

Hygrothermal performance of internal insulation in historic buildings



Tessa Kvist Hansen

PhD Thesis

Department of Civil Engineering
2019

DTU Civil Engineering Report-Byg R-399

Hygrothermal performance of internal insulation in historic buildings

Tessa Kvist Hansen

Ph.D. Thesis

Department of Civil Engineering

Technical University of Denmark

2019

Supervisors

Main supervisor: Associate Professor Søren Peter Bjarløv, Technical University of Denmark

Co-supervisor: Research Director, Ph. D., Ruut Hannele Peuhkuri, Danish Building Research Institute, Aalborg University

Assessment Committee

Professor Carsten Rode (chairman), Technical University of Denmark

Morten Hjorslev Hansen, Ph. D., BYG-ERFA

Professor Andra Blumberga, Riga Technical University

Start date: June 1st, 2015

Submission: October 2nd 2018

Defense: January 11th 2019

Copyright © 2019 by Tessa Kvist Hansen

Publisher:

Department of Civil Engineering

Technical University of Denmark

Building 118

DK-2800 Kgs. Lyngby

Denmark

ISBN: 9788778774965

Report no.: R-399

Preface

The present thesis, *“Hygrothermal performance of internal insulation in historic buildings”* concludes the work from 3 years and 4 months of full-time research conducted at the Technical University of Denmark, Department of Civil Engineering in Kgs. Lyngby, Denmark. The thesis is submitted as a partial fulfillment of the requirements for a Ph.D. degree by Danish standards. The research was financed by the European Union’s Horizon 2020 research and innovation programme through the RIBuild (Robust Internal Thermal Insulation of Historic Buildings) project (grant no. 637268). The research was conducted in the field of energy retrofitting with internal insulation in historic buildings of solid masonry. The case studies included were initiated by Maria Harrestrup in connection with the EUDP 2013-II project “Energy efficient comfort in older apartment blocks”. The rain gauge system for quantification of wind-driven rain was designed in collaboration with Ph.D. student Tommy Riviere Odgaard and with LINATEX A/S.

I would like to take this opportunity to express my utmost gratitude to my wonderful team of supervisors, Associate Professor at the Technical University of Denmark, Søren Peter Bjarløv, and co-supervisor Research Director of the Danish Building Research Institute, Ruut Hannele Peuhkuri. Your guidance, encouragement and positive spirits have been invaluable for me through this process. A further thank you is extended to RIBuild friends; I have enjoyed working with, and learned a lot, from this collaboration. A special thanks must be addressed to friends at Technische Universität Dresden, for welcoming me into your team for 3 months.

Thank you to the people of building 118 and 119; from the reception, to the workshop, to administration and IT, to the laboratory, professors and fellow Ph.D.’s – for always being super helpful, kind, and great colleagues. A special thanks to office 259, both former and present fellows.

Finally, thank you to my family and friends, for proofreading, patience, and so much more.

Tessa Kvist Hansen

Kgs. Lyngby, October 2nd, 2018

Abstract

Global climate change is evident to most, which is why development in the field of renewable energy sources as well as in the reduction of energy consumption is so vital. As the building stock in Europe accounts for 40 % of the energy consumption, we must find possibilities for reducing this figure - not only by the construction of modern and energy efficient buildings, but also through energy retrofitting existing buildings. In these cases, there is a large potential for energy savings, through i.e. low-energy windows, HVAC, and thermal post-insulation of the building envelope. In Denmark, 35 % of the building stock is comprised of historic buildings. These façades are often preservation worthy, and therefore only internal insulation is possible as a strategy for reducing transmission heat losses of the façades.

The application of internal insulation presents potential for other problems, as the existing wall becomes damper and colder, and the risk of interstitial condensation increases. The elevated moisture conditions induce new risks, i.e. the risk of mould growth, wood rot and frost damage. Therefore, moisture safe and robust solutions for internal insulation of solid masonry must be determined. Dynamic simulations are useful tools for prediction of hygrothermal performance of internal insulation. The modelling results however, are naturally highly dependent on the given input. Therefore, the role and relevance of the various inputs is in focus throughout this thesis, as well as conditions contributing to unfavorable moisture conditions.

The purpose of this study was to investigate important parameters with regard to prediction of the hygrothermal performance of internally insulated solid historic masonry with both experimental and numerical methods. Attention was especially given to the effect of wind-driven rain, possibilities with hydrophobization, and the influence of material parameters. Through case studies, the performances of two different internal insulation systems were evaluated. By means of validated hygrothermal simulation models and implementation of predicted future climate, projections of the hygrothermal conditions were calculated and the risks evaluated. A clear but delayed elevated correlation with wind-driven rain and relative humidity behind the insulation was detected in a laboratory study with relatively extreme environmental loads. The effect of wind-driven rain was also apparent through dynamic simulations. However, in situ measurements of wind-driven rain on case buildings did not give definite results on the impact on humidity conditions behind the insulation. Hydrophobization was introduced as a possible measure to prevent water penetration from wind-driven rain and elevated relative humidity behind the insulation in connection with wind-driven rain. The effect of hydrophobization, on water uptake, drying and vapour diffusion was investigated. It was found that hydrophobization in general had a larger effect in brick when compared to lime mortar. Hygrothermal simulations supported these findings, and showed the brick type being a vital parameter. Through dynamic simulations, it was also established that single material parameters, especially water uptake coefficient, had a significant influence on the hygrothermal performance of masonry. Correlations between material parameters were indicated graphically. Linear and logarithmic regression did not, however, yield sufficient models for these correlations.

Dansk resume

Globale klimaændringer er tydelige for de fleste, og derfor er udvikling inden for vedvarende energikilder samt reduktion af energiforbrug afgørende. Da bygningsmassen i Europa udgør 40 % af det samlede energiforbrug, er det nødvendigt at finde muligheder for at reducere dette - ikke kun ved opførelse af moderne og energieffektive bygninger, men også ved energirenovering af eksisterende bygninger. I disse er der et stort potentiale for energibesparelser, f.eks. ved lavenergi vinduer, HVAC optimering og efterisolering af klimaskærmen. I Danmark består 35 % af byggemassen af historiske bygninger, hvoraf mange facader er bevaringsværdige. Derfor er indvendig efterisolering den eneste mulighed for at reducere varmetabet gennem facaderne.

Anvendelsen af indvendig isolering genererer dog muligheden for andre problemer, da den eksisterende væg bliver koldere og fugtigere, og risikoen for kondens og fugtophobning stiger. De forhøjede fugtforhold medfører nye risici, fx risikoen for skimmelvækst, råd i træ og frostskafer. Derfor skal fugtsikre og robuste løsninger til indvendig isolering af fuldmuret murværk findes. Dynamiske simuleringer er nyttige værktøjer i forbindelse med indvendig isolering, da disse kan være med til at forudsige fremtidige hygrotermiske forhold. Modelleringsresultaterne er imidlertid stærkt afhængige af det givne input. Denne afhandling diskuterer derfor rollen og relevansen af de forskellige input, samt andre betingelser, der bidrager til ugunstige fugtforhold.

Formålet med denne afhandling var at undersøge vigtige parametre med hensyn til forudsigelse af de hygrotermiske forhold i indvendigt isoleret historisk murværk med både eksperimentelle og numeriske undersøgelser. Især blev effekten af slagregn, mulighederne med hydrofobering og indflydelse af materialeparametre undersøgt. Gennem casestudier af indvendigt isolerede vægge blev resultaterne af to forskellige indvendige isolationssystemer evalueret. Ved hjælp af validerede hygrotermiske simuleringsskemaer og implementering af forudsagt fremtidigt klima, blev fremskrivninger af de hygrotermiske forhold beregnet og risikoen vurderet. I en laboratorie undersøgelse med relativt ekstreme klimaforhold blev der registreret en tydelig, men forsinket sammenhæng mellem slagregn og forhøjet relativ luftfugtighed bag isoleringen. Derimod gav in situ målinger af slagregn på indvendigt isolerede casestudier ikke konkrete resultater af effekten på fugtforholdene bag isoleringen. Effekten af slagregn var dog tydelig ved dynamiske simuleringer. Af denne grund blev hydrofobering indført som en mulig foranstaltning for at forhindre vandindtrængning og forhøjet relativ luftfugtighed bag isoleringen i forbindelse med slagregn. Effekten af hydrofobering, blev undersøgt i forhold til vandoptagelse, tørring og dampdiffusion. Der blev fundet, at hydrofobering generelt havde en større effekt i mursten sammenlignet med kalkmørtel. Hygrotermiske simuleringer understøttede disse resultater, og viste at tegltypen var afgørende for resultaterne. Gennem dynamiske simuleringer blev det også konstateret, at enkelte materialeparametre, især vandoptagelseskoefficienten, havde en betydelig indflydelse på murværks hygrotermiske ydeevne. Korrelationer mellem materialeparametre blev præsenteret grafisk, men lineær og logaritmisk regression gav imidlertid ikke tilstrækkelige modeller til disse sammenhænge.

Abbreviations and symbols

WDR: Wind-driven rain

T: Temperature

RH: Relative humidity

PUR: Polyurethane

ACC: Autoclaved Cellular Concrete // AAC: Autoclaved Aerated concrete

PCA: Principal Component Analysis

RAF: Rain Admittance Function (rain exposure coefficient)

Contents

1	Introduction.....	1
1.1	Background.....	1
1.2	RIBuild.....	2
1.3	Objective and scope	3
1.3.1	Hypotheses	3
1.4	Structure of the thesis	6
2	State of the art.....	9
2.1	Hygrothermal performance of internally insulated solid historic masonry	9
2.1.1	Risk assessment models	11
2.2	Quantification and effect of wind-driven rain.....	13
2.3	Effect of hydrophobization.....	17
2.4	Material parameters and characterization.....	19
3	Methods for investigation of hypotheses	23
3.1	Hygrothermal performance of internally insulated solid historic masonry	23
3.1.1	In situ measurements	23
3.1.2	Hygrothermal simulations	25
3.2	Quantification and effect of wind-driven rain.....	27
3.2.1	Quantification of wind-driven rain	27
3.2.2	Effect of wind-driven rain	29
3.3	Effect of hydrophobization	31
3.3.1	Laboratory experiments	32
3.3.2	Hygrothermal simulations	34
3.4	Material parameters and characterization.....	35
3.4.1	Influential material parameters with regard to hygrothermal conditions.....	35
3.4.2	Statistical investigation of material parameter correlation	36
4	Results and discussion.....	39
4.1	Hygrothermal performance of internally insulated solid historic masonry	39
4.1.1	In situ measurements	39
4.1.2	Damage models for performance assessment.....	40
4.1.3	Hygrothermal simulations	41
4.2	Quantification and effect of wind-driven rain.....	45
4.2.1	Quantification of wind-driven rain	45

4.2.2	Effect of wind-driven rain	47
4.3	Effect of hydrophobization	50
4.3.1	Laboratory experiments	50
4.3.2	Hygrothermal simulations	54
4.4	Material parameters and characterization.....	54
4.4.1	Influential parameters	55
4.4.2	Parameter correlations.....	56
5	Main findings	59
5.1	Hygrothermal performance of internally insulated solid historic masonry	59
5.2	Quantification and effect of wind-driven rain.....	60
5.3	Effect of hydrophobization	60
5.4	Material parameters and characterization.....	61
6	Conclusion and hypotheses	63
6.1	Hypothesis 1	63
6.2	Hypothesis 2	64
6.3	Hypothesis 3	64
6.4	Hypothesis 4	65
6.5	Perspectives and future research.....	65
	References	67
	Appended papers	75
	Appendix A	77
	Appendix B.....	93
	Appendix C.....	109
	Appendix D	129
	Appendix E.....	137
	Appendix F	149

Appended papers

Journal papers

Paper I [1]: Long term in situ measurements of hygrothermal conditions at critical points in four cases of internally insulated historic solid masonry walls

Authors: Tessa Kvist Hansen (DTU), Søren Peter Bjarløv (DTU), Ruut Hannele Peuhkuri (SBI), Maria Harrestrup (Ekolab)

Publication: Published in Energy and Buildings, Volume 172, August 2018

Paper II [2]: Performance of hydrophobized historic solid masonry – experimental approach

Authors: Tessa Kvist Hansen (DTU), Søren Peter Bjarløv (DTU), Ruut Hannele Peuhkuri (SBI), Kurt Kielsgaard Hansen (DTU)

Publication: Published in Construction and Building Materials, Volume 188, November 2018

Paper III [3]: The effects of wind-driven rain on hygrothermal performance of solid masonry walls with internal insulation

Authors: Tessa Kvist Hansen (DTU), Søren Peter Bjarløv (DTU), Ruut Hannele Peuhkuri (SBI),

Publication: Submitted to Buildings and Environment

Conference papers

Paper IV [4]: Material characterization models and test methods for historic building materials

Authors: Tessa Kvist Hansen (DTU), Ruut Hannele Peuhkuri (SBI), Eva B. Møller (SBI), Søren Peter Bjarløv (DTU), Tommy Odgaard (DTU/COWI)

Conference: 11th Nordic Symposium of Building Physics, 2017

Paper V [5]: Moisture transport properties of brick – comparison of exposed, impregnated and rendered brick

Authors: Tessa Kvist Hansen (DTU), Søren Peter Bjarløv (DTU), Ruut Hannele Peuhkuri (SBI)

Conference: Materials, Systems and Structures in Civil Engineering, 2016

Report

Paper VI [6]: Correlation between certain material parameters in bricks

Author: Tessa Kvist Hansen (DTU)

Course: Introduction to applied statistics and R for PhD students, 02935, Technical University of Denmark

Not appended dissemination

Conference paper [7]: A lime based mortar for thermal insulation of medieval church vaults

Authors: Tessa Kvist Hansen (DTU), Poul Klenz Larsen (National Museum of Denmark), Kurt Kielsgaard Hansen (DTU), Søren Peter Bjarløv (DTU), Ruut Hannele Peuhkuri (SBI)

Conference: 4th Historic Mortars Conference, 2016

Conference paper [8]: A lime based mortar for thermal insulation of medieval church vaults

Authors: Poul Klenz Larsen (National Museum of Denmark), Tessa Kvist Hansen (DTU)

Conference: 2nd International Conference on Energy Efficiency and Comfort of Historic Buildings, 2016

Report [9]: EUDP 2013-II: “Energy efficient comfort in older apartment blocks”, Results and Experience from the Project

Authors: Maria Harrestrup (DTU), Tessa Kvist Hansen (DTU), Rune Haferbier (Ekolab), Jørgen Lange (Ekolab), Leif Rønby Pedersen (rönby.dk), Rasmus Karkov (E&P-service)

1 Introduction

The following introduction elaborates the motivation for the research performed in the present work, and the correlations between 4 main research topics: Hygrothermal performance of internally insulated historic masonry; Quantification and effect of wind-driven rain; Effect of hydrophobization and Material parameters and characterization.

They all share common grounds in relation to the performance of internal insulation in solid historic masonry walls, and the correlation is elaborated through the presented thesis.

1.1 Background

The evident global climate changes have hypothetically urged world leaders, including those of the European Union and even the Danish government, to take action and responsibility for fossil-fuel consumption. Denmark has set a goal of being fossil-fuel-free by the year 2050 [10]. By then Denmark should be able to produce sufficient amounts of renewable energy to cover its national energy consumption. This goal needs to be reached not only by development of and improvements in renewable energy sources, but also by contributing to reduced energy consumption. In Europe, 40 % of the total energy consumption is accounted for by the building stock alone.

35 % of all building stock area in Denmark is historic buildings. In this sense, historic buildings are represented by buildings constructed prior to 1945. In Denmark, the first building code was introduced in 1856, and no changes were made to it before the 1930s [11]. For this reason, most Danish historic buildings were constructed by the same mean principles, using solid masonry with embedded wooden beams for i.e. story partitions. With the introduction of the new building code came new construction techniques, including concrete, steel and cavity walls. Constructions with timber frames were the dominant Danish construction type until 1890's [12]. This dissertation, however, only revolves around solid masonry and wooden beams. Historical buildings in both Denmark and the rest of Europe represent cultural, historic and aesthetic value, whether preservation worthy or not. For this reason, the concept of internal insulation was introduced as a possible energy retrofitting measure in cases where external insulation is not possible. Examples of typical historic solid masonry façades are seen in Figure 1. Not only requirements with regard to reduction in energy, hereunder heat consumption, but also an increased thermal comfort and the avoidance of cold draughts is desired with the application of internal insulation.



Figure 1: Panorama view of a variety of historic façades of solid masonry facades in Copenhagen, Denmark.

Until recently, internal insulation in Denmark has traditionally been installed with mineral wool applied to a timber or steel frame with a vapour barrier installed on the warm side of the insulation. This method, however, often appeared to fail when the wall is solid masonry, because interstitial condensation and mould growth can be caused by the vapour barrier. With the increased focus on energy savings and reduction of heat loss through building envelopes, the attention, research and development in the field of internal insulation has increased in recent years. Several solutions to internal insulation are being introduced, either as complete systems, or stand-alone materials. Products on the internal insulation market include as well vapour tight as vapour open solutions, and capillary active insulation materials.

With the application of internal insulation to a wall, the hygrothermal conditions of that wall inevitably change. Internal insulation reduces both the drying potential and temperature of a masonry wall, inevitably leaving the existing wall colder and damper when compared to pre-retrofitting. Furthermore, the steep drop of temperature gradient may yield interstitial condensation as the temperature at the interface may be less than the dew-point temperature. Undesirable moisture conditions in a construction may lead to mould growth, wood rot and the general deterioration of building materials. Therefore, internal insulation should not be applied without careful consideration to the potential moisture conditions. As masonry consists of porous building materials, the absorption of wind-driven rain is inevitable. It has been proven that wind-driven rain has a significant impact with regard to wetting and water penetration of masonry [13], and it has even been shown to impact indoor climate, energy consumption and the risk of mould growth [14]. Penetration of wind-driven rain may be prevented with the application of a surface treatment. In the case of internal insulation, the constructions are in some cases retrofitted as diffusion open, thus possibly elevated humidity conditions can seek equilibrium with surroundings. Hydrophobization surface treatments have proved to hinder water absorption without compromising the water vapour permeability. For this reason, hydrophobization is particularly relevant in the internal insulation discussion.

In this work the hygrothermal performance of internally insulated historic masonry has been evaluated by means of case studies as well as dynamic 1D simulation. Simulations also assisted in the investigation of most influential material parameters with regard to hygrothermal performance and the influence of surface treatments. The correlations between some single material parameters in brick were investigated statistically, as material parameters are vital for reliable simulations; however, it is not always possible to come by complete material characterizations of historic building materials. The apparent influence of wind-driven rain on hygrothermal conditions within internally insulated solid masonry has been monitored in both case studies and experimental setups in a laboratory. Furthermore, simulations assisted in the evaluation of the significance of wind-driven rain. The effect of hydrophobization treatments of masonry holistically, and on brick and lime mortar as single elements, has also been studied and evaluated through laboratory experimentation.

1.2 RIBuild

The research performed for the present Ph.D. dissertation has been financed by the EU Horizon 2020 project RIBuild – Robust Internal Thermal Insulation of Historic Buildings, under grant agreement no. 637268. RIBuild aims to develop guidelines for the internal thermal insulation of historic buildings, thus allowing for the maintenance of aesthetical and cultural values of the façade expressions while reducing heat loss through external walls. RIBuild introduced the possibility of valuable networking in an international environment with both scientists and other Ph.D. students from 7 participating countries throughout Europe. In addition to the

research performed and disseminated in the presented appended journal and conference papers, compulsive work was performed for several work packages included in RIBuild.

1.3 Objective and scope

The objective of the presented Ph.D. dissertation was to provide research in the field of internal insulation of solid historic masonry. The objective has been met by means of a variety of studies: both in 1:1 case studies and in laboratory, in addition to hygrothermal simulations, literature studies and statistical analysis. The aim was to study the hygrothermal performance of said structures, including defining the impact of wind-driven rain and the possibilities of hydrophobization, in addition to studying material parameter impact and correlations.

The scope of this Ph.D. project is to investigate which aspects are important with regard to prediction of hygrothermal performance of internally insulated historic solid masonry. The scope is investigated through the following hypotheses:

1.3.1 Hypotheses

Hypothesis 1: Long term hygrothermal conditions can be predicted by means of numerical models verified by measurements in critical points in internally insulated case buildings.

Hypothesis 2: Wind-driven rain has a significant effect on the hygrothermal performance of solid masonry walls with internal insulation.

Hypothesis 3: Hydrophobization of the exterior surface has a significant effect on the hygrothermal performance of historic solid masonry.

Hypothesis 4: Certain material properties of brick are more influential with regard to the hygrothermal performance of internally insulated solid masonry structures, and some material parameters can be correlated.

The hypotheses stated above are investigated through the methods and disseminations listed below.

Hypothesis 1: Hypothesis 1 claims that reliable numerical models can be implemented for prediction of hygrothermal conditions in internally insulated solid masonry structures. By establishment of measurements in 4 internally insulated test apartments, the hygrothermal conditions were monitored. In turn, the measurements made up the basis for model verification and validation. By implementing the actual measurements in models with unknown material parameters, the model parameters can be estimated. Provided the postulate cannot be rejected, there is evidence that said models are vital for research in the area, and general improvements are necessary. The hypothesis is tested by various means:

1. Long term measurements of hygrothermal conditions in internally insulated masonry
2. Hygrothermal modelling of case studies of various internal insulation systems
3. Validation of said models based on long term measurements from case studies
4. Future predictions, including climate change, of hygrothermal conditions with implementation of forecasted weather for Denmark in 2020-2050
5. Simulation investigation of vital material parameters with regard to moisture transport and hygrothermal conditions

6. Dynamic simulations of basic moisture transport properties of brick with different surface treatments

On the basis of the above methods, it can be determined whether or not hygrothermal modelling can be used successfully for the prediction of hygrothermal conditions in cases of internally insulated masonry. The investigations should also shed light on the possibilities of building reliable models despite estimations of certain material parameters and boundary conditions. Furthermore, the most vital material parameters for the moisture modelling would be identified. The work revolved around this hypothesis is processed in the work listed below.

- a) **Paper I:** “Long term in situ measurements of hygrothermal conditions at critical points in four cases of internally insulated historic solid masonry walls”. The paper investigated four case buildings and their hygrothermal conditions. Numerical models were created (Delphin 5.8.3) and validated against measurements. On this basis, variations of the models were created for determination of decisive input.
- b) **Paper IV:** “Material characterization models and test methods for historic building materials”. This paper investigated the most decisive material parameters in numerical simulations of hygrothermal conditions by implementing a parameter variation study of 5 material parameters in simulation models.
- c) **Paper V:** “Moisture transport properties of brick – comparison of exposed, impregnated and rendered brick”. Investigation of the moisture transport properties of brick with various surface treatments was investigated experimentally, and numerical models with various brick types were implemented for prediction of the behavior.

Hypothesis 2: The second hypothesis claims that WDR has a significant influence on the hygrothermal conditions within internally insulated historic masonry walls. The hypothesis was tested by implementation of experimental WDR measurements in 2 of the monitored case buildings. Furthermore, a laboratory study investigated water migration and penetration with implementation of climate cycles with rain loads, radiation and a cold climate. If the postulate cannot be rejected, WDR must be seen as a vital parameter with regard to the hygrothermal performance of internally insulated masonry. Thus, WDR must be considered as a parameter in the development of internal insulation systems. For investigation of this hypothesis, the following research was performed;

- 1. Literature studies of existing knowledge on WDR and WDR quantification
- 2. Development of WDR gauges and experimental setup in some case studies
- 3. Monitoring of the WDR coupled with hygrothermal measurements in case studies
- 4. Comparison of experimental quantification and semi-empirical models
- 5. Dynamic simulations for evaluation of the influence of the rain exposure coefficient
- 6. Experimental setup of moisture loads on masonry sections with and without hydrophobization

Through the methods described above, it should be possible to identify if WDR is in fact a main contributor to undesirable moisture conditions within internally insulated masonry. Furthermore, it should be possible to assess the effect of hydrophobization with a constant climate as well as the WDR influence observed with numerical simulations. The hypothesis was studied in the following work:

- a) **Paper III:** “The effects of wind-driven rain on the hygrothermal performance of solid masonry walls with internal insulation”. Wind-driven rain was monitored experimentally and evaluated against monitored hygrothermal performance within the masonry walls (at wall-insulation interface and behind beam ends).
- b) **Paper II:** “Performance of hydrophobized historic solid masonry – experimental approach”. The paper includes a study of the water migration through masonry sections with built-in temperature and relative humidity sensors placed at different depths in the masonry.

Hypothesis 3: The third hypothesis states that hydrophobization of the external surface of internally insulated historic masonry may remedy the ingress of WDR and improve the quality of the moisture performance of said walls. Provided the hydrophobization can reduce the water uptake without compromising drying capability. There is a large variety of hydrophobic treatments available on the market; however they may not have the same efficiency with use on various materials. When studying historic masonry holistically, the efficiency on both brick and lime mortar must be taken into consideration. Provided that hydrophobization can work efficiently on historic masonry holistically (bricks and lime mortar), the hypothesis can be verified. The hypothesis is investigated through the following research:

- 1. Literature review of existing research on hydrophobization agents and their effects on masonry
- 2. Laboratory experiments of a variety of hydrophobization agents and their effects on both brick and air lime mortar
- 3. Study of the effect of the agents with regard to water uptake, drying, penetration depth and vapour diffusion resistance
- 4. Laboratory experiments monitoring moisture ingress in wall sections with and without hydrophobization subjected to extreme climate cycles
- 5. Laboratory investigations of a variety of surface treatments (hydrophobization and render) on brick and associated numerical simulations on various brick types

The above experimentation makes it possible to determine whether hydrophobization yields a positive contribution to hygrothermal conditions within internally insulated historic masonry. The investigations include the effect on individual elements (brick and lime mortar) and also on masonry holistically. The effect of hydrophobization naturally depends on the significance of WDR, which is examined via the previous hypothesis. The following dissemination is related to the third hypothesis:

- a) **Paper II:** “Performance of hydrophobized historic solid masonry – experimental approach”. The paper includes laboratory experiments performed on brick and lime mortar specimens. The investigation includes a variety of types of hydrophobization agents, and their effects on various material properties, i.e. water uptake, drying and vapour diffusion. Furthermore, the water migration through masonry sections – some hydrophobized - was studied.
- b) **Paper V:** “Moisture transport properties of brick – comparison of exposed, impregnated and rendered brick”. The paper studies the transport properties of brick with different surface treatments, including hydrophobization.

Hypothesis 4: The final hypothesis states that certain brick material parameters are more influential than others when it comes to the hygrothermal performance of internally insulated masonry. Furthermore, it is stated that a correlation between certain material parameters can be made, thus yielding the possibility for

in situ and non-destructive determination of brick type and quality. If the hypothesis cannot be rejected, the influential parameters can be estimated, thus improving the quality of predictions and numerical models. The hypothesis was examined by means of the following work:

1. Numerical simulations based on a case study allows for a parameter study on the most influential material parameters with regard to hygrothermal conditions in masonry
2. Statistical investigation of certain material parameters in brick, and their correlations

With the investigations of vital material parameters and their correlations, the 4th hypothesis is investigated. The most influential material parameters could be identified, and possible correlations may lead to simple classification methods based on non-destructive parameter determination. The hypothesis has been investigated through the following studies:

- a) **Paper IV:** “Material characterization models and test methods for historic building materials”. Through numerical simulations a parameter study on 5 material parameters (density, open porosity, thermal conductivity, water uptake coefficient, and water vapour diffusion resistance factor) was performed in order to identify primary influential parameters on hygrothermal conditions and performance.
- b) **Paper VI:** “Correlation between certain material parameters in bricks”. A statistical study of correlations between certain material parameters: density, open porosity, water uptake, thermal conductivity, and water vapour diffusion resistance.

1.4 Structure of the thesis

The present dissertation includes 6 main chapters, as presented in Figure 2. The thesis revolves around 4 main topics: 1) Hygrothermal performance of internally insulated historic masonry, 2) Quantification and effect of wind-driven rain, 3) Effect of hydrophobization, 4) Material parameters and characterization. The research performed within these 4 main topics is disseminated in the appended papers listed on page 13. In the schematic view of the structure, Figure 2, it is seen which main topics and hypotheses are processed in the 6 dissemination items. Chapter 1 includes background and motivation for the research as well as the objective, hypotheses, and the present structure section. Chapter 2 is a state-of-the-art review of all 4 main topics, and Chapter 3 describes the methods implemented for the investigations. Chapter 4 comprises the results and sub-discussions. In Chapter 5, the main findings within the 4 main topics are processed. Finally, Chapter 6 concludes this dissertation; the hypotheses are evaluated in accordance with the performed research. As seen in the graphic presentation of the thesis structure, all the main topics were included in a minimum of 2 dissertation pieces. The same applies to the case of the hypotheses.

Figure 2: Schematic presentation of the thesis structure. In the above scheme, the nomenclature P represents appended Papers I-VI, and Main Topics are denoted with MT.

2 State of the art

The following literature review of the 4 main topics presented in the research is largely contributed by the appended papers. Additions have been made with regard to the completeness of the thesis. Some of the given information and previous research relates to several main topics; however, prioritizing of the associated paragraphs has been made.

2.1 Hygrothermal performance of internally insulated solid historic masonry

Thermal insulation is a common method of reducing the heat loss through the building envelope. Thermal insulation does not only reduce the energy demand for heating, but also provides a better indoor environment with regard to thermal comfort, utilization of indoor space, and indoor air quality [15]. External insulation is usually the most efficient and moisture safe method for reduction of heat transfer through external walls, as it provides the existing construction with protection from the external environment and eliminates thermal bridges [16–21]. This is, however, not possible with many historic buildings, as the façades are either preservation worthy or of too much cultural and aesthetic value to change the exterior aesthetics. Therefore internal insulation is introduced in these cases. Internal insulation however introduces several risks to the existing construction, as the hygrothermal conditions in the original construction are changed. As a result, the risk of interstitial condensation is increased [22–24], and the drying potential inward is reduced as the permeability is reduced by the insulation [23,25,26]. Figure 3 illustrates the principles of condensation risk in connection with internal insulation. It is seen that in the case of internal insulation, the immediate temperature reduction through the internal insulation layer creates the possibility of the temperature cooling below the dew point temperature, yielding the possibility of interstitial condensation [19] at the interface. For this reason, the traditional method of internal insulation includes a vapour barrier to prevent the humid interior air to reach the cold interface and condensate. Especially in cold seasons, the internal vapour pressure exceeds the external and humidity equilibrium is sought, which forces the internal air to diffuse outwardly.

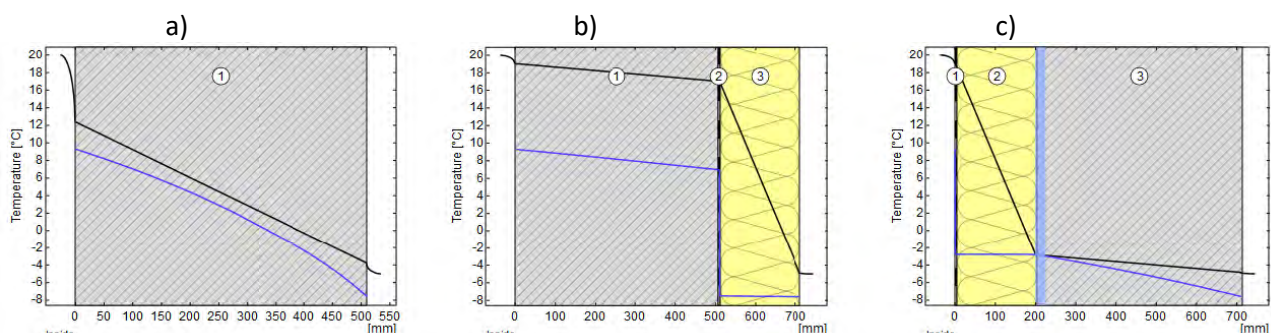


Figure 3: Temperature profiles through external masonry walls with a) no insulation, b) external insulation, and c) internal insulation. The left side represents interior conditions, and the right side exterior climate. The black lines represent the dew point temperature profiles, and blue indicates the temperature gradient. The blue area in c) represents the area where the risk of condensation occurs. Illustration from RIBuild D1.2 [27].

Basic moisture transport mechanisms in and around an internally insulated solid wall with embedded wooden beams are illustrated in Figure 4. The moisture transport mechanisms include vapour diffusion, i.e. diffusion from a higher vapour pressure in the warm interior outwards due to vapour pressure differences. In porous building materials, capillary suction leads to the transport of liquid moisture, whether it is present due to condensation, wind-driven rain, or rising damp. In other words, capillary suction is the driving force of moisture transport in saturated pores, whilst at lower humidities within the pores the main transport

mechanism is vapour diffusion. Convective moisture transport occurs as a consequence of moving damp air through leakages, etc., e.g. around partition walls and floor slabs, where the colder surface temperature due to thermal bridge effect also makes it possible for moisture to accumulate. In addition, the embedded beam end can transport accumulated moisture inwards, in the fiber direction, for evaporation, while the same does not qualify for the wooden lath, which is completely embedded in the masonry perimeter.

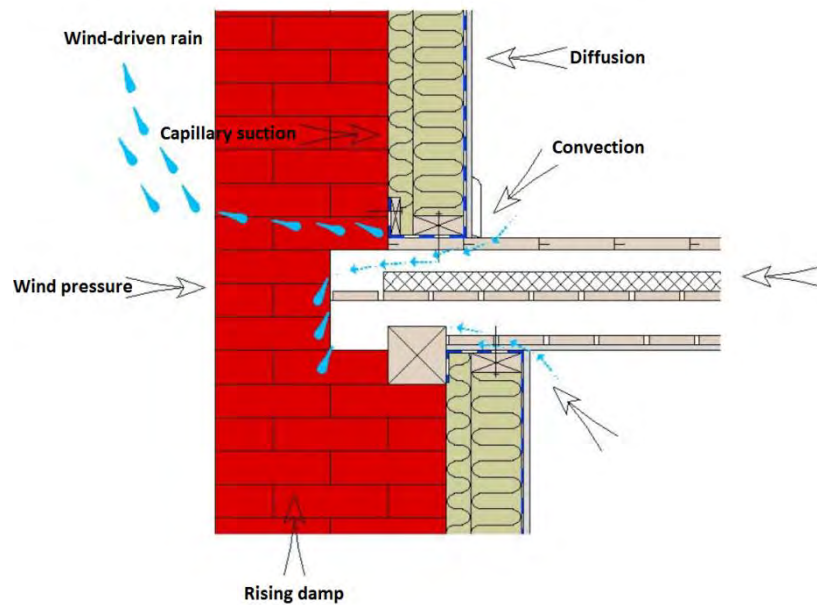


Figure 4: Typical moisture transport mechanisms in an internally insulated wall [28].

The increased risk of high moisture in the wall inevitably leads to an increased risk of mould growth [29] and decay of the existing wood embedded in the structure. Furthermore, as a result of reduced temperature and drying potential of the existing wall, the risk of frost damage to the surface is also increased [21,22,26,29]. Internal insulation should thus not be installed without considerations to the building physics aspects. It might not be possible to achieve the desired U-value, or the desired heat loss reductions, but given the risks involved, it is far more feasible in the long run to implement a moisture safe solution.

There are several types of insulation systems marketed for internal insulation [23], including capillary active and hydrophilic insulation materials [20,22,30,31], and traditional hydrophobic insulation materials in a system including a vapour barrier. Internal insulation systems on the market can be separated into three groups based on their basic properties: 1) capillary active and vapour open, 2) vapour open and 3) vapour tight systems. Capillary active systems have the advantage of a high moisture buffering capacity, yielding the possibility of redistributing absorbed moisture for evaporation [32]. The capillary active systems are also vapour open. Vapour open systems allow transport of water vapour in the construction, but the risk of interstitial condensation increases as moist indoor air reaches the cold external wall. A vapour open system can be combined with a smart vapour retarder, whose vapour resistance varies depending on the relative humidity [33]. A high vapour resistance in cool periods would prevent interstitial condensation, and a reduced vapour diffusion resistance can allow drying of the wall. Vapour tight systems completely inhibit moisture transfer through the insulation system, preventing vapour from diffusing through the insulation and condensing on the external wall. All of these systems naturally have pitfalls; the capillary active system will lose its ability for moisture redistribution if there is not full contact between the materials in the system.

Also, no organic material should exist at the cold surface of the insulation [34] and for systems with vapour barriers, proper installation and complete tightness is needed. Furthermore, these systems leave the wall extra sensitive to external moisture loads, as inward drying is limited.

There has been increasing focus on internal insulation in heritage buildings for the past few years; a limited number of studies with long-term in situ measurements are available. Orlik-Koźdoń *et al.* [23] found no critical moisture conditions in two cases of internal insulation of expanded polystyrene and lightweight aerated concrete on a solid brick wall. However, measurements were only performed for 6 months, and furthermore, there was an external curtain wall, protecting the construction from external moisture loads etc. Klůšeiko *et al.* [25,35], on the other hand, obtained high relative humidities in 4 cases of internal insulation on a brick wall during a 9 month study. The 4 materials tested in that case included: calcium silicate (50 mm), aerated concrete (AAC, 60 mm), polyurethane foam with capillary active calcium silicate channels in a grid of 40X40mm (PUR, 50 mm) and polyisocyanurate foam (PIR, 30 mm). Calcium silicate showed the best performance with regard to moisture performance, however calcium silicate also has the highest thermal conductivity. Harrestrup *et al.* [36] monitored a case of internal insulation of 40mm aerowolle on solid masonry in a heritage building, and the effect of intentional thermal bridges above and below supportive wooden beams. They found that leaving a 200 mm uninsulated gap above and below the beams yielded a lower risk of mould growth; this was found, however, to be very dependent upon the orientation and the thickness of the existing wall. Toman *et al.* [20] ran a long-term study of 4 years on a 19th century building with solid brick walls, external render and paint. It was insulated with a hydrophilic mineral wool insulation board, and had no vapour barrier; a vapour retarder was placed on the interior surface of the existing wall. The study showed excellent hygrothermal conditions and no risk of interstitial condensation at any point in time during the 4 year period. In a recent study by Hamid *et al.* [37], a similar study was performed with in situ measurements in solid masonry with internal insulation, and validated simulation models. This study emphasized the importance of the orientation due to the significant influence of wind-driven rain, and solar-driven vapour. Furthermore, the study emphasized the significant risk of mould growth at the wall-insulation interface and the cold side of an integrated vapour barrier given the presence of biological material.

2.1.1 Risk assessment models

For the investigation and assessment of the hygrothermal performance of building envelope constructions it is useful to implement so called risk assessment models. These risk assessment models provide a basis for comparison of the various hygrothermal conditions and associated risks. In terms of internal insulation, moisture induced deterioration is in focus. Undesirable moisture conditions in masonry yield the possibility of several deterioration processes, including frost damage in brick and mortar, corrosion of embedded metals, rotting of embedded wood, loss of thermal insulation values of porous building materials, and mould growth [38]. Theoretical models are implemented for prediction and magnitude of risks, despite often not being very accurate [38]. One of the failure modes commonly implemented is the risk of mould growth, as such a risk indicates that there is an undesired moisture excess in the construction. Another relevant failure mode for the present research is the degeneration of wood, as wood typically is embedded in historic Danish masonry structures.

Mould growth can occur when the following are present; fungal spore, water and organic material. Mould growth rates are furthermore dependent on temperature conditions. Mould spores are everywhere, even

airborne, and given favorable conditions, mould growth can occur on surfaces. For very sensitive materials, mould growth has the possibility of occurring at relative humidities above 80 % [39]. The time span of the given favorable conditions, influence the mould growth intensity. Mould growth is cause for bad indoor climate, and can initiate general health effects such as eczema and headaches, however also has a negative impact on breathing, and can instigate both asthma and bronchitis [40].

There are several assessment models developed for the theoretical quantification of mould growth, based on hygrothermal conditions. Krus *et al.* [41] introduced the isopleth systems based on boundary conditions of temperature and relative humidity, generating boundaries for lowest possible conditions for mould growth. One of the most acknowledged risk assessment models is a mould growth prediction model presented and described in [39]. This model takes benefit of the time dependence of the favorable mould growth conditions and is based on the original VTT mould growth model [42]. The original model was developed for prediction of mould growth on wooden surfaces, whereas the improved model takes sensitivity classes into consideration. The sensitivity classes are based on experimental results on various building materials [39]. The mould index, M, quantifies the mould growth rate in a range from 0-6, elaborated in Table 1. The mould index can be generated for simulations or measurements of temperature and relative humidity in critical points in a construction. A review of different mould models is found e.g. in [43], [44].

Table 1: Mould growth index classifications [39].

Mould Index (M)	Description of growth rate
0	No growth, spores not activated
1	Small amounts of mould on surface (microscope), initial stages of local growth
2	Several local mould growth colonies on surface (microscope)
3	Visual findings of mould on surface, <10% coverage, or, <50% coverage of mould (microscope)
4	Visual findings of mould on surface, 10-50% coverage, or, >50% coverage of mould (microscope)
5	Plenty of growth on surface, >50% coverage (visual)
6	Very heavy and tight growth, coverage around 100%

For indication of severe moisture problems, i.e. high moisture loads in constructions, risk models have also been developed for e.g. wood decay, which estimates mass loss in wood due to wood rot. The deterioration of wood can cause vital damage to a structure, as wood rot and decay fungi cause mass loss, and in time the wood deteriorates completely. This is naturally an undesired phenomenon, as it can cause life-threatening damage to inhabited buildings. The timeframe for wet conditions is essential for wood rot occurrence. Furthermore a very high relative humidity (95-99 %) of the ambient air in the local microclimate is required for decay fungi occurrence in pine sap wood [45].

The most common model for wood decay is described in Viitanen *et al.* [45]. This model for wood decay accounts for the period of time in which the conditions are favorable in relation to wood decay. The model is developed for worst-case scenario wood; untreated pine sapwood, why the results should be studied with precaution, when it is unknown which type of wood is actually used in the studied cases. Also, the embedded wood may in reality be wrapped in moisture proof materials and/or treated with contemporary substances, e.g. tar, creosote oil or the like in order to make the wood resistant to moisture damage [12]. The output from the wood decay model is evaluated as a percentage of irreversible mass loss, ML, in the wood.

For all risk assessment models apply – due to the high uncertainties connected to the absolute values – that they only should be used relatively to give an indication for which solution gives a higher or lower potential for a risk.

2.2 Quantification and effect of wind-driven rain

The hygrothermal performance of internally insulated solid masonry is inevitably affected by external moisture loads, including wind-driven rain. In fact, wind-driven rain is a significant parameter with regard to the hygrothermal performance of external façades [13,30,46]. Wind-driven rain is rain that passes through a vertical plane in the atmosphere. As opposed to e.g. cavity walls providing a capillary break, solid masonry absorbs and retains the wind-driven rain water [47]. Usually this moisture would evaporate, but the application of internal insulation impedes the evaporation as the temperature in the masonry decreases. In the case of internally insulated masonry, wind-driven rain has proven to be a negative contributor to the hygrothermal performance [48]. Finken *et al.* state that wind-driven rain can be the most critical factor in regards to moisture in a façade of porous building materials, as opposed to interstitial condensation, reduced drying capability and temperature when internal insulation is applied [30]. Blocken *et al.* also found that wind-driven rain was the most influential factor contributing to the wetting and water penetration of external façades, which in turn affects not only hygrothermal properties and durability [13], but also has been shown to influence indoor climate, energy consumption and the risk of mould growth [14]. Through hygrothermal simulations and measurements, Künzle *et al.* found that an estimated 70 % of wind-driven rain is absorbed by means of capillary action [49]. This observation was based on a one-dimensional validation of measured water content in 3 cases of different porous building materials installed in a western wall, and thus susceptible to exterior climate.

In section 2.1, the basic moisture transport mechanisms regarding internal insulation were introduced. As mentioned, transport of liquid moisture occurs due to capillary forces in porous materials such as brick and mortar as a result of cohesive pores. The rate of the moisture transport is dependent on the pore structure, whether they are open or closed pores, and the pore size distribution. Capillary suction occurs in porous materials when the material comes in contact with water. The suction happens as a result of a hydrostatic vacuum and surface tension in a moist pore. The moisture creates a concave water surface, a meniscus, under which a negative hydrostatic pressure is created and the surface tension occurs [50]. In an attempt to equalize the pressure, a force stronger than gravity and friction combined sucks up water which is in contact with the material. As the water takes up more space in the pores, the resistance caused by friction is increased, the pull of gravity also steps in, and the process will slow down [51]. The hydrostatic pressure increases as the meniscus radius decreases, and for larger pores capillary suction is therefore not possible. For very small pores that are filled quickly, a significant resistance from friction occurs although the hydrostatic vacuum is larger. Thus a material with a fine pore structure is in fact able to absorb water from an adjacent material of a coarser pore structure [19]. Capillary migration of wind-driven rain contributes to moisture induced risks, especially where vapour barriers, capillary inactive insulation materials [30], or diffusion tight paint on the interior surface are present, as they make it more difficult for the moisture to evaporate inwards. Damaged façades are less resistant to WDR and therefore internal insulation should only be installed on intact façades. Damaged or weathered bricks, joints and render should be replaced or repaired before internally insulating [18,52]. Mould or wood decaying fungi growth in wooden beams and other woodwork in the wall are not the only risks associated with the accumulation of moisture in the masonry façade. The risks also include a resulting decrease in durability due to frost damage, surface soiling,

and salt migrations [53], not to mention the reduced thermal resistance caused by an accumulation of moisture (especially for capillary active insulation systems) [48].

The magnitude of WDR is a function of rain intensity, size and distribution of raindrops, and wind speed. The simultaneous occurrence of wind and vertical rain generates the WDR, which can be referred to as a sloped vector [13], illustrated in Figure 5. The terminal velocity of the raindrop is dependent on the size of the raindrop; larger droplets fall faster [54], but are less easily carried by wind [55]. The impact on the façade is affected by additional factors, such as the building's geometry, wind direction, local topography, climate, obstructions, façade orientation, rainfall duration, pressure differences, façade surface characteristics, uniformity, condition, and location on the façade. Studies have shown that the edges [56] and top of a building are most exposed to WDR provided there is no existing roof overhang [57]. This phenomenon can be partly explained by the varying wind pattern across an obstacle such as a building, and the fact that the edges are subjected to WDR from two sides. The wetting of edges has also proved to be more prolonged when compared to central areas of the facades, due to the lower temperatures and reduced drying potential [14]. Strong solar loads may also drive moisture from large WDR loads further into the construction [58]. There are various quantification methods for WDR loads, namely experimental, semi-empirical, and numerical models [13,59].

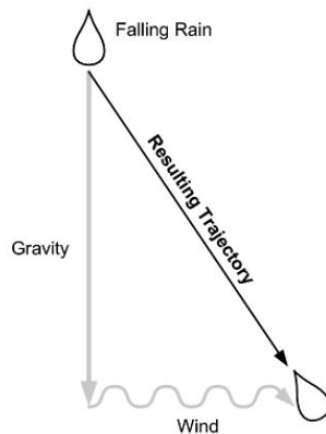


Figure 5: Basic illustration of WDR [54].

Experimental quantification of WDR loads is not a standardized procedure, although it is always performed with a WDR gauge. Wall-mounted WDR gauges have been implemented in experimental work since the 1930's, and a variety of designs have been used. The designs vary in shape, size, material, whether or not they are recessed in the wall, and whether or not they are installed with automatic wipers - variations that have been found to yield discrepancies [13]. The most influential source of error in connection with WDR measurements has been identified as the evaporation of adhered water on the collector plate. Other sources of error include splashing of rain drops, evaporative losses from the reservoir and connecting tube, condensation on the collection area and wind errors. A deeply recessed WDR gauge type has proven to reduce the splashing errors with high wind speed and rain intensity, while in the case of light rain, the large collection area generated large evaporative losses, and splashing in this case was irrelevant [13,59]. The condensation error on the collector surface has been estimated in simulations [59], and shown to be small. This is the only error source that can increase measured results, which are thus liberal. Section 3.2.1 elaborates the development of the wind-driven rain gauge used in the presented research.

Several semi-empirical calculation models for WDR have been developed, and they are continuously under development and improvement. They are all based on the theoretical formula expressed in Eq. 1, where r_{WDR} represents rainfall intensity for WDR and r_h unobstructed horizontal rain [mm], U the wind speed [m/s] and V_t the raindrop terminal velocity of fall [m/s];

$$\text{Wind driven rain} \quad [l/m^2] \quad r_{wdr} = r_h \cdot \frac{U}{V_t} \quad (\text{Eq. 1})$$

In 1955 Hoppestad introduced the WDR coefficient, DRF, [13],[60], which is a proportionality constant between rain on a vertical and horizontal plane, given as $\frac{1}{V_t}$, where V_t is dependent on rain drop diameter [61] and in 1965 Lacy refined the formula (Eq. 1), providing the empirical relationships for functions of median rain drop size and terminal velocity of fall for these raindrops [13,47,60], resulting in Eq. 2, where DRF represents the WDR coefficient, empirically determined as 0.222 on average;

$$\text{Wind driven rain} \quad [l/m^2] \quad r_{WDR} = DRF \cdot U \cdot r_h^{0.88} \quad (\text{Eq. 2})$$

For estimation of rain deposition on a building, Lacy suggests additions to the WDR calculation as seen in Eq. 3, in order to account for wind velocity, wind direction and location on the building.

$$\text{WDR deposition on facade} \quad [l/m^2] \quad r_{bv} = DRF \cdot U \cdot r_h^{0.88} \cdot RAF \cdot \cos(\theta) = r_{WDR} \cdot RAF \cdot \cos(\theta) \quad (\text{Eq. 3})$$

In Eq. 3 RAF is the rain admittance function and θ is the angle between the normal to the wall and the wind direction. RAF varies from <0.20 below a roof overhang up to >1 at the top and edges of high-rise (>10m) buildings without roof overhang, as seen in Figure 6 [54,60]. Equation 3 is most operational, as it accounts for the wall orientation by including cosine of the wind directions angle to a normal of the wall, and furthermore accounts for the location on a façade. The rain admittance function can be equated with the rain exposure coefficient introduced in hygrothermal Delphin simulations.

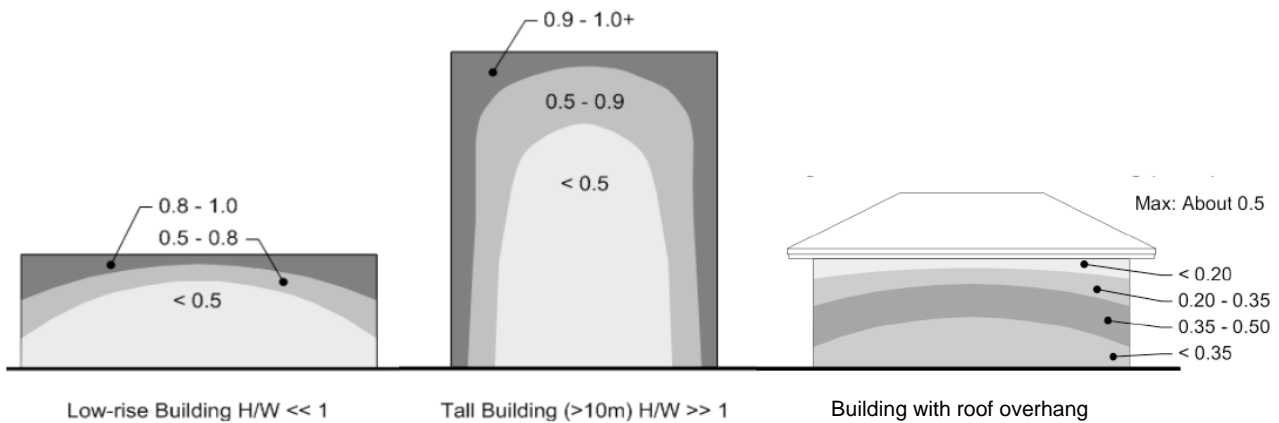


Figure 6: Rain admittance function on areas of building facades for low-rise, high-rise and buildings with roof overhang [54].

Numerical models of WDR are often based on computational fluid dynamics. The numerical method includes various HAM (Heat, Air and Moisture) simulation models performed in various codes, e.g.; HAMFEM [62], WUFI [63] or Delphin [64]. Abuku *et al.* (2012) performed extensive research on WDR, comparing measurements and numerical simulations [62],[65]. A test building was set up for WDR measurements in actual climate conditions. The test building included specially installed test sections for monitoring WDR, weight changes in specimens, surface temperature, and runoff water for monitoring the moisture response

to WDR impact. Large differences were detected between measurements and simulation results. The differences could not all be attributed to the convective moisture transfer coefficient, β_e , used in the HAM simulations. A parameter study of β_e as a function of the reference wind measured did show some influence on results and compatibility. The discrepancies found were also attributed to various error sources such as adhesion, evaporation, splashing, bouncing, and spatial and temporal averaging of rain drops. The fact that many of the parameters interact, makes it is very difficult to make precise numerical simulations of WDR.

Morelli *et al.* (2012) [66] compiled a short review of studies on masonry walls with wooden beams. Most of the reviewed literature at the time stated that WDR was not problematic as long as the façade was intact (no cracks or degraded joints). These studies did not clearly reference WDR loads or climate conditions, and WDR was not included in the hygrothermal simulations. Morelli *et al.* [20] also studied potential moisture risks at beam ends in masonry walls subjected to WDR. The study was based on FMEA (Failure Mode and Effect Analysis) and hygrothermal simulations of retrofitted masonry walls with embedded wooden beams as story-partitions, and internal insulation. See also Figure 7 for an illustration of the construction types. The hygrothermal simulations with WDR of various intensities (3 different rain exposure coefficients) did not show any sign of an effect on the moisture conditions behind the insulation, but with high rain intensity the beam ends could exceed critical moisture content. For medium rain intensity it was seen that in cases with free air flow around the beam (20 mm on three sides) and reduced insulation (omitting 200 mm insulation above and below the beam), the moisture content had a tendency to be lower than in constructions with full insulation, which tended to increase the moisture content. Simulations with vapour barriers applied to the case with reduced insulation indicated no impact on the drying potential of beam ends, so the 20 mm air gap around the beam is the influential factor. It was concluded that WDR had a substantial impact on the moisture conditions in beam ends, and that the rain intensity was a very influential factor. A previous study by Morelli *et al.* (2010) with 2D and 3D simulations of internally insulated masonry with wooden beams embedded, showed that the magnitude of WDR load had a significant impact on the moisture conditions in beam ends [67].

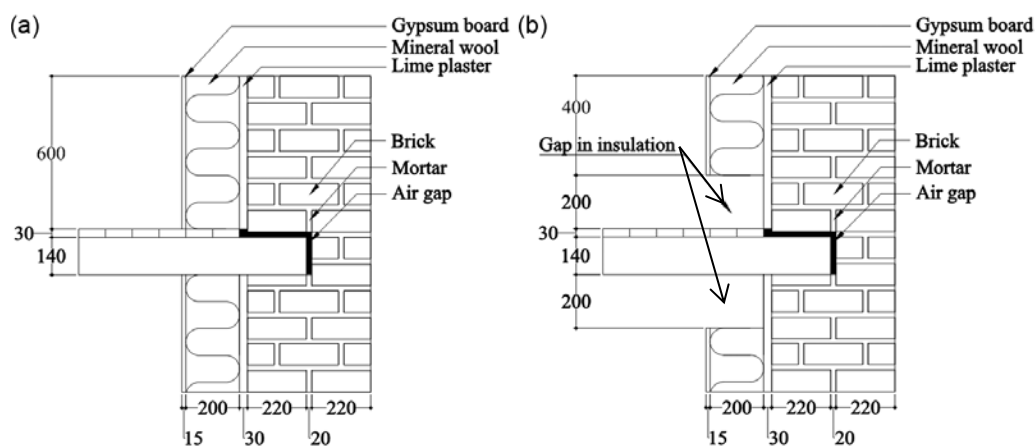


Figure 7: The construction principles around beam ends used FMEA and hygrothermal simulations by in Morelli *et al.* [66].

Abuku *et al.* (2008) investigated the interaction between indoor and outdoor climate and a solid masonry building envelope. Their focus was on WDR impact on hygrothermal response, including mould growth, indoor climate and energy consumption. Using numerical simulations, the hygrothermal conditions in the brick wall and room were determined. The study found a distinct impact of WDR on the humidity of internal wall surfaces and indoor humidity. Critical periods were seen especially in summer and winter, and the walls

were especially affected in the south and west wall-orientations, as this is also the dominant wind direction at the location of the study [14]. A subsequent study by Abuku *et al.* (2009) compared WDR field measurements with numerical simulations, and determined the responses of the walls to WDR loads. The study indicated that predicted WDR loads were often overestimated in numerical modelling of moisture content, partly because of the splashing of raindrops hitting the wall surface not being considered in standard HAM modelling, and partly due to averaging errors in absorption and evaporation [65]. Klößeiko *et al.* (2014) reported a study of field measurements of four different internal insulation systems. They found a certain impact from exterior conditions/rain as increased humidity was measured at the interface between insulation and brick in the case of a vapour tight insulation material [25].

A study by Vereecken *et al.* (2015) on capillary active interior insulation methods demonstrated that driving rain influenced hygrothermal behavior undesirably [48]. The study investigated whether a capillary active solution (calcium silicate) performed better than a vapour tight system (extruded polystyrene (XPS)) on single leaf, exposed masonry constructions with a dynamic indoor environment. Adding (large) WDR loads in numerical simulations resulted in high relative humidity on the interior side of the masonry in both insulation systems, and of the reference wall. The relative humidity in the case of vapour tight insulation reached roughly 100 % for the entire year, whereas the capillary active system illustrated the capability for inward moisture transport and drying potential when the drying to the exterior occurred slowly at low temperatures. With regard to moisture accumulation after WDR loads, the vapour tight system showed slower drying; only external drying could occur in this case. In the case of capillary active insulation and a reference wall without insulation, it was seen that WDR loads also influenced the relative humidity on the interior wall surface. This study also found that at high WDR loads the thickness of the masonry wall had an impact on the masonry moisture content regardless of insulation type, and on the indoor relative humidity in cases of capillary active insulation.

2.3 Effect of hydrophobization

Hydrophobization treatments may prevent, or at least reduce, penetration of liquid water from external conditions. Thus hydrophobization may have a positive effect on the moisture conditions within a wall, and actually impedes moisture accumulation due to rain penetration. Therefore, a hydrophobization treatment may enhance the service life of an internally insulated wall, as the risk of moisture related damages such as frost damage, cracking, wood degradation and mould is also reduced. Hydrophobization will protect the façade from external liquid moisture loads. The façade will however not be protected from internal moisture sources in the form of warm moist air, or possibly condensation. This is why the vapour permeability of a hydrophobized wall should not be affected by the treatment. An old-fashioned method for hydrophobization is found in old surface treatments, such as façade painting. However, this is not desired for protection listed or culturally valued buildings, as it changes the architectural expression. A previous study of internal insulation applied to external walls showed a case with a painted façade yielding excellent results with regard to hygrothermal conditions at critical points [1]. This success may be attributed to the paint serving as a water repellent; however the façade was also northbound and only a thin layer of insulation was applied. Furthermore, both hygrothermal simulation [30] and experimental [68] studies have shown a reduction in heat loss through impregnated external walls, due to the reduced thermal conductivity caused by the dryer state of the wall. In addition, moisture within the insulation material compromises the efficiency [29,30]. There is a large variety of hydrophobization agents on the market, but these may not have the same efficiency

on various building materials, and when studying historic masonry holistically, the efficiency on both brick and lime mortar must be taken into consideration.

Many hydrophobic agents are based on silicone in the form of either silane or siloxane, or even a hybrid of both [69]. Both active compounds react with silicates in the building material and create CH_3 -molecules which are hydrophobic, like the other non-polar carbonaceous groups CH and CH_2 . Lime does not contain silicates in itself, however sand grains as aggregates in lime mortar do. Therefore the silicone based hydrophobic treatments may not bind as well to lime mortar as they do not bind to the binding agent itself as they do on e.g. cement or brick.

The main principle of hydrophobization is illustrated in Figure 8. In a non-surface treated specimen, the surface tension is higher than that of water, and thus the attraction of water from the specimen is higher than the internal attraction of water molecules. Therefore, when the contact angle, θ , becomes small, the droplet becomes big, and the water is absorbed by the surface. In the opposite case, a hydrophobization treatment reduces the surface tension, and the attraction of water molecules within the droplet is larger than the specimen's attraction to the water. In other words, the contact angle becomes larger, and the surface will not absorb the liquid [19].

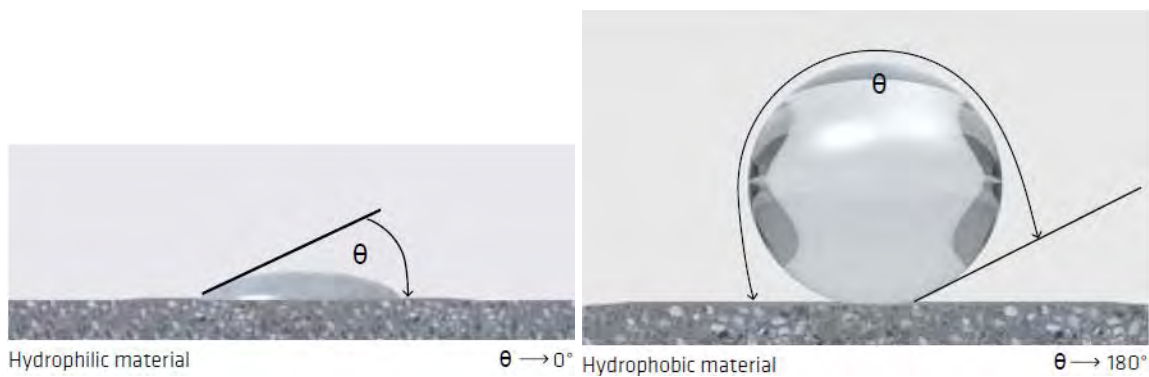


Figure 8: The principle of hydrophobization [70].

The main difference between the silane and the siloxane based agents is that the silane molecules have a smaller structure and lower viscosity, and thus the ability for deeper penetration into porous materials. Silane is also more volatile, and thus higher concentrations are used for achieving good results [71]. Siloxane is a more complex compound and thus larger molecules, decreasing the penetration depth, leaving the porous material more vulnerable if the external surface is damaged. Siloxane is less volatile, and lower concentrations can be used, with good results with regard to repelling water. The molecular structures of silane and siloxane are presented in Figure 9. In some cases, nanotechnology has been implemented in an attempt to improve the efficiency of hydrophobization agents.

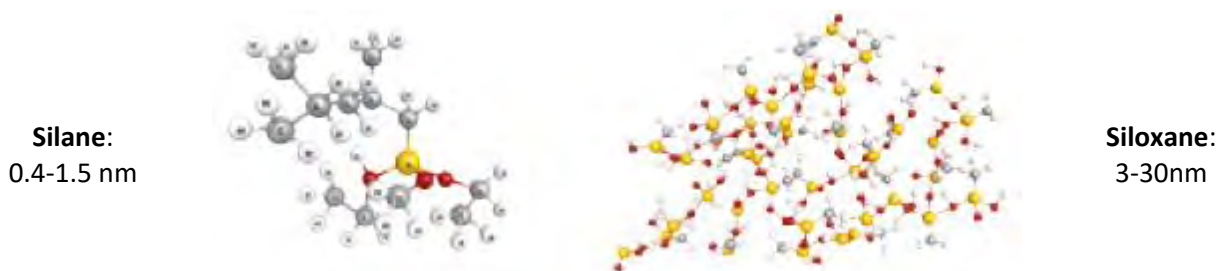


Figure 9: Molecular structure and size of silane (left) and siloxane (right) [70].

Some of the recent research includes investigations of the effect of external moisture loads on the hygrothermal performance of internally insulated walls, and the prevention or reduction of external water penetration, e.g. from wind-driven rain. Solar radiation can be a positive contributor to a wet façade by means of increased drying and reduced condensation potential, but it can also drive the moisture further into the construction [72].

A study by Guizzardi *et al.* from 2015 of masonry walls with severe wetting [73] yielded information about migration of external water loads through masonry. The experiment revealed that interfaces posed as hydraulic resistances/barriers, and that the moisture transport occurred faster in the fine pored bricks than in mortar joints. In contrast, van Hees found that the mortar joints were the weakest part of hydrophobized masonry [74]. He observed a difference in the efficiency of hydrophobization treatments on brick and mortar, yielding mortar joints a possible way for water ingress. Zhang *et al.* have investigated the efficiency of silane water repellent impregnation on cement based mortars and concrete [68], and found that the capillary suction was significantly reduced. Slapø *et al.* have found that fresh mortars with high water content improved masonry's resistance to WDR, as the mortar-brick interface becomes less porous [75]. Engel *et al.* [76] performed a study on water absorption, drying and vapour diffusion of hydrophobized brick specimens. They examined 5 silane based creams of different concentrations along with 2 fluid hybrid agents. They found significant water absorption reduction with no influence on the vapour diffusion resistance. Their drying experiment showed that specimens hydrophobized with agents of a lesser concentration of active ingredients dried faster, thus an impregnation should be applied with the lowest, effective concentration. An older study from 1995 by Charola [71] found a reduction of 5-10 % in water vapour permeability with silicone-based hydrophobization treatments. Couto *et al.* [77], who investigated silicone-based water-repellents on ceramic brick, also found a reduction in vapour permeability of hydrophobized brick specimens in some water-repellent treatments. Van Hees [74] found a limited effect of hydrophobization on vapour diffusion. However, he found the hydrophobization treatments to have a high impact on the drying process, as was also found by Couto *et al.* [77] for most investigated treatments. Lubelli *et al.* [78] tested the efficiency of two nano-coatings on bricks, and found significantly reduced water absorption, and little effect on the drying; however, the penetration depth was found to be much lower than traditional products. Finken *et al.* [30] found, through a study of hydrophobization based on several hygrothermal simulations, that hydrophobization has a positive impact on the hygrothermal conditions within an internally insulated façade. In the simulation, the entire wall became dryer, compared to unhydrophobized cases. Finally, Slapø *et al.* performed a large scale study on masonry panels with high pressure water loads for 5 hours. They found the tested water repellents to be ineffective to high pressure driving rain after a few minutes of water loads; this inefficiency was attributed the extreme testing conditions. Odgaard *et al.* found that hydrophobization had a positive effect on internally insulated walls during summer, however it impeded evaporation of interstitial condensation during winter periods [79].

2.4 Material parameters and characterization

Hygrothermal simulations are valuable tools in the design of a suitable interior insulation system, in both new constructions and retrofitting. Hygrothermal simulations take into account many specific variables for each case in question, e.g. climatic conditions, geometry and material parameters. Materials used in historic buildings are extremely varied, not only in the raw materials and resources used, but also in the production method. If it can be proven that certain material properties are decisive for the hygrothermal performance

and they can be determined feasibly with regard to both time and economic expenditures, it would be beneficial for future analysis of retrofit measures.

As there are numerous uncertainties in hygrothermal simulation, identification of potential discrepancies in material properties and boundary conditions were determined in a sensitivity analysis performed by Kloda [80]. The analysis concluded vital influence on output from parameters such as solar radiation absorption coefficient, thermal conductivity, suction curve, capillary conductivity and surface heat transfer coefficients. Biseniece *et al.* [81] also found material parameters to be vital input with regard to simulations, however they also found that initial conditions were even more influential. Probabilistic methods have previously been introduced by e.g. Zhao *et al.* [82] and Holm *et al.* [83], running 400 and 69 hygrothermal simulations respectively, for determination of the influence of material parameters and boundary conditions, and measurement uncertainties respectively. The findings of these measures were, among others, that the effect of single parameters may be seasonal, and can have positive, negative and/or seasonal-dependent correlations. The studies emphasize the need for full and exact material properties for achieving valid results. By means of statistical tools however, it may be possible to attain reliability ranges for results, and simplify the models by the clustering of materials. Moisture transport in porous media, e.g. building materials, is driven by material characteristics as well as external factors. Driving forces include gradients in partial vapour pressure, total air pressure and external total pressure, as well as gravity and pore width, defining the capillary suction [84]. Moisture transport in a material also depends on the moisture storage potential, which in turn is dependent on specific material characteristics; e.g. water retention curve relates to the porosity, effective and capillary saturation – depending on the hygroscopic range, and the function for liquid water conductivity depends on both effective saturation and the water uptake coefficient. Material functions are vital, as they describe properties at various conditions; therefore material functions are implemented in hygrothermal simulations together with constant material parameters. Some of the material parameters and functions are not directly measurable and therefore the process of determining the parameters also requires a calibration, either experimentally and/or numerically [85].

In hygrothermal simulations some material parameters are more decisive than others and some are interrelated. Unfortunately, some decisive parameters may be difficult to determine; if the interrelated parameters are easier to estimate, it might be possible to estimate the decisive parameters through simple tests. Some materials have similar pore systems e.g. most historic building materials have open pore systems, which means that density and open porosity are interrelated. Parameter studies are useful when determining which parameters are decisive, while determination of which parameters are interrelated can be done by making a statistical analysis on material parameters from materials where these are already known. The purpose of a statistical analysis is twofold:

- Determination of correlations between material parameters; in this way it will be possible to see which parameters can be estimated through other parameters that are easier to determine.
- Clustering of materials. Within groups of materials e.g. bricks there can be significant differences in hygrothermal properties. By defining decisive properties and analyzing how materials differ, it is possible to cluster specific materials in groups and create generic material representing the cluster.

The work of Zhao *et al.* [86] investigated different clustering techniques and methods for deriving a generic material from a cluster. They emphasized that it is important to find correlations between parameters first;

otherwise some parameters will have too much influence on the clustering. Generic materials can be used to overcome the problem of incomplete material data. Zhao *et al.* [87] have also developed a concept for the inclusion of input uncertainties and a stochastic material database for probabilistic simulation rather than deterministic. Including the probability distributions of material properties, it gives better estimations of the realism in achieved hygrothermal simulation results.

3 Methods for investigation of hypotheses

In this chapter, the methods implemented for the investigations of the various hypotheses in this research work are presented. The research has been presented in papers published in scientific journals, conferences and in reports. References to these publications (cf. list of publications on page 13) are used throughout the chapter.

3.1 Hygrothermal performance of internally insulated solid historic masonry

3.1.1 In situ measurements

In **Paper I**, long term in situ measurements of temperature and relative humidity were monitored in 4 historic case buildings for investigation of the performance of internal insulation on solid masonry. All the case buildings were multistory residential buildings in traditional Danish building style, solid masonry of 1½ brick (360 mm) thickness, and of historic date (1877-1932). The cases differ from each other in terms of orientation, height, location and external surface treatment. Two different types of internal insulation were applied to the four cases, and in 4 different thicknesses. The insulation systems included in the case studies, are elaborated in Table 2.

Table 2: Internal insulation systems applied to the case studies [1].

	Insulation material	Complete system	
System 1	Phenolic foam boards (Kingspan Kooltherm K17 insulated plasterboard) $\lambda=0.020\text{W/mK}$	Integrated in Kingspan K17 boards	Glue mortar (2-5mm notched trowel) Glass tissue Phenolic foam (25 or 60mm) Composite foil vapour barrier ($s_d \approx 24\text{m}$) 12.5 mm gypsum based plasterboard Skim coating (3mm) Paint
System 2	Polyurethane (PUR) foam with calcium silicate channels in a grid of 40X40mm (IQ-Therm) $\lambda=0.037\text{W/mK}$		IQ-Fix glue mortar (2-5mm notched trowel) IQ-Therm PUR foam (30 or 80mm) IQ-Top (porous light mortar) IQ-Tex (glass tissue) IQ-top (porous light mortar, 10-15mm total) IQ-Fill (fine putty) Diffusion open paint (e.g. IQ-Paint)

The applied insulation systems varied in thickness and in thermal conductivity. Estimations of the gained U-value reduction were made, based on the assumption of same brick type on a 1½ brick thick (360 mm) wall with internal rendering, and are displayed in Table 3 together with information about the location and the applied insulation system.

Table 3: Overview of case buildings and U-value estimations [1].

Case building	Year of construction	Floor + orientation	Ext surface	Insulation system (see Table 2) + thickness	Theoretical retrofitted U-value [W/m²K]	Theoretical U-value reduction [%]
1	1932	2 nd , East + South	Blank	2, 80mm	0.35	75
2	1877	5 th , South + Southwest	Blank	1, 60mm	0.27	81
3	1905	4 th , North	Render + paint	1, 25mm	0.50	64
4	1899	4 th , East	Blank	2, 30mm	0.65	53

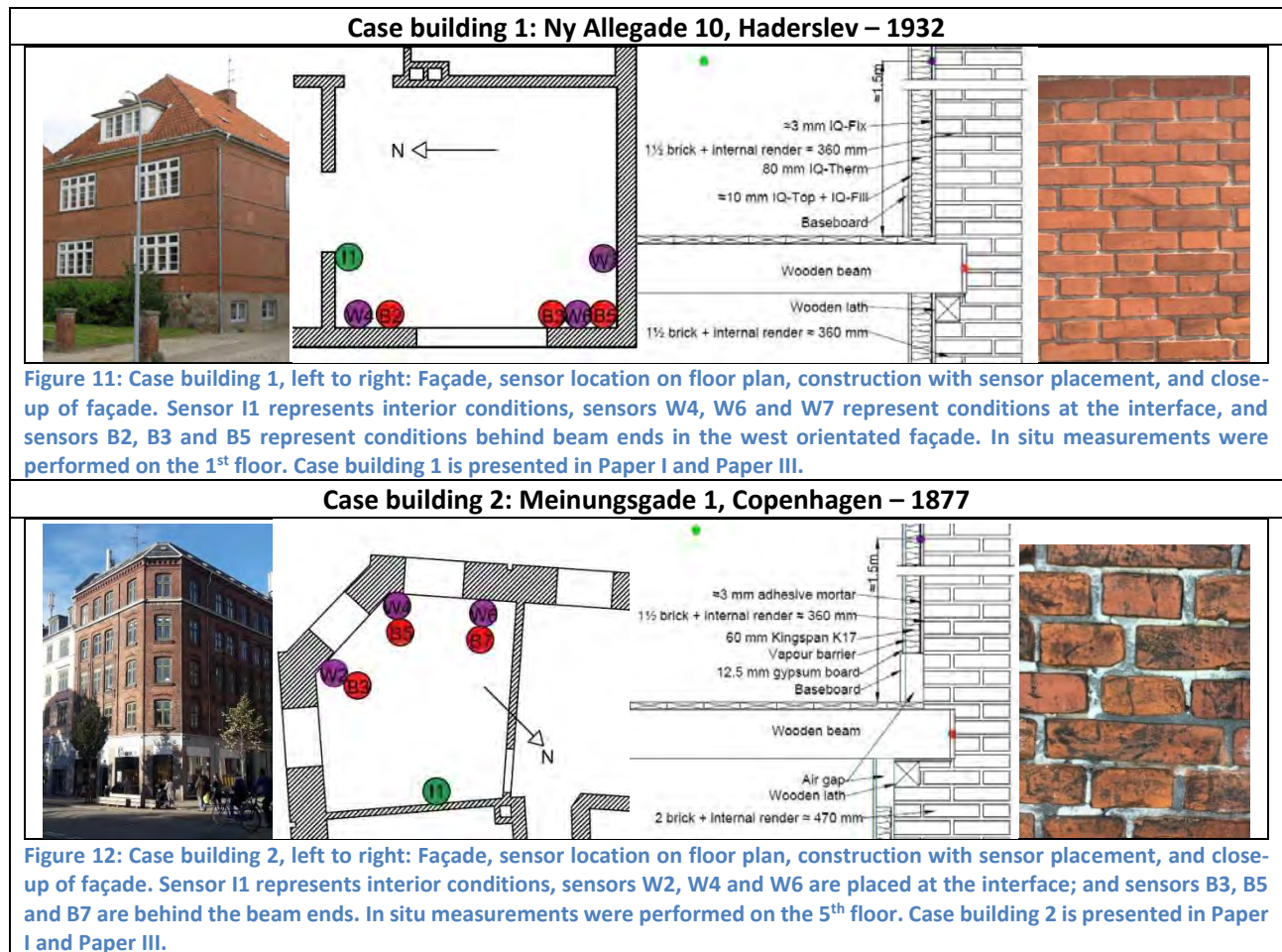
Temperature and relative humidity sensors (Rotronic HygroClip2) were installed at the interface between the existing wall and the insulation, and in ¾ of the cases, sensors were also installed behind the beam ends, as these are areas where potential moisture related risks occur. At the interface there is an increased risk of

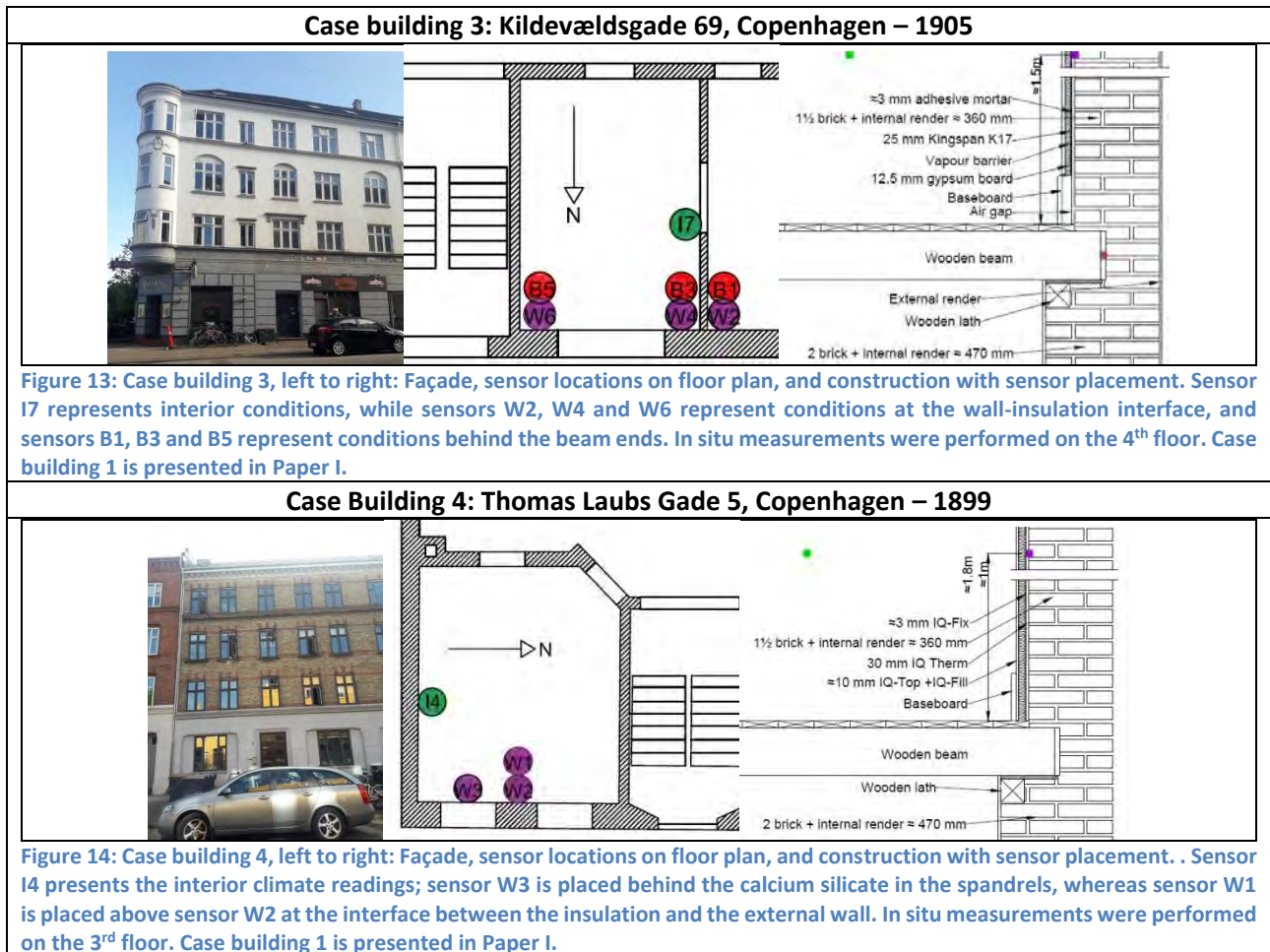
interstitial condensation, which yields the risk of e.g. mould growth. The risk of condensation and moisture accumulation is also present behind the beam ends. This area is also closer to the external conditions as the beam ends are embedded in the masonry. The beam ends in traditional Danish masonry buildings from this time period are of wood, and thus the risk of wood rot is present. The sensors were placed either in existing joints, or in purposely designed notches in the wall, drilled holes in the beam, and subsequently the holes were sealed with foam. Sensor locations are depicted in Figure 10.



Figure 10: Sensor locations, left to right: in existing joint, in man-made notch in existing wall, and sealed in behind beam end [1].

The cases used for in situ measurements are presented in Figure 11 - Figure 14.





A relative humidity of 85% is considered the minimum relative humidity for initiation of mould growth during long term exposure for medium resistant materials, e.g. concrete and glass wool [39], which is why this is considered the threshold value for performance success in the present work.

3.1.2 Hygrothermal simulations

Dynamic, hygrothermal simulations have been implemented several times in the presented research. All the models were created in the numerical simulation program Delphin 5.8, that can simulate coupled heat, moisture, air, pollutant, and salt transport through porous building materials [64,88]. For this research, hygrothermal 1D Delphin models have been used for studying the effect of surface treatments (**Paper V**), investigation of influential material parameters (**Paper IV**), and final simulations were made based on the constructions in the 4 monitored case studies introduced in Figure 11-Figure 14. As in situ measurements were performed in these cases, hygrothermal models could be validated with the monitored data, and the models were thus used for forecasting the hygrothermal behavior of the constructions as well as the hygrothermal response to variations such as insulation thickness, insulation system, and external render (**Paper I**). As mainly 1D modelling is performed in this work, all models were built up as homogenous layers of a certain thickness.

In **Paper I**, hygrothermal simulations were initially used for validation of models of the 4 cases, and subsequently these models were used for predictions of hygrothermal conditions with model variations and 10 years' future climate. None of the material properties for the existing constructions were known; however

the properties for the two insulation systems were both tested and validated at the Technische Universität Dresden, and therefore assumed to be of high quality. As it is not clear whether moisture travels primarily in lime mortar joints, or through bricks, and due to the indefinite material properties of the existing constructions, the initial modelling was performed in 2D on constructions of both brick and lime mortar, with material data from the Delphin material database. A simplified 1D model with lime mortar yielded better results with regard to the measured conditions this is why the subsequent 1D models were based on lime mortar construction, as is apparent in Figure 15. The output from the simulation models was defined as average temperature and relative humidity for a spectrum of 3 elements corresponding to 2.5 mm in the masonry at the interface. This should represent the sensor locations.



Figure 15: 1-dimensional simulation models (Delphin) for the four case studies. Discretization causes the formation of layer thicknesses not being representative in the images. Output locations are marked with a red dot.

In the case of insulation system 1 (phenolic foam with integrated vapour barrier), two models of each case were simulated with varying vapour diffusion resistance factor of the phenolic foam, and varying s_d -value of the integrated vapour barrier, as explained in section 5.1. The material parameters implemented in the models of the four case studies, can be seen in

Table 4. Two years of local climate data (March 2015-March 2017) was gathered from Copenhagen (case buildings 2-4) and Haderslev (case building 1) by means of data from the Danish Meteorological Institute, and implemented in the models. Interior climate was monitored in all the cases, and implemented in the models.

Table 4: Material parameters utilized in the hygrothermal simulations of the 4 cases presented in section 3.1.1.

	Dry density ρ [kg/m ³]	Thermal conductivity λ [W/mK]	Water uptake coefficient A_w [kg/m ² s ^{1/2}]	Water vapour diffusion resistance factor μ [-]	S_d -value [m]
External render	1570	0.7	0.18	11	
Existing wall	1800	0.82	0.13	12	
Adhesive/glue mortar - system 1	830	0.16	0.0031	13	
Adhesive/ glue mortar - system 2	1313	0.50	0.0051	19	
Insulation material – system 1	35	0.020	$8 \cdot 10^{-6}$	dif. tight: 583 dif. open: 1	
Insulation material – system 2	49	0.037	0.013	27	
Vapour barrier (system 1)					$S_{d,dif. open}: 0.5$ $S_{d,dif. tight}: 100$
Top layer – system 1	850	0.2	0.28	10	
Top layer – system 2	1269	0.48	0.22	14	

Subsequent to the model validations, future predictions were modelled in order to evaluate the long term performance and different variations of insulation systems. In these models, the interior climate was set constant to 22 °C and 55 % relative humidity, and 10 years of forecasted weather in the time frame 2020-2050 in Øster-Ulslev in Denmark was used as exterior climate and gathered from the EU project, Climate for Culture [89] and implemented in the models. The variations of the constructions in the simulations are presented in Table 5.

Table 5: Simulated variations of each case.

	1. Ny Allegade	2. Meinungsgade	3. Kildevældsgade	4. Thomas Laubs Gade
Original	No render 80mm system 2	No render 60mm system 1	Paint + render 25mm system 1	No render 30mm system 2
Variation 1 Thickness	No render 30mm system 2	No render 30mm system 1	Paint + render 60mm system 1	No render 80mm system 2
Variation 2 Render	Paint + render 80mm system 2	Paint + render 60mm system 1	No render 25mm system 1	Paint +render 30mm system 2
Variation 3 Insulation system	No render 80mm system 1	No render 60mm system 2	Paint + render 30mm system 2	No render 30mm system 1

In order to estimate the influence of wind-driven rain on the hygrothermal performance of internally insulated solid historic masonry, simulations with variations in the rain exposure coefficient (0.0, 0.4, and 1.0) were also performed. These models took their basis in the validated model of case building 2 from **Paper I**, and the work is presented in **Paper III**.

3.2 Quantification and effect of wind-driven rain

The study of wind-driven rain and its effect on hygrothermal conditions in internally insulated masonry was investigated by means of in situ WDR measurements on case buildings 1 and 2, presented in section 3.1.1, and presented in **Paper III**. In this work, a semi-empirical model for WDR deposition was also implemented. The water migration through masonry was further investigated in a large-scale laboratory experiment in **Paper II**.

3.2.1 Quantification of wind-driven rain

For experimental quantification of wind-driven rain, special wind-driven rain gauges were designed and produced based on extensive literature review. The developed wind-driven rain gauges were first introduced

in the final technical report for the EUDP project Energy Efficient Comfort in Older Apartment Blocks [9]. The gauges were installed on case buildings 1 and 2 in June 2016. The results from the WDR gauge measurements were presented in **Paper III**.

The wind-driven rain gauge designed for the experiment was based on existing types, experience and comparative tests. It was based on the gauges manufactured at K.U. Leuven's Laboratory for Building Physics, with some alterations according to recommendations found in the literature. The area of the collection plate was 300x300 mm, with a 10 mm raised rim around all the edges. The raised rim caught splashing water to some extent [65], and prevented collection of water from outside the collection area [59,90]. The plate was constructed of acrylic glass (PMMA), which had shown better performance and fewer errors due to water adhesion/evaporation in comparison with teflon (PTFE) [13]. The wind-driven rain was monitored by a HOBO Rain Gauge (Metric) Data logger, which was a closed tipping bucket rain gauge that minimized the evaporation losses from the reservoir. The data logger was fixed to the collection plate, and the water drained directly into the HOBO. The HOBO had a diameter of approximately $\varnothing 15$ cm, which meant that the collector plate was extended out slightly from the wall surface. The wind-driven rain gauge is illustrated in Figure 16. The gauge is also described in [9,79]. It was set to monitor rain events, and calibrated prior to use. The calibration showed that one counted rain event corresponded to 3.78 ml and 3.72 ml for case buildings 1 and 2 respectively.

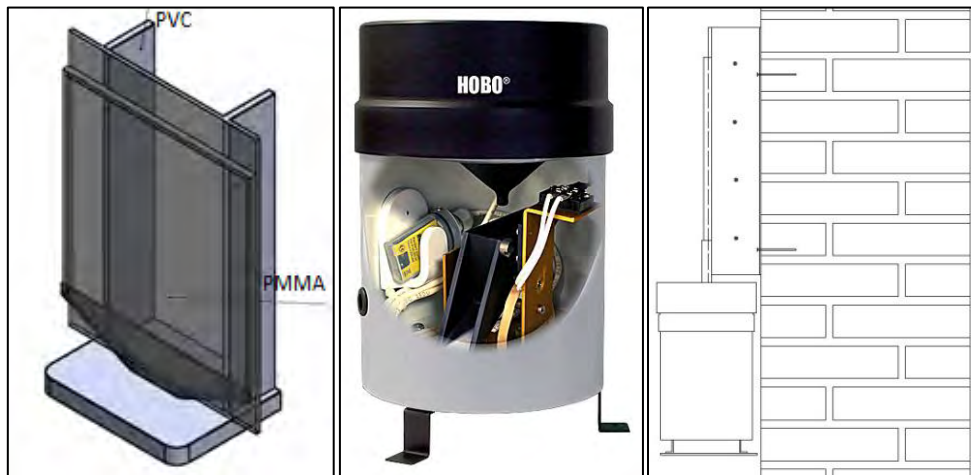


Figure 16: Wall-mounted WDR gauge with HOBO logger. Left: 3D illustration by LINATEX A/S, who assisted with the PMMA construction. Middle: HOBO Rain Gauge (Metric) Data Logger RG3-M (<http://www.onsetcomp.com/products/data-loggers/rg3-m>). Right: shows fixation and extension from surface due to the gauge below.

On case building 1, the WDR gauge was located on the west façade at the 2nd floor height. This façade was facing the street. The distance to the closest neighbor in this direction was approximately 20 m and there were no large trees or other obstructions in the immediate vicinity. On case building 2, the gauge was mounted on the southwest façade, at the 5th floor height. This façade faces a large cemetery, so no buildings or obstructions in the direct vicinity were expected to influence the WDR measurements. In both cases, the gauges were placed near windows with the intention of easier access for data collection and battery changes. Figure 17 depicts the WDR gauges mounted on the 2 case buildings.



Figure 17: Installation of WDR gauge. Top: Case building 1. Bottom: Case building 2.

The WDR deposition was also estimated by means of the semi-empirical model, Equation 3, described in section 2.2. In this case, the rain admittance function was set to 0.2, in accordance with Figure 6, as for buildings with a roof overhang.

3.2.2 Effect of wind-driven rain

In situ measurements of the hygrothermal conditions in the wall-insulation interface and behind beam ends were compared to the registered wind-driven rain loads in **Paper III**. Hygrothermal simulation models were also performed in **Paper III** on validated models from **Paper I** to estimate the importance of wind-driven rain, by alterations in the rain exposure coefficient.

In **Paper II**, a largescale experiment of water migration in masonry is presented. As hydrophobization was applied to some of the masonry sections, the experiment also shed light on the effect of hydrophobization with regard to moisture response. In the following paragraphs, the experiment will be presented in brief. The scope was to monitor the moisture response of internally insulated solid masonry with imitated climatic loads applied to the external surface. In order to imitate the dynamics and the varying nature of the natural climate, a cyclic exposure was designed. The cycles consisted of 30 minutes of rain load, 2 hours of radiation load, and 21½ hours of cold climate. This 24 hour cycle was repeated 5 times. The experiment was conducted on nine 1½ brick thick solid masonry wall sections of 330x348mm² built into the doors of 3 refrigerators, as seen in Figure 18. To ensure adiabatic boundaries, each wall section was surrounded by a vapour barrier tightly taped to the perimeter. Furthermore, the boundaries of the wall surface were sealed with silicone to prevent water penetration through small airgaps at the perimeter. Sensors for the registration of temperature and relative humidity were placed in the vertical middle of the masonry sections, and at the depths seen in Figure 18.

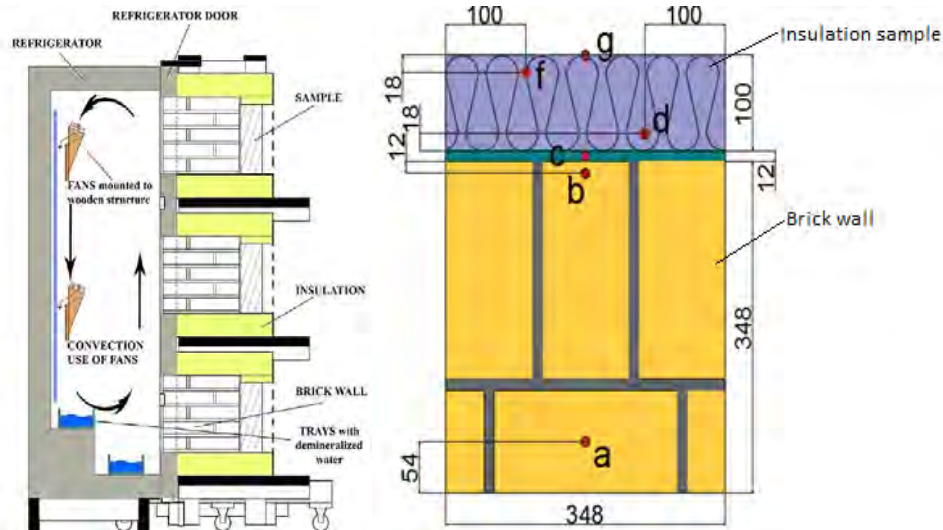


Figure 18: Left: Diagram of the experimental setup with the cooling chamber from Sandholdt *et al.* [91]. Right: Construction of each wall section, and sensor location [91]. Dimensions are stated in [mm]. Sensor locations are denoted a, b, c, d, f, and g.

Table 6 displays the setup of each wall section, with insulation types, as well as whether or not hydrophobization was applied. In the table it is seen that each wall section is denoted with 1.1-1.3, 2.1-2.3, and 3.1-3.3, depending on the refrigerator door, and the height. Furthermore, the table states which sensor locations were in use for each wall section.

Table 6: Overview of wall sections; 1) insulation sample type, 2) with/without hydrophobization, 3) internal surface treatment, 4) sensors used in this wall section. Placements of the sensors are shown in Figure 18.

1.1 Foam concrete Hydrophobization Internal: Diffusion open paint Placement of sensors: a, b, c, d, f	2.1 Insulation type: PUR with CaSi channels Hydrophobization Internal: No treatment Placement of sensors: a, b, c, g	3.1 Insulation type: ACC No hydrophobization Internal: Diffusion open paint Placement of sensors: a, b, c, d, f
1.2 Insulation type: No insulation (ref) No hydrophobization Internal: No paint (ref) Placement of sensors: a, b, c	2.2 Insulation type: Foam concrete No hydrophobization Diffusion open paint Placement of sensors: a, b, c, d, f	3.2 Insulation type: ACC Hydrophobization Internal: Diffusion open paint Placement of sensors: a, b, c, d, f
1.3 Insulation type: Foam concrete Hydrophobization Internal: Ordinary paint Placement of sensors: a, b, c, d, f	2.3 Insulation type: Foam concrete No hydrophobization Internal: Ordinary paint Placement of sensors: a, b, c, d, f	3.3 Insulation type: PUR with CaSi channels No hydrophobization Internal: No treatment Placement of sensors: a, b, c, g

The climatic conditions applied to the wall sections were chosen to be rather severe. The rain loads were of 0.08-0.11 l/min, corresponding to a severe cloudburst by Danish meteorological standards [92]. The radiation loads were provided with Osram ULTRA-VITALUX 300W bulbs, that provide radiation similar to natural sunlight, and are also used in climate simulators for accelerated aging [93]. The bulbs were set at a distance of 20 cm from the wall surfaces, yielding an average black panel temperature of 78.1 °C. The subsequent cold climate was provided by the refrigerators, where the temperature was set to regulate at 3 °C. The relative humidity was kept high at 80-85 %, by the placement of open water baths within the refrigerators. The conditions in the refrigerator were kept steady and stratification was avoided by mounting four fans inside each refrigerator for constant air circulation. The experimental setup is presented in Figure 19.



Figure 19: Experimental setup. A: 3 wall sections mounted in a refrigerator door. B: water loads applied horizontally to the top of the wall section, by perforated pipe. C: view of water loads applied to 3 wall sections. D: radiation loads on 3 wall sections.

The effect of wind-driven rain was also studied in **Paper III**, by comparison of in situ measured hygrothermal conditions in the wall-insulation interface and behind beam ends to in situ measurements of wind-driven rain. In case building 1 and case building 2, presented in section 3.1.1, wind-driven rain gauges were installed and the effect of wind-driven rain studied.

3.3 Effect of hydrophobization

The effect of hydrophobization of historic masonry was investigated experimentally in both the large scale experiment presented above, and through an investigation of a variety of agents, active components, and concentrations, and the effect of these on both ceramic brick and lime mortar was presented in **Paper II**. For the initial part of the study, 16 different hydrophobization agents were tested on brick and lime mortar for the effect on both water uptake and drying. The penetration depth was registered as well. These initial investigations were performed to get an overview of the efficiency and differences in the types of agents.

Furthermore, the effect of hydrophobization on the water vapour permeability of both brick and lime mortar was established. In a separate study, shown in **Paper V**, the effect of surface treatments, hydrophobization and render were investigated experimentally and with dynamic hygrothermal simulations. The active components and concentrations of the included hydrophobization agents are listed in Table 7, along with the associated experiments.

Table 7: Hydrophobization agents that were included in the investigation of the effect on ceramic brick and lime mortar.

	Active component (concentration)	Experiments
A	Siloxane and Fluoro Polymer (16%)	Water uptake, drying, penetration
B	Copolymers (16%)	Water uptake, drying, penetration
C	Various fluoric polymers (16%)	Water uptake, drying, penetration
D	Silane, siloxane and Fluoro Polymer (16%)	Water uptake, drying, penetration
E	Silane/siloxane (16%)	Water uptake, drying, penetration
F	Siloxane copolymers and pefluorinated siloxane (16%)	Water uptake, drying, penetration
G	Nanoparticle dispersion, isopropanol solvent (<13%wt)	Water uptake, drying, penetration
H	Nanoparticle dispersion, isopropanol solvent (<3%wt)	Water uptake, drying, penetration
I	Silane (80%)	Water uptake, drying, penetration
J	Silane (40%)	Water uptake, drying, penetration, vapour diffusion, large-scale, surface treatment
K	Unknown	Water uptake, drying, penetration
L	Chlorophyllane	Water uptake, drying, penetration
M	Flour-Acryl-Polymer and Alkyl-Acoxy Silane	Water uptake, drying, penetration
N	Alkylalcoxysilane	Water uptake, drying, penetration, vapour diffusion
O	Silane >20%	Water uptake, drying, penetration
P	Silane/siloxane (100%)	Water uptake, drying, penetration, vapour diffusion
Q	Reference	Water uptake, drying, penetration, vapour diffusion, large-scale, surface treatment

The hydrophobization agents were applied to the specimens by different methods. For the initial investigation of water uptake, drying and penetration depth, the specimens were shaken in a bag with the liquid agents for 10 seconds. For the vapour diffusion experiments, the liquid agents were sprayed on the surface of the specimens in specified amounts. For all the investigations including the creamy agents, it was applied with a paint brush in specified amounts. All test specimens were oven-dried and conditioned in room conditions prior to hydrophobization, which was minimum 14 days prior to experimental execution. The bricks used for experiments were yellow soft molded bricks from Helligsø Teglværk (1643 kg/m^3 , $0.39 \text{ m}^3/\text{m}^3$). Lime mortar specimens were of 3 different types. Specimens of 7.7 % air lime mortar with 0-4 mm aggregates (1243 kg/m^3 , $0.53 \text{ m}^3/\text{m}^3$) were used for the diffusion experiments and the large scale experiment. For the investigation of water uptake, drying and penetration depth, two unspecified lime mortars were used (A-J: 1881 kg/m^3 , $0.26 \text{ m}^3/\text{m}^3$, K-Q: 1941 kg/m^3 , $0.28 \text{ m}^3/\text{m}^3$). All lime mortar specimens were carbonated before experimentation.

3.3.1 Laboratory experiments

Laboratory experiments were conducted in order to identify the material parameter alterations and the magnitude of these alterations, in connection to surface treatments of brick and lime mortar. The changes in certain parameters with the application of e.g. hydrophobization provide vital information for simulations and the hygrothermal performance of internally insulated masonry. A variety of experiments were performed.

With regard to quantification of water uptake, 3 methods were applied. In **Paper II** full immersion tests were reported, while in **Paper V** partial immersion and Karsten tubes were used. In Figure 20 these experimental methods are depicted. Elaborated descriptions of experimental methods and related calculations can be found in the dissemination items referenced. Karsten tubes were also used for evaluation of the façade conditions in case buildings 1 and 2 disseminated in **Paper III**. The study of influence on vapour diffusion, **Paper II**, was investigated by wet cup tests, and the drying tests performed in a climate chamber. Images from various experiments are seen in Figure 20 and Figure 21.

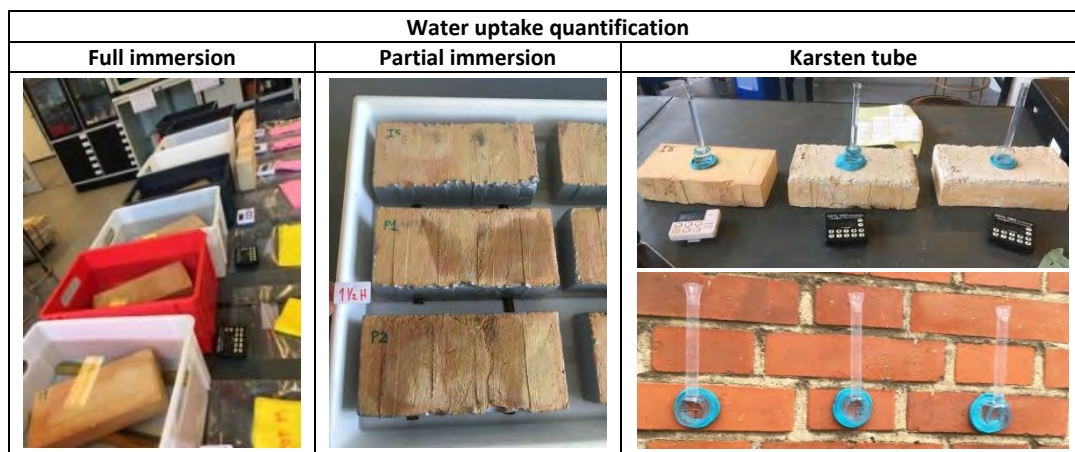


Figure 20: Various experimental setups for determination of water uptake and the effect of hydrophobization. Full immersion (left), partial immersion (middle), and Karsten tube (right) performed in both laboratory on horizontal plane (top), and in situ on a vertical plane (bottom).

For full immersion experiments, specimens were completely submerged in water, and the mass registrations at various time intervals were transformed into mass % increase, and plotted in a diagram over time; thus the absorption of each specimen over time could be studied graphically. In partial immersion experiments,

the specimens were partly submerged in water, and the sides were sealed with epoxy. The mass difference between successive weighings were plotted as a function of the square root of time, and the water absorption coefficient was calculated based on the graphical representations. A Karsten tube is a method for non-destructive testing for porous façade materials. It was used to estimate water absorption of masonry façades and test specimens, for comparative purposes. By means of a method described by Hendrickx [94], estimations of the sorptivity and capillary saturated volume can be made.

In the case of in situ measurements for **Paper III**, the Karsten tube measurements were performed on 3 randomly selected bricks on case buildings 1 and 2, and furthermore on 3 joints in case building 1. The measurements of the joints were performed where mortar is dominant in the tube area, where head and bed joints meet. The test was performed for comparison of the two types of masonry, and to give an indication of relative resistance to wind-driven rain.

The effect of hydrophobization on the permeability of ceramic brick and lime mortar specimens were determined by means of wet cup experiments (DS/EN ISO 12572) and presented in **Paper II**. The principle purpose of the experiment was to determine the amount of vapour diffusion through a specimen due to differential vapour pressure differences on both sides of the specimen, see Figure 21. By daily mass registrations, the rate of water vapour transmission in steady state can be determined, and further transformed into water vapour diffusion resistance factor, μ .

The drying experiment presented in **Paper II** was conducted on hydrophobized specimens subsequent to full immersion water uptake experiments. The specimens were vacuum saturated by means of vacuum desiccators prior to initiating the drying experiment. The specimens were placed on triangular spacers in a climate chamber, seen in Figure 21, of approximately 20°C and 85% relative humidity to dry. The measurements were transformed into moisture content, which is illustrated graphically in the results as a function of time.

The penetration depth of hydrophobization is not in itself a criterion for effectiveness; however, a higher penetration depth may yield higher protection from e.g. frost damage in the case of cracks or other damage to the surface. Different types of active components, viscosity, and application methods in connection with the properties of specimens it is applied to, has an influence on the penetration depth. In **Paper II**, the penetration depth of the 16 different hydrophobization agents was determined by halving the specimens with chisel and hammer, and spraying the broken side with water. Thus, the penetration depth of the various agents became visible, as seen in Figure 21. The average penetration depth is presented in results.



Figure 21: Experimental setups for; vapour diffusion: the principles of the cup setup, drying experiment: brick and mortar specimens in climate chamber, and penetration depth: example of visible penetration depth

The effects of the experimentation of hydrophobization of historic masonry, namely tests of water uptake (full immersion), drying and penetration depth, were evaluated by a simple ranking system. The ranking system was implemented as a very simplified means for interpreting the various results in the complex field. Penetration depth was ranked according to percentage of half the specimen's thickness, and specimens with full penetration were thus given a score of 100%. The water uptake was ranked by the final mass % increase by the end of the experiment, as a percentage relative to the mass increase found in the reference specimen. The drying was ranked by the percentage difference between the initial slopes of the drying graph for each treatment relative to the reference specimen. The final ranking score was the sum of the 3 scores for the 3 categories, and a higher score yielded an overall better performance of this agent. A combined score for brick and mortar consists of the sum of the final score for each material. The formulas used for the ranking system, can be seen below in equations 4-8;

$$1) \text{ Penetration depth} \quad \frac{\frac{\text{registered penetration depth}}{\text{specimen thickness}}}{2} \cdot 100 \quad [\%] \quad \text{Eq. 4}$$

$$2) \text{ Water uptake} \quad \frac{\text{mass increase}_{\text{reference}} - \text{mass increase}_{\text{specimen}}}{\text{mass increase}_{\text{reference}}} \cdot 100 \quad [\%] \quad \text{Eq. 5}$$

$$2a) \text{ Mass increase} \quad \frac{\text{mass}_{\text{end}} - \text{mass}_{\text{initial}}}{\text{mass}_{\text{initial}}} \cdot 100 \quad [\%] \quad \text{Eq. 6}$$

$$3) \text{ Drying} \quad \frac{\text{initial slope}_{\text{reference}} - \text{initial slope}_{\text{specimen}}}{\text{initial slope}_{\text{reference}}} \cdot 100 \quad [\%] \quad \text{Eq. 7}$$

$$3a) \text{ Initial slope}^* \quad \frac{y_2 - y_1}{x_2 - x_1} \quad [-] \quad \text{Eq. 8}$$

*The initial slope is calculated based on values from timestep 0 ($x_1=0$) to timestep 4020 minutes ($x_2=4020$) for brick and 2700 minutes ($x_2=2700$) for lime mortar

3.3.2 Hygrothermal simulations

In **Paper V**, hygrothermal simulations were performed in an attempt to clarify the long term effects of hydrophobization at different depths and on various brick types. Surface treatments of both hydrophobization and a lime plaster render were examined. All material parameters were found in the Delphin database, with the exception of one brick type, yellow brick, which was generated partly based on a Delphin material (Historical Brick (cluster 4)), and partly on experimentally obtained values [91]. The simulations were performed on 4 different brick types, with the same geometry (228 mm thick). Hydrophobization was applied to the external 5 mm of the brick, by reducing the water uptake coefficient by factor 15, as found experimentally with Karsten tubes. External render was applied in a 10 mm layer on the

brick. Output locations for results - temperature and relative humidity - are displayed in Figure 22; on the external surface, 50 mm from the brick surface, the middle of the brick and the internal surface.

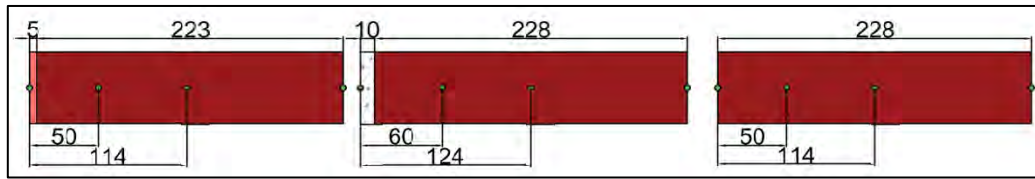


Figure 22: Geometries for the modelling investigation of surface treatments and indication of output locations (green dots). Left: brick with hydrophobization, middle: brick with render, right: reference brick.

The boundary conditions were constructed from a constant internal climate of 20 °C and 50 % RH, and the external climate was designed from a Danish Reference Year. In order to achieve maximum moisture loads, the orientation was set to southwest, the most exposed orientation in Denmark, and the rain exposure coefficient was set to 1. The simulations were run for a 2 year period, and results from the latter were used for further evaluation.

3.4 Material parameters and characterization

As the hygrothermal simulations could potentially be vital for the modelling of hygrothermal conditions and the identification of associated risks, **Paper IV** investigated the most influential material parameters with regard to moisture transport through brick, and possible correlations between these. The presented work had a focus on historic masonry buildings, and associated material parameters. It may be possible to determine or estimate some parameters in situ and non-destructively, but if these are insignificant it may be purposeless. Naturally some material parameters are associated, e.g. porosity and density. Correlations between material parameters were studied statistically in **Paper VI** [6].

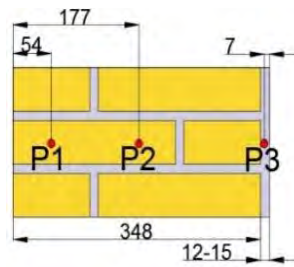
3.4.1 Influential material parameters with regard to hygrothermal conditions

In **Paper IV**, 1D simulation models for planar horizontal moisture transport were made and validated with measured data from an experimental setup at the Technical University of Denmark [79,95], with temperature and relative humidity sensors built into the construction. The models were made of a reference wall without internal insulation. The wall consisted of merely 348 mm brick and 12-15 mm internal render, see Figure 23. The external side faces southwest, and the external climate was measured on site by a local DTU weather station, and 1 year of climate data was implemented in the model- with cyclic repetition for an extra year. The results from the latter were evaluated. The interior climate was set to be constant at 20 °C and 60%, as the interior conditions in the experimental setup. For the initial investigation of the importance of various single basic material parameters, models with ± 10 % values were made for the following brick parameters: density, open porosity, thermal conductivity, water uptake coefficient, and water vapour diffusion resistance factor. For the partial investigation of the correlations between brick material parameters, additional simulations were performed on two types of brick from the Delphin material database with a large difference in density and a significant difference in most of the other parameters as well. The basic material parameters and the alterations can be found in Table 8.

Table 8: Material parameter variations, and materials for correlation investigation.

	Yellow, softmolded brick			High density Brick Bernhard	Low density Brick Schlagmann	Unit
	Original	-10%	+10%			
Density, ρ	1713	1542	1884	2060	1396	kg/m ³
Open porosity, θ_{por}	0.38	0.34	0.41	0.25	0.47	m ³ /m ³
Thermal conductivity, λ	0.52	0.47	0.57	1	0.27	W/mK
Water uptake coefficient, A_w	0.2	0.18	0.22	0.10	0.44	kg/m ² s ^{1/2}
Water vapour diffusion resistance factor, μ	25	22.5	27.5	19	14	-

The simulations were performed with three output locations for both temperature and relative humidity- at the same locations as where sensors were placed in the experimental setup: point 1: 54 mm and point 2: 177 mm from the external side, and point 3: in the internal render layer, as seen in Figure 23.

**Figure 23: Measuring locations for validation of hygrothermal simulation model.**

3.4.2 Statistical investigation of material parameter correlation

The parameters of historic building materials are very often unknown, and there is an interest in the development of methods for determination, or at least estimation or clustering of the historic brick and mortars, for the purpose of building more reliable hygrothermal simulation models. As it may be possible to determine some material parameters in situ and non-destructively, methods for correlating these to other parameters become of interest. In an introductory study with the statistical platform R, the correlations between 5 material parameters in brick were investigated. The investigation was based on material parameters from 63 brick types, found in the Delphin material database. The 5 variables included in the investigation are: density, open porosity, thermal conductivity, water uptake coefficient, and water vapour diffusion resistance factor. These parameters were included in the study, as they are assumed to be the most influential single material parameters, without considering material functions like sorption isotherms. These material parameters were also investigated in the parameter study described in section 3.4.1. A basic description of the analyzed data can be found in Table 9;

Table 9: Summary of data for the statistical analysis of correlations

	Density, ρ [kg/m ³]	Open porosity [m ³ /m ³]	Water uptake coefficient [kg/m ² s ^{1/2}]	Thermal conductivity, λ [W/mK]	Water vapour diffusion resistance factor, μ [-]
Denomination	RHO	POR	AW	LAM	MEW
Min.	1300	0.227	0.006	0.266	6.84
1 st quantile	1700	0.295	0.088	0.551	11.00
Median	1773	0.330	0.177	0.700	17.05
Mean	1769	0.327	0.178	0.704	20.21
3 rd quantile	1868	0.354	0.243	0.810	24.52
Max.	2060	0.474	0.489	1.012	46.21
Std. dev	159.69	0.051	0.113	0.173	11.52

By means of principal component analysis (PCA) and simple linear regression, possible correlations were investigated. The investigation was introduced with the thought of correlations yielding the possibility of material parameter estimation, based on a few, easy-to-get material properties.

4 Results and discussion

In this chapter, the results from the various research performed with regard to the four main topics, are presented together with partial discussions.

4.1 Hygrothermal performance of internally insulated solid historic masonry

The hygrothermal conditions in interior insulated constructions were monitored in situ, and in addition, dynamic simulation models were validated and used for future predictions as well as for construction variations, all presented in **Paper I**.

4.1.1 In situ measurements

Measurements are presented as hourly averages generated from minutely data. The general observed tendencies of the measurements show that insulation system 2 yields unacceptably high relative humidities, whereas insulation system 1 performs successfully.

The relative humidities obtained from measurements in case building 1 are portrayed in Figure 24. With the exception of sensor B2, the relative humidities at both wall interfaces and cavities behind the beam ends are above 95 % during the measurement period with no indication of significantly reduced relative humidity. It is a known fact that built-in moisture, due to the installation of internal insulation takes time to dry out, but after the 1st year the installation moisture from the glue mortar can be considered of no significance [96].

The relative humidity measurements gathered from case building 3 are displayed in Figure 25. The initial building moisture and successive drying out period were very apparent. In the first 6 months, the relative humidity was very high in the wall interface, and hereafter a seasonal dependency was apparent, but the relative humidity did not exceed 80 %.

Measured relative humidities from case buildings 2 and 4 are presented in the appended **Paper I**. Measurements from case building 2 show that the relative humidity rarely exceeds 80% at the wall interfaces. The integrated vapour barrier seems to inhibit drying inwardly when the masonry becomes moist. Sensor W6 was located in southwest orientation and by an indentation in the façade, making the wall thinner, thus the penetration of wind-driven rain may reach closer to the sensor. The same case applies for conditions at beam ends, as the external wall is thinner here, thus leaving the area behind beam ends more exposed to external conditions such as penetrating wind-driven rain. The intentional thermal bridges do not seem to have the desired effect; the temperature behind the beam ends is the same, or less than, the temperature at the wall interfaces, as can be seen in the temperature measurements presented in **Paper I**. The relative humidity measured in case building 4 is very high initially, due to installing the insulation with a wet glue mortar. A decline of the relative humidity is seen during the 20 months of measuring, however, the relative humidity still exceeds 80 %.

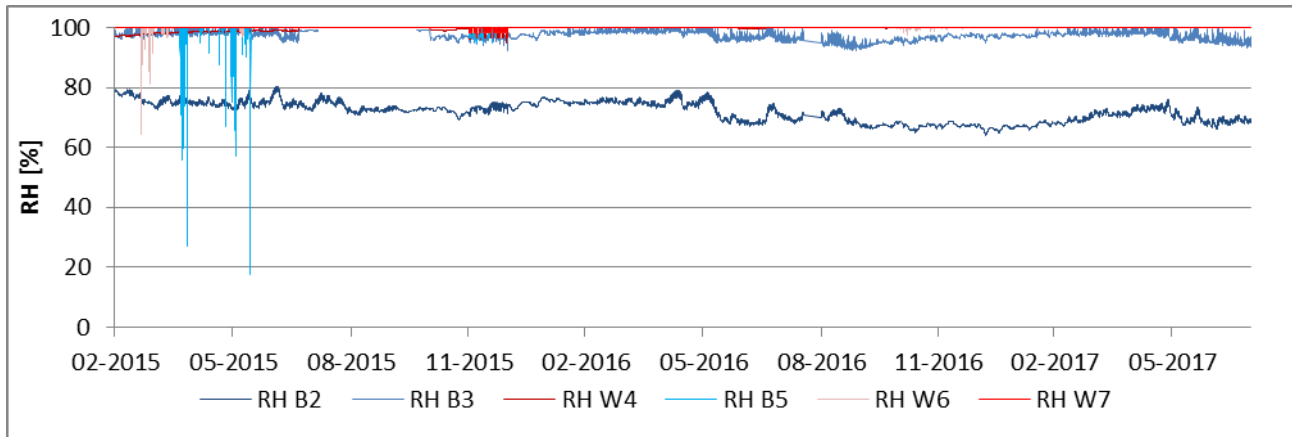


Figure 24: Measured relative humidities from case building 1 (80 mm system 2, western (W4, W6, B2, B3, B5) and southern (W7) façade. The blue nuances represent sensors behind beam ends, whereas the red colors represent sensors at the wall-insulation interface.

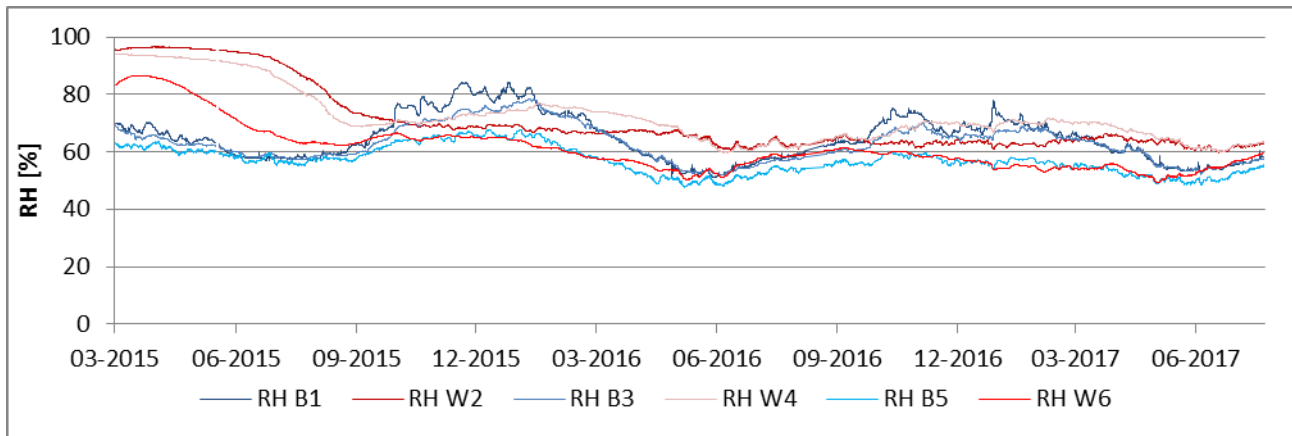


Figure 25: Measured relative humidities from case building 3 (25 mm system 1, northern façade. The blue nuances represent sensors behind beam ends, whereas the red colors represent sensors at the wall-insulation interface.

4.1.2 Damage models for performance assessment

The assessment of the hygrothermal performance of the post insulated façades with damage models (Mould Index and Wood Decay) are presented graphically in Figure 26 and Figure 27. The data from case building 4 is unfortunately insufficient for generation of mould and decay models due of the large data gaps.

Due to basic alkaline conditions in the cementitious glue mortar at the interface, it was assumed that mould growth was prevented for the first year of measurements. Therefore these data have been excluded in the model calculations [96]. The calculated mould indexes are presented in Figure 26. It is seen that in case building 1, the measurements in all sensors yielded mould indexes above 1, thus the theoretical risk of mould growth existed and the conditions can be considered unacceptable. In case building 2 mould growth was only initiated for measurements at sensor W6, where the mould index never exceeded 1, not even with the uncertainty factor of +5% for $RH > 90\%$ included. In case building 3 there was no indication of risk of mould growth for any of the measured data.

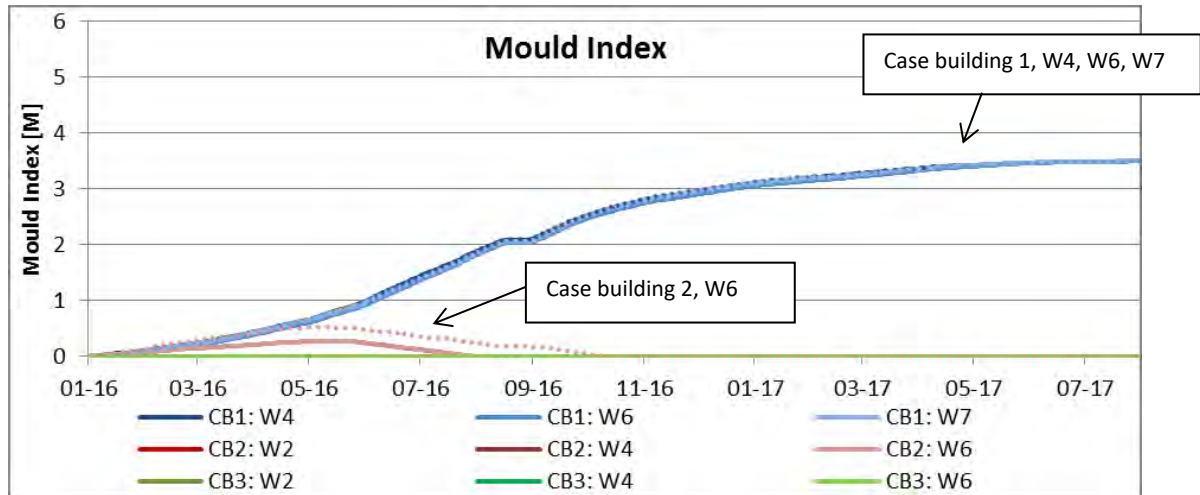


Figure 26: Mould Index for wall-insulation interfaces as a function of time. CB: Case Building. Dashed lines represent measurements with 5% added relative humidity on measurements above 90% RH due to uncertainties.

The calculated mass loss due to the wood decay model is graphically illustrated in Figure 27. A tremendous wood decay is seen in case building 1, where more than 100 % mass loss occurred in the beam, B5, providing an equilibrium between the beam end and the gap behind it, where the measurements were performed. A similar laboratory study with measurements in beam ends and wooden lath, has shown, significantly lower relative humidity in the wooden beam compared to the lath, indicating the inward transport of moisture through the beam end in the fiber direction [79], and thus further reason for evaluating the results with caution. The other case buildings showed no risk of wood decay based on measurements and the theoretical model. No visual inspection of case building 1 and the beams were performed, but the house is inhabited and no signs of this deterioration have become a concern. Thus the model was assessed to be too conservative.

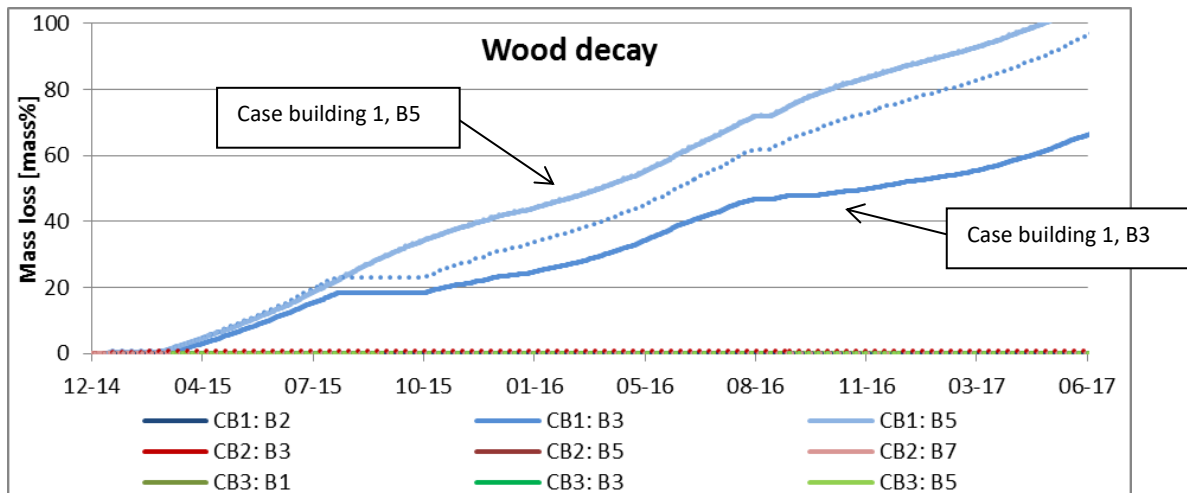


Figure 27: Wood decay (mass loss in percent) behind beam ends, as a function of time. Dashed lines represent measurements with 5% added relative humidity on measurements above 90% RH due to uncertainties.

4.1.3 Hygrothermal simulations

Hygrothermal modelling was made for the purpose validating the reliability of predictions of hygrothermal conditions and risk of mould growth in internally insulated historic buildings, and was presented in **Paper I**. Initially models were created and validated towards the in situ measured data.

The quality of simulation results depends highly on the input variables, and there are numerous unknown parameters estimated in the performed simulations. The following projections of hygrothermal performance were based on validated models, the validation results and average measurements are portrayed in Figure 28. For the two cases of insulation with system 1 (phenolic foam with integrated vapour barrier), case buildings 2 and 3, good validation results were achieved by implementation of a model with significantly decreased S_d -value for the vapour barrier ($S_d=0.5$ m) and reduced water vapour diffusion resistance factor of the phenolic foam ($\mu=1.0$). The vapour barrier was discontinued at the bottom gap as well as in the joints, and screws were placed through the boards. A notched trowel was used for the glue mortar, thus the plates were not fully bonded and yielded the possibility of diffusion in air pockets at the interface. By alterations of the vapour diffusion resistance the validations were achieved. In general modelled relative humidity appears higher than measured, so the models present results that are on the safe side when it comes to moisture risks. The same tendency was found by Hamid *et al.* [37].

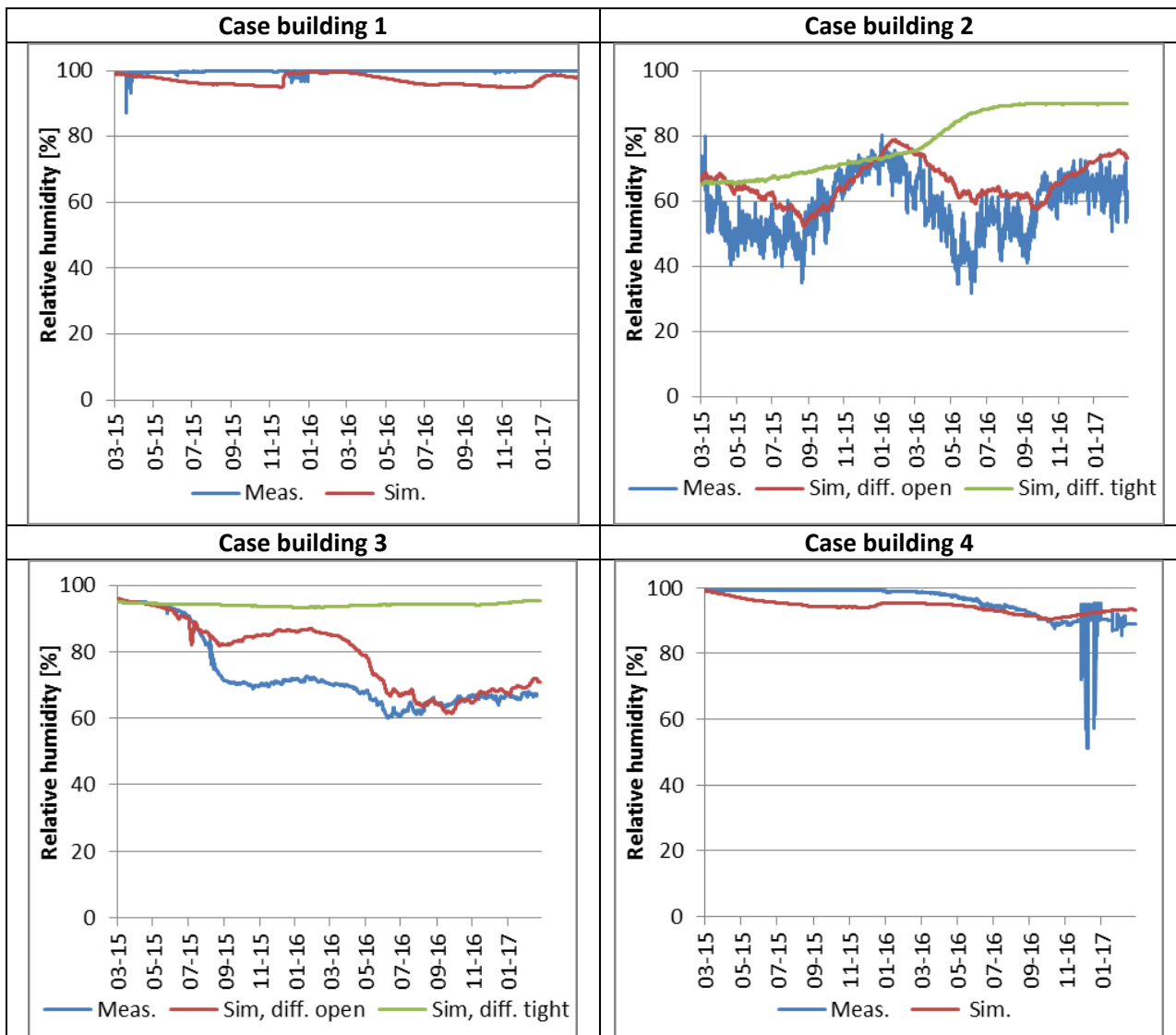


Figure 28: Validated models for the four case buildings. Blue lines represent average in situ measurements. Red and green lines represent simulation results. In case building 2 and 3, the red lines represent simulations made diffusion open, and green lines represent simulations performed diffusion tight.

10 year predictions for each case are represented in Figure 29. All cases show unacceptable hygrothermal conditions ($RH > 85\%$) for the duration of the 10 years of simulations. The worst moisture conditions appear to be in winter periods for the cases of insulation system 2 and diffusion tight system 1. The diffusion open version of system 1 exhibits significantly more seasonal variations and only unacceptable conditions during winter periods.

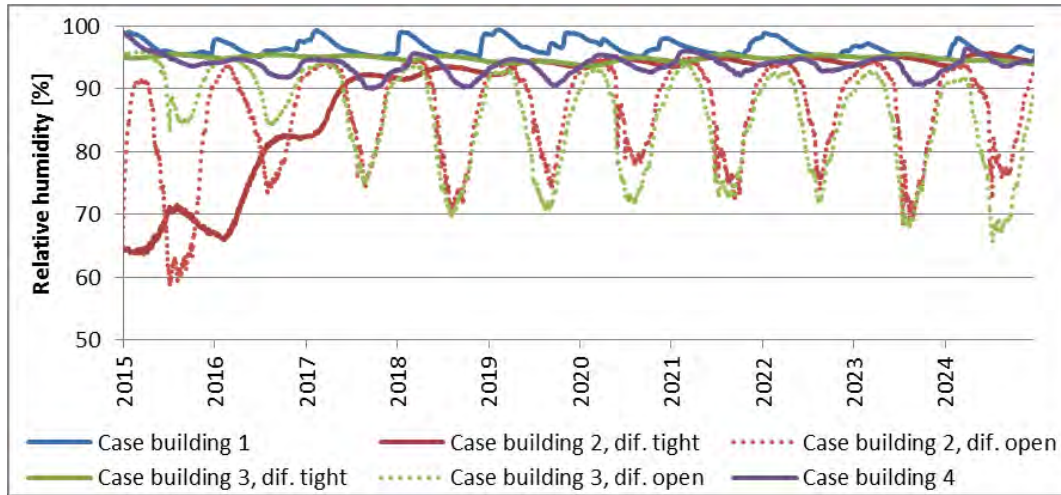


Figure 29: 1-dimensional simulations for 10 years of each presented case at the wall-insulation interfaces. The dotted lines represent the diffusion open version of insulation system 1.

In Figure 30 and Figure 31, the results from the parameter variations are presented for each case. In each case, the original model is presented in blue, the thickness variation in red, the external surface with/without render in green, and finally, the variation between the insulation systems is depicted in purple. Case building 3 with insulation system 2 rather than system 1, is the only case that exhibits a tendency of reduced relative humidity during the 10 year period. For the cases of insulation system 1 (case buildings 2 and 3), it is apparent that the diffusion open version yields better hygrothermal conditions at the interface.

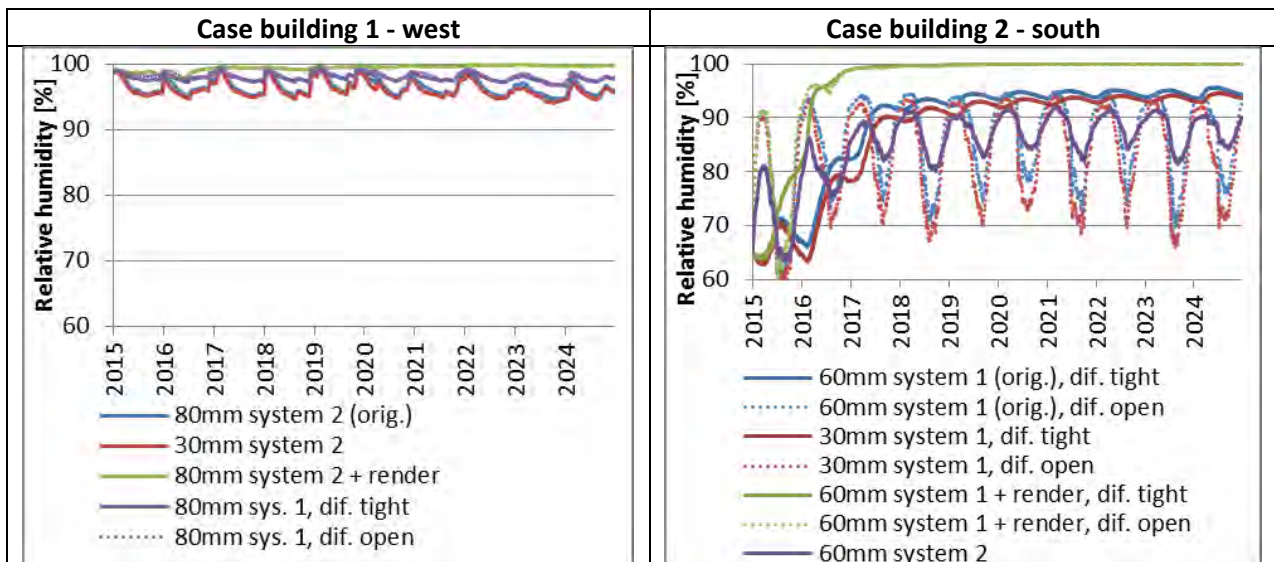


Figure 30: 10 year simulation variations of insulation thickness, external surface (with/without render) and insulation system for case buildings 1 and 2.

Case building 3 – north	Case building 4 - east
-------------------------	------------------------

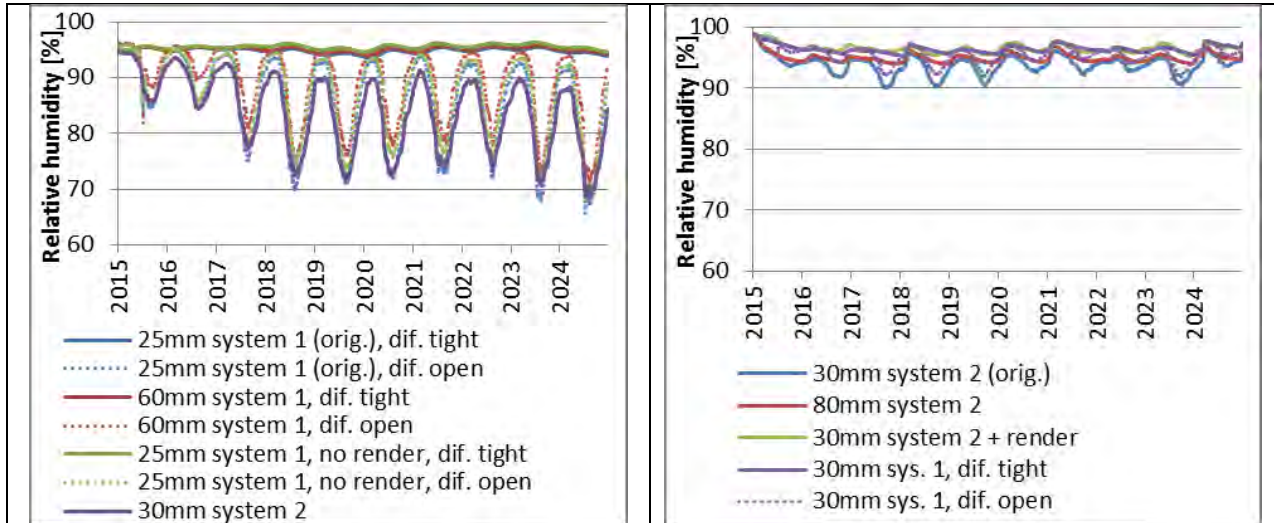


Figure 31: 10 year simulation variations of insulation thickness, external surface (with/without render) and insulation system for case buildings 3 and 4.

The mould indexes for the four 10-year simulations are illustrated in Figure 32 and Figure 33. In case buildings 1 and 4 the mould index quickly reached a steady maximum value of 3.3 and 3 respectively, for all the variations implemented, and thereby presented a moderate risk of visual findings of mould growth. These two cases had continuously high relative humidities and minimal seasonal variation, thus leading to optimal mould growth criteria. The risk of mould growth was significantly less in case buildings 2 and 3, when insulation system 2 is applied to these cases. The reduction of insulation thickness yielded a slightly reduced mould index, which can be expected. It is also seen that the diffusion open version of insulation system 1 yielded more seasonal variation, and in general a lower risk of mould growth in the long run.

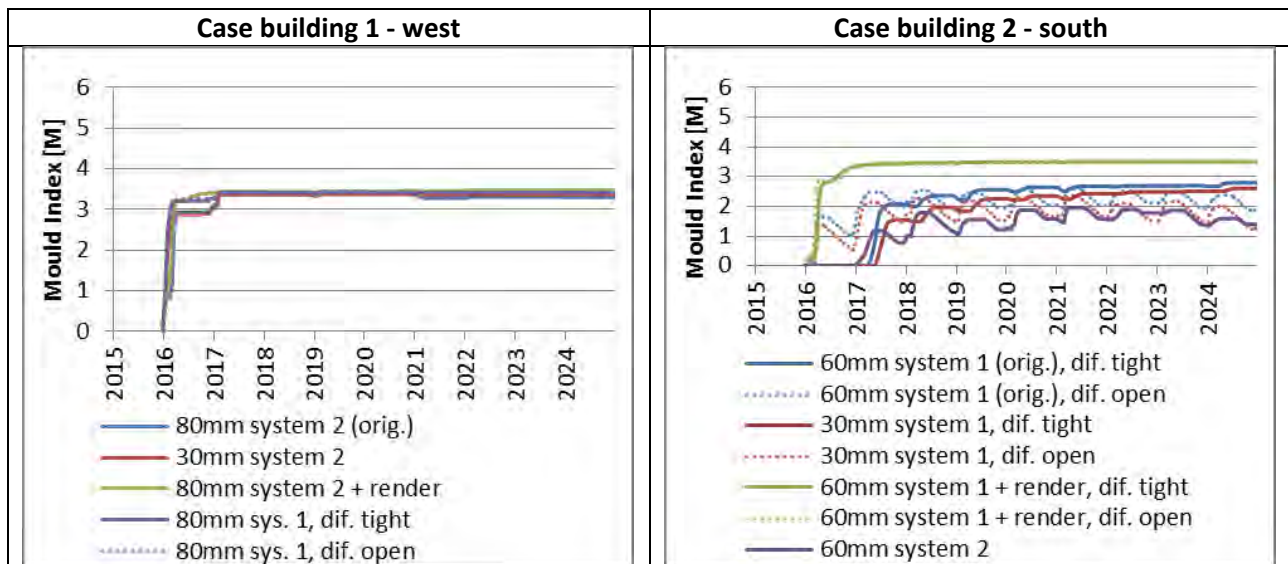


Figure 32: Generated Mould Indexes for simulated variations of insulation thickness, external surface and insulation system for case building 1 and 2.

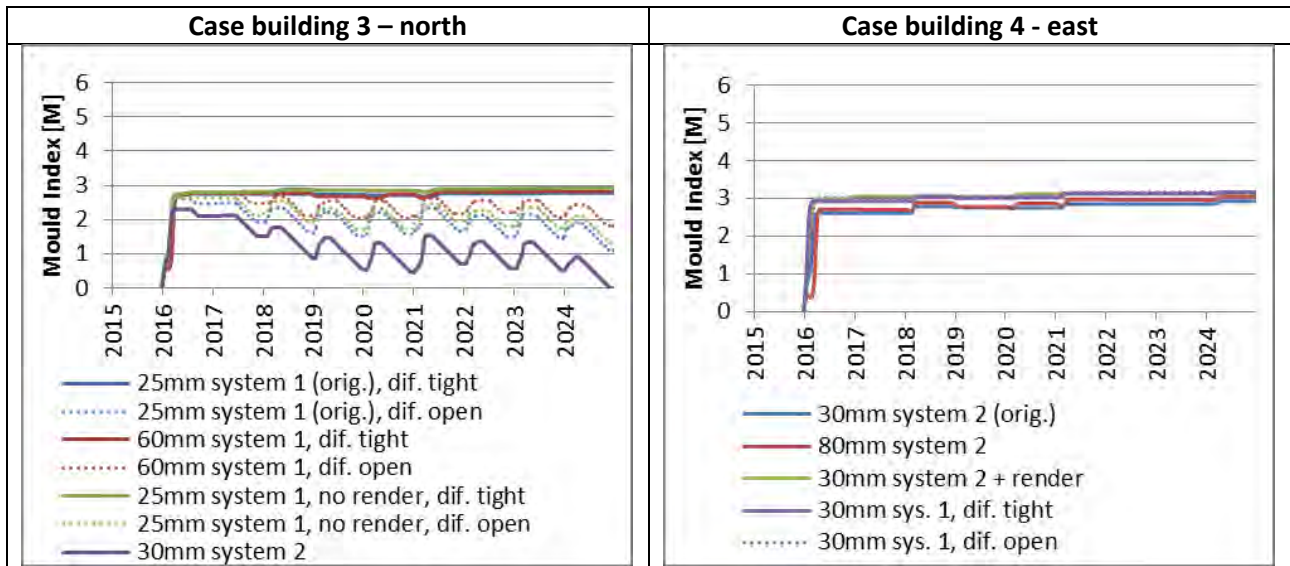


Figure 33: Generated Mould Indexes for simulated variations of insulation thickness, external surface and insulation system for case building 3 and 4.

The impact of the parameter variations on the hygrothermal performance of the studied cases can be summarized as follows: that increasing internal insulation thickness, choosing a vapour tight insulation system, and application of external render results in higher relative humidity in the interface between internal insulation and the original wall. Results from hygrothermal simulations however, should be considered cautiously; as seen, they can present the relative effect of the different variations.

4.2 Quantification and effect of wind-driven rain

Quantification of wind-driven rain deposition was investigated through in situ measurements with a wind-driven rain gauge, and compared to a semi-empirical model developed for wind-driven rain deposition in **Paper III**. Also, the effect of wind-driven rain on the hygrothermal conditions within the internally insulated masonry was studied. In addition, the effect of wind-driven rain on masonry was studied in a large-scale experiment, presented in **Paper II**.

4.2.1 Quantification of wind-driven rain

The wind registrations from the two locations distinctly illustrate the dominant wind direction being from the southwest in both cases. Figure 34 depicts the wind direction with red lines indicating the spectra of which the respective façade would be hit by wind-driven rain.

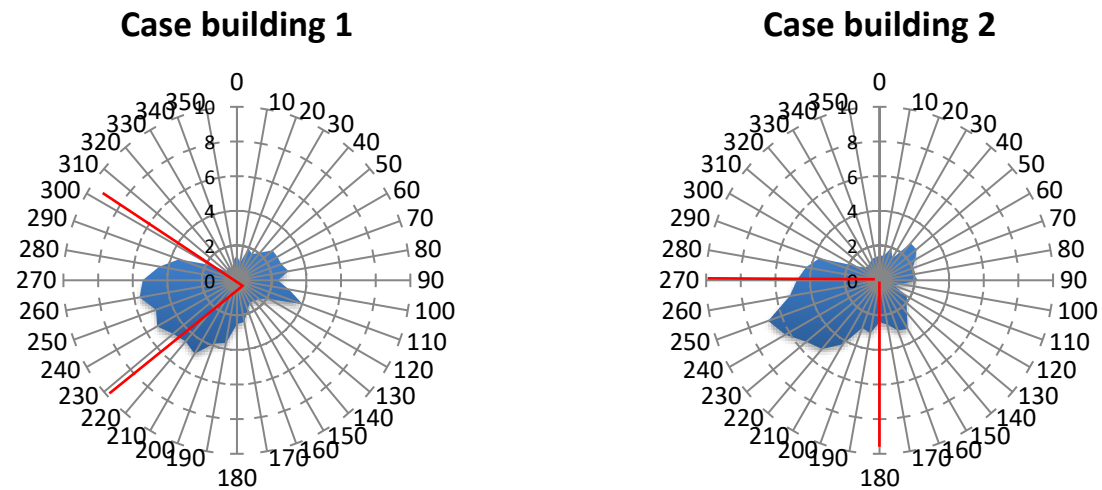


Figure 34: Diagrams of wind direction for the two areas. The outer axis represents the wind direction, 0-360°, and the inner axis represents the percentage of registered wind in 10° intervals. The red lines indicate the spectra of which the respective walls would be hit by WDR.

Calculations of deposited wind-driven rain were performed on the basis of Eq. 3 in section 2.2. Results of cumulative wind-driven rain calculations can be seen in Figure 35, along with cumulative measured wind-driven rain. Wind-driven rain was measured in event counts, and calibrated against the found amount of rain per event, and furthermore corrected to be $l \text{ pr. m}^2$. As seen in the graphs, the lengths of the test periods for the two buildings differed, as well as the time frame for wind-driven rain measurements, and the theoretical wind-driven rain deposition based on climate data. In case building 2 the climate measurements ran slightly longer than the wind-driven rain measuring period, and for case building 1, the wind-driven rain measurements were about a year longer than the climate measurements.

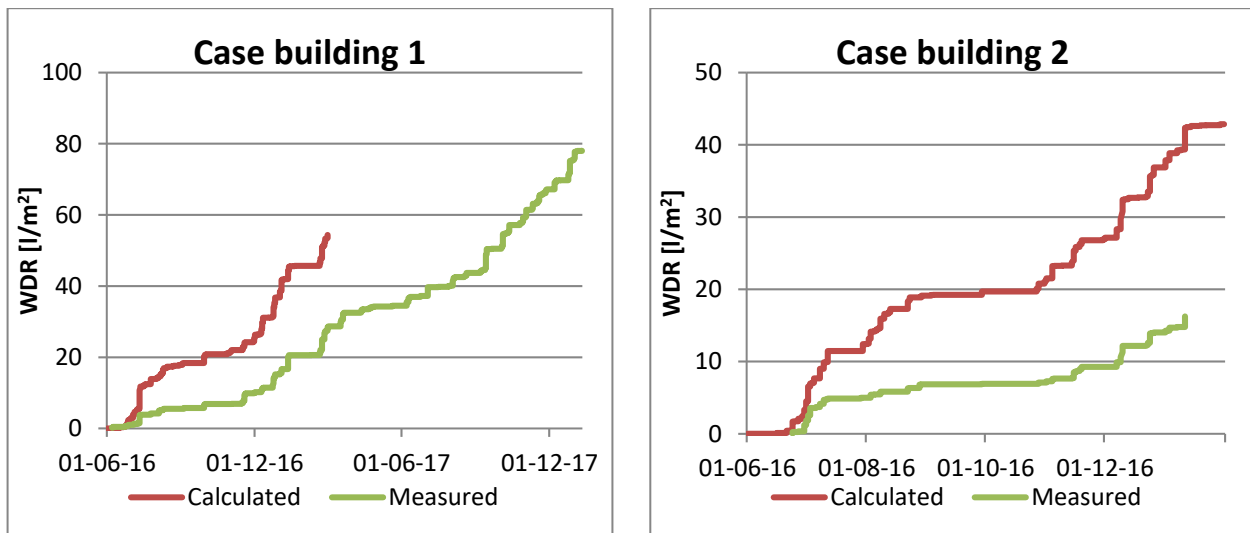


Figure 35: Calculated and measured WDR deposition per m^2 facade for the two case buildings.

As seen in Figure 35, the measured wind-driven rain did not correspond to the theoretically calculated wind-driven rain based on climate measurements. In fact, the theoretical calculations yielded significantly higher results of deposited wind-driven rain. Some of the discrepancies, however, may be explained by the sources of error connected with the wind-driven rain gauge, e.g. adhesion, evaporation and splashing, which were

not accounted for in the theoretical calculations [62]. Nath *et al.* [97] performed a study where they similarly found the semi-empirical model to overestimate WDR up to three times the measured values; the locations and orientations also influenced their results.

4.2.2 Effect of wind-driven rain

The results of hygrothermal measurements in internally insulated solid masonry are presented in **Paper III** together with the in situ measurements of wind-driven rain.

As most of the relative humidity measurements from test building 1, Figure 36, were in the range of 98-100% for the duration of the measurements, it is unfortunately not possible to identify any shifts in connection with monitored wind-driven rain. There seems to be no indication of significant wind-driven rain influence on the measurements behind the beam ends.

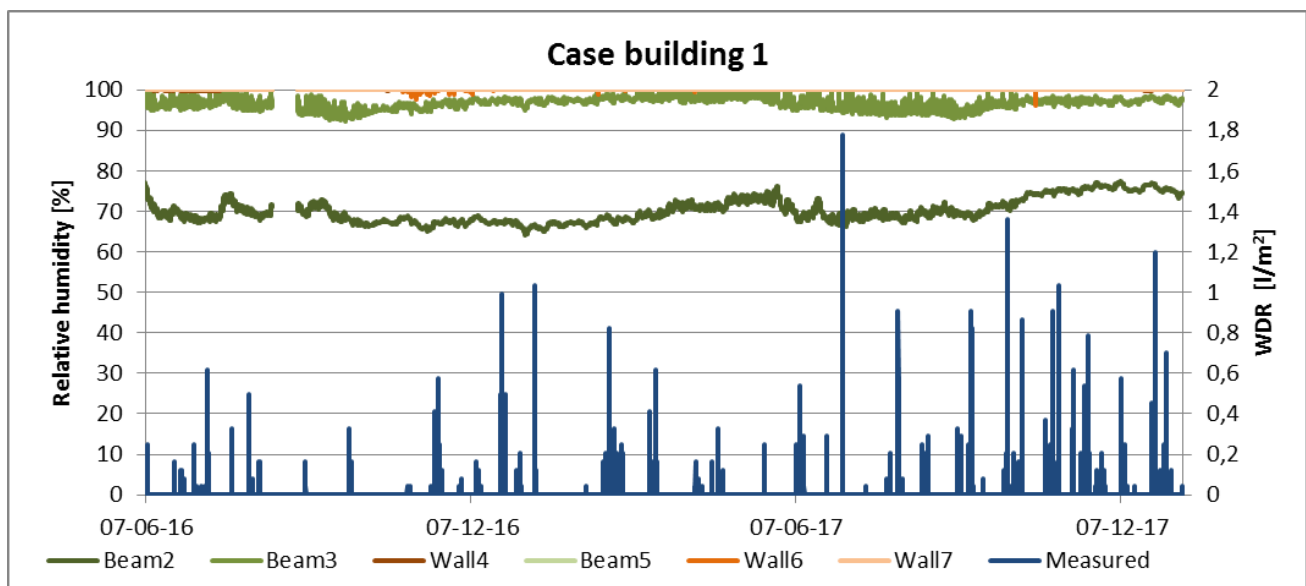


Figure 36: In situ measurements of relative humidity and wind-driven rain for case building 1. Wind-driven rain is portrayed in dark blue, relative humidity in orange colors represent wall-insulation interfaces, and green nuances represent conditions behind beam ends.

Case building 2, Figure 37, also does not give any clear answers as to whether wind-driven rain has a direct impact on the hygrothermal conditions in the wall or behind beam ends. E.g. at the end of September 2016, the relative humidity increased without the occurrence of significant rain events, and the wall interfaces' measurements did peak subsequent to a rainy spell in the beginning of August 2016. The results indicated that in the case of wind-driven rain being influential on the hygrothermal conditions within a masonry wall, there would be a delay. This delay would vary, and likely be dependent upon other climate conditions such as solar radiation, cloud cover and temperature.

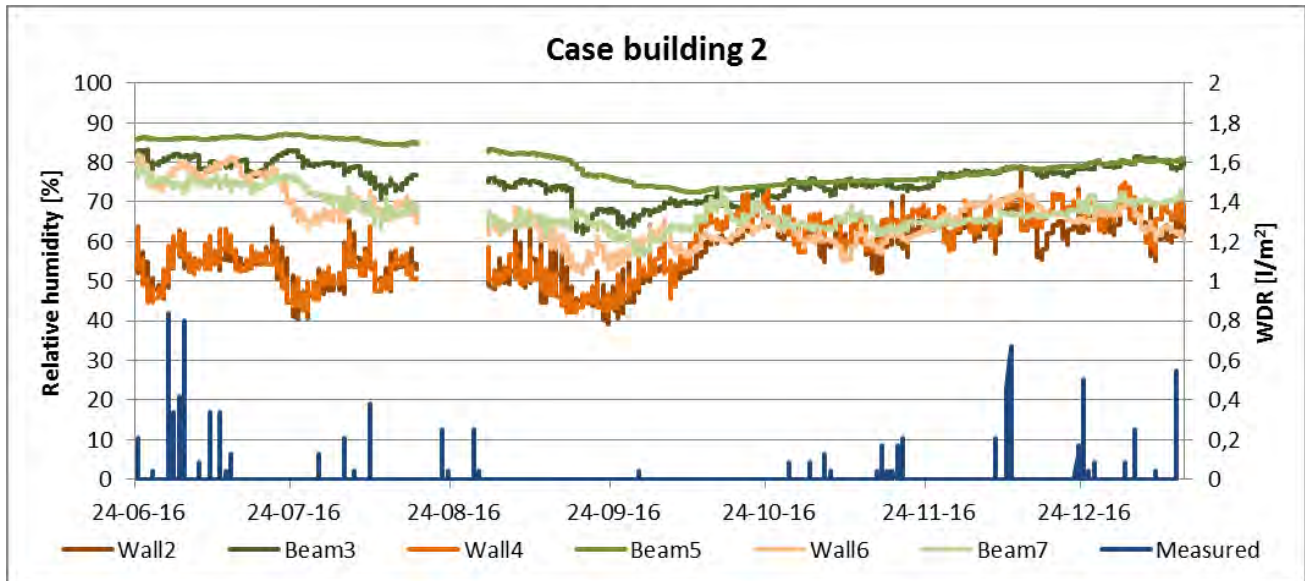


Figure 37: In situ measurements of relative humidity and wind-driven rain for case building 2. Wind-driven rain is portrayed in dark blue, relative humidity in orange colors represent wall-insulation interfaces, and green nuances represent conditions behind beam ends.

In both test buildings, the results could be interpreted in favor of some peaks during summer being due to delayed wind-driven rain penetration; but the results were inconclusive. The delay of water penetration to the interface is likely influenced by solar radiation, cracks and evaporation rates, and the time it takes for wind-driven rain penetration of 1 or 1½ brick thick masonry is unknown. Theoretically, if there was a continuous reservoir of water on the façade and perfect contact with the façade and throughout the façade, the penetration of 350 mm of masonry (of yellow soft molded brick with $A_w = 0.2782 \text{ kg/m}^2\text{s}^{1/2}$, $\rho = 1643 \text{ kg/m}^3$ and $\theta_{\text{cap}} = 0.275 \text{ m}^3/\text{m}^3$) would take about 33 hours. According to a partial immersion experiment performed with the same brick in another study [34], water penetration of 54 mm occurred after 1 hour in yellow soft molded brick types with full water contact. At this rate, a 1½ brick thick construction would be penetrated in less than 7 hours of full water contact.

In the results from hygrothermal simulations, absolute humidity, rather than relative humidity, is presented in Figure 38 to create a better overview of the events. The variety in the rain admittance function indeed illustrated the effect of wind-driven rain. It was seen, that a RAF of 1 and 0.4 in fact generated very similar results, and the result for RAF 0 lies below RAF 1 and 0.4, and tends to follow the external climate conditions. As seen in the models, the effect of WDR appeared larger than the one measured with the wind-driven rain gauge, which confirms the overestimations found in semi-empirical models and numerical models [62].

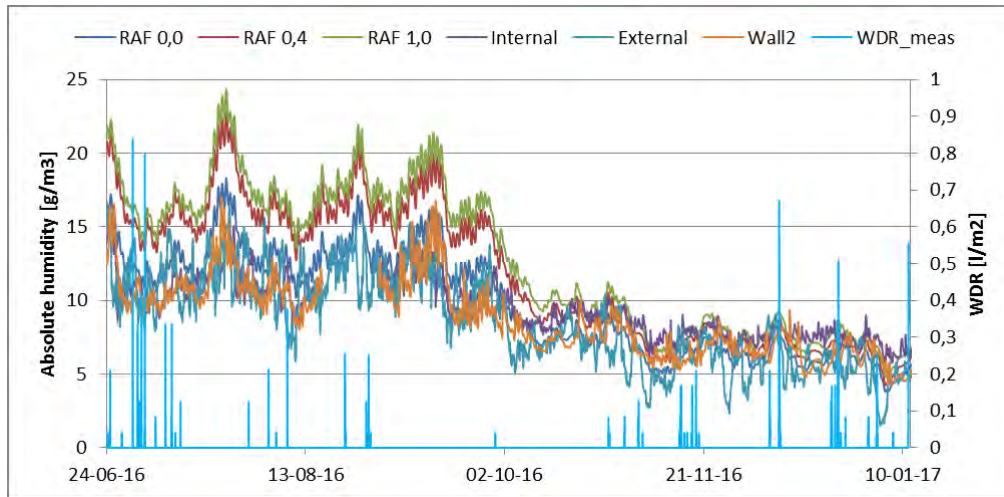


Figure 38: Simulated absolute humidities in case building 2, with varying rain admittance function, and in situ measured absolute humidity at the interface (Wall2), internal and external absolute humidity conditions. RAF indicates the value of the rain admittance function in simulation models, and measured wind-driven rain is presented in blue bars.

The laboratory study of water migration through masonry presented in **Paper II** and displayed in Figure 39, shows that liquid water loads on the external surface can in fact influence the hygrothermal conditions within solid masonry; the relative humidity increased in all the sensor points during the experiment. The results showed that after 3 days of cyclic climatic loads, the relative humidity at the interface between the masonry and internal insulation began to increase, and a steady increase was still apparent on the 7th day, when only 5 cycles of climatic loads had been applied. The results indicated a delay of water penetration reaching the internal surface of the original masonry.

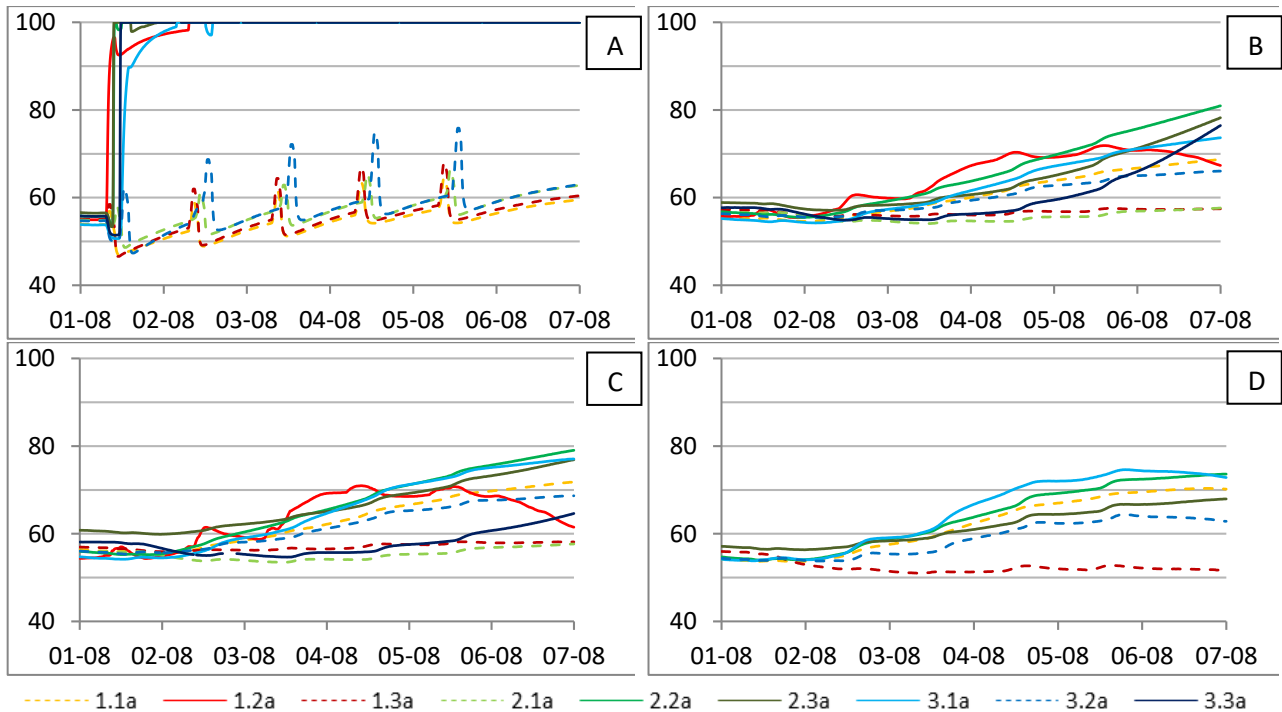


Figure 39: Relative humidity [%] measured in points A, B, C, and D. Hydrophobized cases are presented with dashed lines.

In the interface, the small increase in relative humidity was first detected after three 24 hour cycles, which is consistent to the theoretical time calculated for penetration of 350 mm yellow soft molded brick, described

above. The results from these studies and the present study indicate the effect of wind-driven rain on hygrothermal conditions in internally insulated walls being present, however not necessarily significant. Odgaard *et al.* [79] found that large rain events, or rain events of longer duration did in fact yield temporarily delayed increases in relative humidity during summer seasons. The moisture may be able to partially dry out before it penetrates to the wall-insulation interface. In cases where the masonry is thicker, the penetration is likely delayed further, and the delay allows further drying out. Similarly, Vereecken [48] *et al.* also established the importance of masonry thickness when it comes to wind-driven rain penetration. Finally, several of the referenced studies [4, 5, 19] stated that deteriorated façades were less resistant to wind-driven rain. In the presented study, test building 2 had the most deteriorated façade, and furthermore the highest sorptivity. Despite these facts, the monitored effects on the hygrothermal conditions were nearly negligible.

4.3 Effect of hydrophobization

The effect of hydrophobization on brick, lime mortar, and holistic masonry was investigated and presented in **Paper II**. An investigation of the effect of surface treatments by means of laboratory experiments and hygrothermal simulations was introduced in **Paper V**.

4.3.1 Laboratory experiments

In **Paper V**, the effect of hydrophobization was investigated on brick specimens by means of partial immersion and Karsten tubes. The investigation showed, that hydrophobization treatment J (cf. Table 7) reduced the water uptake with a factor of 15 (Karsten tube) – 400 (partial immersion). The results from the experiments are portrayed in Table 10.

Table 10: Average sorptivity and standard deviation for the reference and hydrophobized brick specimens obtained by Roel Hendrickx' method after Karsten tube experiment and partial immersion experiment.

$\frac{kg}{m^2\sqrt{s}}$	Karsten tube		Partial immersion	
	$S_{average}$	$S_{standard\ deviation}$	$A_{w,average}$	$A_{w,standard\ deviation}$
Reference	0.129	0.070	0.16	0.04
Hydrophobisation	0.009	0.004	0.0004	0.0001

It should be noted that all reference specimens displayed water on the top surface within 1 hour of immersion, and none could be seen in the hydrophobized specimens, as can be seen in Figure 40. It is apparent that in untreated specimens the water appears on the surface, whereas no water is seen in on the top of hydrophobized specimens.

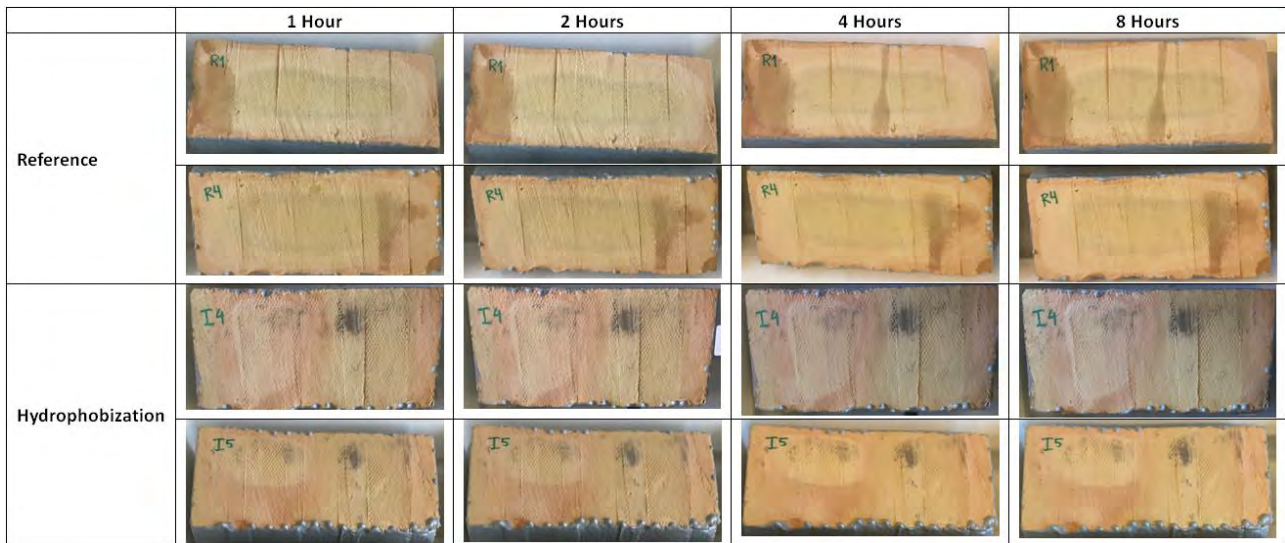


Figure 40: Two examples of reference specimens and hydrophobized specimens during partial immersion experiment.

The investigation of the effect of hydrophobization on brick and lime mortar individually was assessed via water uptake (full immersion), drying and penetration depth in **Paper II**. Results from the water uptake experiments are displayed in Figure 41 and Figure 42 for brick and lime mortar respectively. For the brick specimens, a large difference in water absorption was observed. Agents E, I, J, M, N and O, primarily silane based agents, had a mass increase of less than 2% during the duration of the experiment, and are thus deemed to be the most successful agents with regard to low water uptake.

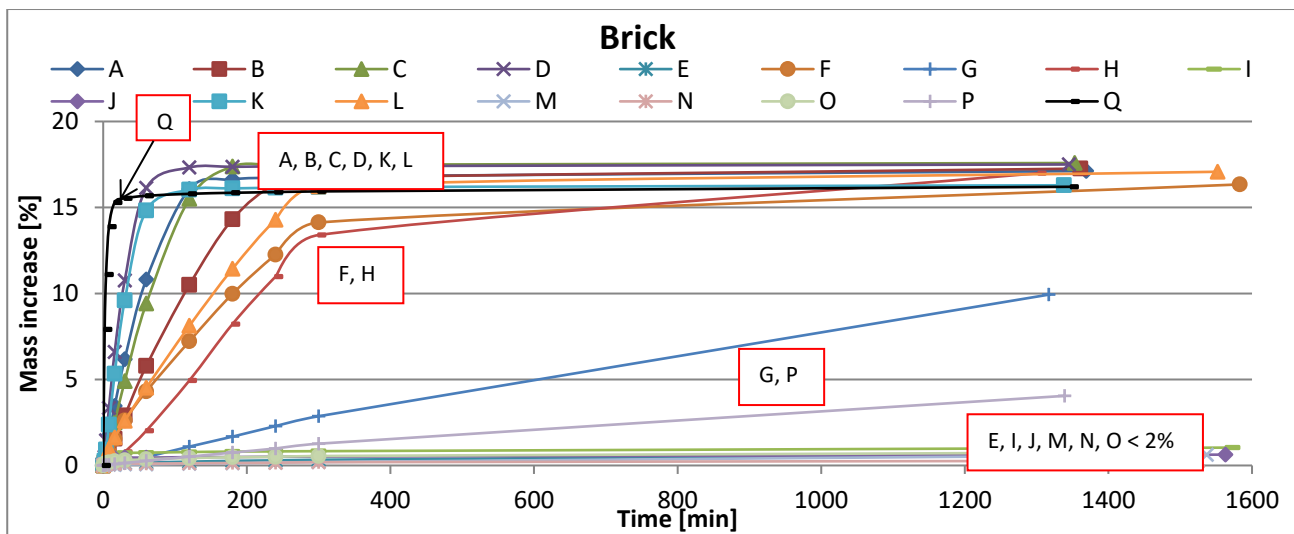


Figure 41: Mass increase by full immersion over time for brick specimens with hydrophobization agents A-P. Q is reference specimen.

For the lime mortar specimens, the results seem more random for the various agents. As can be seen in Figure 42 though, some agents seem to have no effect on the mortar's water absorption.

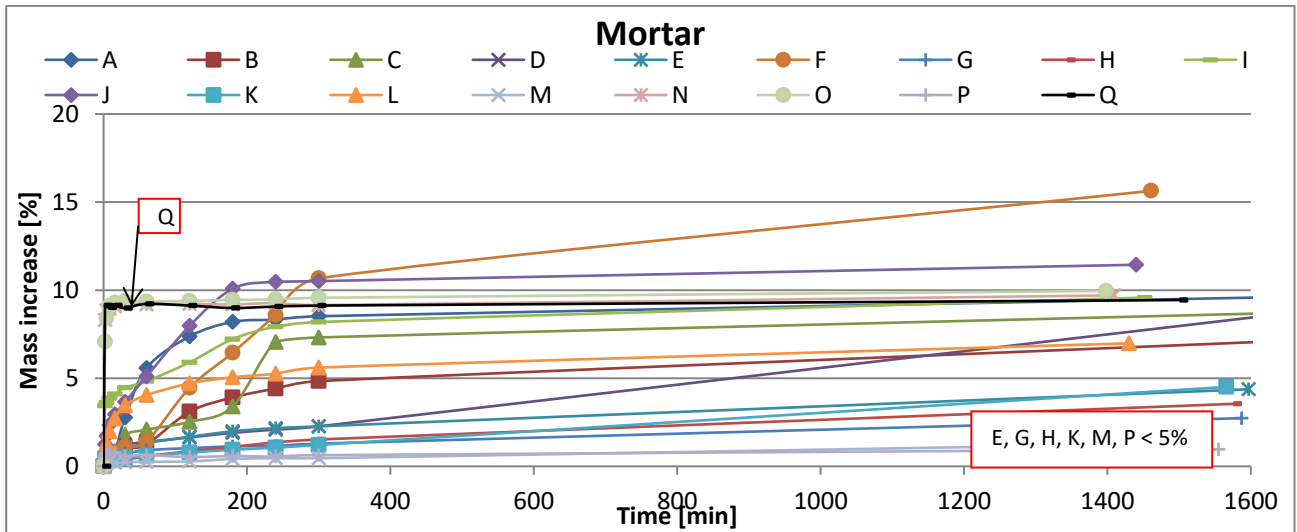


Figure 42: Mass increase by full immersion over time for mortar specimens with hydrophobization agent A-Q. Q is reference specimen.

The initial drying period was of relevance in the presented study, as this was where liquid transport to the surface occurred. Actual rain events are assumed not to yield vacuum saturated materials. The hydrophobization had less effect on the drying of brick, as compared to the drying capabilities of lime mortar. All the mortar specimens showed slower drying compared to the reference, while there was much more variation in the drying velocity in brick specimens, as some bricks exhibited slightly faster initial drying than the reference.

The average penetration depth of the hydrophobization agent is presented below in Figure 43 as a percentage of half the specimen thickness. It is seen that for both brick and mortar, agents I and J, which are both silane based creamy agents, had high penetration depths.

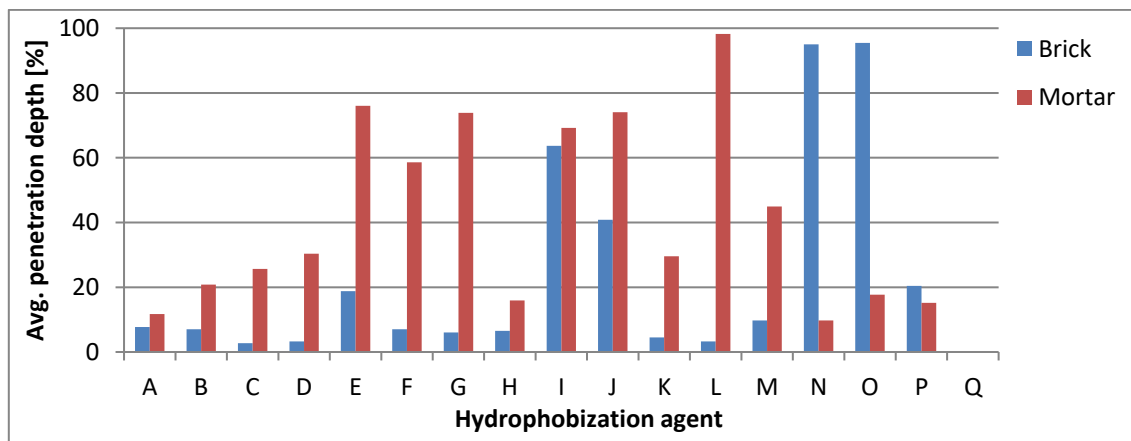


Figure 43: Penetration depths, presented as percentage of $\frac{1}{2}$ specimen thicknesses.

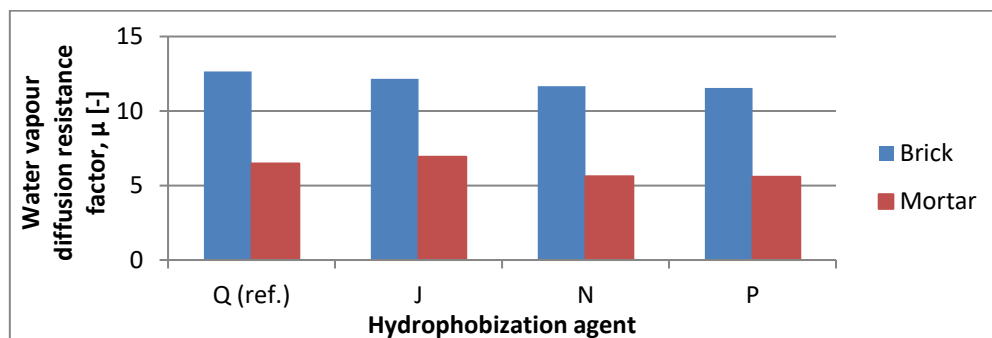
The simplified ranking system described in section 3.3.1 was introduced in order to try to evaluate the various results. Despite some of the results being contradictory, the ranking system yields opportunity for the evaluation of overall results. The results are displayed in Table 11.

Table 11: Ranking of the various hydrophobization treatments for brick and mortar altogether, and brick and mortar individually.

Ranking by 3 categories					
Brick and mortar		Brick		Mortar	
	Σ Score		Σ Score		Σ Score
O	297	O	314	G	116
N	239	N	268	E	90
I	230	I	189	M	85
M	213	J	168	L	82
J	195	M	128	P	57
E	186	E	96	H	44
P	132	P	75	I	41
G	128	A	49	K	40
L	81	G	12	J	27
K	25	B	10	Q (reference)	0
H	17	F	4	O	-17
Q (reference)	0	Q (reference)	0	B	-24
A	-9	L	-1	D	-24
B	-14	D	-15	N	-29
D	-39	K	-15	C	-31
C	-50	C	-19	A	-58
F	-64	H	-27	F	-68

The water uptake experiment distinctly showed the reduction in initial water uptake for most hydrophobization agents, as expected, due to the purpose of the surface treatment. This was also illustrated in **Paper V**, where the water uptake of hydrophobized brick was found to be significantly reduced with hydrophobization. It is evident that hydrophobization treatments of silane rather than siloxane seemed to perform better overall, especially on bricks. Agent M was represented in the top-5 of all the ranking lists.

Results from the water vapour diffusion experiment are seen in Figure 44, as average values for the 3 specimens of each type. It can be seen that the water vapour diffusion resistance factor was not affected significantly by the 3 investigated hydrophobization treatments. There was, however, a slight tendency of reduced water vapour diffusion resistance factor with the application of hydrophobization treatment, which was attributed to uncertainties in the experiment.

**Figure 44: Graphical illustration of water vapour diffusion resistance factor on specimens with no treatment (Q) and treatments J, N and P.**

The investigation of water migration through masonry, presented in **Paper II**, also led to results within the efficiency of hydrophobization, but on masonry holistically. The effect of hydrophobization was most pronounced in point A (54 mm from the external surface), but also had noticeable effects in points B (brick,

near interface), C (interface), and D (insulation, near interface). The results are displayed in Figure 39. The relative humidity in point A, for untreated masonry, reached 100%, and stayed at this level for the duration of the experiment, whereas for hydrophobized specimens, the relative humidity only exceeded 70 % in short peaks when the water loads were applied.

4.3.2 Hygrothermal simulations

Hydrophobization was investigated with hygrothermal simulations in **Paper V**, by means of obtained laboratory experiment results implemented in Delphin. Simulation results of the average water content in the various brick types, with and without hydrophobization, are depicted in Figure 45. The figure distinctly shows that the hydrophobization has a larger positive impact on the denser brick types, Brick Bernhard and Brick Joens. For the lower density brick types, Brick Schlagmann and Yellow brick, the effect of hydrophobization is nonexistent for warm periods, whereas as the effect appears to be negative in colder periods. The implementation of hydrophobization in the modelling was however somewhat conservative as the factor 15 water uptake coefficient reduction (Karsten tube method) was implemented rather than the factor 400 found with partial immersion. The low-density brick types had a higher initial water uptake coefficient, and thus the implementation of factor 15 would have less effect on these bricks, compared to factor 400. The simulations were performed as “worst case scenarios” with regard to wind-driven rain.

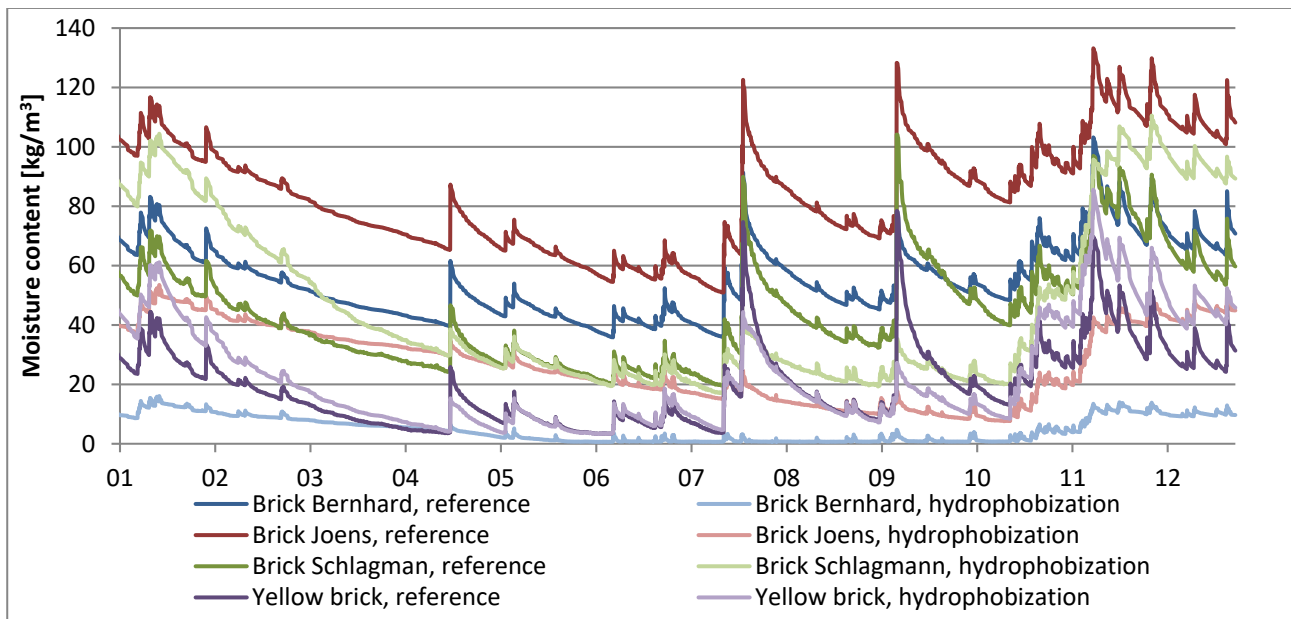


Figure 45: Simulated average moisture content for the 2nd year of simulation and 3 surface types.

These results are only representative of the given input, of the water uptake coefficient being reduced by a factor 15, found by the Karsten tube method. Had the water uptake coefficient been reduced with a factor of 400, as found by the partial immersion experiments, a larger success rate may have occurred.

4.4 Material parameters and characterization

The influential parameters with regard to hygrothermal simulation and performance were investigated in **Paper IV** by means of simulation with varied single parameters, and different brick types. In **Paper VI** possible correlations between these parameters were investigated.

4.4.1 Influential parameters

Hygrothermal simulations were used as a tool for investigation of essential material parameters with regard to hygrothermal conditions in masonry. Initially, a validation with measured values for a case-study was performed, as also described in section 3.4.1. The validation of the simulation model does not reach a perfect fit; the simulations are performed in 1D without consideration to mortar joints, long wave emission has been omitted due to nonexistent data, and surface exchange coefficients were estimated. Despite these things, the validated model gives sufficient correlation in order to investigate the variations in material parameters. Figure 46 illustrates the obtained results in **Paper IV** from the parameter variation investigation, in output location P2, in the middle of a 1½ brick thick masonry wall.

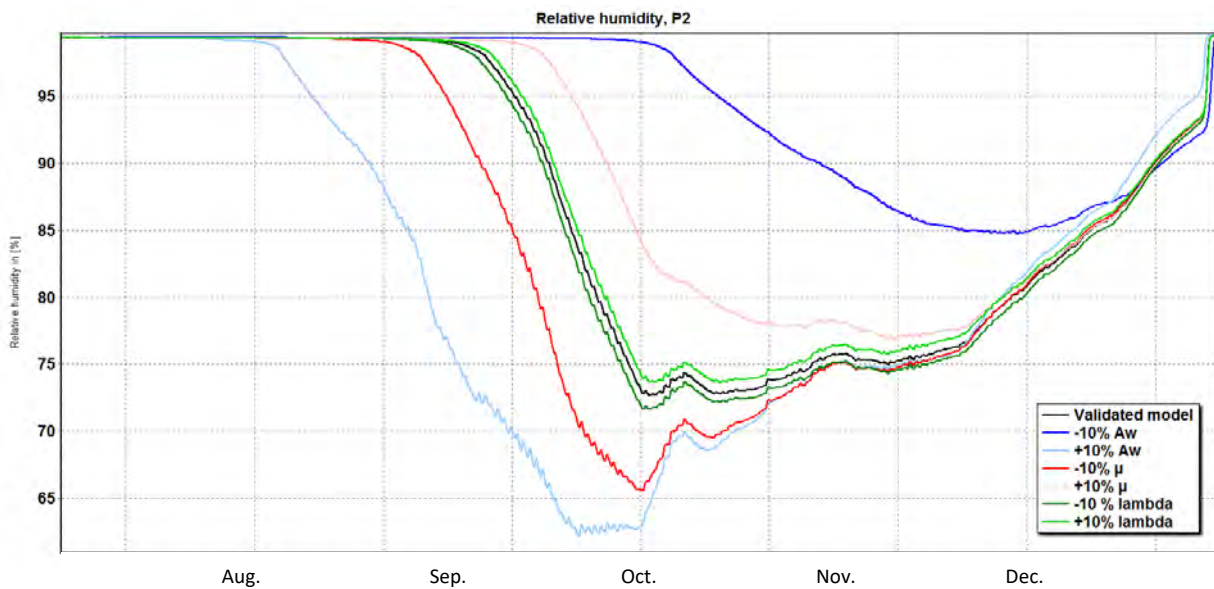


Figure 46: Results from parameter variation in measuring point 2.

Variations in density and open porosity alone showed no effect on the results. The water uptake coefficient showed the largest impact on the results; however vapour diffusion resistance, μ , and thermal conductivity, λ , also influence results. The simulations indicated that the water uptake coefficient (liquid transport) yielded the largest impact on the relative humidity. The seasonal dependency could be explained in part by rain events not succeeded by fast drying from solar radiation during summer. The influence of vapour diffusion resistance could be partly explained by the reduced drying potential due to the increased diffusion resistance. The results were in consistency with findings by Kłoda [80]. The orientation of the wall, which in this case is the “worst case scenario”, may have been a determining factor for the current conclusions. Another series of simulations with a less exposed orientation may result in a different conclusion.

The material parameter variation study presented above was performed relatively simplistically, i.e. studying a single parameter at a time, and the correlation of parameter variation was not included. In reality, many of the parameters correlate: e.g. thermal conductivity will normally decrease for decreasing density, which again decreases for increasing porosity. So the observed negligible effect of density and porosity within the $\pm 10\%$ variation on the temperature and moisture conditions in the studied construction must be linked to the observed effects of thermal conductivity, water vapour diffusion resistance, and water uptake coefficient. For this reason, further simulations were performed with 2 different types of brick, namely a high and a low density brick, and the results are presented in Figure 47.

The results showed that the denser type of brick, Brick Bernhard, yielded results of higher relative humidity. The water uptake coefficient is lower in this brick type, underlining the effect demonstrated by the previous simulations. The lower relative humidity in Brick Schlagmann could partly be explained by the higher temperatures. It is apparent that the material characteristics were predominantly influential in colder periods. The simulations illustrated how different the outcome of hygrothermal simulations can be, depending on which brick was chosen for the simulation. A study of 23 specific bricks by Zhao *et al.* [86] resulted in four different clusters: New bricks, Historical bricks of clay and loam, Historical bricks of clay, loam and sand and Bricks for external facades (high density and low moisture storage and transport capacity). Therefore, information, e.g. the construction period, or information on either density or transport capacity estimated by simple tests, (e.g. Karsten tube), could be sufficient for classification or determination of the correct cluster for a better estimation of the hygrothermal performance via simulations.

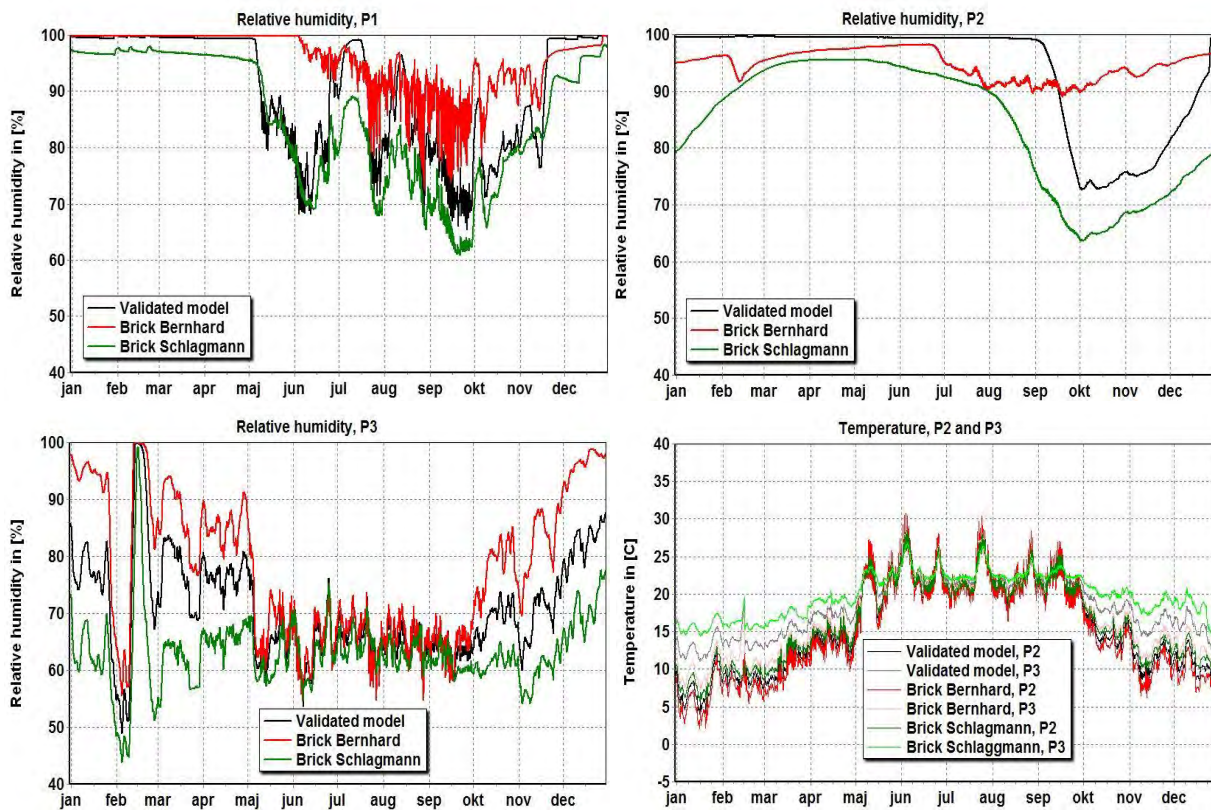


Figure 47: Hygrothermal simulations with varying brick types. Top left: relative humidity in point 1 (54 mm from external surface); top right: relative humidity in point 2 (middle of 1½ brick thick masonry wall); bottom left: relative humidity in point 3 (in internal render); bottom right: temperature in points 2 and 3.

4.4.2 Parameter correlations

By plotting all the parameters from a dataset including a number of similar materials, here brick, indications of linear correlations between density and open porosity, density and thermal conductivity, open porosity and water uptake, and open porosity and thermal conductivity were found. The plots are seen in Figure 48.

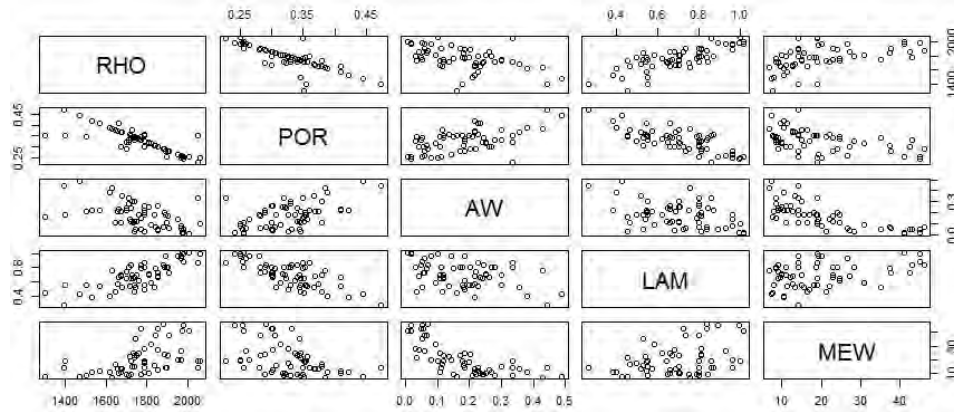


Figure 48: All variables plotted against each other. Indications of linear correlations are when the plots of the parameters against each other are displayed almost linear.

Subsequently generated scatterplots of density against the remaining parameters indicated linear correlations between density and open porosity, and density and thermal conductivity. A principal component analysis (PCA) was implemented to gain knowledge and visualize patterns between the variables (material parameters), as presented in **Paper VI**. A strong positive correlation was seen between density and thermal conductivity, and a strong negative correlation between density and open porosity. Hence the density was expected to decrease with an increased porosity. The same can be explained for the thermal conductivity. Also, a strong negative correlation was seen between water uptake (AW) and water vapour diffusion resistance (MEW). There is also little correlation between the density and water uptake and vapour diffusion respectively.

Simple linear regression was performed on all variables vs. density. As expected, the best results were gathered for correlation between density and open porosity with an R^2 of 0.83, as well as density and thermal conductivity where R^2 was 0.61. Fitted models were generated with the omission of outlying values. The best generated models are presented below in Table 12.

Table 12: Simple linear regression performed on density vs. the remaining parameters. The colors indicate the precision of the model; dark red is worst, over lighter red, dark orange and finally light orange was the best fit generated.

RHO vs.	1 st model		Omitted observations /bricks	Fitted model			Example: prediction if RHO is 1780kg/m ³		
	R^2	p-value		R^2	p-value	function	fit	lower	upper
POR	0.64	3.36e-15	1, 3, 62	0.83	<2.2e-16	$y=0.93 - 0.00034x$	0.33	0.28	0.37
AW	0.19	3.08e-4	1, 61, 62	0.39	1.07e-7	$y=1.04 - 0.00049x$	0.17	-0.01	0.35
LAM	0.60	1.08e-13	1, 3	0.61	1.01e-13	$y=-0.97 + 0.00094x$	0.71	0.49	0.93
MEW	0.26	1.82e-5	3, 59, 62	0.29	7.36e-6	$y=-52.68 + 0.04108x$	20.44	1.09	39.80

Logarithmic transformations of the models were also made and fitted, again by omission of outliers, however no acceptable correlations were generated, as R^2 was 0.26 and 0.40 for the fitted models of density vs. water uptake and water vapour diffusion resistance respectively.

5 Main findings

The following paragraph includes the main findings from the research performed and described above. The most important findings are divided into the four main topics.

5.1 Hygrothermal performance of internally insulated solid historic masonry

The performances of 4 cases of internally insulated historic masonry were monitored for the duration of 1½-2½ years. Furthermore, validated simulation models contributed to the investigation of hygrothermal performance of two insulation systems on solid historic masonry. Lastly, the performance was evaluated integrated with an investigation of the effect of wind-driven rain on the hygrothermal response of a solid masonry façade.

Both case studies of insulation system 2 (PUR foam with calcium silicate channels) generated unacceptable moisture conditions behind the insulation and beam ends, thus risk of mould growth and wood degradation occurred. In case building 4 with 30 mm of insulation, there was a tendency of a slow and slight reduction of relative humidity for the duration of the measurements. While there was no indication of reduction in relative humidity in case building 1 with 80 mm. The influence of insulation thickness is supported by hygrothermal simulations, yielding reduced relative humidity with reduced insulation thickness.

The in situ measurements of case studies with insulation system 1 (phenolic foam with integrated vapour barrier) showed acceptable humidity conditions. Hygrothermal simulations of insulation system 1 yielded better results with regard to validation and measurements when diffusion was included in the models. Simulations with vapour barrier, and vapour tight phenolic foam, resulted in unacceptable humidity conditions, and the accompanying risk of mould growth. The simulations of the vapour tight versions of simulation system 1 even yielded worse results, when compared to simulation system 2. Due to these results, it is assumed that diffusion occurred behind the insulation plates, despite being “fully bonded”. This could be explained by the way the plates were installed; the integrated vapour barrier was discontinued at the plate joints and at the floor and ceiling. Furthermore, the integrated vapour barrier was penetrated with screws during installation. Lastly, the plates were applied with a glue mortar, and a notched trowel, allowing possible convection in air cavities in the channels behind the plates if 100 % contact is not achieved. Furthermore, the influence of masonry thickness was seen in the measurements from case building 2, as sensor W6 had the highest relative humidity, and the wall is ½ brick thinner at this location.

The results and parameter variations support the indication that the hygrothermal performance of internally insulated solid historic masonry is reduced by applications of vapour barriers and vapour tight solutions. The hygrothermal simulations support the statements that the vapour tight solution has the worst performance, and more success is apparent in the vapour open and capillary active solutions. The overall hygrothermal performance, however, is naturally influenced by many parameters. Measurements and hygrothermal simulations both show an increased risk of unfavorable humidity conditions and mould growth increases with increased insulation thickness. [Paper I]

The investigation of wind-driven rain and the effect of wind-driven rain on the hygrothermal performance of internally insulated historic solid masonry indicated that some delayed influence might be present, especially in warmer seasons. The influence is dependent on other external factors, e.g. solar radiation and wind dynamics, and therefore no definite coherence between wind-driven rain and relative humidity at the

interface was established. However high external moisture content, especially in summer influence the hygrothermal conditions in the wall. [Paper III]

In the laboratory, the performance of 3 different internal insulation systems was evaluated after cyclic climatic loads, as described in section 3.2.2. The results showed that the best performance with regard to relative humidity behind the insulation was found in the cases with the insulation material that had shown limited capillary active properties, insulation system 2 described in Table 2. This system even performed better at the interface when compared to the other insulation systems, including a hydrophobizing surface treatment. It can be concluded that the hygrothermal performance of the internally insulated masonry appeared to be significantly improved with the application of hydrophobization. [Paper II]

5.2 Quantification and effect of wind-driven rain

Investigations of wind-driven rain, and the effect of wind-driven rain on hygrothermal conditions in masonry, was investigated both in situ in case buildings 1 and 2, experimentally in a laboratory and with hygrothermal simulations.

In the case of in-situ measurements of wind-driven rain, the results were compared with those generated from a semi-empirical model of wind-driven rain depositions on a façade, presented in Eq. 3. These results showed that the model significantly overestimated the wind-driven rain measured by the gauge, with a factor of up to 2.5. The hygrothermal simulations support the fact that the effect of wind-driven rain is present; the general effect of external humidity conditions, however, appears to be influential too. The hygrothermal simulations do indicate a higher influence of wind-driven rain on the hygrothermal conditions in the masonry when compared to the effect monitored in situ. This in turn indicates the overestimation found in semi-empirical and numerical models, also observed by other researchers, e.g. Abuku *et al.* [62]. [Paper III]

Laboratory experimentation, with imitated climatic loads of rain, radiation and cold climate on masonry sections, showed the effect of wind-driven rain on masonry. The relative humidity was monitored through the masonry. It became apparent that the most significant influence of wind-driven rain was observed at the outermost external part of the wall, and the effect declined inwardly. In wall sections without hydrophobization, the relative humidity within 54 mm of the surface reached 100 % succeeding the first induced daily rain load, and did not decrease for the duration of the experiment. At the interface between the masonry and internal insulation, an increase in relative humidity was observed 3 days after the first induced daily rain load, which increased steadily with time, up to 80 %, for the cases without hydrophobization. [Paper II]

5.3 Effect of hydrophobization

In a large-scale laboratory experiment on water migration through masonry (section 3.2.2) influence of hydrophobization on masonry holistically was investigated. Relative humidity measurements through the masonry sections distinctly illustrate the effects of hydrophobization. In the external measuring point, 54 mm from the surface, all un-hydrophobized specimens reached 100 % relative humidity subsequent to the first induced daily rain load. In the cases of hydrophobized wall sections, the relative humidity peaked at a maximum of 80 % relative humidity following the applied rain loads, but these elevated relative humidities were dried out before the next rain load was applied. Further in the wall, the effect of hydrophobization varies between the cases, but the relative humidity at the interface did not exceed 60 % - 70 %. Diffusion open paint on the internal surface resulted in the higher relative humidity inside the construction. [Paper II]

The effect of a variety of hydrophobization agents on both brick and air lime mortar were investigated by several means. These investigations showed that, the most successful effect of hydrophobization was found in specimens of brick rather than lime mortar. A tendency of silane-based products being more efficient in bricks was apparent for both water absorption, drying and penetration depth. The success of these parameters in lime mortar specimens was granted a variety of types of hydrophobization; silane-based, hybrid, and nano. With regard to penetration depth, the creamy agents, I and J, performed well in both types of specimens, this being attributed to their creamy consistency, yielding better means for absorption into the specimens. The drying of hydrophobized brick specimens did not appear to be affected significantly, however the drying of hydrophobized lime mortar specimens appeared slightly impeded. The water vapour diffusion resistance of 3 hydrophobization agents, on both brick and lime mortar specimens, showed that hydrophobization did not have any significant effect on the water vapour diffusion resistance. [Paper II]

The effect of hydrophobization was evaluated separately on brick and lime mortar specimens, and the efficiency between the active components varied between the 2 types of specimens. Thus the success of individual hydrophobization agents cannot definitely be attributed masonry holistically. In order for hydrophobization to be efficient on masonry, the water absorption must be reduced in both the bricks and the joints. The large-scale experiment however, did yield positive results for holistically efficient hydrophobization. This agent, hydrophobization treatment J cf. Table 7, performed very well in brick specimens, and medium well in specimens of lime mortar. Furthermore, the creamy consistency appears to be successful and yield a higher penetration depth. Theoretically, the hydrophobization agents will have a better bonding to cementitious mortars. Repairing of many historic façades may have included the application of cementitious mortars in degraded joints, this possibly being why the success of hydrophobization may be larger in these cases. The aspects of application method, aging, and consistency of the agents are not treated in the presented study, but should be taken into account.

The effect of hydrophobization was also tested on a smaller scale. In this case, both partial immersion and Karsten tube were performed on specimens of brick. Despite discrepancies between the two methods linked to the duration of the experiments it was found that hydrophobization decreased the water uptake in the brick specimens with a factor of 15 (obtained by Karsten tube for 30 minutes) and up to factor 400 (obtained by partial immersion for 24 hours). Very little water was absorbed in the hydrophobized specimens. Hygrothermal simulations were also performed, with hydrophobization applied as a factor 15 reduction in water uptake coefficient in the external 5 mm. Four brick types were investigated. The simulation models showed that the effect on the hygrothermal performance of hydrophobized brick depended highly on the brick type. Most successes with hydrophobization were found in brick types with higher densities, and an initially lower water uptake coefficient. The results may have been different with different agents, and the laboratory application may have bonded differently on these brick types, which would yield other results. Furthermore, the simulation results on the various brick types may have turned out differently if the factor 400 reduction in water uptake coefficient gained by partial immersion experiments had been applied to simulations rather than the factor 15 found by Karsten tube. [Paper V]

5.4 Material parameters and characterization

Some of the material characterization performed in this project includes the alterations in moisture transport mechanisms due to the application of hydrophobization, and are thus described in paragraphs above.

Karsten tube measurements are not a standard method for quantification of water uptake coefficient, but it may be used for simple comparison purposes, or for the demonstration of the effect of hydrophobization, as previously described. Karsten tube measurements may even yield the possibility for in situ classification estimations of historic masonry. The Karsten tube measurements performed on case buildings 1 and 2 indicate, however, no significant differences in the water absorption capabilities in severely weathered masonry from 1877, when compared to well-maintained masonry from 1932. **[Paper III]**

A parameter study of vital material parameters with regard to hygrothermal simulations was performed simplistically and based on 1D Delphin simulation models with $\pm 10\%$ in 5 single material characteristics. The investigation showed that the water uptake coefficient led to the highest impact on the relative humidity through the masonry of the investigated parameters. As the water uptake was reduced, relative humidity increased in cold periods. The water vapour diffusion resistance was also found to be influential on the relative humidity observed in the masonry, as increased diffusion resistance led to higher relative humidity in winter. The thermal conductivity also influenced results to some extent, as a higher thermal conductivity led to a lower temperature and increased relative humidity. Density and open porosity were initially found to have an insignificant influence on the results; however water uptake, thermal conductivity and water vapour diffusion are functions dependent on just density and/or porosity. Simulations were therefore performed on a high density brick and a low density brick. These simulations showed that the denser brick type yielded higher relative humidity. The water uptake coefficient was also lower in this brick type, underlining the previous statement of reduced water uptake coefficient increasing the relative humidity. The influence of the material characteristics and their differences was pronounced in cold periods, as also seen in the parameter variation study. The large difference in results obtained by different brick types underlines the importance of at least correct classification, and if this can be done in situ and nondestructively, e.g. by using the construction period, location, density or transport capacities estimated by simple tests, e.g. Karsten tube, it is favorable, and could be sufficient for the determination of correct cluster/classification. **[Paper IV]**

In connection with the above, a simple investigation of parameter correlations was performed on the same 5 single material parameters as in the parameter variation study. The PCA indicated a strong positive correlation between density and thermal conductivity, and a strong negative correlation between density and open porosity. Furthermore, a strong negative correlation between water vapour diffusion resistance factor and water uptake coefficient was established. Simple linear regression was performed on all the parameters with regard to the density. The best fitted models were established for density and open porosity with an R^2 of 0.83, and density and thermal conductivity with an R^2 of 0.61. Unfortunately, these correlations were not found to be strong enough to provide a basis for the correlation functions to be linear, but the correlation appears to be present. **[Paper VI]**

6 Conclusion and hypotheses

In the following paragraphs, the conclusions of the demonstrated research are related to the defined hypotheses and the scope of the thesis. Lastly, suggestions for future research, based on the present, will be listed.

The scope was to investigate important parameters with regard to prediction of the hygrothermal performance of internally insulated solid historic masonry. In addition to focus on hygrothermal simulations and performance, attention was also given to the effect of wind-driven rain, possibilities with hydrophobization, and the influence of material parameters.

6.1 Hypothesis 1

The first hypothesis states that:

Long term hygrothermal conditions can be predicted by means of numerical models verified by measurements in critical points in internally insulated case buildings.

The hypothesis was investigated through **Paper I**, **Paper IV**, and **Paper V**, as these disseminations include hygrothermal simulations (Delphin 5.8.3). The hypothesis could not be rejected, as obtained results support the statement. The results of simulations however, depended highly on input.

Through hygrothermal simulations, it was found that predictions could in fact be made for conditions under the given input. However, this input proved to be vital for the results and the reliability of the modelling. Craftsmanship showed to be of importance as well. In **Paper I** it was proven that despite a system including a vapour barrier and phenolic foam being diffusion tight, the system in reality was diffusion open and there was possibly an air cavity behind the plates. This was proven by simulating the same model, just vapour open with a resulting match with measured results. The vapour tight models generated undesirable hygrothermal conditions. Good validation models were achieved for both the diffusion open models of insulation system 1 and for insulation system 2, despite unknown material parameters for the existing construction. These 1D models consisted of lime mortar rather than brick, as initial simulations suggested this alteration. This indicates that the main means for moisture transport in historic masonry, at least in these cases, is through the lime mortar joints. After model validation, the models were used for forecasting future conditions. Predictions were performed for both cases; the diffusion tight original system as well as the diffusion open, and the performance of both cases could be predicted. Thus the hygrothermal models can be used for predictions of hygrothermal conditions under the given circumstances. **Paper IV** showed that as single parameters, density and open porosity did not influence the temperature or relative humidity, whereas water uptake coefficient, vapour diffusion resistance, and thermal conductivity all influenced results. As the material parameters are correlated, the simulations were repeated with two different brick types, and the effect of water absorption was reestablished. **Paper V** also established the importance of brick types and water uptake coefficient, as the simulation models showed different responses in surface treatments on the different brick types. The results of hygrothermal simulations were dominated by the main characteristics found in the application method and craftsmanship, as this showed to be a decisive and critical factor with regard to a successful hygrothermal performance. In the end, reliable hygrothermal conditions can be predicted with hygrothermal simulations, with regard to the given modelling input.

6.2 Hypothesis 2

The second hypothesis reads:

Wind-driven rain has a significant effect on the hygrothermal performance of solid masonry walls with internal insulation.

The hypothesis stated above, was investigated in **Paper II** and **Paper III**, both of which included a study of water penetration in masonry subsequent to rain loads. This hypothesis was partly supported by results.

In situ measurements of wind-driven rain performed in two case buildings with in situ measurements (T and RH) taken at wall-insulation interfaces and behind beam ends (**Paper III**), did not show conclusive direct influence of wind-driven rain on the hygrothermal conditions. There was only a slight indication of delayed elevated humidity at the interface successive to rain events. However, most of these changes observed in the relative humidity in the masonry could more likely be attributed to the variations in external relative humidity. Thus the in situ measurements of wind-driven rain did not give conclusive determination of the effect of wind-driven rain on the hygrothermal performance of internally insulated solid masonry.

In the large-scale laboratory experiment described in **Paper II**, the effects of wind-driven rain on hygrothermal conditions at the interface were, however, detected. This study was built up as a worst case scenario, with extreme climatic conditions of daily cloudbursts succeeded by solar radiation and cold climate. Furthermore, the experiment showed that the insulation system and internal surface influenced the results. This indicates that the effect of wind-driven rain is less pronounced in cases with capillary active systems and diffusion open surfaces. Indications of slightly increased relative humidity in warmer periods from in situ measurements and the detectable humidity increase from the laboratory experiment with applied solar radiation may indicate the significant influence of the solar radiation on the penetration of wind-driven rain. However, this hypothesis was not investigated in this study.

The effect of wind-driven rain on hygrothermal conditions behind internal insulation, were also seen by means of hygrothermal simulations, as presented in **Paper III**. These results, together with the above conclusions, indicate that WDR in fact does yield elevated relative humidity behind the insulation, why the effect of hydrophobization is highly relevant for the hygrothermal performance of internal insulation.

6.3 Hypothesis 3

The third hypothesis is that:

Hydrophobization of the exterior surface has a significant effect on the hygrothermal performance of historic solid masonry.

This hypothesis was studied through both **Paper II** and **Paper V** by means of experimental methods on material parameter levels, in a large-scale experiment, and with hygrothermal simulations. The hypothesis could not be rejected based on the performed research.

Hydrophobization of the exterior surface has a significant effect on the hygrothermal performance of historic solid masonry. This was illustrated in **Paper II**, by means of the large-scale investigation, where hydrophobization showed to have a distinct impact on the hygrothermal conditions detected at the critical interface. Most of the effect of hydrophobization was seen in the outermost part of the masonry, but the

effect was also apparent deeper in the construction. The highest obtained relative humidity at the interface of the hydrophobized wall section barely exceeded 70 %, whereas untreated wall sections reached 80 %. The laboratory investigations of the obtained changes in material parameters due to hydrophobization, also in **Paper II**, showed a distinct effect of hydrophobization on water absorption properties of historic masonry. The effect of hydrophobization was more pronounced in specimens of brick when compared to the effect achieved in lime mortar specimens. Silane based agents performed better in specimens of brick, and in lime mortar specimens a variety of active components was most efficient. Essentially the studies showed that hydrophobization induces the desired effect of reduced water penetration without significantly compromising drying potential or vapour permeability. By means of the hygrothermal simulations performed in **Paper V**, it could be seen that the effect of hydrophobization also varied between brick types. Despite the lesser effect on water absorption properties in specimens of lime mortar, a successful hydrophobization of historic masonry appears to be beneficial with regard to the hygrothermal performance of internally insulated solid masonry.

6.4 Hypothesis 4

The fourth hypothesis reads:

Certain material properties of brick are more influential with regards to the hygrothermal performance of internally insulated solid masonry structures, and some material parameters can be correlated.

The statement was tested by means of **Paper IV** and **Paper VI**, through parameter and correlation investigations. The hypothesis could not be rejected as the investigation supported the statement.

Through the parameter analysis based on hygrothermal simulations in **Paper IV**, a distinct difference in the effect of single material parameters on hygrothermal conditions in masonry was found. It was seen that variations in density and open porosity alone did not affect the masonry, whereas thermal conductivity, water vapour diffusion resistance, and especially the water uptake coefficient showed an influence on the humidity conditions in the masonry. The effects of the parameter variations were found to be more pronounced in colder seasons. This was further supported by simulations on high- and low-density brick types that stressed the fact that high density bricks with high thermal conductivity resulted in increased relative humidity, especially in cold periods. The investigation of parameter correlations presented in the **Paper VI** did not yield perfect regression models but tendencies of parameter correlations were apparent.

6.5 Perspectives and future research

The present study has given valuable knowledge on how to predict performance of internally insulated solid historic masonry, and which parameters are important when designing internal insulation solutions. A number of open questions remain, and therefore further studies of hygrothermal performance of internally insulated solid historic masonry need to be done. In the presented study, only little focus was given to the effect of indoor climate and orientation when these factors actually appear to be vital with regard to the hygrothermal performance of internally insulated solid masonry. More case studies with long term in situ measurements would be preferred, including several types of insulation systems in 1:1 case studies, with varying orientations and indoor climates would add to the existing research in the area, including in terms of increasing validity of simulation models. The effect of indoor climate should be taken into consideration in future modelling, as the success of the diffusion open systems relies on suitable interior moisture conditions. In terms of theoretical models of mould index, wood decay and wind-driven rain, the presented study

suggests overestimation in all cases. For this reason, updated and improved models could be relevant in future research. In terms of the wind-driven rain effect on hygrothermal conditions in masonry, the delay in penetration, and the influential parameters for this, needs to be studied further. The slight indications of increased relative humidity in warmer periods from in situ measurements, and the detectable humidity increase from the laboratory experiment with applied solar radiation may indicate the influence of the sun on the penetration of wind-driven rain. This may, however, be partially explained by summer condensation. With regard to hydrophobization, it is important to note that the presented research of various hydrophobization agents was performed on specimens of lime mortar and brick, and the effect clearly showed to be more successful in brick. As masonry must be considered holistically, it is vital that a hydrophobization agent reduces the water uptake in joints as well as brick. It is equally important to point out that the type of brick appeared to be influential on results. Furthermore, the effect of hydrophobization on cementitious mortars should be investigated on the same level as ceramic brick and lime mortar. The application method of hydrophobization treatment, as well as the consistency of the agents used, appears to be influential on obtained results. This area warrants more in-depth study. The aging of hydrophobization agents is a crucial aspect in the case of hydrophobization applied for enhanced performance of internal insulation systems; the application of an aging agent could have a degrading effect and would thus influence the hygrothermal performance negatively. The material parameters implemented in simulation models appear to be of significant influence with regard to hygrothermal performance. For this reason, the possibility of simple, in situ, non-destructive material classification, possibly based on clusters, would be a valuable tool for aiding research in the field.

References

- [1] T.K. Hansen, S.P. Bjarløv, R.H. Peuhkuri, M. Harrestrup, Long term in situ measurements of hygrothermal conditions at critical points in four cases of internally insulated historic solid masonry walls, *Energy Build.* 172 (2018) 235–248. doi:10.1016/j.enbuild.2018.05.001.
- [2] T. Kvist Hansen, S.P. Bjarløv, R.H. Peuhkuri, K.K. Hansen, Performance of hydrophobized historic solid masonry - experimental approach, *Constr. Build. Mater.* 188 (2018) 695–708. doi:10.1016/j.conbuildmat.2018.08.145.
- [3] T. Kvist Hansen, S.P. Bjarløv, R.H. Peuhkuri, The effects of wind-driven rain on the hygrothermal performance of solid masonry walls with internal insulation, *Energy Build.* (2018).
- [4] T.K. Hansen, R.H. Peuhkuri, E.B. Møller, S.P. Bjarløv, T.R. Odgaard, Material characterization models and test methods for historic building materials, in: *Energy Procedia*, 2017. doi:10.1016/j.egypro.2017.09.738.
- [5] T.K. Hansen, S.P. Bjarløv, R. Peuhkuri, Moisture transport properties of brick – comparison of exposed, impregnated and rendered brick, in: *Int. RILEM Conf. Mater. Syst. Struct. Civ. Eng. 2016 Segm. Moisture Mater. Struct., Kgs. Lyngby*, 2017: pp. 351–360. http://orbit.dtu.dk/ws/files/128040737/Pages_from_Moisture_conf_proceedings_3.pdf.
- [6] T.K. Hansen, Correlation between certain material parameters in bricks, Kgs. Lyngby, 2017.
- [7] T. Kvist Hansen, P. Klenz Larsen, K. Kielsgaard Hansen, S.P. Bjarløv, R.H. Peuhkuri, A lime based mortar for thermal insulation of medieval church vaults, in: *4th Hist. Mortars Conf. 2016*, Kgs. Lyngby, 2016.
- [8] P. Klenz Larsen, T. Kvist Hansen, A lime based mortar for thermal insulation of medieval church vaults, in: *M. de Bouw, S. Dubois, L. Dekeyser, Y. Vanhellemont (Eds.), 2nd Int. Conf. Energy Effic. Comf. Hist. Build. — 2nd Int. Conf. Energy Effic. Comf. Hist. Build., Flanders Heritage Agency*, 2016: pp. 198–204.
- [9] Department of Civil Engineering at the Technical University of Denmark, Technische Universität Dresden, Rønby.dk, Ekolab, E&P service, Kingspan, et al., Results and experience from the project: EUDP 2013-II “Energy efficient comfort in older apartment blocks”. Final report, (2016) 203.
- [10] Energistyrelsen, Energistyrelsen: Dansk Energi politik, (n.d.). <https://ens.dk/ansvarsomraader/energi-klimapolitik/fakta-om-dansk-energi-klimapolitik/dansk-energipolitik> (accessed September 10, 2018).
- [11] T. Odgaard, S.P. Bjarløv, C. Rode, M. Vesterlørkke, Building renovation with interior insulation on solid masonry walls in Denmark - A study of the building segment and possible solutions, *Energy Procedia*. 78 (2015) 830–835. doi:10.1016/j.egypro.2015.11.003.
- [12] J. Engelmark, Københavnsk etageboligbyggeri 1850-1900 - En byggeteknisk undersøgelse. SBI-Rapport 142, 1983.
- [13] B. Blocken, J. Carmeliet, A review of wind-driven rain research in building science, *J. Wind Eng. Ind. Aerodyn.* 92 (2004) 1079–1130. doi:10.1016/j.jweia.2004.06.003.
- [14] M. Abuku, H. Janssen, S. Roels, Impact of wind-driven rain on historic brick wall buildings in a moderately cold and humid climate : Numerical analyses of mould growth risk , indoor climate and energy consumption, *Energy Build.* 41 (2009) 101–110. doi:10.1016/j.enbuild.2008.07.011.
- [15] C. Balocco, G. Grazzini, A. Cavalera, Transient analysis of an external building cladding, *Energy Build.* 40 (2008) 1273–1277. doi:10.1016/j.enbuild.2007.11.008.

-
- [16] E. Kossecka, J. Kosny, Influence of insulation configuration on heating and cooling loads in a continuously used building, *Energy Build.* 34 (2002) 321–331. doi:10.1016/S0378-7788(01)00121-9.
 - [17] S.P. Bjarløv, G.R. Finken, T. Odgaard, Retrofit with interior insulation on solid masonry walls in cool temperate climates - An evaluation of the influence of interior insulation materials on moisture condition in the building envelope, *Energy Procedia.* 78 (2015) 1461–1466. doi:10.1016/j.egypro.2015.11.171.
 - [18] J. Munch-Andersen, SBI-anvisning 221: Efterisolering af etageboliger, 1., Statens Byggeforskningsinstitut, Hørsholm, 2008.
 - [19] E. Brandt, SBI-anvisning 224 Fugt i bygninger, 1., Statens Byggeforskningsinstitut, Hørsholm, 2009.
 - [20] J. Toman, A. Vimmrová, R. Černý, Long-term on-site assessment of hygrothermal performance of interior thermal insulation system without water vapour barrier, *Energy Build.* 41 (2009) 51–55. doi:10.1016/j.enbuild.2008.07.007.
 - [21] P. Mensinga, J. Straube, C. Schumacher, Assessing the freeze-thaw resistance of clay brick for interior insulation retrofit projects, in: 11th Int. Conf. Therm. Perform. Exter. Envel. Whole Build. Build. XI, 2010. doi:10.1081/E-EEE2-120046011.
 - [22] J. Zhao, J. Grunewald, U. Ruisinger, S. Feng, Evaluation of capillary-active mineral insulation systems for interior retrofit solution, *Build. Environ.* 115 (2017) 215–227. doi:10.1016/j.buildenv.2017.01.004.
 - [23] R. Walker, S. Pavía, Thermal performance of a selection of insulation materials suitable for historic buildings, *Build. Environ.* 94 (2015) 155–165. doi:10.1016/j.buildenv.2015.07.033.
 - [24] D.I. Kolaitis, E. Malliotakis, D.A. Kontogeorgos, I. Mandilaras, D.I. Katsourinis, M.A. Founti, Comparative assessment of internal and external thermal insulation systems for energy efficient retrofitting of residential buildings, *Energy Build.* 64 (2013) 123–131.
 - [25] P. Klöšeko, E. Arumägi, T. Kalamees, Hygrothermal performance of internally insulated brick wall in cold climate: A case study in a historical school building, *J. Build. Phys.* (2014) 1744259114532609-. doi:10.1177/1744259114532609.
 - [26] J. Straube, C. Schumacher, Interior Insulation Retrofits of Load-Bearing Masonry Walls in Cold Climates, *J. Green Build.* 2 (2007) 42–50. doi:10.3992/jgb.2.2.42.
 - [27] A. Blumberga, K. Kass, E. Kamendere, G. Zogla, A. Kamenders, D. Blumberga, et al., State of the art on historic building insulation materials and retrofit strategies, 2015. doi:10.1002/ejoc.201200111.
 - [28] R. Peuhkuri, C. Rode, Indvendig efterisolering: Sådan dimensioneres løsninger, som giver holdbare konstruktioner, Taastrup, 2010.
 - [29] E. Vereecken, L. Van Gelder, H. Janssen, S. Roels, Interior insulation for wall retrofitting - A probabilistic analysis of energy savings and hygrothermal risks, *Energy Build.* 89 (2015) 231–244. doi:10.1016/j.enbuild.2014.12.031.
 - [30] G.R. Finken, S.P. Bjarløv, R.H. Peuhkuri, Effect of façade impregnation on feasibility of capillary active thermal internal insulation for a historic dormitory – A hygrothermal simulation study, *Constr. Build. Mater.* 113 (2016) 202–214. doi:10.1016/j.conbuildmat.2016.03.019.

-
- [31] Z. Pavlík, R. Černý, Hygrothermal performance study of an innovative interior thermal insulation system, *Appl. Therm. Eng.* 29 (2009) 1941–1946. doi:10.1016/j.applthermaleng.2008.09.013.
 - [32] E. Vereecken, S. Roels, Capillary Active Interior Insulation Systems for Wall Retrofitting: A More Nuanced Story, *Int. J. Archit. Herit.* 10 (2016) 558–569. doi:10.1080/15583058.2015.1009575.
 - [33] T. Bunch-Nielsen, G. Christensen, Byg-Erfa Erfaringsblad (27) 05 12 29 Uventilerede paralleltage med dampbremse af hygrodioder, (2005). <https://byg-erfa.dk/uventilerede-hygrodioder>.
 - [34] S. Kirkeskov Jensen, C. Rode, K. Kielsgaard Hansen, N.P. Kloch, Non-isothermal Laboratory Measurements of Moisture Profiles in Calcium Silicate for Interior Insulation Applications, in: 2. Int. Innendämmkongress, 2013: pp. 97–106.
 - [35] P. Klöšeko, E. Arumägi, T. Kalamees, Hygrothermal performance of internally insulated brick wall in a cold climate: field measurement and model calibration, in: *Proc. 2nd Cent. Eur. Symp. Build. Phys.*, 2013. doi:10.1081/E-EEE2-120046011.
 - [36] M. Harrestrup, S. Svendsen, Internal insulation applied in heritage multi-storey buildings with wooden beams embedded in solid masonry brick façades, *Build. Environ.* 99 (2016) 59–72. doi:10.1016/j.buildenv.2016.01.019.
 - [37] A. Abdul Hamid, P. Wallentén, Hygrothermal assessment of internally added thermal insulation on external brick walls in Swedish multifamily buildings, *Build. Environ.* 123 (2017) 351–362. doi:10.1016/j.buildenv.2017.05.019.
 - [38] VTT Technical Research Centre of Finland, T. Häkkinen, Sustainable refurbishment of exterior walls and building facades, 2012. <https://www.vtt.fi/inf/pdf/technology/2012/T30.pdf>.
 - [39] T. Ojanen, R. Peuhkuri, Viitanen, Lähdesmäki, Vinha, Salminen, Classification of material sensitivity–new approach for mould growth modeling, in: 9th Nord. Symp. Build. Phys., 2011: pp. 867–874. http://webhotel2.tut.fi/nsb2011/sites/webhotel2.tut.fi/nsb2011/files/b10_02_tuomo_ojanen_vtt_nordic_9th_classification__mould_growth_final2.pdf.
 - [40] OBH gruppen, Skimmelsvampsymptomer, (n.d.). <https://www.obh-gruppen.dk/da/privat/skimmelsvamp/skimmelsvamp-symptomer> (accessed September 26, 2018).
 - [41] M. Krus, K. Sedlbauer, Mold Growth Prediction by Computational Simulation Mold Growth Prediction by Computational Simulation, in: *IAQ 2001 Moisture, Microbes, Heal. Eff. Indoor Air Qual. Moisture Build.*, 2001.
 - [42] A. Hukka, H. Viitanen, A mathematical model of mould growth on wooden material, *Wood Sci. Technol.* 33 (1999) 475–485. doi:10.1007/s002260050131.
 - [43] E. Vereecken, S. Roels, Review of mould prediction models and their influence on mould risk evaluation, *Build. Environ.* 51 (2012) 296–310. doi:10.1016/j.buildenv.2011.11.003.
 - [44] E. Vereecken, K. Vanoirbeek, S. Roels, Towards a more thoughtful use of mould prediction models: A critical view on experimental mould growth research, *J. Build. Phys.* 39 (2015) 102–123. doi:10.1177/1744259115588718.
 - [45] H. Viitanen, T. Toratti, L. Makkonen, R. Peuhkuri, T. Ojanen, L. Ruokolainen, et al., Towards modelling of decay risk of wooden materials, *Eur. J. Wood Wood Prod.* 68 (2010) 303–313. doi:10.1007/s00107-010-0450-x.

-
- [46] G.B.A. Coelho, F.M.A. Henriques, Influence of driving rain on the hygrothermal behavior of solid brick walls, *J. Build. Eng.* 7 (2016) 121–132. doi:10.1016/j.jobbe.2016.06.002.
 - [47] J.F. Straube, E.F.P. Burnett, Driving rain and masonry veneer, in: *ASTM Spec. Tech. Publ.* 1998, Vol. 1314, ASTM, 1998: pp. 73–87.
 - [48] E. Vereecken, S. Roels, Capillary active interior insulation: do the advantages really offset potential disadvantages?, *Mater. Struct.* 48 (2015) 3009–3021. doi:10.1617/s11527-014-0373-9.
 - [49] H.M. Künzeli, *Simultaneous Heat and Moisture Transport in Building Components One- and two-dimensional calculation using simple parameters .*, 1995. doi:ISBN v.3-8167-4103-7.
 - [50] A. Nielsen, *Bygningsmaterialers egenskaber: Definitioner og tabeller*, 1992.
 - [51] DTU Civil engineering, Porøsitet, densitet of kapillarsugning, DTU Byg, n.d.
 - [52] G. Christensen, T. Bunch-Nielsen, Indvendig efterisolering af ældre ydermure | BYG-ERFA, BYG-ERFA. (2009). <https://byg-erfa.dk/indvendig-efterisolering-aeldre-ydermure>.
 - [53] B. Blocken, M. Abuku, S. Roels, J. Carmeliet, Wind-driven rain on building facades: some perspectives, in: *EACWE 5*, 2009.
 - [54] J. Straube, Simplified Prediction of Driving Rain on Buildings : ASHRAE 160P and WUFI 4.0, *Build. Sci. Dig.* (2010) 1–16. file:///C:/Users/tekhan/Downloads/BSD-148_Simplified_Prediction_Driving_Rain.pdf.
 - [55] E.C.C. Choi, Velocity and Impact Direction of Wind-Driven Rain on Building Faces, *Proc. ICBES'97.* (1997) 465–472. www.bath.ac.uk/cwct/cladding_org/icbest97/paper69.pdf.
 - [56] H. Ge, R. Krpan, Field measurement of wind-driven rain on a low-rise building in the coastal climate of British Columbia, *Sci. Technol.* (2007).
 - [57] DS/EN ISO 15927-3 Hygrothermal performance of buildings - Calculation and presentation of climatic data - Part 3: Calculation of a driving rain index for vertical surfaces from hourly wind and rain data, 2009.
 - [58] G. Christensen, A.P. Koch, E.B. Møller, Indvendig efterisolering - ældre ydervægge og murværk, BYG-ERFA. (2015).
 - [59] B. Blocken, J. Carmeliet, On the accuracy of wind-driven rain measurements on buildings, *Build. Environ.* 41 (2006) 1798–1810. doi:10.1016/j.buildenv.2005.07.022.
 - [60] B. Blocken, J. Carmeliet, Overview of three state-of-the-art wind-driven rain assessment models and comparison based on model theory, *Build. Environ.* 45 (2010) 691–703. doi:10.1016/j.buildenv.2009.08.007.
 - [61] N. Sahal, M. a. Lacasse, Water entry function of a hardboard siding-clad wood stud wall, *Build. Environ.* 40 (2005) 1479–1491. doi:10.1016/j.buildenv.2004.11.019.
 - [62] M. Abuku, B. Blocken, S. Roels, Field measurement and numerical analysis of wind-driven rain absorption and evaporation on building facades, *Building.* 32 (2009).
 - [63] A.N. Karagiozis, M. Salonvaara, A. Holm, H. Künzeli, Influence of Wind-Driven Rain Data on Hygrothermal Performance, *Eighth Int. IBPSA Conf.* (2003) 627–634.

-
- [64] A. Nicolai, J. Grunewald, Delphin 5 User Manual and Program Reference, Program. (2006).
- [65] M. Abuku, B. Blocken, S. Roels, Moisture response of building facades to wind-driven rain: Field measurements compared with numerical simulations, *J. Wind Eng. Ind. Aerodyn.* 97 (2009) 197–207. doi:10.1016/j.jweia.2009.06.006.
- [66] M. Morelli, S. Svendsen, Investigation of interior post-insulated masonry walls with wooden beam ends, *J. Build. Phys.* 36 (2012) 265–293. doi:10.1177/1744259112447928.
- [67] M. Morelli, T.R. Nielsen, G.A. Scheffler, S. Svendsen, Internal Insulation of Masonry Walls with Wooden Floor Beams in Northern Humid Climate, *Therm. Perform. Exter. Envel. Whole Build. XI Int. Conf.* (2010).
- [68] J. Macmullen, Z. Zhang, E. Rirsch, H. Nath, N. Bennett, Brick and mortar treatment by cream emulsion for improved water repellence and thermal insulation, *Energy Build.* 43 (2011) 1560–1565. doi:10.1016/j.enbuild.2011.02.014.
- [69] H. Mayer, Masonry Protection with Silanes, Siloxanes and Silicone Resins, *Surf. Coatings Int.* 81 (1998) 89–93.
- [70] Sika, Refurbishment: Sika Technology and Concepts for Hydrophobic Impregnations, Zurich, 2015. https://www.sika.com/dms/getdocument.get/f234bf04-fb9b-39ea-9ed9-d0913f239079/technology_hydrophobic_impregnations.pdf.
- [71] E. Charola, Water-Repellent Treatments for Building Stones, *J. Preserv. Technol. Technol.* 26 (1995) 10–17. <http://www.jstor.org/stable/1504480>.
- [72] H.R. Trechsel, M.T. Bomberg, *Moisture Control in Buildings: The Key Factor in Mold Prevention*, 2nd ed., ASTM International, 1994. http://books.google.com/books?id=_pc6X3yvYsIC&pgis=1.
- [73] M. Guizzardi, D. Derome, R. Vonbank, J. Carmeliet, Hygrothermal behavior of a massive wall with interior insulation during wetting, *Build. Environ.* 89 (2015) 59–71. doi:10.1016/j.buildenv.2015.01.034.
- [74] R.P.J. Van Hees, The performance of surface treatments for the conservation of historic brick masonry, in: *Proc. CIB World Build. Congr. Gaevle, Sweden, 7-12 June 1998*, 1998.
- [75] F. Slapø, T. Kvande, N. Bakken, M. Haugen, J. Lohne, Masonry's Resistance to Driving Rain: Mortar Water, *Buildings* 7 (2017) 70–86. doi:10.3390/buildings7030070.
- [76] J. Engel, P. Heinze, R. Plagge, Adapting Hydrophobizing Impregnation Agents to the Object, *Restor. Build. Monum.* 20 (2014) 1–8. doi:10.12900/RBM14.20.6-0029.
- [77] S. Couto, T.D. Goncalves, J.M.G. Lopes, Drying of Red Ceramic Brick. The effect of five Silicone-based Water-Repellent Treatments., in: *Hydrophobe VI. 6th Int. Conf. Water Repel. Treat. Build. Mater.*, 2011: pp. 81–92.
- [78] B. Lubelli, R.P.J. Van Hees, Evaluation of the Effect of Nano-Coatings with Water Repellent Properties on the Absorption and Drying Behaviour of Brick, *136* (2011) 125–135.
- [79] T. Odgaard, S.P. Bjarløv, C. Rode, Influence of hydrophobation and deliberate thermal bridge on hygrothermal conditions of internally insulated historic solid masonry walls with built-in wood, *Energy Build.* 173 (2018) 530–546. doi:10.1016/j.enbuild.2018.05.053.

-
- [80] P. Kloda, Computational investigation of moisture problems related to internal insulation, DTU, 2017.
- [81] E. Biseniece, R. Freimanis, R. Purvins, A. Gravelins, A. Pumpurs, A. Blumberga, Study of Hygrothermal Processes in External Walls with Internal Insulation, *Environ. Clim. Technol.* 22 (2018) 22–41. doi:10.1515/rtuect-2018-0002.
- [82] J. Zhao, R. Plagge, A. Nicolai, J. Grunewald, Stochastic study of hygrothermal performance of a wall assembly — The influence of material properties and boundary coefficients, *HVAC R Res.* 17 (2011). <http://www.tandfonline.com/doi/abs/10.1080/10789669.2011.585421>.
- [83] A.H. Holm, H.M. Künzle, The influence of Measurement Uncertainties on the Calculated Hygrothermal Performance, in: *Insul. Mater. Test. Appl. 4th Vol. Astm Spec. Tech. Publ.*, American Society for Testing and Materials, 2002: pp. 335–347.
- [84] H. Hens, *Building Physics - Heat, Air and Moisture. Fundamentals and Engineering Methods with Examples and Exercises*, Ernst & Sohn, A Wiley Company, 2007.
- [85] G.A. Scheffler, Validation of hygrothermal material modelling under consideration of the hysteresis of moisture storage, Dresden University of Technology, 2008.
- [86] J. Zhao, R. Plagge, N.M. Ramos, M.L. Simoes, J. Grunewald, Application of clustering technique for definition of generic objects in a material database, *J. Build. Phys.* 39 (2015) 124–146. doi:10.1177/1744259115588013.
- [87] J. Zhao, R. Plagge, N.M.M. Ramos, M.L. Simões, J. Grunewald, Concept for development of stochastic databases for building performance simulation - A material database pilot project, *Build. Environ.* 84 (2015) 189–203. doi:10.1016/j.buildenv.2014.10.030.
- [88] E.B. Møller, Robust internal thermal insulation of historic buildings - D2.1, 2018. <https://www.ribuild.eu/work-packages>.
- [89] EU, Climate for Culture, (2014). <https://www.climateforculture.eu/>.
- [90] B. Blocken, Guidelines for wind, rain and wind-driven rain measurements at test-building sites, (2004).
- [91] H. Sandholdt, D. Dysted, Experimental and theoretical investigation of Interior insulations of solid brick walls with foam concrete and other silicate based materials, 2015.
- [92] D. Niels Hansen, Hvad kan du forvente, når DMI varsler skybrud?: DMI, (2015). <https://www.dmi.dk/nyheder/arkiv/nyheder-2015/05/hvad-kan-du-forvente-naar-dmi-varsler-skybrud/> (accessed March 21, 2017).
- [93] H. Kaaris, By og Byg Dokumentation 048, Klimasimulatorer. Teknisk dokumentation for accelereret ældning, perioden 1994-2002, 2003.
- [94] R. Hendrickx, Using the Karsten tube to estimate water transport parameters of porous building materials, *Mater. Struct.* (2012) 1–12. doi:10.1617/s11527-012-9975-2.
- [95] N.F. Jensen, S.P. Bjarløv, C. Rode, T.R. Odgaard, Hygrothermal assessment of internally insulated solid masonry walls fitted with exterior hydrophobization and deliberate thermal bridge, *Ce/Papers.* 2 (2018) 79–87. doi:10.1002/cepa.868.

-
- [96] H. Viitanen, M. Krus, T. Ojanen, V. Eitner, D. Zirkelbach, Mold risk classification based on comparative evaluation of two established growth models, *Energy Procedia*. 78 (2015) 1425–1430. doi:10.1016/j.egypro.2015.11.165.
- [97] U.K. Deb Nath, V. Chiu, H. Ge, Field measurements of wind-driven rain on mid-and high-rise buildings in three Canadian regions, *Build. Environ.* 116 (2017) 228–245. doi:10.1016/j.buildenv.2017.02.016.

Appended papers

- A **Paper I:** Long term in situ measurements of hygrothermal conditions at critical points in four cases of internally insulated historic solid masonry walls
- B **Paper II:** Performance of hydrophobized historic solid masonry – experimental approach
- C **Paper III:** The effects of wind-driven rain on hygrothermal performance of solid masonry walls with internal insulation
- D **Paper IV:** Material characterization models and test methods for historic building materials
- E **Paper V:** Moisture transport properties of brick – comparison of exposed, impregnated and rendered brick
- F **Paper VI:** Correlation between certain material parameters in bricks

Appendix A

Paper I

**Long term in situ measurements of hygrothermal conditions at critical points in
four cases of internally insulated historic solid masonry walls**



Long term in situ measurements of hygrothermal conditions at critical points in four cases of internally insulated historic solid masonry walls



Tessa Kvist Hansen^{a,*}, Søren Peter Bjarløv^a, Ruut Hannele Peuhkuri^b, Maria Harrestrup^c

^aTechnical University of Denmark, Department of Civil Engineering, Brovej 118, Kongens Lyngby 2800, Denmark

^bAalborg University, Danish Building Research Institute, A. C. Meyers Vænge 15, Copenhagen SV 2450, Denmark

^cEkolab, Vestergade 48H, 2. tv, 8000, Aarhus C, Denmark

ARTICLE INFO

Article history:

Received 5 January 2018

Revised 4 April 2018

Accepted 1 May 2018

Available online 8 May 2018

Keywords:

Internal insulation

In situ measurements

Hygrothermal conditions

Mould index

ABSTRACT

In heritage buildings with solid masonry walls, where external insulation is not an option, insulating internally is an alternative way to improve indoor climate and reduce energy consumption and heat loss through external walls. This study presents results from hygrothermal measurements performed in four different buildings in Denmark where internal insulation has been installed. The buildings are all heritage buildings from 1877–1932 and of solid masonry walls. The insulated façades differ in orientation, surface treatments, location, and insulation system. The insulation materials used are phenolic foam and polyurethane (PUR) foam, with calcium silicate channels in a grid of 40 × 40 mm. Measurement results and hygrothermal assessments indicate that a vapour barrier does not contribute positively to the performance of the system and the more vapour open, the better performance on solid masonry. However, the performance is highly dependent on other parameters like insulation thickness and surface treatment, and above all: the external hygrothermal loads. Therefore, before the application of internal insulation, every case should be carefully assessed in order to find the most suitable solution with regards to both thermal and hygrothermal performance.

© 2018 Elsevier B.V. All rights reserved.

1. Introduction

As society's urge for reduction of energy consumption is on the rise, so is the need for energy retrofitting measures to be implemented in the existing building stock. The European building stock itself accounts for 40% of European energy consumption [1]. Also, more than 40% of European residential buildings were built prior to 1960 [2], thus being prior to any attention being given to energy consumption, including heat loss through external walls in cold and temperate climates. Thermal insulation is a natural measure in order to reduce the heat loss through the building envelope. Thermal insulation does not only reduce the energy demand for heating, but also provides a better indoor environment in regards to thermal comfort, utilization of indoor space, and indoor air quality [3]. External insulation is usually the moisture safest and most efficient method for reduction of heat transfer through the external walls, as it provides the existing construction with protection from the external environment and eliminates thermal bridges [4–9]. This is however not possible in many historic buildings, as the façades are either preservation worthy, or of too much cultural and

aesthetic value, to change the exterior aesthetics. Therefore, internal insulation is introduced in these cases. Internal insulation however introduces several risks to the existing construction, as the hygrothermal conditions in the original construction are changed. As a result, the risk of interstitial condensation is increased [10–12], and the drying potential inward is reduced as the permeability is reduced by the insulation [11,13,14]. The increased risks of high moisture in the wall, inevitably leads to an increased risk of mould growth [15], and decay of the existing wood embedded in the structure. Furthermore, as a result of reduced temperature and drying potential of the existing wall, the risk of frost damage to the surface is also increased [9,10,15,14]. Internal insulation should thus not be installed without considerations to the building physics aspects. It might not be possible to achieve the desired *U*-value, or the desired heat loss reductions, but given the risks involved, it is far more feasible in the long run, to implement a moisture safe solution.

There are several types of insulation marketed for internal insulation [11], including capillary active and hydrophilic insulation materials [8,10,16,17], and traditional hydrophobic insulation materials including a vapour barrier. Internal insulation systems on the market can be separated into three groups based on their basic properties: 1) capillary active and vapour open, 2) vapour open

* Corresponding author.

E-mail addresses: tekhau@byg.dtu.dk (T.K. Hansen), spba@byg.dtu.dk (S.P. Bjarløv).

<https://doi.org/10.1016/j.enbuild.2018.05.001>
0378-7788/© 2018 Elsevier B.V. All rights reserved.

and 3) vapour tight systems. Capillary active systems have the advantage of a high moisture buffering capacity, yielding the possibility of redistributing absorbed moisture for evaporation [18]. The capillary active systems are also vapour open. Vapour open systems allow transport of water vapour in the construction, but the risk of interstitial condensation increases as moist indoor air reaches the cold external wall. A vapour open system can be combined with a smart vapour retarder, whose vapour resistance varies depending on the relative humidity [19]. A high vapour resistance in cool periods would prevent interstitial condensation, and a reduced vapour diffusion resistance can allow drying of the wall. Vapour tight systems completely inhibit moisture transfer through the insulation, preventing vapour from diffusing through the insulation and condensing on the external wall. All these systems naturally have pitfalls; the capillary active system will lose its ability for moisture redistribution if there is not full contact between the materials in the system. Also, no organic material should exist at the cold surface of the insulation [20] and for systems with vapour barriers, proper installation and complete tightness is needed. Furthermore, these systems leave the wall extra sensitive to external moisture loads, as inward drying is limited.

There has been increasing focus on internal insulation in heritage buildings for the past few years; a limited number of studies with long-term in situ measurements are available. Orlik-Kozłowski et al. [11] found no critical moisture conditions in two cases of internal insulation of expanded polystyrene and lightweight aerated concrete on a solid brick wall. However, measurements were performed for only 6 months, and furthermore, there was an external curtain wall, protecting the construction from external moisture loads etc. Klöseko et al. [13,21] on the other hand, obtained high relative humidities in four cases of internal insulation on a brick wall during a 9 month study. The four materials tested in this case include; calcium silicate 50mm, aerated concrete (AAC) 60mm, polyurethane foam (PUR) with capillary active calcium silicate channels in a grid of 40 × 40 mm (IQ-Therm) 50mm and polyisocyanurate foam (PIR) 30mm. Calcium silicate proved the best performance in regard to moisture performance, however calcium silicate also has the highest thermal conductivity. Harrestrup et al. [22] monitored a case of internal insulation of 40 mm aerowolle on a heritage brick building, and the effect of intentional thermal bridges above and below supportive wooden beams. They found that leaving a 200mm uninsulated gap above and below the beams yielded a lower risk of mould growth, however this was found to be very dependent on the orientation and the thickness of the existing wall. Toman et al. [8] ran a long-term study of 4 years, on a 19th century building, with solid brick walls, external render and paint, insulated with a hydrophilic mineral wool insulation board, and no vapour barrier, however, a vapour retarder was placed on the interior surface of the existing wall. The study showed excellent hygrothermal conditions and no risk of interstitial condensation at any point in time during the 4 year period. In a recent study by Hamid et al. [23], a similar study was performed with in situ measurements in solid masonry with internal insulation, and validated simulation models. The study emphasized the importance of the orientation due to the significant influence of wind driven rain, and solar driven vapour. Furthermore, the study emphasized the significant risk of mould growth at the wall-insulation interface, and the cold side of an integrated vapour barrier given the presence of biological material.

This study aims to add to the knowledge of internal insulation systems by investigating the success or failure of two different insulation systems and thicknesses on four different case buildings with long-term monitoring in real climate conditions. Initially the measurements were initiated in order to gain empirical data for research of internal insulation of historical brick buildings with regard to moisture performance of the wall and beam ends. Based

on the measured data, and hygrothermal simulations performed in Delphin 5.8 [24], it is sought to gain an understanding of how internal insulation can safely be applied.

2. Method

The presented study is built around long-term monitoring of hygrothermal performance of historic building façades retrofitted with internal insulation. Monitoring results are assessed with mathematical risk models and with 1D hygrothermal numerical simulations. In the case of Meinungsgade, the 1D simulation has also been verified by 2D simulations.

2.1. Insulation systems

Two different insulation systems with different insulation thicknesses are studied. In total, four cases are presented. Both insulation materials in this study are highly insulating rigid foams, however they are initially not vapour permeable or capillary active potentially trapping possible moisture accumulation. One of the systems included in this study, system 2, has been provided with channels of calcium silicate with the purpose of enabling capillary transport of possible condensate, as well as leaving the system vapour permeable. The complete insulation systems in this study are set up as fully adhered to the existing wall and the systems are described in Table 1;

The two systems have thermal conductivities of 0.02 W/mK and 0.037 W/mK for system 1 and system 2 respectively. In all cases, the insulation is applied to a 1½-brick (360mm) thick solid masonry wall with internal rendering. The *U*-values are estimated based on an assumed identical brick type and the theoretical *U*-value reductions in each are displayed in Table 2 together with an overview of the presented cases. Each case is elaborated in Sections 2.2.1–2.2.4.

2.2. In situ measurements and case buildings

In all cases, temperature and relative humidity sensors of the type Rotronic HygroClip2 (accuracy ± 0.8% RH, ± 1 K, up to 90% RH) have been installed at the interfaces between the original wall, and the insulation, as well as at the end of the beams. The case of Thomas Laubs Gade however, only has sensors at the wall-insulation interface. These are considered the areas of interest, as this is where potential risks concerning damaging moisture can arise. At the interfaces, there is an increased risk of interstitial condensation, which produces e.g. the risk of mould growth. The same goes for the beam ends with an increased risk of wood rot, as the drying potential and temperature are reduced when internal insulation is applied, and thus increasing the relative humidity. The sensors at the interfaces are placed in either existing joints, or purposely designed notches in the existing wall. Sensors behind beam ends are placed through holes drilled in the beam, and the holes then sealed with foam. Examples of sensor locations can be seen in Fig. 1.

The sensors are set to log every 1 minute; and hourly averages have been generated and will be presented in the results section. The data was acquired by an online system provided by the company Electromec Engineering Service. The test buildings presented in this paper, are all multistorey residential brick buildings from 1877–1932, built in a traditional Danish building style, with wooden beams and wooden lath to support intermediate floors. The four cases are located in Denmark; three of them in Copenhagen, and one in Haderslev.

2.2.1. Ny Allegade 10, Haderslev

The case building in Haderslev is a 2 story building from 1932, with a bare brick surface, as seen in Fig. 2. In the spring of 2015,

Table 1
Internal insulation systems used in the presented cases.

	Insulation material	Complete system
System 1	Phenolic foam boards (Kingspan Kooltherm K17 insulated plasterboard) $\lambda=0.020\text{W/mK}$	Integrated in Kingspan K17 boards Glue mortar (2–5mm notched trowel) Glass tissue Phenolic foam (25 or 60mm) Composite foil vapour barrier ($s_d=24\text{m}$) 12.5 mm gypsum based plasterboard Skim coating (3mm) Paint
System 2	Polyurethane (PUR) foam with calcium silicate channels in a grid of 40X40mm (IQ-Therm) $\lambda=0.037\text{W/mK}$	IQ-Fix glue mortar (2–5mm notched trowel) IQ-Therm PUR foam (30 or 80mm) IQ-Top (porous light mortar) IQ-Tex (glass tissue) IQ-top (porous light mortar, 10–15mm total) IQ-Fill (fine putty) Diffusion open paint (e.g. IQ-Paint)

Table 2
Overview of the four cases including the calculated U-values.

Case	Year of construction	Floor + orientation	Ext surface	Insulation system (see Table 1) + thickness	Theoretical retrofitted U-value [$\text{W/m}^2\text{K}$]	Theoretical U-value reduction [%]
Ny Allegade	1932	2nd, East + South	Blank	2, 80 mm	0.35	75
Meinungsgade	1877	5th, South + Southwest	Blank	1, 60 mm	0.27	81
Kildevældsgade	1905	4th, North	Render + paint	1, 25 mm	0.50	64
Th. Laubs Gade	1899	4th, East	Blank	2, 30 mm	0.65	53



Fig. 1. Sensor locations. From left to right: sensor in existing joint, purposely designed notch and in hole through beam end.

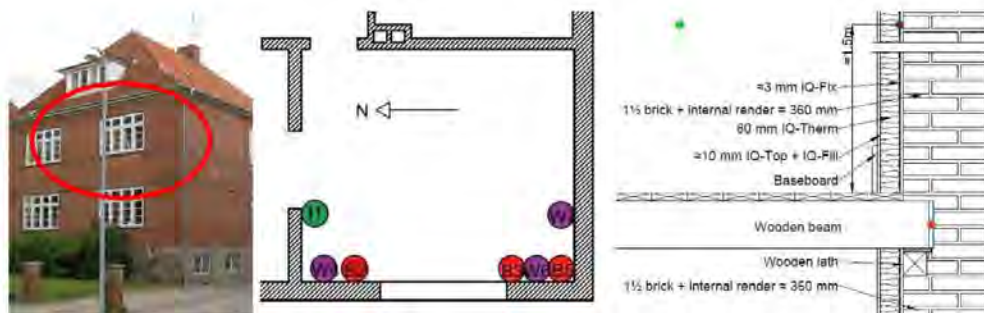


Fig. 2. Left to right: Ny Allegade facade with indication of insulated walls, sensor placement on floor plan, and construction with sensor placement.

80 mm of system 2 (30 mm at spandrels) was installed on the west and south facades of both the 1st and 2nd floor. Fig. 2 also displays the sensor locations on the floor plan, and construction plan. Sensor I1 represents interior conditions, sensors W4, W6 and W7 represent conditions at the interface, and sensors B2, B3 and B5 represent conditions behind beam ends in the west orientated façade.

2.2.2. Meinungsgade 1, Copenhagen

This case building is from 1877, and the measurements are performed on the south and southwest walls on the 5th floor. During

the winter of 2015 the walls on the 4th and 5th floor, were insulated with 60 mm of system 1 (20 mm for spandrels). Furthermore, a gap of 20 cm was left above the floor, for the creation of an intentional thermal bridge; the construction is seen in Fig. 3. A floor plan with indications of sensor locations is also seen in Fig. 3; sensor I1 represents interior conditions, sensors W2, W4 and W6 are placed at the interface; and sensors B3, B5 and B7 are behind the beam ends. Fig. 3 also displays the façade, and as it can be seen, there is no visible surface treatment.

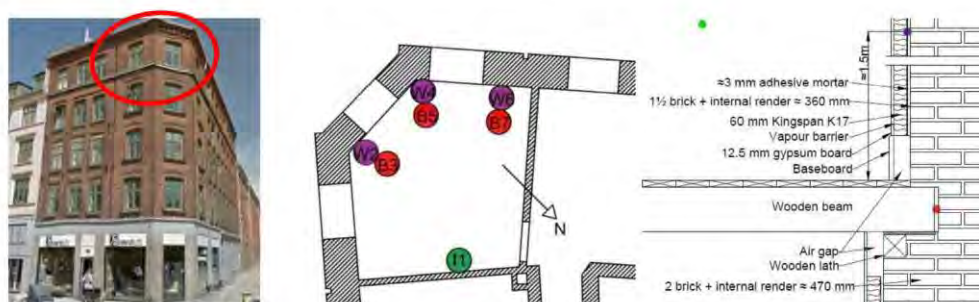


Fig. 3. left to right; Meinungsgade facade with indication of insulated walls, sensor placement on floor plan, and construction with sensor placement.

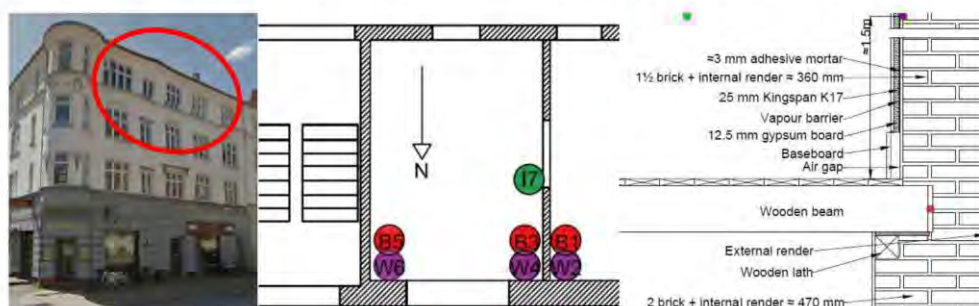


Fig. 4. left to right; Kildevældsgade facade with indication of insulated walls, sensor placement on floor plan, and construction with sensor placement.

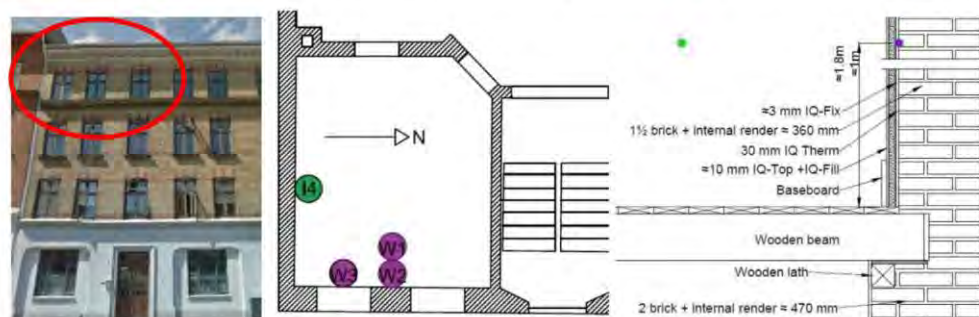


Fig. 5. left to right; Thomas Laubs Gade facade with indication of insulated walls, sensor placement on floor plan, and construction with sensor placement.

2.2.3. Kildevældsgade 69, Copenhagen

The case on Kildevældsgade is a building from 1905, and has a rendered facade, as can be seen in Fig. 4. 25 mm of system 1 (20 mm for spandrels) was installed in March 2015 on the northern facade of the 3rd floor. As indicated in Fig. 4, a 20 cm air gap above the beam was included for the intention of creating a thermal bridge, thus increasing the temperatures at the beam end. Fig. 4 also displays a floor plan with an indication of sensor locations. Sensor I7 represents interior conditions, while sensors W2, W4 and W6 represent conditions at the wall-insulation interface, and sensors B1, B3 and B5 represent conditions behind the beam ends. Note that the floor beneath has not been insulated, and thus higher temperatures at the beam ends are expected compared to if both walls were insulated.

2.2.4. Thomas Laubs Gade 5, Copenhagen

The case on Thomas Laubs Gade is a building from 1899 with an exposed brick surface, as seen in Fig. 5. The eastern facade on the 3rd floor was in the fall of 2015 insulated with 30 mm system 2 except the spandrels which were insulated with 50 mm calcium silicate (SLP CS 50). Fig. 5 also illustrates the floor plan with indication of sensor placements, and the construction. In this case there are no sensors in the beam ends. Sensor I4 presents the interior climate readings; sensor W3 is placed behind the calcium silicate in the spandrels, whereas sensor W1 is placed above sensor W2 at the interface between the insulation and the external wall. Unfortunately sensor W3 lost all contact during the summer of 2016. And all sensors lost connection for a period of about 3 months, March 2017 – June 2017.

Table 3
Mould growth index classifications [25].

Mould index (M)	Description of growth rate
0	No growth, spores not activated
1	Small amounts of mould on surface (microscope), initial stages of local growth
2	Several local mould growth colonies on surface (microscope)
3	Visual findings of mould on surface, <10% coverage, or, <50% coverage of mould (microscope)
4	Visual findings of mould on surface, 10–50% coverage, or, >50% coverage of mould (microscope)
5	Plenty of growth on surface, >50% coverage (visual)
6	Very heavy and tight growth, coverage around 100%

2.3. Risk assessment model – mould index

For assessment of risks associated with the altered hygrothermal conditions following installment of internal insulation, a risk assessment model for mould growth is introduced. The assessment is performed on measured data at the wall-insulation interface from the four case studies. The risk assessment model provides a basis for comparison of the various hygrothermal conditions and associated risks. However, the risk assessment models – like the one used – should only be used relatively to give an indication for which solution gives a higher or lower potential for a risk.

In order to assess the mould risks in these cases, an improved mould model described in [25] and based on the original VTI mould growth model [26], was implemented. This model is one of the most acknowledged mould growth prediction models and takes benefit of the time dependence of the favourable mould growth conditions. A review of different mould models is found e.g. in [27,28]. The original model was developed for prediction of mould growth on wooden surfaces, whereas the improved model takes sensitivity classes into consideration. The sensitivity classes are based on experimental results on various building materials [25]. The mould model can be implemented for the wall-insulation interfaces, however the mould growth intensity may be less, due to the limited air flow at the interface contra at the surface [29]. In the current study, the sensitivity class is set to medium resistant, corresponding to “cement or plastic based materials” and a relatively low decline (0.25) during unfavourable growth conditions was implemented. Furthermore, the factors surface quality, SQ, and wood species, W, are included in the model and set to 0 for non-wood materials, and pine respectively. The mould index, M , quantifies the mould growth rate in a range from 0–6, elaborated in Table 3.

The mould model is described in Eq. (1), and the factors k_1 and k_2 represent intensity of growth and moderation of growth intensity in the late stage respectively. For determination of k_1 and k_2 , time factors are used; $t_{M=1}$ represents the time needed for the growth to start (when M reaches 1), and $t_{M=3}$ represents the time needed for the material to reach a mould index of 3. Pine is the reference material, and why it is included in the calculations. M_{\max} , the maximum mould index, depends on conditions and sensitivity class, in which the constants A , B and C are defined [25]. For the medium resistant sensitivity class, the parameters are given as: $A=0$, $B=5$, and $C=1.5$. RH_{crit} is the minimum limit to start the mould growth, dependent on the temperature [26] and the sensitivity class:

$$\frac{dM}{dt} = \frac{1}{7 \cdot e^{-0.68 \ln(T)} - 13.9 \ln(RH) + 0.14W - 0.33SQ + 66.02} \cdot k_1 k_2 \quad (1)$$

$$k_1 = \begin{cases} \frac{t_{M=1, \text{pine}}}{t_{M=1}}, & M < 1 \\ 2 \cdot \frac{t_{M=3, \text{pine}} - t_{M=1, \text{pine}}}{t_{M=3} - t_{M=1}}, & M > 1 \end{cases} \quad (2)$$

$$k_2 = \max \left\{ \begin{array}{l} 1 - e^{2.3 \cdot (M - M_{\max})} \\ 0 \end{array} \right. \quad (3)$$

$$M_{\max} = A + B \cdot \frac{RH_{\text{crit}} - RH}{RH_{\text{crit}} - 100} - C \cdot \left(\frac{RH_{\text{crit}} - RH}{RH_{\text{crit}} - 100} \right)^2 \quad (4)$$

2.4. Hygrothermal simulation

1D simulations of the hygrothermal conditions in the wall-insulation interface of each of the four cases were carried out in Delphin 5 in order to study the long term performance of the specific cases as well as other variations of the studied systems. The models were first validated relative to measured data, yielding the possibility of forecasting the hygrothermal behaviour of the cases in a longer perspective. The models for validation were built up as the constructions shown in Figs. 2–5. For simplification, the preliminary simulations for initial validation of the 1-dimensional models were performed on both brick and lime mortar constructions, and the mortar wall yielded better results in regard to validation, as well as closer to results gained from a 2D-simulation. Therefore the following simulations are performed on walls consisting of lime mortar. In addition, local weather data from Copenhagen and Haderslev from March 2015–March 2017, as well as measured indoor conditions, were used for the validations. Indoor boundary conditions were set to constant conditions of 22 °C and 55% RH for the future predictions. Material data for all materials was imported from the Delphin material library, with the exception of phenolic foam, which is based on extruded polystyrene board from the Delphin material database, altered in accordance to generic material parameters for phenolic foam and product specific information given by the manufacturer [30]. Material parameters are presented in Table 4. Thus the validation was achieved by constructing the 1D model with the correct layer thicknesses and assumptions in regards to the existing materials, and the climate files being similar to the local climate. Furthermore, assumptions on various exchange coefficients, including the rain exposure coefficients and absorption coefficient of the surface in regards to short wave radiation. As 1D simulations are performed, it should be noted that insulation system 2 is assumed homogenized despite the calcium silicate channels, however the material has been defined in the material database as one material. Hence the result may deviate from reality on this basis. In the cases of insulation system 1, two versions of each case have been simulated, as explained in Section 3.3.

After model validation, 10 year simulations were performed based on 10 years of forecasted weather data for 2020–2050 in Øster-Ulslev in Denmark, from the EU project Climate for Culture [31]. Finally, variations of each case were simulated in order to study the effect of insulation thickness (based on product specific thicknesses), material and rendered façade surface. The variations are described in Table 5 below.

Table 4
Material parameters for hygrothermal simulations in Delphin 5.

	Dry density ρ [kg/m ³]	Thermal conductivity λ [W/mK]	Water uptake coefficient A_w [kg/m ² s ^{0.5}]	Water vapour diffusion resistance factor μ [-]	$S_{d, \text{value}}$ [m]
External render	1570	0.7	0.18	11	
Existing wall	1800	0.82	0.13	12	
Adhesive/glue mortar - system 1	830	0.16	0.0031	13	
Adhesive/ glue mortar - system 2	1313	0.50	0.0061	19	
Insulation material - system 1	35	0.020	$8 \cdot 10^{-6}$	dif. tight: 583 dif. open: 1	
Insulation material - system 2	49	0.037	0.013	27	
Vapour barrier					$S_{d, \text{diff. open}}: 0.5$ $S_{d, \text{diff. tight}}: 100$
Top layer - system 1	850	0.2	0.28	10	
Top layer - system 2	1269	0.48	0.22	14	

Table 5
Simulation variations of each case.

	Kildevældsgade	Meinungsgade	Ny Allegade	Thomas Laubs Gade
Original	Paint + render 25 mm system 1	No render 60 mm system 1	No render 80 mm system 2	No render 30 mm system 2
Variation 1 Thickness	Paint + render 60 mm system 1	No render 30 mm system 1	No render 30 mm system 2	No render 80 mm system 2
Variation 2 Render	No render 25 mm system 1	Paint + render 60 mm system 1	Paint + render 80 mm system 2	Paint + render 30 mm system 2
Variation 3 Insulation system	Paint + render 30 mm system 2	No render 60 mm system 2	No render 80 mm system 1	No render 30 mm system 1

3. Results and discussion

3.1. In situ measurements

Measurements for each case are presented as hourly averages generated from minutely data. A relative humidity of 85% is considered the minimum relative humidity for initiation of mould growth during long term exposure for very medium resistant materials, e.g. concrete and glass wool [25], why this is considered the threshold value in the following paragraphs.

3.1.1. Ny Allegade, Haderslev, 80 mm system 2

Hourly averages of measurements performed are presented in Fig. 6. The relative humidities at both wall interfaces and cavities behind the beam ends are above 95% during the measurement period, with the exception of sensor B2. During the 2½ year measurement period, there is no indication of significantly reduced relative humidity in either the wall interfaces or behind the beam ends. It is a known fact that built-in moisture, due to the installation of internal insulation takes time to dry out, but after the first year the installation moisture from the glue mortar can be considered of no influence [29]. There is no observable difference in wall measurements on the west and south façades. The outlier, sensor B2 however, exhibits acceptable conditions below 80% relative humidity for the entire period. Sensor B2 is placed towards the middle of the wall, as opposed to B3 and B5, which may reduce the impact of driving rain in this position [32]. The temperature measurements however, also reveal higher temperatures at B2 during winter, thus increasing the drying potential. The higher temperature may indicate the placement of a hot water pipe or the like, or that the sensor is not placed at the end of the beam, but rather within the beam, and thus closer to the warmer interior conditions. Also, the beam end might be dryer than the cavity behind the beam, as the wood fibers of the beam end transport the moisture inwards. In these cases, the measurements in B2 are not representative and should be discarded. The measured interior conditions seem stable at 20 °C and seasonal variation of 30–70% RH. The interior conditions do not seem to effect the hygrothermal conditions in sensor locations, although temperature measurements in sensors resemble the interior temperature during summer seasons.

3.1.2. Meinungsgade, Copenhagen, 60 mm system 1

Generated hourly averages from measurements performed in Meinungsgade are represented in Fig. 7. For wall interfaces, sensors W2 and W4, it is seen that the relative humidity rarely exceeds 80%. It is seen that for warmer periods, the relative humidity resembles interior conditions, whereas the external moisture influences during winter are apparent, as the relative humidity increases. The integrated vapour barrier inhibits drying inwardly in the colder periods when the masonry becomes moist. The relative humidity at the wall interfaces fluctuates between 40–80% which is considered acceptable. In the first 2 years, sensor W6 generally exhibits higher relative humidity. This sensor is located by an indentation in the wall for the previous installation of a downspout. This indentation makes the wall thinner, thus the penetration of wind driven rain may reach closer to the sensor. The indentation furthermore limits the drying potential in form of both radiation and wind. Additionally, sensor W6 is placed in southwest orientation as opposed to south, as W2 and W4. This again contributes to more wind-driven rain and less sun at W6 compared to W2 and W4. The conditions behind the beam ends are rather high, 70–90%, during the first 2 years of measurements. For the last months of measurements, the relative humidity barely exceeds 80%. Neither weather data from Copenhagen or interior conditions indicate any obvious explanations for the 2-year drying period. The beam ends are embedded in the wall, so the external wall is thinner at the location behind the beam ends, thus leaving this area more exposed to external conditions, such as penetrating wind-driven rain. The intentional thermal bridges do not seem to have the desired effect; the temperature behind the beam ends is the same, or less than, the temperature at the wall interfaces. The temperature conditions show very similar results for all sensors. During summer, the temperatures resemble the interior conditions. This tendency also applies to the relative humidity measurements after the initial drying period.

3.1.3. Kildevældsgade, Copenhagen, 25 mm system 1

In the case of internal insulation installed in Kildevældsgade, the initial building moisture and successive drying out period is very apparent; see Fig. 8. In the first 6 months, the relative humidity is very high in the wall interface, sensors W2, W4, W6, and hereafter a seasonal dependency is apparent, but the relative humidity does not exceed 80%. During the course of measurements, sensor W6 exhibits a significantly faster decline and gen-

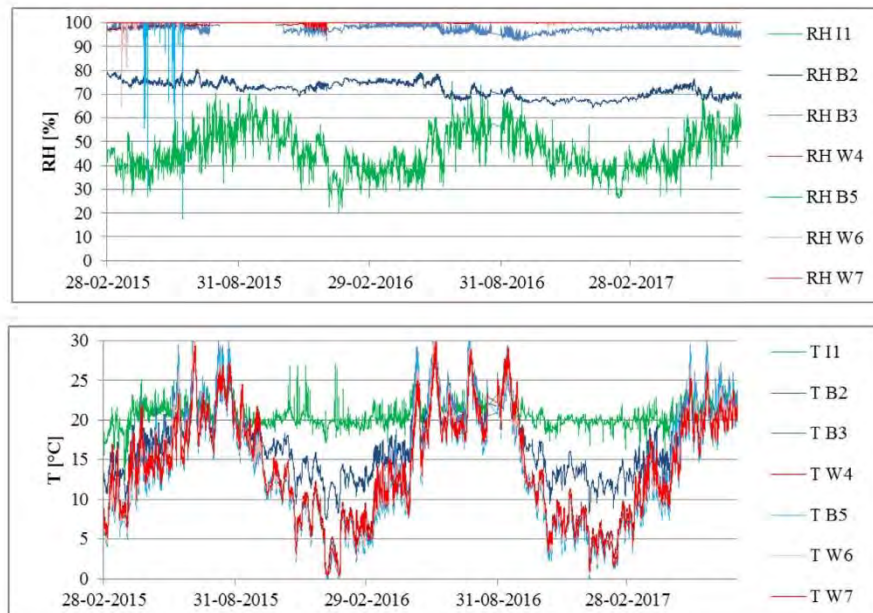


Fig. 6. Measured hygrothermal conditions measured in Ny Allegade (80 mm, system 2, western (W4, W6, B2, B3, B5) and southern (W7) façade). The blue nuances represent sensors behind the beam ends, whereas the red colors represent sensors at the wall-insulation interface.

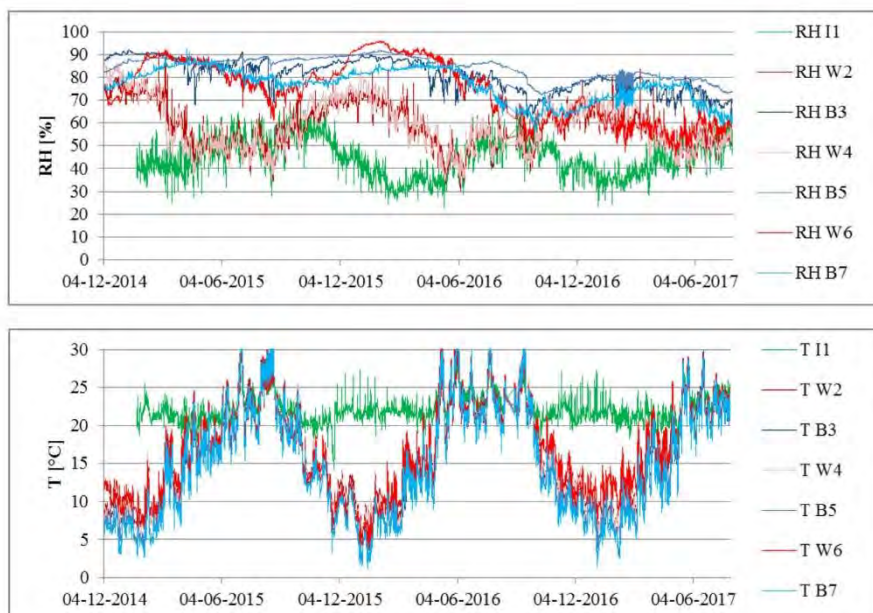


Fig. 7. Measured hygrothermal conditions in Meinungsgade (60 mm, system 1, southern (B3, W2) and southwestern (B5, B7, W4, W6) façade). The blue nuances represent sensors behind the beam ends, whereas the red colors represent sensors at the wall-insulation interface.

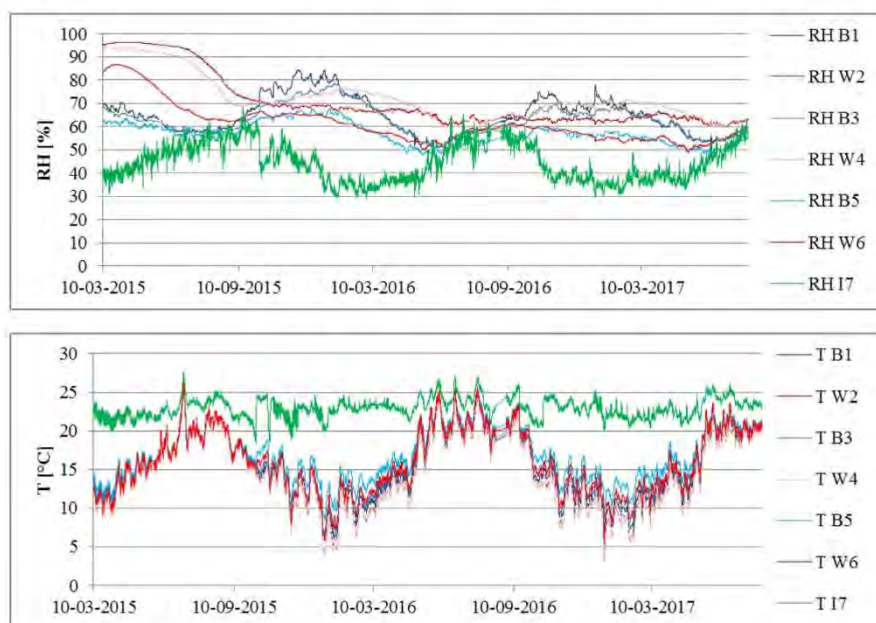


Fig. 8. Measured hygrothermal conditions in Kildevældsgade (25 mm, system 1, southern (B3, W2) and southwestern (B5, B7, W4, W6) façade). The blue nuances represent sensors behind the beam ends, whereas the red colors represent sensors at the wall-insulation interface.

erally lower relative humidity compared to the other wall sensors. There is a slightly higher temperature measured by W6, and by studying pictures from the installment of insulation, it is seen that hot water pipes are installed in the vicinity of sensor W6, increasing the drying potential in this area. The beam end sensors also do not exceed 80% relative humidity, with the exception of sensor B1 that exceeds 80% for shorter periods during the first winter. It is seen that sensor B5 has the lowest relative humidity, and again this can be explained by a slightly higher temperature, or possibly the location of the sensor not drilled all the way into the cavity behind the beam end. The temperature and relative humidity both behind the beam ends and at the wall-insulation interfaces resemble the interior conditions measured.

3.1.4. Thomas Laubs Gade, Copenhagen, 30 mm system 2

At Thomas Laubs Gade, the relative humidity is initially very high, due to installing the insulation with a wet glue mortar. Despite unreliable sensors and missing data, a decline of the relative humidity is seen, Fig. 9. During the 20 months of measuring however, the relative humidity still exceeds 80% in sensor W2, whereas sensor W1 seems to decrease to acceptable conditions. For the initial period, sensor W1 exhibits the highest relative humidity, but also the lowest temperature. This is the sensor placed below the window. The spandrels are thinner (one brick thick with render=240 mm) and thus this measuring point is more exposed to exterior conditions. It is seen that the temperatures measured at the wall-insulation interfaces resemble the interior conditions during summer seasons.

3.2. Hygrothermal assessment of the measurements – mould index

The assessment of the hygrothermal performance of the post insulated façades with damage model (mould Index) is presented graphically in this section. Furthermore, due to the expected in-

creasing uncertainty of the measured relative humidity, the assessment has been performed as well on measured data as +5% RH for relative humidity above 90% RH in each case. The results for +5% relative humidity are presented with dashed lines. The results for the damage models are presented in Fig. 10. The data from Thomas Laubs Gade is unfortunately insufficient for generation of mould model, due to the large data gaps, as seen in Fig. 9.

The basic alkaline conditions in the cementitious glue mortar, prevent mould growth for the first year of measurements, why these data have been excluded in the model calculations [29]. The calculated mould indexes are presented in Fig. 10. It is seen that at Ny Allegade the measurements from all sensors yield mould indexes above 1, thus the theoretical risk of mould growth exists, and the conditions can be considered unacceptable. There is no sign of decline, as the measured RH is so high. In these cases, the mould index peaks at 3.5 and stays there. At Meinungsgade it is seen that for the measured values, the mould growth is only initiated for measurements of sensor W6, however it never exceeds Mould Index 1, not even with the uncertainty factor included. Furthermore, the mould index in this sensor declines to 0 after a short period. At Kildevældsgade there is no indication of risk of mould growth from any of the measured data.

3.3. Hygrothermal simulations

The quality of simulation results depends highly on the input variables, and there are numerous unknown parameters estimated in the performed simulations, they include material parameters of the existing walls as well as climate data being from nearby weather stations, and not necessarily representing e.g. wind patterns at the exact locations. However validated models were made based on measured data, and the following projections were based on the validated models. In general, as also seen in Fig. 11, for the two cases of insulation with system 1 (phenolic foam), Kilde-

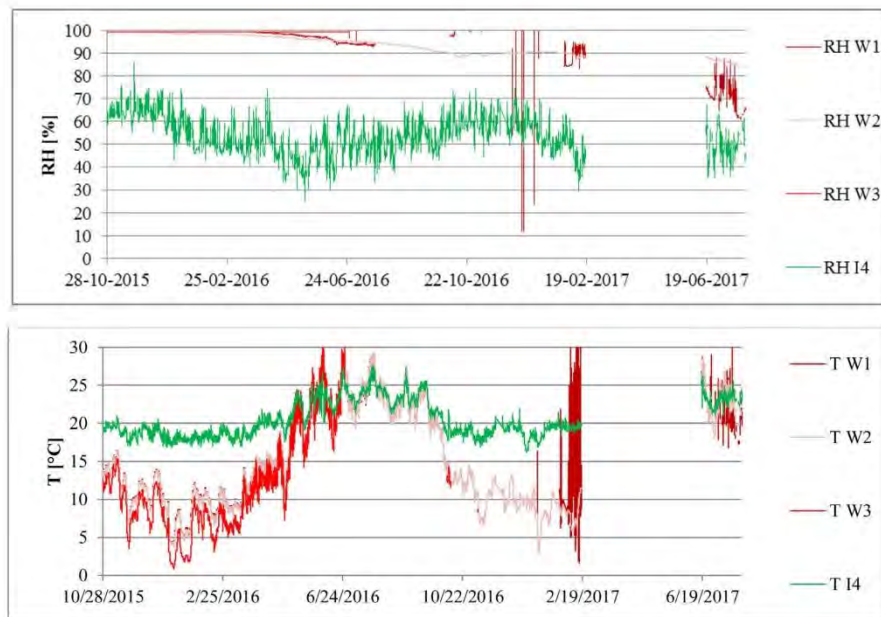


Fig. 9. Measured hygrothermal conditions in Thomas Laubs Gade (30 mm, system 2, eastern façade). The blue nuances represent sensors behind the beam ends, whereas the red colors represent sensors at the wall-insulation interface.

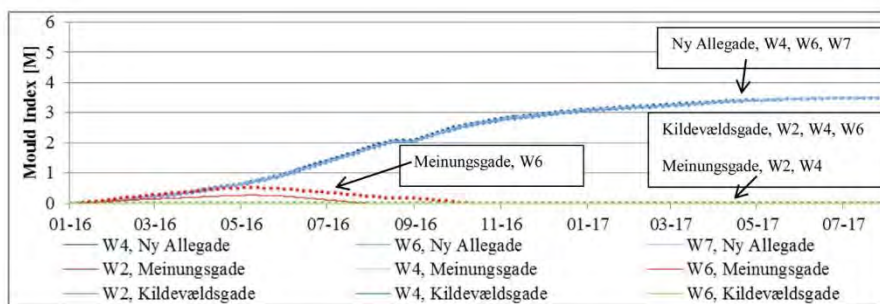


Fig. 10. Mould index for wall-insulation interfaces as a function of time. W: interface. Dashed lines represent cases where 5% uncertainty was added to measurements above 90% RH.

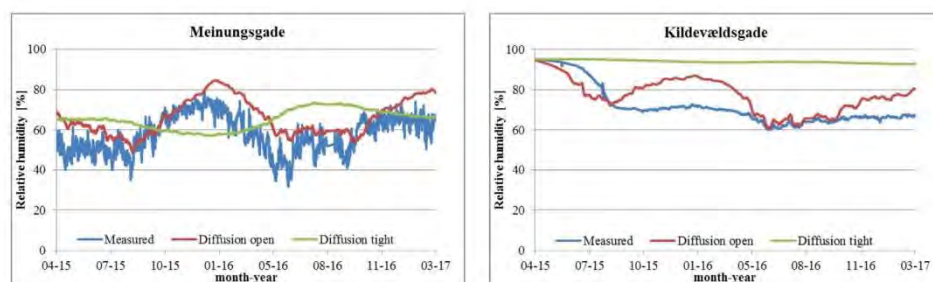


Fig. 11. Validation of cases with insulation system 1 were achievable when making the phenolic foam diffusion open and omitting the vapour barrier.

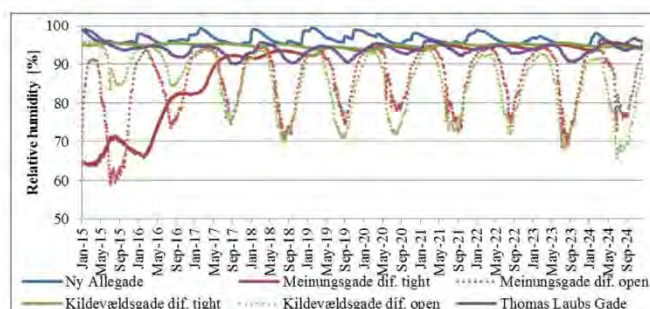


Fig. 12. 1-dimensional simulations for 10 years of each presented case at the wall-insulation interfaces. The dotted lines represent the diffusion open version of insulation system 1.

vældsgade and Meinungsgade, good validation results could not be achieved. Initially insulation system 1 was simulated as diffusion tight, as phenolic foam is diffusion tight, and furthermore the system includes a vapour barrier. These simulations generated very different moisture levels than the measured data in the interface between insulation and the existing wall. By implementation of a model without a vapour barrier and reduced water vapour diffusion resistance factor of the insulation to $\mu = 1.0$ better agreements were achieved, as seen in Fig. 11. The discrepancies in simulation results are assumed to be caused by the installation method. In both cases, the insulation systems were installed with a 20 cm gap left at the bottom of the wall, for an intentional thermal bridge in order to achieve higher temperatures at the beam ends. The vapour barrier, incorporated in the insulation boards, was discontinued at the bottom gap as well as joints. In addition, a notched trowel was used for the glue mortar, and likely not smoothed out. Thus the plates were not fully bonded and yielded the possibility of convection or vapour diffusion in air pockets at the interface. For the 1D hygrothermal simulations, this air movement was attempted to be incorporated in the models, by alterations of the vapour diffusion resistance of the phenolic foam and removal of the vapour barrier, as stated above. Thus the further simulations include both the diffusion tight (fully bonded plates) and the diffusion open (validated model) version of insulation system 1. Simulations indicate, that despite the vapour barrier, and diffusion tight phenolic foam, the system performs diffusion open in the measured cases presented. In regards to 1D simulation, the application method is critical to avoid air channels behind the plates and hence allowing convection and vapour diffusion. This was taken into account by alteration of material parameters, and the achieved validations are illustrated in Fig. 11. As it can also be seen in Fig. 11, the simulation results resemble measured data mostly for summer and fall periods, whereas the relative humidity seems to lie a bit higher in the simulations for the winter periods. This means, that at least the models present results that are on the safe side according to moisture risks. The same tendency was found by Hamid et al. [23].

10 year predictions for each case are represented in Fig. 12. All cases show unacceptable hygrothermal conditions ($RH > 80\%$) during the 10 years of simulations - with the exception of the diffusion open version of insulation system 1. The worst moisture conditions appear to be in winter periods for the cases of insulation system 2 and diffusion open system 1. The case with 80 mm of insulation system 2 (Ny Allegade) appears to show the worst performance, whereas the case with only 30 mm of system 2 insulation (Thomas Laubs Gade) appears to perform better during the 10 year period. Unacceptable conditions still apply however. The diffusion tight versions of Meinungsgade and Kildevældsgade, both insulated with system 1, show significantly less seasonal variation. The diffu-

sion open version of system 1 exhibits significantly more seasonal variations and only unacceptable conditions during winter periods.

In Fig. 13 the results from the parameter variations are presented for each case. In each case, the original model is presented in blue, the thickness variation in red, the external surface with/without render in green, and finally the variation between the insulation systems is depicted in purple. Kildevældsgade with system 2 insulation rather than system 1, is the only case that exhibits a tendency of reduced relative humidity during the 10 year period. For the cases of insulation system 1 (Meinungsgade and Kildevældsgade), it is apparent, that the diffusion open version yields better hygrothermal conditions at the interface.

The mould indexes for the four 10-year simulations are illustrated in Fig. 14. For both cases with insulation system 2 (Ny Allegade and Thomas Laubs Gade), the mould index quickly reaches a steady maximum value of 3.3 and 3 respectively, for all the variations implemented, and thereby presenting a high risk of visual findings of mould growth. As seen in the relative humidities displayed in Fig. 13, these two cases have continuously high relative humidities and minimal the seasonal variation thus leading to optimal mould growth criteria. The risk of mould growth is also apparent in both cases of insulation system 1. The risk of mould growth is significantly less, when insulation system 2 is applied to these cases. In the case of Meinungsgade, the largest display of the effects of the variations is seen. The addition of external render to the surface yields a higher mould index. This could be attributed to the reduction in drying potential from the sun and increased diffusion resistance on the southern façade, which is the most exposed to wind driven rain. The reduction of insulation thickness yields a slightly reduced mould index, which can be expected. It is also seen that the diffusion open version of system 1 yields more seasonal variation, and in general a lower risk of mould growth in the long run.

The impact of the parameter variations on the hygrothermal performance of the studied cases is summarized in Table 6. These observations can be summarized as follows: that increasing internal insulation thickness and choosing a vapour tight insulation system results in higher relative humidity in the interface between internal insulation and the original wall. Results from hygrothermal simulations however, should be considered cautiously; as seen they can present the relative effect of the various variations.

3.4. Discussion of the monitored and simulated results

Results from in situ measurements show the tendency of a larger success rate in cases of insulation system 1, whereas the simulations of the diffusion tight system 1 show the opposite tendency. These discrepancies can be explained by the way instal-

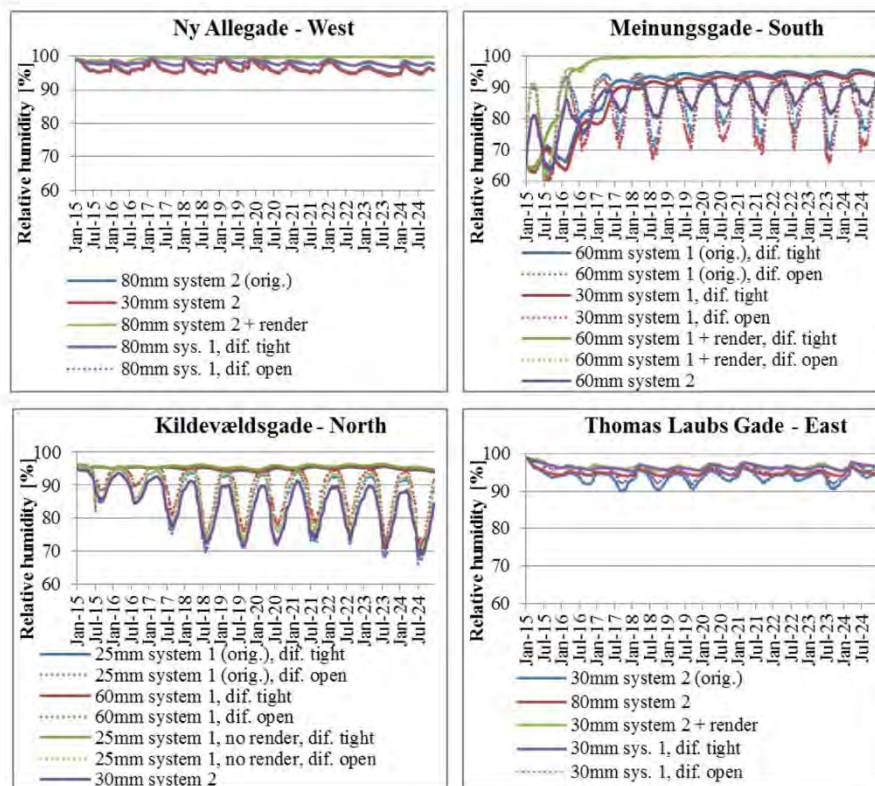


Fig. 13. 10 year simulation variations of insulation thickness, external surface (with/without render) and insulation system.

Table 6
Observed changes in simulated hygrothermal conditions as a result of parameter variations.

	Thickness	Paint + render	Material
Ny Allegade	Reduction of insulation thickness from 80 mm to 30 mm does not yield significant changes in the relative humidity.	Application of external render and paint yields a continuous increase in relative humidity, and no sign of decline	Application of 80 mm system 1 instead of system 2 yields slightly higher relative humidity and less drying in summer periods
Meinungsgade	Reduction of insulation thickness, 60 mm to 30 mm yields relative humidities reduced with up to 5%.	Application of external render increases the relative humidity, and yields no indication of drying in warmer periods.	60 mm system 2 exhibits lower relative humidity than 60 mm system 1. System 2 also yields more seasonal variation, however with an opposite tendency than system 1 where higher relative humidities are found in summer, system 2 yields higher relative humidities during winter. This indicates the diffusion of moist warm air from the inside through the wall during winter with system 2.
Kildevældsgade	Increasing the insulation thickness from 25–60 mm yielded no significant influence on relative humidity.	Removing the external render did not have a significant effect on the relative humidity, but it increased slightly.	Replacing 25 mm of system 1 with 30 mm system 2 yielded reduced relative humidity. System 2 also yielded larger seasonal variation with high relative humidity during winter, which is the opposite tendency of system 1.
Thomas Laubs Gade	Increasing the insulation thickness from 30 to 80 mm yielded higher relative humidities, especially in summer. 80 mm system 2 in this case seems to have less seasonal variation, as less drying is apparent during summer.	Application of render on the external surface increases the relative humidity, and yields less seasonal variation; hence less possibility for drying during summer.	Substitution of system 2 with system 1 causes the relative humidity to increase with a few percentages for all seasons.

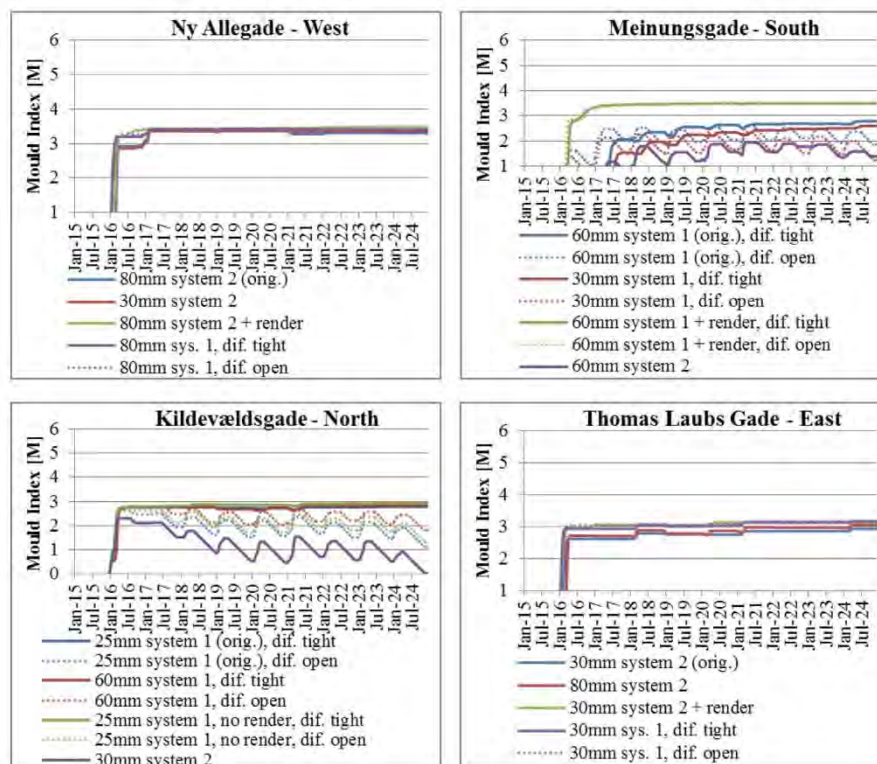


Fig. 14. Generated Mould indexes for simulated variations of insulation thickness, external surface and insulation system for the four cases.

lation has been executed at the site, which does not result in a vapour tight system but instead allows vapour diffusion and perhaps also convection in air pockets behind the insulation system 1, as described in Section 3.3. Inclusion of a vapour barrier in the simulation therefore seems to have a negative effect in regards to interior insulation for the presented cases. The simulation results indicate that an insulation system, where the plates are not fully bonded to the walls, and yield some space for convection and/or vapour diffusion at the interface, results in the lowest risk for moisture damage. Simulations as well as in situ measurements do not indicate the capillary active effect of insulation system 2 being as efficient as intended. Again, this may be explained by the installation process, and the possibility of the insulation plates not being fully bonded and distributing moisture as intended. Capillary active systems are often promoted as being vapour open and able to avoid interstitial condensation due to the capillary forces and buffering in the material, however the calcium silicate channels in system 2 may not be sufficient for achieving the desired effect. The capillary absorption coefficient of system 2 and the associated glue mortar has been found to be very low [18] compared to other claimed capillary active insulation systems which impedes the redistribution of potential moisture from either driving rain or interstitial condensation. The capillary active system should be diffusion open for the allowance of redistribution of water vapour, for evaporation on the internal side, however system 2, comprising mostly of vapour tight PUR, has a 2–3 times higher $S_{d,dry}$ value, compared to other capillary active insulation systems [18]. A more capillary active material, such as pure calcium silicate, may also yield better hygrothermal results, but the thermal conductivity of

such a product would be about 50% higher than that of system 2. In both cases of system 1, Meinungsgade and Kildevældsgade, a 20 cm air gap has been left above the floor, as an intentional thermal bridge in an attempt to increase the temperature and drying potential at the beam ends. The gap seems to yield the desired effect, as the conditions behind the beam ends are not critical. Harrestrup et al. [22] found through measurements and hygrothermal simulations, that internal insulation on northern-oriented façades could not be recommended as the lack of solar radiation yields little drying potential. On the other hand, the case at Kildevældsgade represents a northern oriented internally insulated façade that performs quite well. This case, however, also features external render and paint, which may act as a form of protection from external moisture sources. At Kildevældsgade a thin layer of insulation was applied and the simulation did show slightly increased risk of mould growth when either increasing the insulation thickness or removing the external render. Meinungsgade exhibits a significantly larger risk of mould growth with the inclusion of external render and paint. This may be explained by the orientation of the façade; south and southwest are the most exposed façades in regard to wind driven rain. An extra external layer of render with a higher water absorption coefficient may mean increased water uptake during rain spell, and decreased drying potential from the sun and the increased diffusion resistance. Klöfseiko et al. [13] tested several insulation systems on a northern oriented, externally rendered facade, and found that critical relative humidities after the installation of internal insulation were highest in the case of IQ-Therm, indicating the extended drying period for built in moisture, which may be the case for Ny Allegade and Thomas Laubs Gade.

At Thomas Laubs Gade, there is an indication of slow reduction in the relative humidity at the interface. But this tendency is not apparent in Ny Allegade. It should be kept in mind, that some insulation materials, especially ones containing gas, have shown to have variable thermal conductivities, and also be dependent on temperature [33], why the hygrothermal simulations may be subjected to further errors than the various estimations made, and the theoretical U -value reductions presented may vary. However, as described above, the best hygrothermal performance, with regard to in situ measurements, were found to be in the cases of insulation system 1. This system has a lower thermal conductivity than system 2, and thus the theoretical energy savings are higher, despite lower thickness. In both cases of insulation system 1, an intentional thermal bridge was incorporated at the floor, by means of a 20 cm uninsulated gap. The conditions in the beam ends were acceptable in these cases, indicating the effectiveness of the intentional thermal bridge. This was also demonstrated by Odgaard et al. [34]. In regard to the in situ measurements, it should be noted, that during the long term measurement period, re-calibration of the sensors was not possible, and the results might drift to a little extent [35], however the results give clear indications of the actual hygrothermal conditions. Finally, the simulations indicate that there is no significant difference in the long-term performance between the two insulation systems, which to a greater extent depends on the external loads on the façade.

4. Conclusion

The study presents results from long-term measurements of four cases of solid historical masonry with internal insulation and predicted performance of them according to hygrothermal simulations. The cases vary in location, façade orientation, external surface, insulation thickness and insulation system/material. For the two cases of insulation system 2, the in situ measurements proved very high and unacceptable relative humidities. In Thomas Laubs Gade, where 30 mm was applied, the relative humidity did show a tendency of decrease, which was not the case for Ny Allegade with 80 mm, despite the longer time frame. Hygrothermal simulations also showed reduction in relative humidity with reduction of thickness. For insulation system 1, the in situ measurements in both cases presented acceptable hygrothermal conditions within the wall. The case with thicker insulation, and facing the most exposed orientation (south and southwest), Meinungsgade, showed a longer initial period for drying out of the wall post insulation. Kildevældsgade was found to be sufficiently dry 6 months post insulation, but this case also faces north (less exposed to wind driven rain), the surface is rendered and painted, and the insulation thickness is less. Hygrothermal simulations revealed a better performance, when air flow or convection on the inside was included, and unacceptable conditions for the vapour tight system. Hence, results from in-situ measurements and simulations showed opposite conclusions: while systems with vapour tight insulation and vapour barrier performed better than the system with calcium silicate channels according to the in situ measurements, the opposite was the case according to hygrothermal simulations. This discrepancy was explained by the method insulation systems are mounted in reality that allows vapour diffusion in the interface of insulation and the original wall. This indicates that the vapour barrier in reality doesn't contribute positively to the performance of the system. Hygrothermal simulations show that the inclusion of a vapour tight membrane increases the relative humidity and the risk of mould growth. Simulated parameter variations supported this observation: the more vapour open and the capillary active system, the better the performance, but this conclusion is highly dependent on other parameters, e.g. different external climatic loads on the façade. In addition, an increase in the insula-

tion thickness seems to slightly increase the relative humidity and risk of mould growth. The study essentially enlightens the fact that all cases behave differently to parameter changes. Therefore, before application of internal insulation, the case should be carefully assessed with hygrothermal assessment methods, in order to find the most suitable solution with regard to both thermal and hygrothermal performance.

Acknowledgements

The presented work is a part of RIBuild project that has received funding from the European Union's Horizon 2020 research and innovation programme under grant agreement No 637268. The measurement data used for this study are a continuation of measurements performed for the EUDP project 2013-II: "Energy efficient comfort in older apartment blocks". The cases have been provided by Arup & Hvidt (Meinungsgade), Klimakarré Østerbro (Kildevældsgade and Thomas Laubs Gade), and privately (Ny Allégade).

References

- [1] J. Ruzek, D. López Garrido, Directive 2010/31/EU of the European Parliament and of the Council of 19 May 2010 on the energy performance of buildings, 2010. <http://eur-lex.europa.eu/legal-content/EN/ALL/?uri=CELEX:32010L0091>.
- [2] M. Economidou, J. Laustsen, P. Ruyssevelt, D. Staniszek, Europe's buildings under the microscope, 2011. <http://bpie.eu/publication/europes-buildings-under-the-microscope/>.
- [3] C. Balocco, G. Grazzini, A. Cavallera, Transient analysis of an external building cladding, *Energy Build.* 40 (2008) 1273–1277, doi:10.1016/j.enbuild.2007.11.008.
- [4] E. Kossecka, J. Kosny, Influence of insulation configuration on heating and cooling loads in a continuously used building, *Energy Build.* 34 (2002) 321–331, doi:10.1016/S0378-7788(01)00121-9.
- [5] S.P. Bjarlov, G.R. Finken, T. Odgaard, Retrofit with interior insulation on solid masonry walls in cool temperate climates – an evaluation of the influence of interior insulation materials on moisture condition in the building envelope, *Energy Procedia* 78 (2015) 1461–1466, doi:10.1016/j.egypro.2015.11.171.
- [6] J. Munch Andersen, SBI-anvisning 221: efterisolering af etageboliger, 1., Statens Byggeforskningsinstitut, Hørsholm (2008).
- [7] E. Brandt, SBI-Anvisning 224 Fugt i Bygninger, Statens Byggeforskningsinstitut Hørsholm, 1. (2009).
- [8] J. Toman, A. Vimmrová, R. Černý, Long-term on-site assessment of hygrothermal performance of interior thermal insulation system without water vapour barrier, *Energy Build.* 41 (2009) 51–55, doi:10.1016/j.enbuild.2008.07.007.
- [9] P. Mensinga, J. Straube, C. Schumacher, Assessing the freeze-thaw resistance of clay brick for interior insulation retrofit projects, In: 11th Int. Conf. Therm. Perform. Exter. Envel. Whole Build. Build. XI, 2010, doi:10.1081/E-EEE2-120046011.
- [10] J. Zhao, J. Grunewald, U. Ruisinger, S. Feng, Evaluation of capillary-active mineral insulation systems for interior retrofit solution, *Build. Environ.* 115 (2017) 215–227, doi:10.1016/j.buildenv.2017.01.004.
- [11] R. Walker, S. Pavia, Thermal performance of a selection of insulation materials suitable for historic buildings, *Build. Environ.* 94 (2015) 155–165, doi:10.1016/j.buildenv.2015.07.033.
- [12] D.I. Kolaitis, E. Malliotakis, D.A. Kontogeorgos, I. Mandilaras, D.I. Katsourinis, M.A. Founti, Comparative assessment of internal and external thermal insulation systems for energy efficient retrofitting of residential buildings, *Energy Build.* 64 (2013) 123–131.
- [13] P. Klößeiko, E. Arumägi, T. Kalamees, Hygrothermal performance of internally insulated brick wall in cold climate: a case study in a historical school building, *J. Build. Phys.* (2014) 1744259114532609, doi:10.1177/1744259114532609.
- [14] J. Straube, C. Schumacher, Interior insulation retrofits of load-bearing masonry walls in cold climates, *J. Green Build.* 2 (2007) 42–50, doi:10.3992/jgb.2.2.42.
- [15] E. Vereecken, L. Van Gelder, H. Janssen, S. Roels, Interior insulation for wall retrofitting – a probabilistic analysis of energy savings and hygrothermal risks, *Energy Build.* 89 (2015) 231–244, doi:10.1016/j.enbuild.2014.12.031.
- [16] G.R. Finken, S.P. Bjarlov, R.H. Peuhkuri, Effect of façade impregnation on feasibility of capillary active thermal internal insulation for a historic dormitory – a hygrothermal simulation study, *Constr. Build. Mater.* 113 (2016) 202–214, doi:10.1016/j.conbuildmat.2016.03.019.
- [17] Z. Pavlik, R. Černý, Hygrothermal performance study of an innovative interior thermal insulation system, *Appl. Therm. Eng.* 29 (2009) 1941–1946, doi:10.1016/j.applthermaleng.2008.09.013.
- [18] E. Vereecken, S. Roels, Capillary active interior insulation systems for wall retrofitting: a more nuanced story, *Int. J. Archit. Heritage* 10 (2016) 558–569, doi:10.1080/15483058.2015.1009575.
- [19] T. Bunch Nielsen, G. Christensen, Byg erfaringsblad (27) 05 12 29 uventilerede parallelte med dampbremse af hygrodiode, 2005. <https://byg-erfa.dk/nyventilerede-hygrodiode>.

- [20] S. Kirkeskov Jensen, C. Rode, K. Kleisgaard Hansen, N.P. Knoch, Non-isothermal laboratory measurements of moisture profiles in calcium silicate for interior insulation applications, in: 2. Int. Innendämmkongress (2013) 97–106.
- [21] P. Klöfseiko, E. Arumägi, T. Kalamees, Hygrothermal performance of internally insulated brick wall in a cold climate: field measurement and model calibration, in: Proc. 2nd Cent. Eur. Symp. Build. Phys., 2013, doi:10.1081/E.FEE2-120046011.
- [22] M. Harrestrup, S. Svendsen, Internal insulation applied in heritage multi-storey buildings with wooden beams embedded in solid masonry brick façades, Build. Environ. 99 (2016) 59–72, doi:10.1016/j.buildenv.2016.01.019.
- [23] A. Abdul Hamid, P. Wallentén, Hygrothermal assessment of internally added thermal insulation on external brick walls in Swedish multifamily buildings, Build. Environ. 123 (2017) 351–362, doi:10.1016/j.buildenv.2017.05.019.
- [24] A. Nicolai, J. Grunewald, Delphin 5 User Manual and Program Reference, Program, 2006.
- [25] T. Ojanen, R. Peuhkuri, L. Viitanen, S. Vinha, Classification of material sensitivity—new approach for mould growth modeling, in: 9th Nord. Symp. Build. Phys., 2011, pp. 867–874. http://webhotel2.tut.fi/nsb2011/sites/webhotel2.tut.fi/nsb2011/files/b10_02_niomo_ojanen_vtt_nordic_9th_classification_mould_growth_final2.pdf.
- [26] A. Hukka, H. Viitanen, A mathematical model of mould growth on wooden material, Wood Sci. Technol. 33 (1999) 475–485, doi:10.1007/s002260050131.
- [27] E. Vereecken, S. Roels, Review of mould prediction models and their influence on mould risk evaluation, Build. Environ. 51 (2012) 296–310, doi:10.1016/j.buildenv.2011.11.003.
- [28] E. Vereecken, K. Vanoirbeek, S. Roels, Towards a more thoughtful use of mould prediction models: a critical view on experimental mould growth research, J. Build. Phys. 39 (2015) 102–123, doi:10.1177/1744259115588718.
- [29] H. Viitanen, M. Krus, T. Ojanen, V. Eitner, D. Zirkelbach, Mold risk classification based on comparative evaluation of two established growth models, Energy Procedia 78 (2015) 1425–1430, doi:10.1016/j.egypro.2015.11.165.
- [30] Kingspan Insulation ApS, Produktoversigt Danmark Marts 2016 - Super Effektiv og Højtydende Isolering til Alle Formål, Roskilde, 2016. <file:///C:/Users/camil/Downloads/Produktoversigt-Danmark-Marts-2016.pdf>.
- [31] EU, Climate for Culture, 2014. <https://www.climateforculture.eu/>.
- [32] J. Straube, Simplified prediction of driving rain on buildings: ASHRAE 160P and WUFI 4.0, Build. Sci. Digests (2010) 1–16 file:///C:/Users/tekhan/Downloads/BSD-148_Simplified_Prediction_Driving_Rain.pdf.
- [33] U. Berardi, M. Naldi, The impact of the temperature dependent thermal conductivity of insulating materials on the effective building envelope performance, Energy Build. 144 (2017) 262–275, doi:10.1016/j.enbuild.2017.03.052.
- [34] T. Odgaard, S.P. Bjarlov, C. Rode, Influence of hydrophobation and deliberate thermal bridge on hygrothermal conditions of internally insulated historic solid masonry walls with built-in wood, Energy Build. (2018) (n.d.).
- [35] S. Ahola, J. Lahdensivu, Long term monitoring of repaired external wall assembly, Energy Procedia 0 (2017) 11–14, doi:10.1016/j.egypro.2017.09.635.

Appendix B

Paper II

Performance of hydrophobized historic solid masonry – experimental approach



Contents lists available at ScienceDirect

Construction and Building Materials

journal homepage: www.elsevier.com/locate/conbuildmat

Performance of hydrophobized historic solid masonry – Experimental approach

T.K. Hansen^{a,*}, S.P. Bjarløv^a, R.H. Peuhkuri^b, K.K. Hansen^a^aDTU Civil Engineering, Technical University of Denmark, Kgs. Lyngby, Denmark^bSBI, Danish Building Research Institute, Aalborg University Copenhagen, Denmark

HIGHLIGHTS

- Evaluation of 16 different hydrophobization agents on brick and lime mortar.
- Investigation of penetration depth, water absorption, drying and vapour diffusion.
- Studying water migration through masonry sections with lime mortar joints.
- The efficiency of hydrophobization varies based on active component and material applied to.
- Silane based showed good performance on brick and masonry with lime mortar.

ARTICLE INFO

Article history:

Received 22 June 2018

Received in revised form 21 August 2018

Accepted 22 August 2018

Available online 28 August 2018

Keywords:

Hydrophobization
Historic masonry
Internal insulation
Surface treatment
Ceramic brick
Air lime mortar

ABSTRACT

The hygrothermal conditions in historic solid masonry are expected to change for the worse, with the application of internal insulation. Nevertheless, internal insulation plays a role in a holistic energy retrofit of historic buildings. With careful considerations and correct application, hydrophobic treatment may help remedy moisture ingress from external rain loads. This study includes experimental investigations of the effect on hygrothermal performance of various hydrophobization treatments on both brick and air lime mortar. An investigation of water migration through masonry applied with imitated climatic loads is also reported. The study showed a larger efficiency of hydrophobization on specimens of brick compared to the efficiency of hydrophobization of specimens of air lime mortar, which may be problematic in cases where mortar joints are the primary means for water ingress. Silane-based treatments generally proved to be most efficient in brick, whereas a variety of other active components were most successful in air lime mortar treatment. The investigation of water migration showed a distinct effect of silane, cream hydrophobization, though most evident in the external part of the brick.

© 2018 Elsevier Ltd. All rights reserved.

1. Introduction

Reducing the energy consumption in the existing building stock is a vital measure in the goal of global reduction of energy consumption. In Europe, the energy consumption from the building sector constitutes 40% of the overall energy consumption [1], yielding a large potential for improvements in the field. The improvements should not be limited to new, sustainable constructions, but can also be attributed historical buildings by means of energy efficient renovations. In Denmark, 60% of the existing building stock of multistory residential buildings were constructed prior to 1950 [2], often yielding preservation worthy façades as the aes-

thetic expression presents cultural, local and traditional importance. This excludes the possibility of external insulation.

Internal insulation is therefore often the only way to reduce heat loss through the external walls in historic buildings. In addition to the reduction in energy consumption, an advantage of reducing heat loss through façades is the improved thermal comfort, as the surface temperature of the interior wall increases. However, the application of internal insulation to an old façade will dramatically change the hygrothermal conditions of the wall, as the temperature and drying potential is reduced, yielding the possibility for interstitial condensation [3]. The hygrothermal conditions in the construction can reach undesirable states due to both internal (vapour) and external (vapour and liquid) moisture loads, and there are several risks associated with the undesirable moisture conditions, e.g. mould growth, frost damage, decay of embedded wood, and general degeneration of the construction.

* Corresponding author at: DTU Civil Engineering, Brovej 118, DK-2800 Kgs. Lyngby, Denmark.

E-mail address: tekhan@byg.dtu.dk (T.K. Hansen).

<https://doi.org/10.1016/j.conbuildmat.2018.08.145>
0950-0618/© 2018 Elsevier Ltd. All rights reserved.

External moisture loads appear in the form of vapour/humidity and wind-driven rain (WDR). WDR is a significant parameter in regards to the hygrothermal performance of external facades [4,5]. When it comes to internally insulated masonry walls, WDR has also proven to be a negative contributor to the hygrothermal performance [6]. Finken et al. state that WDR can be the most critical factor in regards to moisture in a façade of porous building materials, as opposed to interstitial condensation, reduced drying capability and temperature when internal insulation is applied [5]. Through hygrothermal simulations and measurements, Künzle et al. found that an estimated 70% of WDR is absorbed by means of capillary action [7]. This observation was based on a one-dimensional validation of measured water content in three cases of different porous building materials installed in a western wall, and thus susceptible to exterior climate. Odgaard et al. found that hydrophobization had a positive effect on internally insulated walls during summer, however it impeded evaporation of interstitial condensation during winter periods [8].

Hydrophobization treatments may prevent, or at least reduce, penetration of liquid water from external conditions. Thus it may have a positive effect on the moisture conditions within a wall, and impede moisture accumulation due to rain penetration. Therefore, a hydrophobization treatment may enhance the service life of an internally insulated wall, as the risk of moisture related damages such as frost damage, cracking, wood degradation and mould is also reduced. An old-fashioned method for hydrophobization is found in old surface treatments, such as façade painting. However, this is not desired for listed or culturally valued buildings, as it changes the architectural expression. A previous study of internal insulation applied to external walls showed a case with a painted façade yielding excellent results in regards to hygrothermal conditions at critical points [9]. This success may be attributed to the paint serving as a water repellent; however the façade was also northbound and only a thin layer of insulation was applied.

Furthermore, both hygrothermal simulation [5] and experimental [10] studies have shown a reduction in heat loss through impregnated external walls, due to the reduced thermal conductivity caused by the dryer state of the wall. In addition, moisture within the insulation material compromises the efficiency [5,3]. There is a large variety of hydrophobic treatments available on the market, however they may not have the same efficiency with use on various materials, and when studying historic masonry holistically, the efficiency on both brick and lime mortar must be taken into consideration.

Many hydrophobic agents are based on silicone in the form of either silane or siloxane, or even a hybrid of both [11]. Both active compounds react with silicates in the building material and create CH_3 -molecules which are hydrophobic, like the other non-polar carbonaceous groups CH and CH_2 . Lime does not contain silicates in itself, however sand grains as aggregates in lime mortar do. Therefore the silicone based hydrophobic treatments may not bind as well to lime mortar as they do not bind to the binding agent itself as they do on e.g. cement or brick.

The main difference between the silane and the siloxane based agents is that the silane molecules have a smaller structure and lower viscosity, and thus the ability for deeper penetration into porous materials. Silane is also more volatile, and thus higher concentrations are used for achieving good results [12]. Siloxane is a more complex compound and thus larger molecules, decreasing the penetration depth, leaving the porous material more vulnerable if the external surface is damaged. Siloxane is less volatile, and lower concentrations can be used, with good results in regards to repelling water. In some cases, nanotechnology has been implemented in an attempt to improve the efficiency of hydrophobization agents.

Recent research includes investigations of the effect of external moisture loads on the hygrothermal performance of internally insulated walls, and the prevention or reduction of external water penetration, e.g. from wind driven rain. Solar radiation can be a positive contributor to a wet façade by means of increased drying and reduced condensation potential, but it can also drive the moisture further into the construction [13].

The following studies in the field of hydrophobization relate to the present study. A study by Guizzardi et al. from 2015 of masonry walls with severe wetting [21] yielded information about migration of external water loads through masonry. The experiment revealed that interfaces posed as hydraulic resistances/barriers, and that the moisture transport occurred faster in the fine pored bricks than in mortar joints. In contrast, van Hees found that the mortar joints were the weakest part of hydrophobized masonry [22]. He observed a difference in the efficiency of hydrophobization treatments on brick and mortar, yielding mortar joints a possible way for water ingress. Zhang et al. have investigated the efficiency of silane water repellent impregnation on cement based mortars and concrete [10], and found that the capillary suction was significantly reduced. Slapø et al. have found, that fresh mortars with high water content improved masonry's resistance to WDR, as the mortar-brick interface becomes less porous [23]. Engel et al. [24] performed a study on water absorption, drying and vapour diffusion of hydrophobized brick specimens. They examined 5 silane based creams of different concentrations, and two fluid hybrid agents. They found significant water absorption reduction, and with no influence on the vapour diffusion resistance. Their drying experiment showed that specimens hydrophobized with agents of lesser concentration should be applied with the lowest, effective concentration. An older study from 1995 by Charola [12] found a reduction of 5–10% in water vapour permeability with silicon-based hydrophobization treatments. Couto et al. [25], who investigated silane-based water-repellents on ceramic brick, also found a reduction in vapour permeability of hydrophobized brick specimens in some water-repellent treatments. Van Hees [22] found a limited effect of hydrophobization on vapour diffusion however, he found the hydrophobization treatments to have a high impact on the drying process, as also found by Couto et al. [25] for most investigated treatments. Lubelli et al. [26] tested the efficiency of two nano-coatings on bricks, and found significantly reduced water absorption, and little effect on the drying, however, the penetration depth was found to be much lower than traditional products. Finken et al. found, through a study of hydrophobization based on several hygrothermal simulations, that hydrophobization has a positive impact on the hygrothermal conditions within an internally insulated façade. In the simulation, the entire wall became dryer, compared to unhydrophobized cases [5]. Finally, Slapø et al. performed a similar large scale study on masonry panels however, the water loads were provided with high pressure for 5 h. They found the tested water repellents to be ineffective to high pressure driving rain after a few minutes of water loads; this inefficiency was attributed the extreme testing conditions.

This investigation focuses on the efficiency and effect of various hydrophobization agents on historic masonry from a holistic point of view. Initially a screening of 16 different hydrophobization agents is performed. The initial investigation includes experiments on brick and lime mortar in regards to penetration depth of hydrophobization agent, water absorption, and drying. Furthermore, the effect of hydrophobization on vapour diffusion is examined as well as a large scale experiment involving monitoring of the migration of water through masonry wall sections and the recorded effects of hydrophobization.

2. Method

As stated in the introduction, this study includes 3 laboratory experiments performed on historic brick, and air lime mortar with properties resembling historic masonry. These parts consist of:

- 1) Initial investigation: 16 different hydrophobization agents (silane, siloxane, hybrids, and nanotechnology) were applied to specimens of ceramic brick and air lime mortar. The performance of each agent was evaluated based on penetration depth, water absorption and drying.
- 2) Influence on vapour diffusion: 3 hydrophobization agents (N, J, P) were applied to specimens of ceramic brick and air lime mortar to determine a possible effect on vapour diffusion properties.
- 3) Water migration through masonry: The effect of a creamy, silane based hydrophobization agent (J) on masonry was investigated by monitoring water migration.

The initial investigation was performed to get an overview of the efficiency and differences between the various types of agents. Steps 2 and 3 of the investigation were partially based on results from the initial investigation, and partially chosen to test a variety of types of hydrophobization agents. For part 2, the chosen agents included N, a silane based liquid agent, J, a silane based creamy agent, and P, a hybrid agent that is a 2-component agent diluted in an organic solvent. For the 3rd investigation, hydrophobization on entire masonry sections, the creamy agent J was used again. The cream based agent, J, used in steps 2) and 3) was chosen because it had shown good properties in regards to hydrophobization of brick, and medium performance with air lime mortar. N and P both showed a good efficiency in brick specimens; however P showed good performance in lime mortar, whereas N did not perform well.

The three studies were conducted in collaboration in order to study the effects of various hydrophobization agents on the hygrothermal behavior of historic masonry components individually, as well as investigating the combined effects of hydrophobization on masonry. By initially investigating a variety of types of agents from various manufacturers, the field could be reduced for the investigation of the influence on vapour permeability, and more specimens of each type could be included. For the investigation of water migration through masonry, only one hydrophobization treatment was used. This agent was chosen prior to the initial tests performed, however it was chosen due to some preliminary experimentation with the product.

2.1. Materials

As the study refers to historic masonry, the experiments have been carried out on specimens of brick and lime mortar. Both the brick and mortar included in the study, were chosen to imitate historic building materials, and are also the materials used in larger scale studies of historic masonry at the Technical University of Denmark [8]. The bricks were all yellow soft-molded bricks from Helligsø Teglværk in Denmark, with a dry density of approximately 1677 kg/m³. For the initial investigation, the mortar specimens provided were unspecified, carbonated lime mortar with an open porosity between 0.26 (K-Q)–0.28 (A-J) m³/m³, and dry density of 1881 (A-J)–1941 (K-Q) kg/m³. The lime mortar used for the remaining experiments was a 7.7% lime mortar (air lime) with aggregates of 0–4 mm grain size with an open porosity of 0.33 m³/m³ and dry density of 1752 kg/m³.

For the initial investigation, 16 different hydrophobization agents were included; these are presented in Table 1 below. Some

of these agents were also used for the further experimentation, which is expressed in the far right column. Most of the agents included in this study are based on silane or siloxane, or a hybrid of both. A few are based on nanotechnology. The silane or siloxane based agents are regarded as pore liners. The pore liners penetrate the open pores of the specimens, and create a hydrophobic lining to the pores without obstructing the vapour diffusion of the material. The agents based on nanotechnology, take advantage of “self-assembly” of the nanoparticles, which is a phenomenon where the particles arrange and assemble themselves in a fashion with the purpose of creating a larger unit with a specific function, as explained by Boostani et al. [14]. As the hydrophobization treatment should not affect the vapour permeability, water vapour in the material still has the possibility to diffuse inside the specimen, and evaporate at the surface. This is the desired effect when surface treating interior insulated facades. The hydrophobization treatment makes the water rebound and runoff rather than being absorbed into the material.

For the water migration experiment, 3, some internal insulation materials were applied to the wall sections. These internal insulation materials were a foam concrete developed at the Technical University of Denmark [15], PUR insulation with channels of calcium silicate (PUR with CaSi channels) and aerated cellular concrete (ACC). Material parameters for the included insulation materials are seen in Table 2 below.

2.2. Experimental methods

In this section the various experimental methods applied will be described.

2.2.1. Initial investigation

The initial investigation of 16 different hydrophobization agents (displayed in Table 1) consists of 3 different parts, described in Sections 2.2.1.1–2.2.1.3. The hydrophobization agents were applied to the specimens by two different methods. The liquid agents were applied to all sides of the specimens by shaking them in a plastic bag containing the agent for 10 s. The creamy products (I and J) were applied with a paint brush, in the amounts recommended by the manufacturer, see Table 1. The brick specimens were whole bricks, as it was desired to study the unbroken, external brick surface's susceptibility to the hydrophobization agents. Standard Danish brick dimensions are 228 × 108 × 54 mm³. The carbonated air lime mortar specimens were significantly smaller, and cut from a larger plate. The specimens were on average 93 × 40 × 30 mm³. 1 specimen of both brick and lime mortar was investigated for each hydrophobization treatment. The specimens were initially oven-dried at 105 °C, and hereafter conditioned in room conditions before the application of hydrophobic treatment. The specimens were hydrophobized 14 days prior to the experimental execution.

The various hydrophobization agents were evaluated by means of a ranking system applied to the 3 categories – penetration depth, water uptake and drying, for both brick and mortar. The ranking system is implemented as a very simplified mean for interpreting the various results in the complex field. Penetration depth was ranked according to percentage of half the specimen's thickness, and specimens with full penetration were thus given a score of 100%. The water uptake was ranked by the final mass% increase by the end of the experiment, as a percentage relative to the reference specimen. The drying was ranked by the percentage difference between the initial slopes of the drying graph for each treatment relative to the reference specimen. The drying experiment is described in Section 2.2.1.2. The final ranking score was the sum of the three scores for the 3 categories, and a higher score yielded an overall better performance of this agent. A combined score for brick and mortar consists of the sum of the final score

Table 1

Hydrophobization agents included in the study, information as stated in technical data sheets of each agents. Highlights in "application method" indicate methods and amounts used for steps 2 and 3.

	Active component (concentration of active component)	Liquid/cream	Application method + coats	Consumption pr. coat [l/m ² or m ² /g]	Included in experiments
A	Siloxane and Fluoro Polymer (16%)	Liquid	Roll, paint brush, low-pressure sprayer or air-less sprayer, 1–2 coats	0.1–0.2 l/m ²	1
B	Copolymers (16%)	Liquid	Roll, paint brush, low-pressure sprayer or air-less sprayer, 1–2 coats	0.1–0.2 l/m ²	1
C	Various fluoroc polymers (16%)	Liquid	Roll, paint brush, low-pressure sprayer or air-less sprayer, 1–2 coats	0.1–0.2 l/m ²	1
D	Silane, siloxane and Fluoro Polymer (16%)	Liquid	Roll, paint brush, low-pressure sprayer or air-less sprayer, 1–2 coats	0.1–0.2 l/m ²	1
E	Silane/siloxane (16%)	Liquid	Roll, paint brush, low-pressure sprayer or air-less sprayer, 1–2 coats	0.1–0.2 l/m ²	1
F	Siloxane copolymers and pefluorinated siloxane (16%)	Liquid	Roll, paint brush, low-pressure sprayer or air-less sprayer, 2–3 coats	0.1–0.2 l/m ²	1
G	Nanoparticle dispersion, isopropanol solvent (<13%wt)	Liquid	Airless standard low-pressure sprayer, roll or paint brush, min. 2 coats	0.062–0.075 l/m ²	1
H	Nanoparticle dispersion, isopropanol solvent (<3%wt)	Liquid	Roll, paint brush or air-less sprayer, 2 coats	0.1–0.125 l/m ²	1
I	Silane (80%)	Cream	Roll, paint brush or air-less sprayer, 1 coat	0.20–0.50 l/m ²	1
J	Silane (40%)	Cream	Roll, paint brush or air-less sprayer, 1 coat	0.15–0.20 l/m ²	1,2,3
K	Unknown	Liquid	Sponge, paint pad, cotton-cloth or sprayer, 2 coats	0.025–0.1 l/m ²	1
L	Chlorophyllane	Liquid	Roll, paint brush or low-pressure sprayer	0.08–0.17 l/m ²	1
M	Flour-Acryl-Polymer and Alkyl-Acoxy Silane	Liquid	ND-sprayer with Viton seal, airless sprayer, roll, paint brush, 1–2 coats	90–170 g/m ²	1
N	Alkylalcoxy silane	Liquid	Brush or low-pressure sprayer, 1–3 coats	180–230 g/m ²	1,2
O	Silane > 20%	Liquid	Low-pressure sprayer with Viton seal, 2–3 coats	2–300 g/m ²	1
P	Silane/siloxane (100%)	Liquid	Roll, Paintbrush or sprayer, 2 coats	10–40 g/m ² (110–440 g/m ² diluted)	1,2
Q	Reference				1,2,3

*Agent P is a 2-component hydrophobization agent, diluted 1:11 with organic solvent (e.g. mineral turpentine).

Table 2

Material parameters of internal insulation systems applied to the wall sections in the large scale experiment.

Insulation material	Density, ρ_d [kg/m ³]	Thermal conductivity, λ [W/(mK)]	Water uptake coefficient, [kg/(m ² s ^{1/2})]	Water vapour diffusion resistance factor, μ [–]
Foam concrete*	147	0.057–0.064	0.078	2
PUR with CaSi channels**	49	0.037	0.013	27
ACC**	99	0.042	0.006	7

* Material parameters derived from the work by Sandholdt and Dysted [15].

** Material parameters derived from material database of simulation software Delphin 5.8.3 [16].

for each material. The formulas used for the ranking system, can be seen below in Eqs. (1)–(5);

$$1) \text{ Penetration depth } \frac{\text{registered penetration depth}}{\text{specimen thickness}} \cdot 100 [\%] \quad (1)$$

$$2) \text{ Water uptake } \frac{\text{mass}_{\text{end}} - \text{mass}_{\text{initial}}}{\text{mass}_{\text{initial}}} \cdot 100 [\%] \quad (2)$$

$$2a) \text{ Mass increase } \frac{\text{mass}_{\text{end}} - \text{mass}_{\text{initial}}}{\text{mass}_{\text{initial}}} \cdot 100 [\%] \quad (3)$$

$$3) \text{ Drying } \frac{\text{initial slope}_{\text{reference}} - \text{initial slope}_{\text{specimen}}}{\text{initial slope}_{\text{reference}}} \cdot 100 [\%] \quad (4)$$

$$3a) \text{ Initial slope }^* \frac{y_2 - y_1}{x_2 - x_1} [-] \quad (5)$$

*The initial slope is calculated based on values from timestep 0 ($x_1 = 0$) to timestep 4020 min ($x_2 = 4020$).

2.2.1.1. Water uptake. The water uptake experiment was performed as full immersion experiments. The treated specimens were weighed and then placed on triangular spacers in a water tank, with a water level above the top of the specimen, as seen in



Fig. 1. Experimental setup of full immersion water absorption experiments on brick (left) and mortar (right).

Fig. 1. The mass of the specimen was recorded before immersion, and after immersion at the following intervals; 2, 4, 8, 16, 30, 120, 180, 240, 300 min, as well as one final measurement 20–28 h after immersion. At every weighing, each specimen was dried off with a damp cloth, to avoid hanging water affecting the results. The measurements were transformed into mass% increase, and

plotted in a diagram over time; thus the absorption of each specimen over time can be studied graphically.

2.2.1.2. Drying experiment. After the water absorption experiment has finalized, all treated specimens and reference specimens were saturated by means of vacuum in desiccators (Fig. 2) prior to initiating the drying experiment. For the vacuum saturation, boiled and cooled demineralized water was used. Hereafter, the specimens were placed on triangular spacers in a climate chamber of approximately 20 °C and 85% relative humidity to dry. The initial drying was monitored with 6 weighings during the first hour, and hereafter one measurement per day or two days was carried out during the duration of 6 weeks for bricks and 17 days for mortar. The measurements were transformed into moisture content, which is illustrated graphically as a function of time.

2.2.1.3. Penetration depth. The specimens were broken in half with a hammer and chisel as seen in Fig. 3, and the broken side sprayed with water to visually define the penetration depth of the hydrophobization agents. The penetration depth was measured at 7 evenly distributed locations on both of the long sides, and one location on each short edge. A large penetration depth does not necessarily equal the highest efficiency of water repellent in a hydrophobization agent. With a large penetration depth however, the agent may further prevent deeper water ingress, and e.g. frost damage.

2.2.2. Influence on vapour diffusion

Hydrophobization of historic masonry repels liquid water from external sources, such as wind-driven rain. However, the façade will not be protected from internal moisture sources, in the form of warm, moist air, or possible condensation, why the vapour diffusivity of a hydrophobized wall should not be affected by the treatment. This is investigated by the cup experiment (wet cup) for measurement of water vapour diffusion resistance factor of untreated and hydrophobized specimens of both brick and mortar. For this experiment, 3 agents (J, N and P) were examined on 3 specimens with each agent, in addition to 3 reference specimens of both brick and mortar. Prior to the experiment the specimens were cut into Ø80 mm specimens and sealed in Ø100 mm plastic rings designed for the cups. Mortar specimens were sealed in a plastic ring with silicone, and the brick specimens were sealed with epoxy, as seen in Fig. 4. The specimens were hydrophobized on the top side against the measurement chamber, with the recommended application methods; the liquid agents, N and P, were applied with a sprayer, and the cream, J, in the amounts and layers (J: 1 layer, N: 3 layers, P: 2 layers) as specified in the datasheets. Specimens were weighed before and after application of each layer, and the specific amounts are presented in Table 3.

The experiment was carried out according to DS/EN ISO 12572 – Hygrothermal performance of building materials and products – Determination of water vapour transmission properties. The principle of the experiment is sealing a specimen in a cup containing an aqueous saturated solution, in this case KNO_3 (94% relative humidity). The cup was placed in a climate chamber with controlled temperature (23 °C) and relative humidity (50%) conditions. Due to different partial vapour pressures on both sides of the specimen vapour flow occurs, and by daily weighings for a week, the rate of water vapour transmission in steady state can be determined, and further transformed into water vapour diffusion resistance factor, μ . Fig. 4 illustrates the specimen preparation and experimentation.

2.2.3. Water migration through masonry

One of the hydrophobization agents included in the initial investigation was tested in a larger perspective. The experimental method was chosen with the purpose of monitoring the resulting hygrothermal behavior of solid masonry with and without hydrophobization, when exposed to typical climatic loads. To imitate the dynamics and the varying nature of the natural climate, a cyclic exposure was designed. The hydrophobization was applied with a paint brush and in amounts according to specifications [17]. The investigation of water migration was performed to study the effect of hydrophobization within masonry walls rather than with the masonry components individually. The experiment was conducted on nine 1½ brick thick solid masonry wall sections of $330 \times 348 \text{ mm}^2$ built into the doors of 3 refrigerators, as seen in Fig. 5. Each wall section was surrounded by a vapour barrier tightly taped to the perimeter, to ensure adiabatic boundaries. Furthermore, the boundaries of the wall surface were sealed with silicone, to prevent water penetration through small airgaps at the perimeter. To prevent excess water influencing neighboring wall sections, gutters were incorporated for each wall section 100 mm of the various insulation materials were applied to the internal side of the wall section, with the exception of the reference wall, which was uninsulated. Each wall section was built up as seen in Fig. 5. For registration of the temperature and relative humidity in the wall sections as well as in the refrigerator itself (cold climate) HYT-221 sensors were used. The sensors were placed in drilled holes that were subsequently sealed with silicone. Each sensor was set for logging measurements every 5 min during the experiment, and the data was logged directly to a computer for data storage. The placements of each sensor are also seen in Fig. 5. Vertically, the sensors were placed in the middle of each wall section. The sensors logged temperature and relative humidity.

As mentioned, there are 3 wall sections in each of the 3 refrigerator doors. Table 4 displays the setup of each wall section, with insulation types, as well as whether or not hydrophobization was



Fig. 2. Vacuum saturation of brick in desiccator (left), and drying in climate chamber of brick (middle) and mortar (right).



Fig. 3. Halving of brick specimens with hammer and chisel (left), marking of 7 measuring locations on both sides (agent L), and example of visible penetration depth, the lighter area around the brick (agent E).

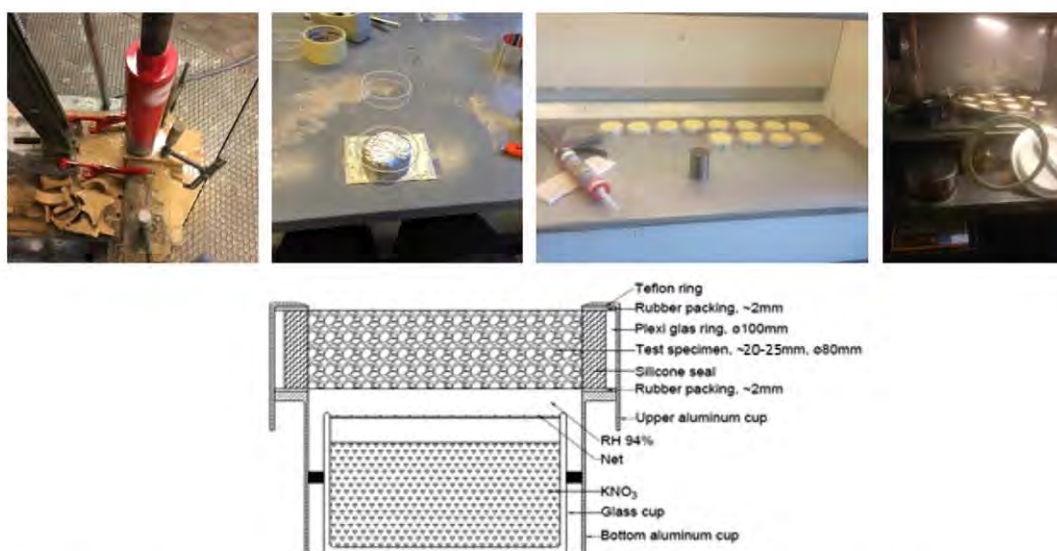


Fig. 4. Top row: Preparation of specimens for cup experiment; brick cutting with a core drill, sealing lime mortar specimen in plexi glass rings with silicone, specimens in cups placed in climate chamber (right). Bottom: Illustration of the specimen in the specially designed cup.

Table 3

Applied hydrophobization agent on test specimens for water vapour diffusion experiment.

	Consumption of hydrophobization agent [g]						Producer specified consumption pr. layer [g]
	Brick			Mortar			
	Layer 1	Layer 2*	Layer 3*	Layer 1	Layer 2*	Layer 3*	
J1	1	–	–	1,3	–	–	~0.8
J2	0,9	–	–	1,5	–	–	
J3	1,1	–	–	1,5	–	–	
N1	1,1	1,2	1,2	1,3	0,9	1,2	~0.9–1.1
N2	1,3	1,1	1,3	1,1	1	1,6	
N3	1,2	1,2	1	1,2	1,2	1,3	
P1	1,3	1,3	–	1,1	0,9	–	~0.5–2.0
P2	1,3	1,1	–	1,4	0,9	–	
P3	1,2	1,1	–	1,1	1	–	

*Layers 2 and 3 were applied wet in wet.

applied. In the table, it is seen that each wall section is denoted with 1.1–1.3, 2.1–2.3, and 3.1–3.3, depending on the refrigerator door, and the height. Furthermore, the table states which sensor locations were in use for each wall section.

2.2.3.1. Boundary conditions. The experiment was conducted in a laboratory. Measurements from a sensor placed at internal surfaces of the walls, represent the interior conditions that were found to be steady with a temperature of 22–23 °C and relative humidity of

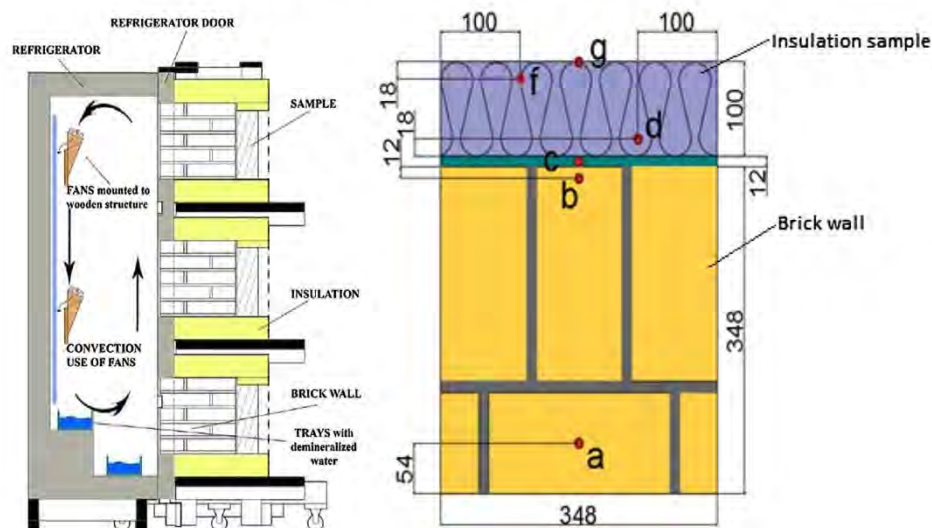


Fig. 5. Left: Diagram of the experimental setup with the cooling chamber from Sandholdt et al. [15]. Right: Construction of each wall section, and sensor location. Dimensions are stated in [mm]. Sensor locations are denoted a, b, c, d, f, and g.

Table 4

Overview of wall sections 1) insulation sample type, 2) with/without hydrophobization, 3) internal surface treatment, 4) sensors used in this wall section. Placements of the sensors are shown in Fig. 5 right.

1.1	2.1	3.1
1) Foam concrete	1) Insulation type: PUR with CaSi channels	1) Insulation type: ACC
2) Hydrophobization	2) Hydrophobization	2) No hydrophobization
3) Internal: Diffusion open paint	3) Internal: No treatment	3) Internal: Diffusion open paint
4) a, b, c, d, f	4) a, b, c, g	4) a, b, c, d, f
1.2	2.2	3.2
1) Insulation type: No insulation (ref)	1) Insulation type: Foam concrete	1) Insulation type: ACC
2) No hydrophobization	2) No hydrophobization	2) Hydrophobization
3) Internal: No paint (ref)	3) Diffusion open paint	3) Internal: Diffusion open paint
4) a, b, c	4) a, b, c, d, f	4) a, b, c, d, f
1.3	2.3	3.3
1) Insulation type: Foam concrete	1) Insulation type: Foam concrete	1) Insulation type: PUR with CaSi channels
2) Hydrophobization	2) No hydrophobization	2) No hydrophobization
3) Internal: Ordinary paint	3) Internal: Ordinary paint	3) Internal: No treatment
4) a, b, c, d, f	4) a, b, c, d, f	4) a, b, c, g

The diffusion open paint system is a combination of a primer and a silicate based paint ($s_d < 0.01$ m), whereas the ordinary paint used was a standard acrylic paint ($s_d < 0.18$ m).

55–60%. The minor fluctuations in the internal hygrothermal conditions are not thought to impact the experimental results obtained. The experiment was conducted in 24 h cycles. Each 24 h cycle consisted of 30 min of rain, 2 h of solar radiation, and 21½ hours of cold climate. This cycle was repeated 5 times.

The rain loads were applied to the wall sections by means of a purposely designed test stand, seen in Fig. 6, C. A perforated (holes of Ø0.5 mm pr. 50 mm) 340 mm long pipe in the length of each wall section was placed at the top, and provided a horizontal water load of 0.08–0.11 l/min. The water distribution was therefore more direct than actual rain, but the intention here was also to create severe climatic conditions. By Danish meteorological standards, a severe cloud burst rain storm is defined as a rain intensity of 15 mm in 30 min or less [18]. This corresponds to 30 mm/h, or 30 l/m² h. The provided water load of approximately 0.1 l/min thus represents a severe cloudburst of 50 mm/h, corresponding to each wall being subjected to 3 l of water over 30 min.

The solar radiation loads were provided by Osram ULTRA-VITALUX 300 W bulbs for simulation of heat and UV-radiation. These bulbs provide a radiation similar to natural sunlight, and are also used in climate simulators for accelerated aging [19]. The bulbs were fixed in a stand as seen in Fig. 6, D, with lightbulbs placed at 3 different heights, corresponding to the center of each wall section. The distance between the bulbs and the wall sections was determined by the so-called black panel temperature. In order to achieve a black panel temperature of 75 ± 5 °C, the distance between the wall and the bulb was set at 20 cm, yielding an average black plate temperature of 78.1 °C.

As mentioned, the wall sections were built into the doors of refrigerators, and these refrigerators provided the cold climate. The refrigerator doors with the wall sections were mounted on wooden rigs that were supplied with hinges. These hinges and the original rubber gaskets on the doors were utilized to ensure a tight fit to the original refrigerator. When the refrigerators/cold cli-

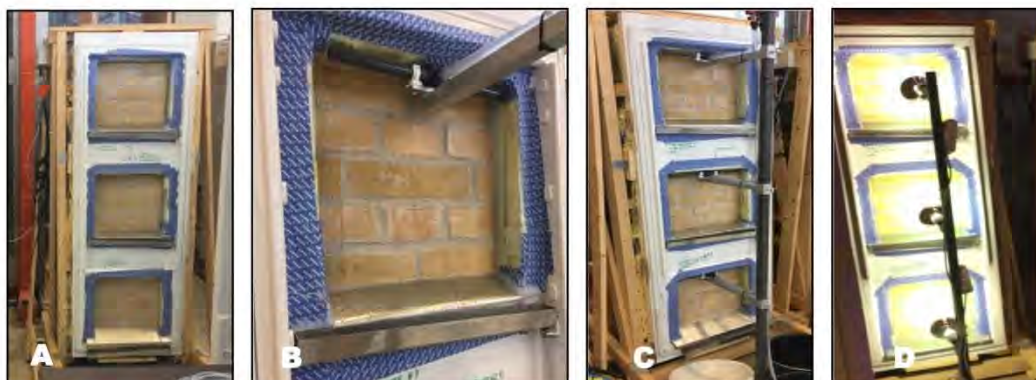


Fig. 6. Experimental setup. A: 3 wall sections in mounted in a refrigerator door. B: water loads applied horizontally to the top of the wall section, by perforated pipe. C: view of water loads applied to 3 wall sections. D: radiation loads on 3 wall sections.

mate assimilators were not in use, the opening was covered with XPS plates to help maintain the cold climate conditions inside. The temperature in the refrigerators was controlled by a temperature regulated on/off switch, Sygonix® room thermostat, which was set to a temperature of 3 °C, and set to switch on at 3.2 °C and off at 2.8 °C. The original thermostat was moved outside of the refrigerator, to induce constant cooling until switching off by the Sygonix® [15]. The relative humidity was less controlled, however kept high by having a water bath inside the refrigerator. The conditions were monitored, and by the above mentioned means it was possible to keep the temperature at 4 °C and the relative humidity at 80–85%, interrupted only when moving the refrigerators to provide water and radiation loads. The conditions in the refrigerator were kept steady and stratification avoided by mounting four fans inside each refrigerator for constant air circulation.

3. Results

3.1. Initial investigation

Results from the experiments included in the initial investigation, are presented in sections 3.1.1–3.1.3.

3.1.1. Water uptake

Results from the water uptake experiments are displayed in Figs. 7 and 8 for brick and mortar respectively. For the brick specimens, a large difference in water absorption was observed. After 300 min, agents A, B, C, D, K and L had reached saturation to the same degree as the reference specimen Q. Agents F and H followed closely with initial absorption, but took the duration of the experiment to reach saturation. Agents G and P are in the middle of the absorption range, and finally agents E, I, J, M, N and O have a mass increase of less than 2% during the duration of the experiment, and are thus deemed to be the most successful agents in regards to low water uptake.

For the mortar specimens, the results seem more random for the various agents. However, as can be seen in Fig. 8, treatments N and O seem to have no effect on the mortar, as they quickly absorb the same amount of water as the reference specimen. Agents M and P gain less than 2% mass during the duration of the experiment, and agents E, G, H and K gain less than 5% mass during the experiment.

Fig. 9 distinctly shows the effectiveness of the various hydrophobization agents, and it is clear that there is relatively no mass increase in brick specimens treated with E, I, J, M, N and O, all silane based except E which is a hybrid. For the mortar speci-

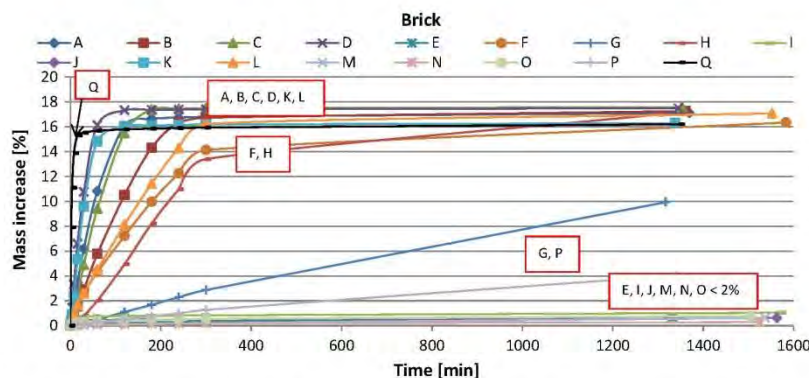


Fig. 7. Mass increase by full immersion over time for brick specimens with hydrophobization agent A-P. Q is reference specimen.

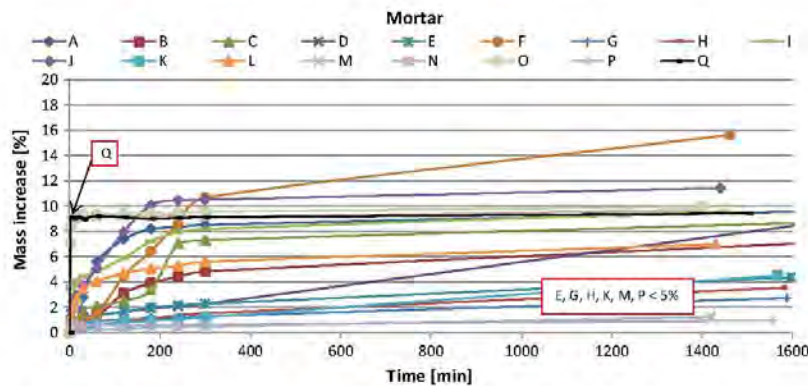


Fig. 8. Mass increase by full immersion over time for mortar specimens with hydrophobization agent A–P. Q is reference specimen.

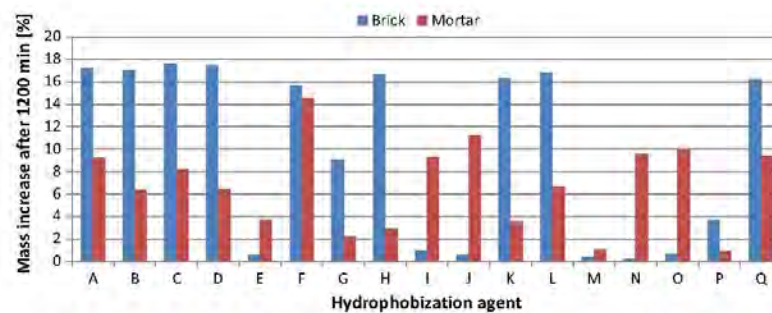


Fig. 9. Bar chart of the mass increase of each specimen after 1200 min of full immersion. Q is reference specimen.

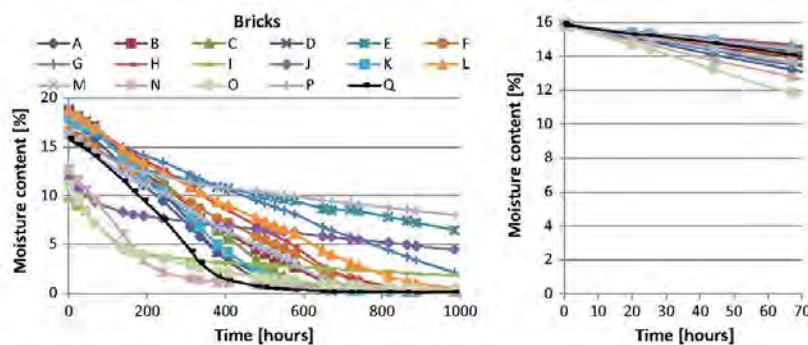


Fig. 10. Moisture content reduction of brick during drying time in climate chamber. Right: All moisture contents are adjusted to the same initial moisture content.

mens, the largest effect of hydrophobization is seen from agents M and P, silane based and hybrid.

3.1.2. Drying experiment

The results from the drying experiments are shown in Figs. 10 and 11 below. To the right, the initial drying period is shown as a section, where all the specimens' initial moisture content is adjusted, for a better visualization of the various slopes for different hydrophobization agents. The initial slopes of the drying curves are especially interesting, as this is where liquid transport to the

surface occurs. Actual rain events are assumed not to yield vacuum saturated materials however.

It can be seen that brick specimens, A, I, J, N, and O have the fastest initial drying, and several specimens showed a faster drying than the reference. In terms of long-term drying, brick specimens with agents A, B, C, D, F, H, K, M, N and O reach levels of relatively constant moisture content, and are all less than 1% moisture content. In regards to mortar specimens, the initial drying is most rapid in specimens with agents H, K, L, N and O.

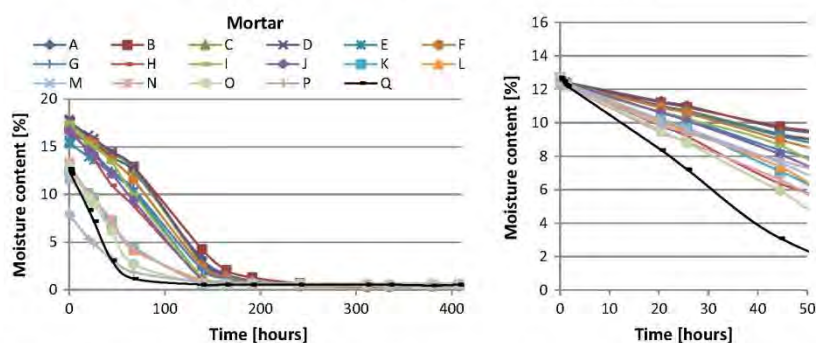


Fig. 11. Moisture content reduction of mortar during drying time in climate chamber. Right: All moisture contents are adjusted to the same initial moisture content.

Table 5

Initial slopes of the various drying curves, generated for the first 67 h of the experiment for brick, and 45 h for mortar specimens.

Hydrophobization agent	Brick		Mortar	
	Initial slope	Relative to reference [%]	Initial slope	Relative to reference [%]
A	−0,0403	47	−0,0681	−68
B	−0,0301	9	−0,0658	−69
C	−0,0239	−13	−0,0755	−65
D	−0,0248	−10	−0,0767	−64
E	−0,0225	−18	−0,0783	−64
F	−0,0268	−3	−0,0833	−61
G	−0,0186	−32	−0,0972	−55
H	−0,0196	−29	−0,1421	−34
I	−0,0362	31	−0,0910	−58
J	−0,0361	31	−0,1028	−52
K	−0,0223	−19	−0,1254	−42
L	−0,0279	1	−0,1197	−44
M	−0,0336	22	−0,1141	−47
N	−0,0468	70	−0,1371	−36
O	−0,0602	118	−0,1520	−29
P	−0,0220	−20	−0,1111	−48
Q(ref)	−0,0276	—	−0,2154	—

Table 6

Penetration depth [mm].

	Brick	Mortar
A	2,1	2,6
B	1,9	4,6
C	0,7	5,6
D	0,9	6,6
E	5,1	16,0
F	2,0	13,0
G	1,6	16,2
H	1,7	3,4
I	17,6	15,4
J	11,4	16,1
K	1,2	3,3
L	0,9	10,9
M	2,7	5,0
N	26,7	1,1
O	27,1	2,0
P	5,4	1,7
Q	0,0	0,0

In Table 5 an overview of the different initial slopes can be seen. The drying slopes for the mortar specimens are generally higher than those for the brick specimens. All the mortar specimens show slower drying compared to the reference, while there is much more variation in the drying velocity in brick specimens, as some bricks (A, B, I, J, L, M, N, O) exhibit faster initial drying than the reference, and the rest of the specimens show slightly slower initial drying.

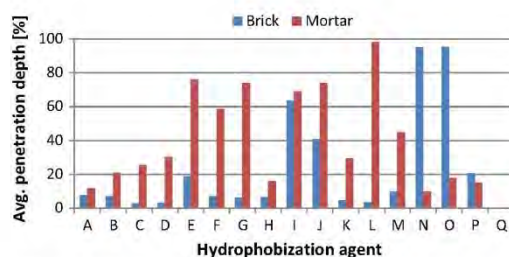


Fig. 12. Penetration depths, presented as percentage of $\frac{1}{2}$ specimen thicknesses.



Fig. 13. Penetration depth of agent I on brick and mortar.



Fig. 14. Penetration depth of agent F on brick and mortar.



Fig. 15. Penetration depth of agent O on brick and mortar.

3.1.3. Penetration depth

The average penetration depth of the hydrophobization agent is presented below, in Table 6 and in Fig. 12 as a percentage of half the specimen thickness. It is seen that for both brick and mortar, agents I and J, which are both silane based, creamy agents, have high penetration depths. Furthermore, agents E, F, G, and L (hybrid, siloxane, nanotechnology and chlorophyllane) have high penetration depths in the mortar samples. Brick specimens with agent N and O, both silane based, leave an undefinable pattern of a dark/wet ring around the edges when compared to other samples, rather than being dry. However no water absorption in the specimen yields the conclusion of almost full penetration; see Figs. 13–15.

Figs. 13–15 illustrate three examples of penetration depth in brick and mortar of agent I, F and O respectively. The difference in penetration depth in the brick specimens was very apparent. For the brick specimen with agent F, there was only a thin, external line of dry material, whereas agent I was seen to penetrate deep into the brick. For mortars, agent I had fully penetrated the specimen, and water-drops lay on top of the specimen. The penetration of agent F on the mortar sample was very uneven.

3.2. Influence on vapour diffusion

Results from the water vapour diffusion experiment are seen in Table 7 and Fig. 16 as average values for the three specimens of each type, and standard deviation is presented. It can be seen that

Table 7
Average water vapour diffusion resistance factor and standard deviation.

	μ [–]	Standard deviation [–]
Brick Q, reference	12.7	1.0
Mortar Q, reference	7.7	1.2
Brick J	12.2	2.8
Mortar J	7.7	1.1
Brick N	11.7	0.7
Mortar N	5.5	2.0
Brick P	11.5	1.3
Mortar P	6.7	0.9

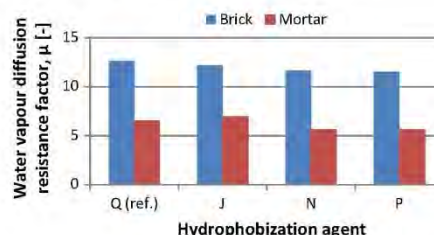


Fig. 16. Graphical illustration of water vapour diffusion resistance factor on specimens with no treatment (Q) and treatments J, N and P.

the water vapour diffusion resistance factor was not affected significantly by the three investigated hydrophobization treatments. There is however, a slight tendency of reduced water vapour diffusion resistance factor with the application of hydrophobization treatment. This tendency is attributed to uncertainties in the experiment.

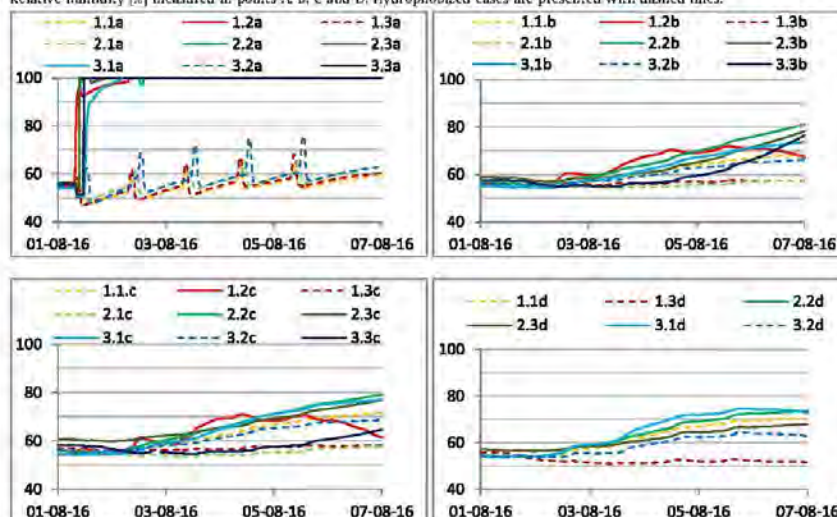
3.3. Water migration through masonry

Studying the relative humidity in points A, B, C, and D, presented in Table 8, the effects of hydrophobization was clear – especially in point A. The relative humidity in point A, for untreated masonry, reached 100%, and stayed at this level for the duration of the experiment, whereas for hydrophobized specimens, the relative humidity only exceeded 70% in short peaks when the water loads were applied. When studying the migration of moisture through the wall, it was seen that the relative humidity increased in all the sensor points during the experiment. In point D however, the relative humidity for all the cases seemed to reach individual maximum limits of 40–75% that were not further affected by the climatic loads. It was seen that the hydrophobized walls 1.3 and 2.1 had the lowest relative humidities monitored in points B, C and D (although the sensor D was missing for wall 2.1). In these points, the hydrophobized walls 1.1 and 3.2 had conditions resembling the untreated walls. These two walls both had diffusion open paint on the interior side, indicating more influence from interior conditions. Unfortunately, walls 2.1 and 3.3 did not have internal surface treatment. However, 1.3 had ordinary paint, which left it less susceptible to the indoor climate, and thus resulted in the lower relative humidity. Wall 2.2 with diffusion open paint, also exhibited higher RH in points B, C and D compared to 2.3 with ordinary paint. The same tendency applies to wall 3.1 that also had ordinary paint on the internal surface. At the critical point C, the interface between internal insulation and masonry, the relative humidities seemed to be continually increasing, with the exception of the hydrophobized walls 1.3 and 2.1. The unhydrophobized wall 3.3 without internal surface treatment yielded a lower relative humidity, also when compared to the hydrophobized walls 1.1 and 3.2. Both the hydrophobized and unhydrophobized wall with insulation of PUR with capillary active channels (2.1 and 3.3), seemed to generate some of the lowest relative humidities at point C, likely due to the capillary active properties, despite the fact that the foam concrete exhibited both a higher water uptake coefficient and a lower vapour diffusion resistance factor.

4. Discussion

It should be noted, that for the initial investigation, agent P was not diluted, as this was unknown information at the time. Agent P was developed for calcareous materials; however the erroneous application may be the reason for the less pronounced effect on

Table 8
Relative humidity [%] measured in points A, B, C and D. Hydrophobized cases are presented with dashed lines.



lime mortar. As previously mentioned, specimens were vacuum saturated with hydrophobization agent on the drying surfaces prior to the drying experiment. As seen in Figs. 10 and 11, brick specimens with agents I, J, N, and O did not reach the same saturation as other specimens. The vacuum saturation of these specimens was repeated to check for error in the saturation procedure. There was no error however, and the explanation was found during the penetration depth experiment. These silane based agents simply penetrated the brick to such an extent that there was less room for water in the pores. It could also have been, that despite the vacuum, these agents blocked the saturation, as they all exhibited low water absorption (>2%) as well. The high penetration depth and effectiveness exhibited by agents I and J, may be attributed to the application method, as these creamy agents were applied with a paint brush and in specified amounts, as opposed to the liquid agents which were applied to specimens by a 10 s exposure. The 10 s exposure time was applied in order to achieve equal hydrophobization on all sides, and to be able to gain the same curing periods for all sides. The method cannot be applied in reality; however e.g. spraying for 10 s is in fact a rather long time frame. The application method does, however, give basis for the comparative study. In regards to mortar specimens, it should be noted that specimens K, L, M, N, O, P, and Q had a slightly lower porosity (as specified in Section 2.1), also yielding these specimens a lower degree of saturation compared to other specimens. The water uptake experiment took place for 24 h, and naturally it is not assumed that an actual rain event will strain a façade to the same degree, however, the experiment was conducted for the purpose of comparison between the different agents. Only one specimen of each agent, on brick and mortar, respectively, were investigated in the initial investigation, yielding the possibility of error, or erroneous results due to minor varieties in the samples. Also, a masonry wall will never undergo the same level of saturation as the vacuum saturated specimens prior to the drying experiment did. In reality, a wall would be much less saturated. The vacuum saturation was performed to achieve a similar moisture content basis. For all of the experiments there are sources of error con-

nected to measurement equipment and human error. For experiments with weight and dimension registration, the scale and caliper both have limitations. Scales used for the drying experiment were only ± 0.1 g, for the water uptake experiment the precision was ± 0.01 g, and for the investigation of influence on vapour diffusion, a ± 0.001 g scale was used. The caliper used for determination of specimen dimensions was 2 decimals. All specimens, especially mortar specimens, were irregular and the square (water uptake, drying and penetration depth) and round shapes (vapour diffusion) were assumed for determination of dimensions. As the errors should be the same for all specimens in this comparative analysis, the effect of the errors is neglected. The sensors used in the investigation of water migration through masonry had an accuracy of $\pm 1.8\%$ RH and ± 0.2 °C.

For water absorption experiments on brick specimens, the best performances were seen in agents E, I, J, M, N, and O, which were primarily silane based agents and one hybrid. For specimens of lime mortar, the effectiveness of the different agent types was not pronounced, as the best performers were a variety of types (silane, hybrid and nano). The drying experiment showed that brick specimens A, I, J, N, and O (primarily silane based) had the most rapid initial drying, whereas H, K, L, N, and O (a variety of types) exhibit fastest initial drying for mortar specimens. Brick specimens A, B, C, D, F, H, K, L, M, N, O, and Q reached constant levels of less than 1% after 1000 h in the drying chamber, whereas all mortar specimens reached this level within 250 h, but these specimens were also rather small. As stated in the experiment's description, the drying experiment was carried out in a climate chamber with a temperature of 20 °C and 85% RH. These conditions may not have been representative for real boundary conditions for a masonry wall, as it is also exposed to e.g. solar radiation and wind. However, for comparison purposes, these conditions were expected to give a correct picture of the influence of surface treatment on drying potential.

The simplified ranking system described in Section 2.2.1 was introduced in order to try and evaluate the various results, despite some of the results being contradictory, the ranking system yields

Table 9
Ranking of the various hydrophobization treatments for brick and mortar altogether, and brick and mortar individually.

Ranking by 3 categories					
Brick and mortar	Σ Score	Brick	Σ Score	Mortar	Σ Score
O	297	O	314	G	116
N	239	N	268	E	90
I	230	I	189	M	85
M	213	J	168	L	82
J	195	M	128	P	57
E	186	E	96	H	44
P	132	P	75	I	41
G	128	A	49	K	40
L	81	G	12	J	27
K	25	B	10	Q (reference)	0
H	17	F	4	O	–17
Q (reference)	0	Q (reference)	0	B	–24
A	–9	L	–1	D	–24
B	–14	D	–15	N	–29
D	–39	K	–15	C	–31
C	–50	C	–19	A	–58
F	–64	H	–27	F	–68

opportunity for evaluation of overall results. The ranking was performed as described in Section 2.2.1, of the various hydrophobization agents based on the initial investigation is seen in Table 9.

The water uptake experiment distinctly showed the reduction in initial water uptake for most hydrophobization agents, as expected, due to the purpose of the surface treatment. This was also illustrated in [20]. It is evident that hydrophobization treatments of silane rather than siloxane (O, N, I, J, and M) seemed to perform better overall, and especially on bricks. However they seemed less efficient on the lime mortar. I and J performed better on the mortar, compared to O and N, which may be explained by the creamy consistency and application method. On the mortar, agents G, E, M, L and P seemed the most efficient; these are hybrids, silane and nanotechnology based.

Overall, it was seen that brick generally is more susceptible to hydrophobization treatment, and the effect is more pronounced in brick samples. The silane based agents seemed to perform better in the initial investigation, and agent M was represented in top-5 of all the ranking lists.

With regard to the study by Guizzardi et al. [21] stating that moisture transport occurred faster in bricks rather than mortar, the lesser efficiency observed in hydrophobization of the lime mortar may not be crucial for the overall effect of hydrophobization on a masonry construction. On the other hand, the study by Van Hees proved the opposite, why mortar joints may in fact be the weakest part of the masonry, emphasizing the need for hydrophobization efficiency of masonry in a holistic perspective. Many historic façades have been renovated since the 1940's; thus it can be expected that the external part of the joints in some cases has been replaced with a cementitious, siliceous mortar, and why the effect of hydrophobization on this type of mortar should be investigated. Based on the studies by Zhang et al. [10] and Slapø et al. mortar with a high water content is recommended for façade renovations, as it reduces the water ingress in itself, and enhances the effect of a hydrophobization treatment.

The hydrophobization treatments examined did not seem to have a negative effect on the drying capability of specimens, nor the diffusion resistance, as also seen in the study by Engel et al. [24]. The present study did not show the same results in regards to concentrations and drying, as different agents were used, and not only various concentrations of an active component. Previous studies found that water vapour permeability was reduced by application of hydrophobization [12,25], however that is not the case in the present study or in the work by Van Hees, who observed only a limited effect on the vapour permeability. Van Hees [22] and

Couto et al. [25] did find the treatments to have a high impact on the drying capabilities, however that was not the case in the present study.

Similar to the study by Lubelli et al. [26], the nano-coating included in this study, namely G and H, performed well on mortar specimens in regards to water uptake and drying, and the penetration depth here was found to be similarly small. In the present study, the performance of nano coatings on brick specimens in the, were however not of noteworthy character.

From the investigation of water migration through masonry, it was seen that the hydrophobization treatment had the largest effect on the external part of the masonry, and to a lesser extent through the wall. Hydrophobization combined with ordinary paint on the internal side, however, seemed to generate the lowest relative humidities and moisture content in internal measuring points. Thus the hydrophobization treatment on the masonry seemed to have the desired effect, despite the initial investigation showing less effect of hydrophobization on the lime mortar. The moisture migrations in walls with foam concrete and ACC seemed to be unaffected by the insulation type, however, the walls insulated with PUR with integrated capillary active channels showed the best results in the interface between insulation and masonry, regardless of the hydrophobization treatment. The internal surface treatments seemed to be influential on the results, as the cases with ordinary paint (1.3 and 2.3) exhibit lower relative humidities compared to cases with diffusion open paint. The results are similar to those found by Finken et al. [5], that the hydrophobization has a positive effect on the hygrothermal conditions of internally insulated masonry walls.

The 24 h cycles implemented did not represent true nature, as the repeatability of the exact loads is highly unlikely. Despite this fact, the setup and the cycles represented realistic loads and gave results suitable for interpretation of WDR penetration of solid masonry, both with and without hydrophobization. It should be mentioned, that the rain loads hit only the top of each wall section, and water ingress through the lower masonry occurred due to run-off. As mentioned, the sensors were located in the middle of the wall section, and thus rather than a severe rain event, it may in fact have been of lesser severity at this location.

Future investigations could include the durability of each hydrophobization treatment, e.g. in masonry with a high salt content, or how various chemicals affect the effectiveness of hydrophobization. Furthermore, the durability in regards to climatic exposure in the form of UV-radiation, rain and erosion could be studied. In addition, the large scale experiment could have been

equipped with sensors in the mortar joints as well, for determination of moisture migration in these.

5. Conclusion

The study concludes that a hydrophobization treatment had the desired effect of reduced rain water penetration on historic masonry, however this effect was more pronounced in the brick as compared to the lime mortar. For specimens of ceramic brick, silane based agents proved to have the best properties, however, for mortar a variety of active components were most efficient. Drying of treated specimens was not significantly influenced for brick; however the drying of lime mortar was slightly impeded by the hydrophobic treatment. Furthermore, the investigation showed that the vapour diffusion, through both brick and mortar, was not influenced by the hydrophobization treatments. The investigation of moisture migration through masonry showed a distinctive effect of hydrophobization, especially in the external part of the wall, indicating a potential for protection from frost damages and biological growths. The hydrophobization treatment in general also yielded lower relative humidities throughout the wall in most cases; however walls insulated with PUR with calcium silicate channels generally performed better in the critical interface, regardless of hydrophobization. The internal surface treatments also seemed to influence the results, and the two cases with ordinary paint show better results compared to their equivalents with diffusion open paint.

6. Declarations of interest

None.

Acknowledgements

The presented work is a part of RIBuild project that has received funding from the European Union's Horizon 2020 research and innovation programme under grant agreement No 637268.

References

- [1] H. Tommerup, S. Svendsen, Energy savings in Danish residential building stock, *Energy Build.* 38 (2006) 618–626, <https://doi.org/10.1016/j.enbuild.2005.08.017>.
- [2] T. Odgaard, S.P. Bjarlov, C. Rode, M. Vesterlökke, Building renovation with interior insulation on solid masonry walls in Denmark – a study of the building segment and possible solutions, *Energy Procedia* 78 (2015) 830–835, <https://doi.org/10.1016/j.egypro.2015.11.003>.
- [3] E. Vereecken, L. Van Gelder, H. Janssen, S. Roels, Interior insulation for wall retrofitting – a probabilistic analysis of energy savings and hygrothermal risks, *Energy Build.* 89 (2015) 231–244, <https://doi.org/10.1016/j.enbuild.2014.12.031>.
- [4] B. Blocken, J. Carmeliet, A review of wind-driven rain research in building science, *J. Wind Eng. Ind. Aerodyn.* 92 (2004) 1079–1130, <https://doi.org/10.1016/j.jweia.2004.06.003>.
- [5] G.R. Finken, S.P. Bjarlov, R.H. Peuhkuri, Effect of façade impregnation on feasibility of capillary active thermal internal insulation for a historic dormitory – a hygrothermal simulation study, *Constr. Build. Mater.* 113 (2016) 202–214, <https://doi.org/10.1016/j.conbuildmat.2016.03.019>.
- [6] E. Vereecken, S. Roels, Capillary active interior insulation: do the advantages really offset potential disadvantages?, *Mater. Struct.* 48 (2015) 3009–3021, <https://doi.org/10.1617/s11527-014-0373-9>.
- [7] H.M. Künzel, Simultaneous heat and moisture transport in building components – one- and two-dimensional calculation using simple parameters, 1995, doi: ISBN v.3-8167-4103-7.
- [8] T. Odgaard, S.P. Bjarlov, C. Rode, Influence of hydrophobation and deliberate thermal bridge on hygrothermal conditions of internally insulated historic solid masonry walls with built-in wood (unpublished results/in press), *Energy Build.* (n.d.).
- [9] T.K. Hansen, S.P. Bjarlov, R.H. Peuhkuri, M. Harrestrup, Long term in situ measurements of hygrothermal conditions at critical points in four cases of internally insulated historic solid masonry walls, *Energy Build.* (2018), <https://doi.org/10.1016/j.enbuild.2018.05.001>.
- [10] J. Macmillen, Z. Zhang, E. Ritsch, H. Nath, N. Bennett, Brick and mortar treatment by cream emulsion for improved water repellence and thermal insulation, *Energy Build.* 43 (2011) 1560–1565, <https://doi.org/10.1016/j.enbuild.2011.02.014>.
- [11] H. Mayer, Masonry protection with silanes, siloxanes and silicone resins, *Surf. Coat. Int.* 81 (1998) 89–93.
- [12] E. Charola, Water-repellent treatments for building stones, *J. Preserv. Technol. Technol.* 26 (1995) 10–17, <http://www.jstor.org/stable/1504480>.
- [13] H.R. Trechsel, M.T. Bomberg, Moisture Control in Buildings: The Key Factor in Mold Prevention, second ed., ASTM International, 1994, <http://books.google.com/books?id=pr6X3yVYSIC&pgis=1>.
- [14] H. Boostani, S. Modirrousta, Review of nanocoatings for building application, *Procedia Eng.* 145 (2016) 1541–1548, <https://doi.org/10.1016/j.proeng.2016.04.194>.
- [15] H. Sandholdt, D. Dysted, Experimental and Theoretical Investigation of Interior Insulations of Solid Brick Walls with Foam Concrete and Other Silicate Based Materials, DTU Civil Engineering, 2015.
- [16] A. Nicolai, J. Grunewald, Delphin 5 User Manual and Program Reference, Program, 2006.
- [17] Kemmers, Technical data sheet – Fungosil FC, (n.d.) 1–3.
- [18] D. Niels Hansen, Hvad kan du forvente, når DMI varsler skybrud? DMI, 2015, <https://www.dmi.dk/nyheder/arkiv/nyheder-2015/05/hvad-kan-du-forvente-naar-dmi-varsler-skybrud/> (accessed 21.03.2017).
- [19] H. Kaaris, By og Byg Dokumentation 048, Klimasimulatorer. Teknisk dokumentation for accelereret ældning, perioden 1994–2002, 2003.
- [20] T.K. Hansen, S.P. Bjarlov, R. Peuhkuri, Moisture transport properties of brick – comparison of exposed, impregnated and rendered brick, International RILEM Conference on Materials, Systems and Structures in Civil Engineering 2016 Segment on Moisture in Materials and Structures, 2017, pp. 351–360, http://orbi.dtu.dk/ws/files/128040737/Pages_from_Moisture_conf_proceedings_3.pdf.
- [21] M. Guizzardi, D. Derome, R. Vonbank, J. Carmeliet, Hygrothermal behavior of a massive wall with interior insulation during wetting, *Build. Environ.* 89 (2015) 59–71, <https://doi.org/10.1016/j.buildenv.2015.01.034>.
- [22] R.P.J. Van Hees, The performance of surface treatments for the conservation of historic brick masonry, in: Proc. CIB World Build. Congr. Gävle, Sweden, 7–12 June 1998, 1998.
- [23] F. Slapo, T. Kvande, N. Bakken, M. Haugen, J. Lohne, Masonry's resistance to driving rain: mortar water, *Buildings* 7 (2017) 70–86, <https://doi.org/10.3390/buildings7030070>.
- [24] J. Engel, P. Heinze, R. Plagge, Adapting Hydrophobizing Impregnation Agents to the Object, *Restoration of Buildings and Monuments* 20 (2014) 1–8, <https://doi.org/10.12900/RBM14.20.6-0029>.
- [25] S. Couto, T.D. Gonçalves, J.M.G. Lopes, Drying of Red Ceramic Brick. The effect of five Silicone-based Water-Repellent Treatments, in: *Hydrophobe VI. 6th International Conference on Water Repellent Treatment of Building Materials*, 2011, pp. 81–92.
- [26] B. Lubelli, R.P.J. Van Hees, Evaluation of the effect of nano-coatings with water repellent properties on the absorption and drying behaviour of brick, *35 (2011) 125–135*.

Appendix C

Paper III

The effects of wind-driven rain on the hygrothermal performance of solid masonry walls with internal insulation

The effects of wind-driven rain on the hygrothermal performance of solid masonry walls with internal insulation

Tessa Kvist Hansen^{a*}, Søren Peter Bjarløv^a, Ruut Peuhkuri^b

^aDepartment of Civil Engineering, Technical University of Denmark, Brovej 118, 2800 Kgs. Lyngby, Denmark

^bDanish Building Research Institute, Aalborg University, Denmark, A.C. Meyers Vænge 15, 2450 Copenhagen, Denmark

*Corresponding Author: Tessa Kvist Hansen, tekhan@byg.dtu.dk, +45 45251803

Abstract

An inevitable measure when energy retrofitting historic buildings in Europe, is the reduction of building envelope heat loss. On preservation-worthy facades where external insulation is not an option, installation of internal insulation is gaining pace. The historic buildings are often constructed with solid masonry facades and wooden decks. The internal insulation may, however, entail potential hygrothermal risks in walls and embedded wood. Measures such as vapour barriers and capillary active insulation materials are continuously evolving and the subject of much current research. The hygrothermal conditions are of great importance for the durability of the building constructions, and for the health and wellbeing of occupants. Wind-driven rain (WDR) is a central factor contributing to water penetration and moisture loads of the exterior walls. Numerous studies have shown that WDR loads influence the moisture conditions in masonry walls and embedded wooden beams, and can even affect interior relative humidity. In the present paper WDR loads on existing façades in a cold temperate climate were determined by measurements and compared to a semi-empirical model. Simultaneously, the hygrothermal conditions within internally insulated walls with exposed brick and embedded wooden beams were monitored. Implementation of a semi-empirical model for calculations of WDR confirmed previous studies in predictions being too conservative. Results from the field measurements did not confirm that WDR has a clear impact on the relative humidity measured in walls behind interior insulation. Hygrothermal simulations and previous studies, however, inevitably show that high WDR loads result in higher relative humidity behind the interior insulation.

Keywords: wind-driven rain, internal insulation, hygrothermal performance, moisture transport, in situ measurements

1 Introduction

Driving or wind-driven rain is rain that passes through a vertical plane in the atmosphere. Wind-driven rain (WDR) is generally assumed to be one of the most important factors that must be taken into account in hygrothermal assessments of external vertical structures, particularly with porous building materials such as brick and mortar. WDR is the most influential factor contributing to the wetting and water penetration of external façades, which in turn affects not only hygrothermal properties and durability [1], but also has been shown to influence indoor climate, energy consumption and the risk of mould growth [2]. Internal insulation is vital in energy retrofits of historic buildings where external changes are unacceptable. Unfortunately, interior insulation increases the risk of interstitial condensation, as changes in the temperature gradient increases the relative humidity, and the lower temperature also reduces the drying potential of the walls. Capillary migration of WDR contributes to moisture induced risks, especially where vapour barriers, capillary

inactive insulation materials [3], or diffusion tight paint on the interior surface are present, as they make it more difficult for the moisture to evaporate inwards. Damaged façades are less resistant to WDR and therefore internal insulation should only be installed on intact façades. Damaged or weathered bricks, joints and render should be replaced or repaired before internally insulating [4][5]. Mould or wood decaying fungi growth in wooden beams and other woodwork in the wall are not the only risks associated with the accumulation of moisture in the masonry façade. The risks also include a resulting decrease in durability due to frost damage, surface soiling, and salt migrations [6], not to mention the reduced thermal resistance caused by an accumulation of moisture (especially for capillary active insulation systems) [7]. Basic moisture transport mechanisms in and around an internally insulated solid wall with embedded wooden beams are illustrated in Figure 1. The moisture transport mechanisms include vapour diffusion, typically from a higher vapour pressure in the warm interior outwards due to vapour pressure differences. Through porous building materials capillary suction leads to the transport of liquid moisture, whether it is present due to condensation, WDR, or rising damp. In other words, capillary suction is the driving force of moisture transport in saturated pores, whilst at lower humidities within the pores the main transport mechanism is diffusion. Convective moisture transport occurs as a consequence of moving damp air through leakages, etc. At thermal bridges, e.g. partition walls and floor slabs, the colder surface temperature also makes it possible for moisture to accumulate.

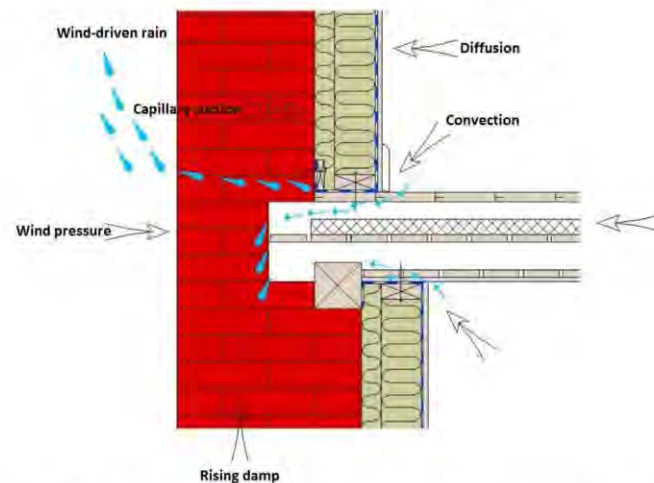


Figure 1: Typical moisture transport mechanisms in an internally insulated wall [8].

The magnitude of WDR is a function of rain intensity, size and distribution of raindrops, and wind speed. The simultaneous occurrence of wind and vertical rain generates the WDR, which can be referred to as a sloped vector [1], illustrated in Figure 2. The terminal velocity of the raindrop is dependent on the size of the raindrop; larger droplets fall faster [9], but are less easily carried by wind [10]. The impact on the façade is affected by additional factors, such as the building geometry, wind direction, local topography, climate, obstructions, façade orientation, rainfall duration, pressure differences, façade surface characteristics, uniformity, condition, and location on façade. Studies have shown that the edges [11] and top of a building are most exposed to WDR provided there is no existing roof overhang [12]. This phenomenon can be partly explained by the varying wind pattern across an obstacle such as a building, and the fact that the edges are subjected to WDR from two sides. The wetting of edges has also proved to be more prolonged when compared to central areas of the façades, due to the lower temperatures and reduced drying potential [2]. Strong solar loads may also drive moisture from large WDR loads further into the construction [13]. There are various quantification methods for WDR loads, namely experimental, semi-empirical, and numerical models [1][14].

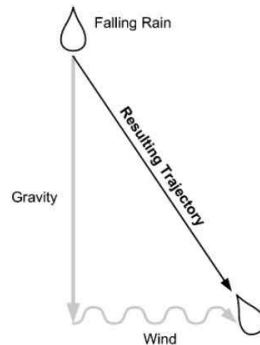


Figure 2: Basic illustration of WDR [9].

There are three methods for WDR quantification, namely experimental quantification by measurements, numerical simulations models, and semi-empirical models. The present work includes experimental methods as well as implementation of semi-empirical and numerical models based on climate data. The semi empirical models have been developed and improved over time, as described in section 2.5.

Experimental quantification of WDR loads is not a standardized procedure, although it is always performed with a WDR gauge. Wall-mounted WDR gauges have been implemented in experimental work since 1930's and a variety of designs have been used. The designs vary in shape, size, materials, whether or not they are recessed in the wall, and whether or not they are installed with automatic wipers; variations that have been found to yield discrepancies [1]. The most influential source of error in connection with WDR measurements has been identified as the evaporation of adhered water on the collector plate. Other sources of error include splashing of rain drops, evaporative losses from the reservoir and connecting tube, condensation on the collection area and wind errors. A deeply recessed WDR gauge type has proven to reduce the splashing errors with high wind speed and rain intensity, while in the case of light rain, the large collection area generated large evaporative losses, and splashing in this case was irrelevant [1][14]. The condensation error on the collector surface has been estimated in simulations [14], and shown to be small. This is the only error source that can increase measured results, which are thus liberal.

Numerical models of WDR are often based on computational fluid dynamics. The numerical method includes various HAM (Heat, Air and Moisture) simulation models performed in various codes, e.g.; HAMFEM [15], WUFI [16] or Delphin [17]. Abuku et. al. (2012) performed extensive research on WDR, comparing measurements and numerical simulations [15] [18]. A test building was set up for WDR measurements in actual climate conditions. The test building included specially installed test sections for monitoring WDR, weight changes in specimens, surface temperature, and runoff water for monitoring the moisture response to WDR impact. Large differences were detected between measurements and simulation results. The differences could not all be attributed to the convective moisture transfer coefficient, β_e , used in the HAM simulations. A parameter study of β_e as a function of the reference wind measured did show some influence on results and compatibility. The discrepancies found were also attributed to various error sources such as adhesion, evaporation, splashing, bouncing, and spatial and temporal averaging of rain drops. The fact that many of the parameters interact, makes it is very difficult to make precise numerical simulations of WDR.

Morelli et. al. (2012) [19] compiled a short review of studies on masonry walls with wooden beams. Most of the reviewed literature stated that WDR was not problematic as long as the façade was intact (no cracks or degraded joints). These studies did not clearly reference WDR loads or climate conditions, and WDR was not included in the hygrothermal simulations. Morelli et. al.[20] also studied potential moisture risks at beam ends in masonry walls subjected to WDR. The study was based on FMEA (Failure Mode and Effect Analysis) and hygrothermal simulations of retrofitted masonry walls with embedded wooden beams as story-partitions, and internal insulation. See also Figure 3 for illustration of the construction types. The hygrothermal simulations with WDR of various intensities (3 different rain

exposure coefficients) did not show any sign of an effect on the moisture conditions behind the insulation, but with high rain intensity the beam ends could exceed critical moisture content. For medium rain intensity it was seen that in cases with free air flow around the beam (20 mm to three sides) and reduced insulation (omitting 200 mm insulation above and below the beam), the moisture content had a tendency to be lower than in constructions with full insulation, which tended to increase the moisture content. Simulations with vapour barriers applied to the case with reduced insulation indicated no impact on the drying potential of beam ends, so the 20 mm air gap around the beam is the influential factor. It was concluded that WDR had a substantial impact on the moisture conditions in beam ends, and that the rain intensity was a very influential factor.

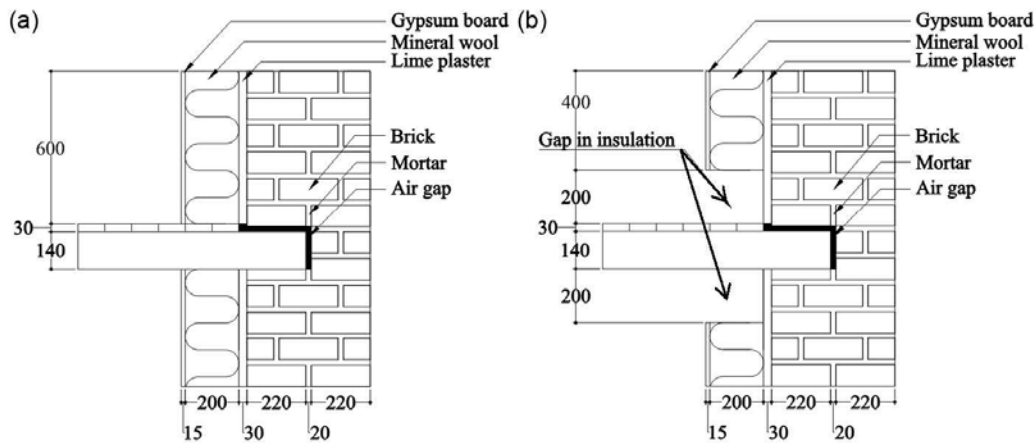


Figure 3: The construction principles around beam ends used in Morelli et. al's FMEA and hygrothermal simulations in [19]. Illustration from [19]. A previous study by Morelli et. al. (2010) with 2D and 3D simulations of internally insulated masonry with wooden beams embedded, showed that the magnitude of WDR load had a significant impact on the moisture conditions in beam ends [20].

Abuku et. al. (2008) investigated the interaction between indoor and outdoor climate and a solid masonry building envelope; with a focus on WDR impact on hygrothermal response, including mould growth, indoor climate and energy consumption. Using numerical simulations, the hygrothermal conditions in the brick wall and room were determined. The study found a distinct impact of WDR on the humidity of internal wall surfaces and indoor humidity. Critical periods were seen especially in summer and winter, and the walls were especially affected in the south and west wall-orientations, as this is also the dominant wind direction at the location of the study [2]. A subsequent study by Abuku et. al. (2009) compared WDR field measurements with numerical simulations, and determined the responses of the walls to WDR loads. The study indicated that predicted WDR loads were often overestimated in numerical modelling of moisture content, partly because of the splashing of raindrops hitting the wall surface not being considered in standard HAM modelling, and partly due to averaging errors in absorption and evaporation [18]. Klöšerko et. al. (2014) reported a study of field measurements of four different internal insulation systems. They found a certain impact from exterior conditions/rain as increased humidity was measured at the interface between insulation and brick in the case of a vapour tight insulation material [21].

A study by Vereecken et. al. (2015) on capillary active interior insulation methods demonstrated that driving rain influenced hygrothermal behaviour undesirably [7]. The study investigated whether a capillary active solution (calcium silicate) performed better than a vapour tight system (extruded polystyrene (XPS)) on single leaf, exposed brick external wall constructions with a dynamic indoor environment. Adding (large) WDR loads in numerical simulations resulted in high relative humidity on the interior side of the masonry in both insulation systems, and of the reference wall. The relative humidity in the case of vapour tight insulation reached roughly 100 % for the entire year, whereas the capillary active system illustrated the capability for inward moisture transport and drying potential when the drying to the

exterior occurred slowly at low temperatures. In regards to moisture accumulation after WDR loads, the vapour tight system showed slower drying; only external drying could occur in this case. In the case of capillary active insulation and a reference wall without insulation, it was seen that WDR loads also influenced the relative humidity on the interior wall surface. This study also found that at high WDR loads the thickness of the masonry wall had an impact on the masonry moisture content regardless of insulation type, and on the indoor relative humidity in cases of capillary active insulation.

The purpose of the present study was to investigate the moisture distribution in the façade after actual WDR loads and possibly establish a correlation between WDR and unacceptable moisture conditions in an internally insulated façade of exposed brick. The aim was also to quantify the real WDR loads on a façade and to identify the impact of this WDR on the moisture content in the masonry wall by monitoring conditions behind the internal insulation as well as at the beam ends. Furthermore, theoretical semi-empirical models and numerical simulation models were investigated with regard to actual measurements. The study included experimental work with WDR measurements on internally insulated masonry facades of two test buildings. It also included monitoring of moisture conditions, as well as implementing semi-empirical WDR models to determine the reliability of the models, as well as to determine the hygrothermal response.

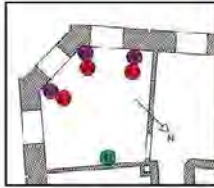

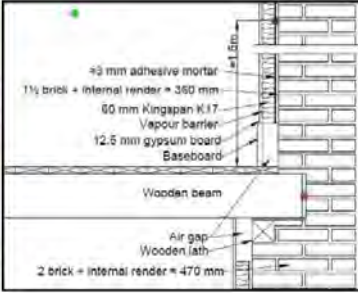
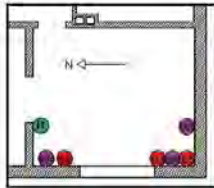

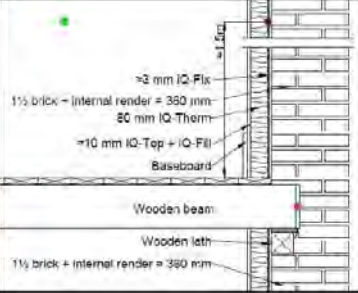
2 Methods and experimental setup

In order to identify the possible water ingress from WDR, gauges measuring WDR and sensors monitoring the hygrothermal conditions within the masonry wall were installed on two test buildings in Denmark.

2.1 Test buildings

The test buildings were two multi-story buildings of typical Danish masonry construction (1850-1950) with embedded wooden beams between the stories. Danish constructions from this time are assumedly constructed with lime mortar, however renovations may have occurred and weathered joints may have been replaced by a cementitious mortar. Both buildings had retained their original construction, with 350 mm solid bare brick external walls at the top story. Table 1 shows the construction after internal insulation had been applied. The differences included the insulation material and its thickness as well as the thickness of the masonry below each story partition and the elevation of the insulated wall. In addition, the major difference between the two buildings is the fact that the insulation system in test building 1 comprises of phenolic foam boards, with integrated vapour barrier and plaster board. This system was installed with 20cm air gaps above and below the beam to create intentional thermal bridges and thus warmer conditions and better drying potential at the beam ends. The insulation system in test building 2 was installed directly to around the beam, with no air gaps. The system itself comprises of PUR foam boards made capillary active with calcium silicate channels in a grid of 40x40 mm. The thermal conductivities of the two systems are 0.020 W/mK and 0.037 W/mK for test building 1 and 2 respectively. The respective U-values are estimated based on unknown brick types, and displayed in the figures. In both buildings measurements behind the insulation and behind beam ends, as marked on the illustrations in Table 1, were obtained.

Table 1: The two test buildings, sensor locations, façade images and section view of insulated façade. The green, red and purple dots represent measuring points indoors, behind beam ends and behind insulation, respectively. The numbered dots represent locations for outputs. In both cases one measurement is made for interior conditions and three measurements behind both beam ends and insulation.

Test building 1: Meinungsgade, Copenhagen, East Denmark			
<p>From 1877 story building 4th floor Residential SW façade Retrofit: Dec. 2014</p> <p>U-values before /after renovation: 1.24 W/m²K / 0.26 W/m²K</p>			
Test building 2: Ny Allégade, Haderslev, South west Denmark			
<p>From 1932 3 story building 2nd floor Residential W façade Retrofit Jan. 2015</p> <p>U-values before /after renovation: 1.24 W/m²K / 0.33 W/m²K</p>			

2.2 Inspection of façades

Before installing WDR measuring equipment, the façades of the test buildings were examined in order to identify potential surface defects which could influence the results. The façades of both test buildings were inspected visually, as cracks, high moisture content, frost damage, salt precipitation or other abnormalities could influence WDR penetration [13]. As for an estimation of water absorption of the masonry façades, and for comparative purposes, a non-destructive test for porous façade materials was made with Karsten tubes [22] on both brick and joints. A Karsten tube consists of a glass/plastic tube with a capacity of 5 ml, affixed to a surface with modelling clay (plasticine). The tube is filled with water and the amount of absorption and size of the visibly wet area is monitored every 5 minutes for 30 minutes, after which the sorptivity and capillary saturated volume moisture content can be determined. The estimations of sorptivity, S , is based on Hendrickx [22]. The calculation steps are described by equations 1-4 below;

$$\text{Penetration distance of the wet front} \quad [mm] \quad x(t) = R_{wet} - R_e \quad (\text{Eq. 1})$$

$$\text{Wet volume for each time step} \quad [mm^3] \quad V_{wet}(t) = \frac{2}{3} \cdot \pi \cdot (x(t)^3 + R_e \cdot x(t)) + \pi \cdot R_e^2 \cdot x(t) \cdot 10^{-3} \quad (\text{Eq. 2})$$

$$\text{Capillary saturated moisture content} \quad \left[\frac{m^3}{m^3}\right] \quad \theta_{cap} = \frac{V_{abs}(t)}{V_{wet}(t)} \quad (\text{Eq. 3})$$

$$\text{Sorptivity, } S, \text{ by isolation (and multiplication with } \frac{10}{\sqrt{60}} \text{ for unit)} \quad \left[\frac{kg}{m^2 \cdot \sqrt{s}}\right] \quad V_{abs} = \pi \cdot R_e^2 \cdot S \cdot \sqrt{t} + \frac{\pi \cdot R_e \cdot \gamma \cdot S^2}{\theta_{cap}} \cdot t \cdot \frac{10}{\sqrt{60}} \quad (\text{Eq. 4})$$

In Eq. 4-7, the following denotations are applied; t : timestep, R_{wet} : radius of wet area [mm], R_e : effective radius of contact zone [mm], V_{abs} : absorbed amount of water [ml], γ : empirically found factor of 0.75.

The test was performed on 3 randomly selected bricks on each test building, and furthermore on 3 joints in test building 2. The measurements of the joints were performed where mortar is dominant in the tube area, where head and bed joints meet, as seen in Figure 4. The Karsten tube measurements were made for comparison between masonry types in the two test buildings which could influence results and for an indication of relative WDR resistance as well as to assist in the classification of brick and mortar.



Figure 4: Karsten tube measurement on brick (left) and mortar joints (right). (Images from test building 2).

2.3 Climate data

Climate data was gathered from local weather stations from the Danish Meteorological Institute (DMI). All the DMI weather stations do not collect all data, which is why the data is spread out on several weather stations, as provided in Table 2.

Table 2: Climate data and origin.

Case	Climate data	Weather station no.
Test building 1	Precipitation	5725
Measurement period: 24/06-16 – 11/01-17	Temperature, relative humidity, wind velocity, wind direction, cloud cover	6180
	Global radiation	6187
Test building 2	Precipitation	5390
Measurement period: 07/06-16 – 10/01-18	Temperature, relative humidity, wind velocity, wind direction, cloud cover	6110
	Global radiation	6123

The climate data was used for WDR calculations and to compare these to the WDR gauge measurements for validation of the WDR gauge measurements.

2.4 Wind-driven rain gauge

The WDR gauge designed for the experiment was based on existing types, experience and comparative tests. It was based on the gauges manufactured at K.U. Leuven's Laboratory for Building Physics, with some alterations according to recommendations found in the literature. The area of the collection plate was 300x300 mm, with a 10 mm raised rim around all the edges. The raised rim caught splashing water to some extent [18], and prevented collection of water from outside the collection area [14][23]. The plate was constructed in acrylic glass (PMMA), which has shown better performance and fewer errors due to water adhesion/evaporation in comparison with teflon (PTFE) [1]. The WDR was monitored by a HOBO Rain Gauge (Metric) Data logger, which was a closed tipping bucket rain gauge that minimizes the evaporation losses from the reservoir. The data logger was fixed to the collection plate, and the water drained directly into the HOBO. The HOBO had a diameter of approximately Ø15 cm, which meant that the collector plate was extended out slightly from the wall surface. The WDR gauge is illustrated in Figure 5. The gauge is also described in [24,25] It was set to monitor rain events, and calibrated prior to use. The calibration showed that one counted rain event corresponded to 3.78 ml and 3.72 ml for test buildings 1 and 2 respectively.



Figure 5: Wall-mounted WDR gauge with HOBO logger. Illustration (left) shows fixation and extension from surface. Image (right) illustrates fixation to façade (test building 1)

As indicated in Table 1, the WDR gauge on test building 1 was mounted on the SW façade, at the 4th floor height. This faces a large cemetery, so no buildings or obstructions in the direct vicinity were expected to influence the WDR measurements. On test building 2, the WDR gauge was located on the W façade at 1st floor height. This façade was facing the street. The distance to the closest neighbor in this direction was approximately 20 m and there were no large trees or other obstructions in the immediate vicinity.

2.5 WDR calculations

Several semi-empirical calculation models for WDR have been developed, and they are continuously under development and improvement. They are all based on the theoretical formula expressed in Eq. 1, where r_{WDR} represents rainfall intensity for WDR and r_h unobstructed horizontal rain [mm], U the wind speed [m/s] and V_t the raindrop terminal velocity of fall [m/s].

$$\text{Wind driven rain} \quad [l/m^2] \quad r_{wdr} = r_h \cdot \frac{U}{V_t} \quad (\text{Eq. 5})$$

In 1955 Hoppestad introduced the WDR coefficient [1][26], which is a proportionality constant between rain on a vertical and horizontal plane, given as $\frac{1}{V_t}$, where V_t is dependent on rain drop diameter [27] and in 1965 Lacy refined the formula (Eq. 5), providing the empirical relationships for functions of median rain drop size and terminal velocity of fall for these raindrops [1][26][28], resulting in Eq. 6, where DRF represents the WDR coefficient, empirically determined as 0.222.

$$\text{Wind driven rain} \quad [l/m^2] \quad r_{WDR} = DRF \cdot U \cdot r_h^{0.88} \quad (\text{Eq. 6})$$

For estimation of rain deposition on a building, Lacy suggests additions to the WDR calculation as seen in Eq. 7, in order to account for wind velocity, wind direction and location on the building.

$$\text{WDR deposition on facade} \quad [l/m^2] \quad r_{bv} = DRF \cdot U \cdot r_h^{0.88} \cdot RAF \cdot \cos(\theta) = r_{WDR} \cdot RAF \cdot \cos(\theta) \quad (\text{Eq. 7})$$

In Eq. 7 RAF is the rain admittance function and θ is the angle between the normal to the wall and the wind direction. RAF varies from <0.20 below a roof overhang up to >1 at the top and edges of high-rise ($>10\text{m}$) buildings without roof overhang, as seen in Figure 6 [26][9]. Equation 7 was implemented in the present study, as it accounts for the wall orientation by including cosine of the wind directions angle to a normal of the wall, and furthermore accounts for the location on a façade.

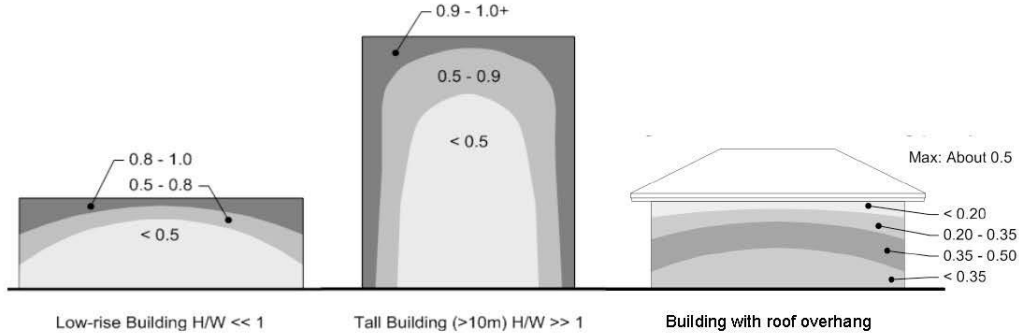


Figure 6: Rain admittance function, RAF, on areas of building facades for low-rise, high-rise and buildings with roof overhang [9].

2.6 Temperature and relative humidity sensors

Temperature and relative humidity sensors were placed behind the internal insulation and behind the beam ends, as marked on the illustrations in Table 1. As seen on the floor plans, three measurements behind the beam ends, three measurements behind the insulation, and one measurement of interior conditions were performed in both cases. Rotronics HygroClip2 HC2-S were used and built into the construction before installing the insulation. Sensors behind the insulation were placed in existing joints or in purposely designed indentations. Sensors behind the beam ends were placed in holes drilled from the inside. The holes were subsequently filled with insulation and sealants to avoid any external influence on the measurements. The temperature and humidity conditions in the interior environment were also monitored with similar equipment. The data was logged every minute, and connected directly to an online service for transmitting the data. The gathered data was later generated into hourly averages and in turn converted to absolute humidity, considering both temperature and relative humidity, as seen in the results, section 3.3. The absolute humidity, or water vapour content, is calculated by means of temperature, and vapour pressure based on the measured relative humidity. Equations 8, 9, and 10 below elaborate the calculations [29]:

$$\text{Absolute humidity} \quad [g/m^3] \quad v = \frac{p_v}{461.4 \cdot T} \cdot 1000 \quad (\text{Eq. 8})$$

$$\text{Vapour pressure} \quad [Pa] \quad p_v = p_s \cdot \frac{RH}{100} \quad (\text{Eq. 9})$$

$$\text{Saturated vapour pressure} \quad [Pa] \quad p_s = 610.5 \cdot e^{\frac{17.269 \cdot \theta}{237.3 + \theta}} \quad (\text{Eq. 10})$$

In the above equations, v denotes the absolute humidity, T is absolute temperature [K], p_v is the vapour pressure [Pa], p_s is the saturated vapour pressure [Pa], RH is relative humidity [%], and θ represents the temperature [°C].

2.7 Hygrothermal simulations

In order to further investigate the effect of WDR on hygrothermal conditions in internally insulated masonry, numerical simulation in Delphin [17] was performed. The numerical models are able to quantify the WDR effect, and with various values of RAF, and thus possibly contribute to support the experimental findings. 1D models were based on the validated models of test building 1, and described in [30]. The climate data gathered from the weather stations described in section 2.3 was implemented in the models. The simulation models were set to quantify the relative humidity and temperature at the wall-insulation interface. RAF of 0.4 was used as best estimate in the model. To further investigate the importance of RAF, two other models were calculated with RAF 0.0 and RAF 1.0, respectively.

3 Results

3.1 Façade conditions

The façades were inspected in connection with the installation of WDR measuring equipment, in June 2016 for both cases. The visual inspection revealed significant differences in the masonry of the two test buildings. Images of the masonry can be seen in Figure 7. Test building 1, from 1877, appears to be significantly weathered and several cracks are apparent when compared to test building 2. Furthermore, test building 1 exhibits many signs of (attempted) masonry renovation, as several mortar types are visually apparent. Test building 1 is 55 years older than test building 2, and located directly adjacent to a central traffic route in the heart of Denmark's capital, Copenhagen. It is reasonable to assume that the concentration of the city's air pollution, and the building's age, have contributed to the deterioration apparent in the façade. In test building 2, from 1932, the masonry appears much more intact, and only a few minor damages are apparent.



Figure 7: Masonry on façades of test building 1 (left) and test building 2 (right)

The Karsten tube measurements yielded sorptivities found in Table 3. The adhesive used for the Karsten tube experiments unfortunately did not fixate sufficiently to the mortar in test building 1, thus, there are no results from the joints in this case. This might also be the reason for the large uncertainty/standard deviation found in the measurements for the bricks in test building 1. If the adhesive was not fixated completely to the surface, water may have seeped through micro cracks in the adhesion. As seen in the results, the bricks in test building 1 exhibit a vaguely higher sorptivity than those of test building 2, however they are in the same range. Furthermore, it is seen that the mortar joints in test building 2 have a higher sorptivity than the bricks. The WDR resistance in the bricks of test building 2 therefore appears to be slightly higher than the WDR resistance in the bricks in test building 1.

Table 3: Estimated sorptivities by means of Hendrickx method [22]

	S_{avg} and standard deviation $\left[\frac{kg}{m^2 \sqrt{s}}\right]$	Absorption in 5 minutes [ml]
Test building 1, brick	0.007 ± 0.006	3.2 ± 3.5
Test building 2, brick	0.006 ± 0.0008	1.8 ± 0.3
Test building 2, mortar	0.017 ± 0.0004	12.5 ± 5.4

3.2 Climate data, WDR calculations and WDR measurements

The wind registrations from the two locations distinctly illustrate the dominant wind direction being from SW in both cases. Diagrams of the wind in the respective time periods (test building 1: 01/06-2016 – 31/01-2017, test building 2: 01/06-2016 – 01/03-2017) are seen in Figure 8 with red lines indicating the spectra of which the respective façade would be hit by WDR.

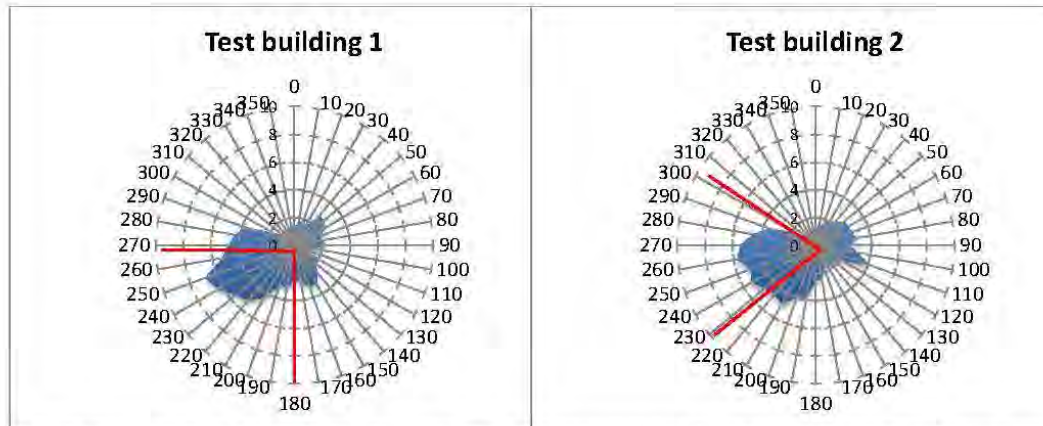


Figure 8: Diagrams of wind direction for the two areas. The outer axis represents the wind direction, 0-360°, and the inner axis represents the percentage of registered wind in 10° intervals. The red lines indicate the spectra of which the respective walls would be hit by WDR.

Calculations of deposited WDR were performed on the basis of Eq. 7 in section 2.5, thus based on the climatic data of wind speed, wind direction, and unobstructed horizontal rain. The rain admittance function was set to 0.2, in accordance with Figure 6, as buildings with roof overhang. Results of cumulative WDR calculations can be seen in Figure 9, along with cumulative measured WDR. WDR was measured in event counts, and calibrated against the found amount of rain per event, and furthermore corrected to be 1 pr. m². As seen in the graphs, the lengths of the test periods for the two buildings differ, as well as the time frame for WDR measurements, and theoretical WDR calculations based on climate data. In test building 1 the climate measurements ran slightly longer than the WDR measuring period, and for test building 2, the WDR measurements were about a year longer than the climate measurements.

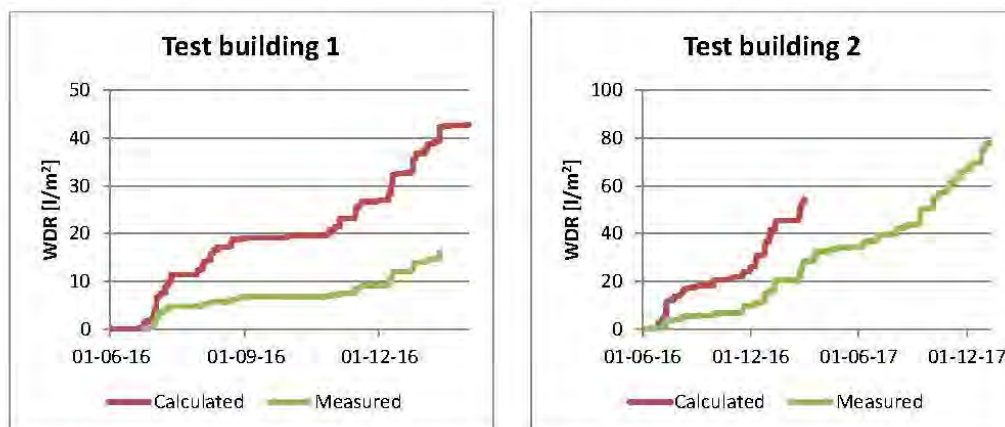


Figure 9: Calculated and measured WDR deposition per m² facade for the two test buildings.

3.3 Hygrothermal conditions in wall and beam ends in relation to WDR

In order to investigate the possible correlations between WDR and the hygrothermal conditions of internally insulated masonry walls, the measured WDR is presented in diagrams together with the relative humidity in the interface between the original wall and the thermal insulation in the two test buildings, as seen in Figure 10 and Figure 11. The WDR is portrayed in blue colors, relative humidity in orange colors that represent wall-insulation interfaces, and green nuances representing conditions behind beam ends.

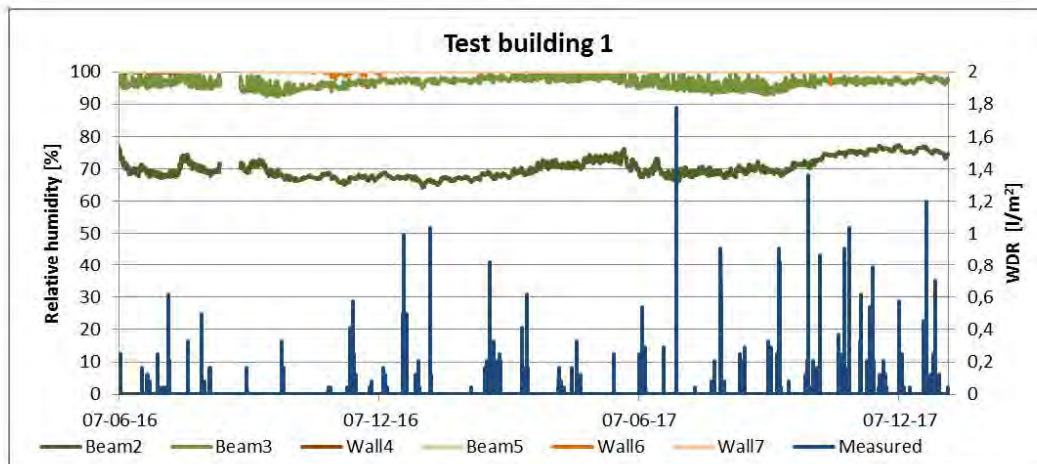


Figure 10: Relative humidities behind beam ends and at wall-insulation interfaces, as well as measured WDR in test building 1. Green colors indicate measurements behind beam ends, and orange colors represent measurements at wall-insulation interfaces. The blue color shows the measured WDR.

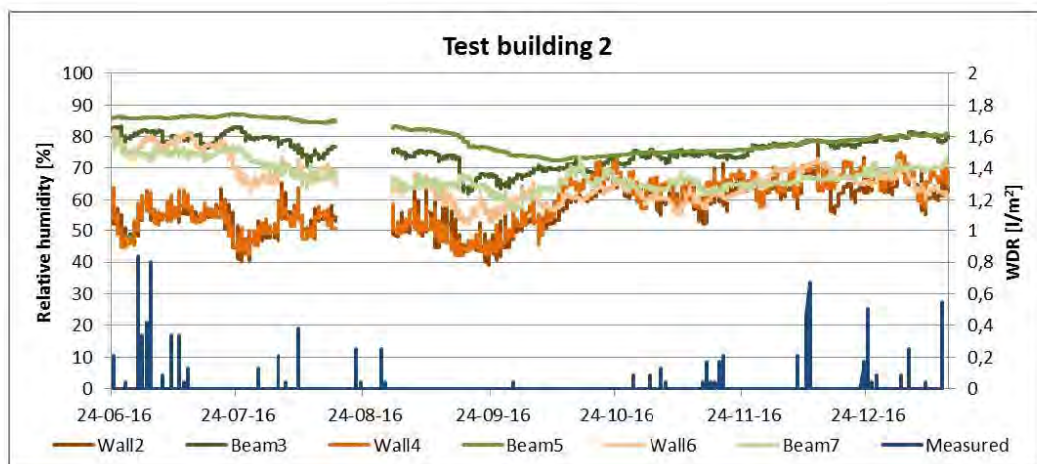


Figure 11: Relative humidities behind beam ends and at wall-insulation interfaces, as well as measured WDR in test building 2. Green colors indicate measurements behind beam ends, and orange colors represent measurements at wall-insulation interfaces. The blue color shows the measured WDR.

The results from the numerical simulation models are found in Figure 12. Besides the generated absolute humidities from the simulation results for the interface between the original wall and the thermal insulation for different rain admittance functions (RAF), the graph contains measured WDR, internal and external moisture content, and lastly the measurements from sensor "Wall2", which can be seen as representative for the interface between the original wall and the thermal insulation.

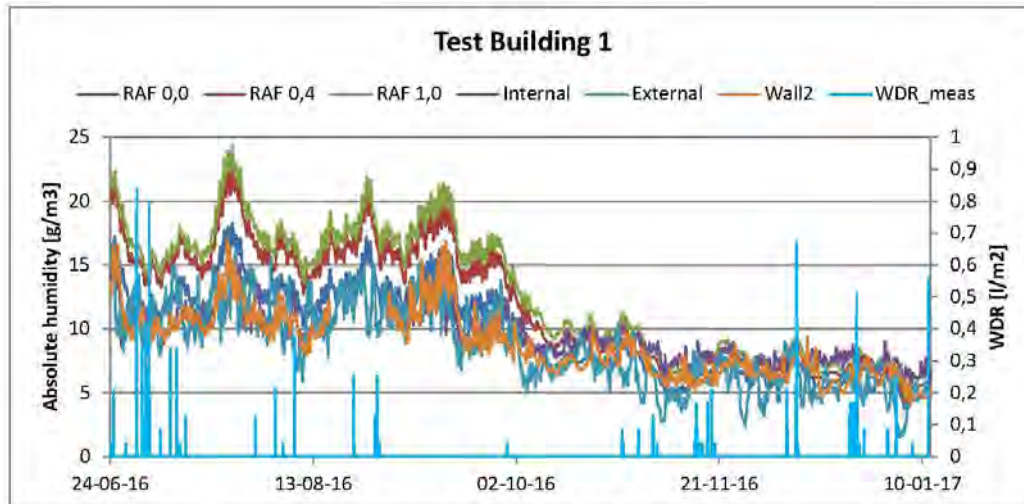


Figure 12: Absolute humidities gathered from simulations; RAF 0,0, RAF 0,4, and RAF 1,0 stand for simulation results for interface between the original wall and the thermal insulation for different rain admittance functions (RAF). Internal and external absolute humidity is also portrayed, as well as measurements from "Wall2" and measured WDR.

4 Discussion

The Karsten tube measurements showed distinct differences in the sorptivity of the bricks in the test buildings; bricks from test building 1 had a higher sorptivity than bricks from test building 2, which may be explained by the age of the building, and the general state of the façade in test building 1. In test building 2, the sorptivity of the mortar joints was also estimated by the Karsten tube, and found to have an even higher sorptivity. This was expected, as the mortar joints are assumed to be of lime mortar. A previous study on moisture transport properties in brick [31] also showed a higher sorptivity on a lime mortar rendered brick specimen compared to a brick specimen that was not rendered. The Karsten tube measurements indicate that WDR would have a higher influence on hygrothermal conditions within test building 1, as test building 2 appears more robust in the brick type. The results from the mortar joints in test building 2, however, yield the possibility of WDR penetration in mortar joints being dominant. According to literature [32], the sorptivity of brick lies in the range of $0.06\text{--}0.6\text{ kg}/(\text{m}^2\text{s}^{1/2})$, and lime mortar $0.25\text{ kg}/(\text{m}^2\text{s}^{1/2})$ on average. As seen from the results gained in this experiment, the estimations from Hendrickx' calculations [22] can be used for comparison purposes.

The wind roses generated from the gathered wind data, Figure 8, stress that southwest is in fact the most exposed façade in terms of WDR. The present investigations therefore are based on worst case scenarios with regard to orientation.

The measured WDR did not correspond to the theoretically calculated WDR based on measured weather. In fact, the theoretical calculations yielded significantly higher results of deposited WDR. For test building 1 the calculated results were 2.5 times larger than the measured; for test building 2 the calculated results were nearly twice the measured at the end of the studied period. It appears that the model overestimates WDR. Some of the discrepancies, however, may be explained by the sources of error connected with the WDR gauge, e.g. adhesion, evaporation and splashing, which were not accounted for in the theoretical calculations [15]. Furthermore, the design of the WDR gauge, protruding from the façade surface, may have caused disturbances in the wind pattern. Finally, the calculations were based on climate data gathered from the closest weather stations and not the exact locations. Especially the wind patterns in a city may vary very locally, influencing the calculation results. Despite the fact that the rain admittance function was set to 0.2 which is in the low end of the RAF interval, the calculation method yielded overestimated results. As seen in Figure 9 however, the tendencies were very similar, and the rain events occurred simultaneously, as did the dry periods. The calculated accumulated WDR load, however, tended to increase too steeply. Nath et al. [33] performed a study on mid- and high-

rise buildings in Canada for the comparison of measurements and theoretical WDR by means of a different WDR model (ISO 15927-3:2009 [12]). In nearly all cases, they similarly found the semi-empirical model to overestimate WDR up to three times the measured values.

The hygrothermal conditions measured behind the beam ends and at the wall-insulation interfaces for the two test buildings were presented and elaborated in a previous journal article by the authors [30]. These measurement results of hygrothermal conditions from the test buildings do not give any clear answers as to whether WDR has a direct impact on the moisture conditions in the wall or behind beam ends. Most of the relative humidity measurements in test building 1 were in the range of 98-100% for the duration of the measurements, and therefore it is impossible to identify any shifts in connection with monitored wind-driven rain in the wall. Neither seems there to be any indication of wind-driven rain influence on the measurements behind the beam ends. The measured relative humidity measurements from test building 2, Figure 11, were on much lower level, but also here it is difficult to see a clear impact of WDR on the hygrothermal conditions. E.g. at the end of September 2016, the relative humidity increased without any occurrence of significant rain events, which indicates that other environmental factors like exterior moisture conditions and solar radiation have a more significant influence. Some peaks in the relative humidity subsequent to rainy spells, e.g. in the beginning of August 2016, are present. But if these and other changes in the hygrothermal conditions within the wall are the result of wind-driven rain other climate conditions such as solar radiation, cloud cover and temperature, remains unclear.

The results from the hygrothermal simulations in Figure 12 show that peaks in the external humidity occur simultaneously to rain events, as expected. Other peaks in the external conditions represent elevated temperatures that increase the moisture capacity of the ambient air, and e.g. other rain events that will not be registered as WDR on the SW façade. The variety in the influence of the rain admittance function (RAF) indeed illustrated the effect of WDR. It is seen, that a RAF of 1 and 0.4 in fact generates very similar results, and results for RAF 0 lies below, and tends to follow the external climate conditions. The peaks are assumed to represent the combination of summer condensation due to high external humidity, lower internal temperatures and other factors like solar radiation. It is important to keep in mind that the numerically higher peaks in the warm season than in the cold season are only an expression of the higher temperatures and following higher moisture capacity of the air. The resulting relative humidity behind the insulation of the other two models is higher than that of RAF = 0, indicating a clear presence and influence of WDR. The results illustrate that the modelled effect of WDR appears larger than the one measured with the WDR gauge, which confirms the overestimations found in semi-empirical models and numerical models (Abuku et al. 2009 [15]).

In both test buildings, some peaks behind the insulation may exist as a result of delayed WDR penetration, however the results are inconclusive. Other factors that may play a role are solar radiation and cracks allowing not only water penetration, but also air flow and wind, contributing to faster evaporation and drying. The time it takes for WDR penetration of 1 or 1½ brick thick masonry is unknown, and may be delayed in such a manner that it is not detectable in the present study. Theoretically, if there was a continuous reservoir of water on the façade and perfect contact with the façade and throughout the façade, the penetration of 350 mm of masonry (of yellow soft molded brick with $A_w = 0.2782 \text{ kg/m}^2\text{s}^{1/2}$, $\rho = 1643 \text{ kg/m}^3$ and $\theta_{\text{exp}} = 0.275 \text{ m}^3/\text{m}^2$) would take about 90 hours. According to a partial immersion experiment performed with brick in another study [34], showed water penetration of 54 mm after 1 hour in yellow soft molded brick types with full water contact. At this rate, a 1½ brick thick construction would be penetrated in less than 7 hours of full water contact.

In a previous laboratory study by the authors [34] on WDR ingress on internally insulated masonry, a clear increase in the relative humidity in the interface between insulation and masonry was observed. The effect however, was delayed. In the interface, the small increase in RH was first detected after three 24 hour cycles, each with 30 minutes of severe rain, 2 hours of radiation and 21½ hours of cold climate. This observation is consistent to the theoretical calculation of penetration time presented above. Smaller increases in RH could even be detected in the internal insulation layer. Odgaard et al. [24] found that large rain events, or rain events of longer duration did in fact yield temporary delayed increases in relative humidity during summer seasons. At the same time he found that hydrophobization hindered drying of the walls after large rain events, and thus WDR in fact had a larger influence on hydrophobized walls, however the

effect was not of significant magnitude. Coelho et. al. [35], did a study on solid brick walls of 220 mm, and it was established through simulations that WDR indeed is a main contributor to moisture content in façades. The results from Odgaard et al. yielded delayed and minor, yet visible, increases in relative humidity at the wall plate.

The results from these studies and the present study indicate the effect of WDR on hygrothermal conditions in internally insulated walls being present, however not necessarily significant. The moisture may be able to dry out somewhat before it penetrates to the wall-insulation interface. In cases where the masonry is thicker, the penetration is likely delayed further, and the delay allows further drying out. Similarly Vereecken et al. [7] also established the importance of masonry thickness when it comes to WDR protection. Morelli et al. [19, 20] did research on WDR based on numerical simulations showing the opposite of the present study - that with high intensity rain events, the beam ends, rather than the wall-insulation interface, were affected by the WDR. Furthermore, Morelli's study showed the positive effect of the 200 mm air gap above and below the beam. This may be why the negative effects of WDR in beam ends were not visible in the present study; however they did generally have a higher relative humidity than the interfaces (test building 1). Finally, several of the references studies [4, 5, 19] stated that deteriorated façades were less resistant to WDR. In the present study, test building 1 had the most deteriorated façade, and furthermore the highest sorptivity. Despite these facts, the monitored effects of the WDR events on the hygrothermal conditions were directly nearly negligible, but a tendency of delayed response and elevated relative humidity is highly likely, and previously addressed.

4.1 Future studies

To further clarify the effects of WDR on internally insulated masonry walls more research is needed. WDR modelling requires optimization, e.g. by taking better account of various error sources that affect the quantification of WDR loads. Standard WDR gauges could be implemented to reduce errors in the experimental quantification of WDR. With respect to internal insulation and WDR effects, more studies need to be made, preferably including hygrothermal measurements at more points in the construction and at more areas of the façade. Also, reference measurements should be made for similar constructions without internal insulation. A further parameter analysis of variations between simulations would identify the most vital parameters affecting the impact of WDR on internal hygrothermal conditions. Non-destructive methods for determining the hygrothermal properties of existing constructions should be developed. Finally, the effect of various ways of protecting masonry from WDR should be studied experimentally.

5 Conclusion

- A distinct coherence is found between external moisture conditions and moisture content at the wall-insulation interface in internally insulated solid masonry.
- The WDR loads have an influence on the moisture conditions in the masonry and behind the applied internal insulation, but the direct detection of WDR rain events behind the insulation was not achieved.
- The research shows that the effect of WDR on internally insulated solid masonry can not only be explained by external moisture conditions, direct WDR loads and pure capillary transport of this liquid water that highly depends on material parameters, but must also be influenced by other factors, e.g. solar radiation and air flow as well as seasonal effects and the internal moisture loads.
- Karsten tube measurements did not yield essential differences in the water uptake of severely weathered and cracked masonry from 1877 and well maintained masonry from 1932.
- Semi-empirical models as well as numerical simulations implemented in the present study for quantification of WDR were found to considerably overestimate the WDR load compared to measurements.
- To improve the hygrothermal performance of interior insulated historic masonry walls, façades should be protected from high loads of WDR as it has a clear impact on the moisture levels in the construction.

6 Acknowledgements

The work in this paper is a part of project RIBuild "Robust Internal Thermal Insulation of Historic Buildings" that has received funding from the European Union's Horizon 2020 research and innovation program under grant agreement No

637268. We would like to thank building owners for allowing measurements to be taken. Also acknowledgement for Ph.D. student Tommy Odgaard and LINATEX A/S for collaboration on the development of the WDR gauge.

7 References

- [1] B. Blocken, J. Carmeliet, A review of wind-driven rain research in building science, *J. Wind Eng. Ind. Aerodyn.* 92 (2004) 1079–1130. doi:10.1016/j.jweia.2004.06.003.
- [2] M. Abuku, H. Janssen, S. Roels, Impact of wind-driven rain on historic brick wall buildings in a moderately cold and humid climate : Numerical analyses of mould growth risk , indoor climate and energy consumption, *Energy Build.* 41 (2009) 101–110. doi:10.1016/j.enbuild.2008.07.011.
- [3] G.R. Finken, S.P. Bjarlov, R.H. Peuhkuri, Effect of façade impregnation on feasibility of capillary active thermal internal insulation for a historic dormitory – A hygrothermal simulation study, *Constr. Build. Mater.* 113 (2016) 202–214. doi:10.1016/j.conbuildmat.2016.03.019.
- [4] G. Christensen, T. Bunch-Nielsen, Indvendig efterisolering af ældre ydermure | BYG-ERFA, BYG-ERFA. (2009). <https://byg-erfa.dk/indvendig-efterisolering-aeldre-ydermure>.
- [5] J. Munch-Andersen, SBI-anvisning 221: Efterisolering af etageboliger, 1., Statens Byggeforskningsinstitut, Hørsholm, 2008.
- [6] B. Blocken, M. Abuku, S. Roels, J. Carmeliet, Wind-driven rain on building facades: some perspectives, in: *EACWE 5*, 2009.
- [7] E. Vereecken, S. Roels, Capillary active interior insulation: do the advantages really offset potential disadvantages?, *Mater. Struct.* 48 (2015) 3009–3021. doi:10.1617/s11527-014-0373-9.
- [8] R. Peuhkuri, C. Rode, Indvendig efterisolering: Sådan dimensioneres løsninger, som giver holdbare konstruktioner, Taastrup, 2010.
- [9] J. Straube, Simplified Prediction of Driving Rain on Buildings : ASHRAE 160P and WUFI 4.0, *Build. Sci. Dig.* (2010) 1–16. file:///C:/Users/tekhan/Downloads/BSD-148_Simplified_Prediction_Driving_Rain.pdf.
- [10] E.C.C. Choi, Velocity and Impact Direction of Wind-Driven Rain on Building Faces, *Proc. ICBES'97*. (1997) 465–472. www.bath.ac.uk/cwct/cladding_org/icbest97/paper69.pdf.
- [11] H. Ge, R. Kpan, Field measurement of wind-driven rain on a low-rise building in the coastal climate of British Columbia, *Sci. Technol.* (2007).
- [12] European committee for standardization, DS/EN ISO 15927-3 Hygrothermal performance of buildings - Calculation and presentation of climatic data - Part 3: Calculation of a driving rain index for vertical surfaces from hourly wind and rain data, 2009.
- [13] G. Christensen, A.P. Koch, E.B. Møller, Indvendig efterisolering - ældre ydervægge og murværk, BYG-ERFA. (2015).
- [14] B. Blocken, J. Carmeliet, On the accuracy of wind-driven rain measurements on buildings, *Build. Environ.* 41 (2006) 1798–1810. doi:10.1016/j.buildenv.2005.07.022.
- [15] M. Abuku, B. Blocken, S. Roels, Field measurement and numerical analysis of wind-driven rain absorption and evaporation on building facades, *Building.* 32 (2009).
- [16] A.N. Karagiozis, M. Salonvaara, A. Holm, H. Künzel, Influence of Wind-Driven Rain Data on Hygrothermal

- Performance, Eighth Int. IBPSA Conf. (2003) 627–634.
- [17] A. Nicolai, J. Grunewald, Delphin 5 User Manual and Program Reference, Program. (2006).
- [18] M. Abuku, B. Blocken, S. Roels, Moisture response of building facades to wind-driven rain: Field measurements compared with numerical simulations, *J. Wind Eng. Ind. Aerodyn.* 97 (2009) 197–207. doi:10.1016/j.jweia.2009.06.006.
- [19] M. Morelli, S. Svendsen, Investigation of interior post-insulated masonry walls with wooden beam ends, *J. Build. Phys.* 36 (2012) 265–293. doi:10.1177/1744259112447928.
- [20] M. Morelli, T.R. Nielsen, G.A. Scheffler, S. Svendsen, Internal Insulation of Masonry Walls with Wooden Floor Beams in Northern Humid Climate, *Therm. Perform. Exter. Envel. Whole Build. XI Int. Conf.* (2010).
- [21] P. Klößeiko, E. Arumägi, T. Kalamees, Hygrothermal performance of internally insulated brick wall in cold climate: A case study in a historical school building, *J. Build. Phys.* (2014) 1744259114532609. doi:10.1177/1744259114532609.
- [22] R. Hendrickx, Using the Karsten tube to estimate water transport parameters of porous building materials, *Mater. Struct.* (2012) 1–12. doi:10.1617/s11527-012-9975-2.
- [23] B. Blocken, Guidelines for wind, rain and wind-driven rain measurements at test-building sites, (2004).
- [24] T. Odgaard, S.P. Bjarlov, C. Rode, Influence of hydrophobation and deliberate thermal bridge on hygrothermal conditions of internally insulated historic solid masonry walls with built-in wood, *Energy Build.* 173 (2018) 530–546. doi:10.1016/j.enbuild.2018.05.053.
- [25] Department of Civil Engineering at the Technical University of Denmark, Technische Universität Dresden, Ronby.dk, E&P service, Kingspan, et al., Results and experience from the project: EUDP 2013-II “Energy efficient comfort in older apartment blocks” Final report, (2016) 203.
- [26] B. Blocken, J. Carmeliet, Overview of three state-of-the-art wind-driven rain assessment models and comparison based on model theory, *Build. Environ.* 45 (2010) 691–703. doi:10.1016/j.buildenv.2009.08.007.
- [27] N. Sahal, M. a. Lacasse, Water entry function of a hardboard siding-clad wood stud wall, *Build. Environ.* 40 (2005) 1479–1491. doi:10.1016/j.buildenv.2004.11.019.
- [28] J.F. Straube, E.F.P. Burnett, Driving rain and masonry veneer, in: *ASTM Spec. Tech. Publ.* 1998, Vol. 1314, ASTM, 1998: pp. 73–87.
- [29] E. Brandt, SBI-anvisning 224 Fugt i bygninger, 1., Statens Byggeforskningsinstitut, Hørsholm, 2009.
- [30] T.K. Hansen, S.P. Bjarlov, R.H. Peuhkuri, M. Harrestrup, Long term in situ measurements of hygrothermal conditions at critical points in four cases of internally insulated historic solid masonry walls, *Energy Build.* 172 (2018) 235–248. doi:10.1016/j.enbuild.2018.05.001.
- [31] T.K. Hansen, S.P. Bjarlov, R. Peuhkuri, Moisture transport properties of brick – comparison of exposed, impregnated and rendered brick, in: *Int. RILEM Conf. Mater. Syst. Struct. Civ. Eng. 2016 Segm. Moisture Mater. Struct., Kgs. Lyngby, 2017: pp. 351–360.* http://orbit.dtu.dk/ws/files/128040737/Pages_from_Moisture_conf_proceedings_3.pdf.
- [32] F.R. Gottfredsen, A. Nielsen, Bygningmaterialer - Grundlæggende egenskaber, 1., Polyteknisk Forlag, 2010.

-
- [33] U.K. Deb Nath, V. Chiu, H. Ge, Field measurements of wind-driven rain on mid-and high-rise buildings in three Canadian regions, *Build. Environ.* 116 (2017) 228–245. doi:10.1016/j.buildenv.2017.02.016.
 - [34] T. Kvist Hansen, S.P. Bjarlov, R.H. Peuhkuri, K.K. Hansen, Performance of hydrophobized historic solid masonry - experimental approach, *Constr. Build. Mater.* 188 (2018) 695–708. doi:10.1016/j.conbuildmat.2018.08.145.
 - [35] G.B.A. Coelho, F.M.A. Henriques, Influence of driving rain on the hygrothermal behavior of solid brick walls, *J. Build. Eng.* 7 (2016) 121–132. doi:10.1016/j.jobe.2016.06.002.

Appendix D

Paper IV

Material characterization models and test methods for historic building materials



Available online at www.sciencedirect.com

ScienceDirect

Energy Procedia 132 (2017) 315–320

Energy
Procedia
www.elsevier.com/locate/procedia

11th Nordic Symposium on Building Physics, NSB2017, 11-14 June 2017, Trondheim, Norway

Material characterization models and test methods for historic building materials

Tessa Hansen^{a,*}, Ruut Hannele Peuhkuri^b, Eva B. Møller^b, Søren Peter Bjarløv^a,
Tommy Odgaard^{a,c}

^a*Technical University of Denmark, Department of Civil Engineering, Brovej 118, 2800 Kgs. Lyngby, Denmark*

^b*Danish Building Research Institute, Aalborg University, A.C. Meyers Vænge 15, 2450 Copenhagen SV, Denmark*

^c*COWI A/S, Parallelvej 2, 2800 Kgs. Lyngby, Denmark*

Abstract

Predictions of long term hygrothermal performance can be assessed by dynamic hygrothermal simulations, in which material parameters are crucial input. Material parameters for especially historic materials are often unknown; therefore, there is a need to determine important parameters, and simple ways for estimation of these. A case study of a brick wall was used to create and validate a hygrothermal simulation model; a parameter study with five different parameters was performed on this model to determine decisive parameters. Furthermore, a clustering technique has been proposed to estimate decisive parameters through simple testing of interrelated parameters that are easier to determine.

© 2017 The Authors. Published by Elsevier Ltd.

Peer-review under responsibility of the organizing committee of the 11th Nordic Symposium on Building Physics.

Keywords: Historic building materials; hygrothermal simulation; moisture; material characterization; test methods

1. Introduction

In historic buildings with façades of cultural and preservation worthy values, interior insulation is the only measure to decrease heat loss through the exterior walls. The mounting of interior insulation may introduce moisture risks. Hygrothermal simulations are therefore valuable tools in the design of a suitable interior insulation system. Hygrothermal simulations take into account many specific variables for each case in question, e.g. climatic conditions, geometry and material parameters. This study has focus on material parameters and their importance in regards to said

* Corresponding author. Tel.: +45 45251803.

E-mail address: tekhan@byg.dtu.dk

hygrothermal simulations. Materials used in historic buildings are extremely varied, not only in the raw materials and resources used, but also in the production method. If it can be proven that certain material properties are decisive for the hygrothermal performance and they can be determined feasibly in regards to both time and economy, it would be beneficial for future analysis of retrofit measures.

As there are numerous uncertainties in hygrothermal simulation, identification of potential discrepancies in material properties and boundary conditions were determined in a sensitivity analysis performed by Kloda [1]. The analysis concluded vital influence on output from parameters such as solar radiation absorption coefficient, thermal conductivity, suction curve, capillary conductivity and surface heat transfer coefficients. Probabilistic methods have previously been introduced by e.g. Zhao et. al. [2] and Holm et. al. [3], running 400 and 69 hygrothermal simulations respectively, for determination of the influence of material parameters and boundary conditions, and measurement uncertainties respectively. The findings of these measures were, among others, that the effect of single parameters may be seasonal, and can have both positive, negative and seasonal-dependent correlations. The studies emphasize the need for full and exact material properties for achieving valid results. By means of statistical tools however, it may be possible to attain reliability ranges for results, and simplifying the models by clustering of materials.

This paper aims to clarify the importance of the single material parameters in regards to characterization of historic building materials with limited information. It is a step towards for better prediction of hygrothermal performance by finding a linkage between clustering and simple experimental methods for material characterization.

2. Material Characterization

A major challenge in hygrothermal simulations of walls in historic buildings is to establish necessary knowledge of the material parameters. Material characterization is in the following described as a combination of the experimental and theoretical approach.

2.1. Practical determination of material properties

There are number of well-defined and standardized methods for determination of many material properties in laboratory. The methods for determination of the parameters included in this study are seen in Table 1.

Table 1: Test methods for determination of some material parameters.

Parameter	Standard method	Alternatives
Density	EN 772-13:2002 [4]	EN 1936:1999 [5]
Open porosity	EN 772-3:1998 [6]	EN 1936:1999 [5]
Thermal conductivity	EN 12664:2001 [7]	ISOMET Heat Transfer Analyzer
Water uptake coefficient	ISO 15148:2002 [8]	Plagge et. al. [9], automatic logging system Hendrickx [10], estimation by Karsten tube
Water vapour diffusion resistance factor	EN ISO 12572:2001 [11]	Bertelsen [12], considering moisture content dependency

2.2. Theoretical hygrothermal models

Moisture transport in porous media, e.g. building materials, is driven by material characteristics as well as external factors. Driving forces include gradients in partial vapour pressure, total air pressure and external total pressure, as well as gravity and pore width, defining the capillary suction [13]. Moisture transport in a material also depends on the moisture storage potential, which in turn is dependent on specific material characteristics; e.g. water retention curve relates to the porosity, effective and capillary saturation – depending on the hygroscopic range, and the function for liquid water conductivity depends on both effective saturation and water uptake coefficient. Material functions are vital as they describe properties at various conditions, therefore material functions are implemented in hygrothermal simulations together with constant material parameters. Some of the material parameters and functions are not directly measurable and therefore the process of determining the parameters also requires a calibration, either experimentally and/or numerically [14]. Simplified, the process of the material characterization can be seen in Figure 1;



Figure 1: Flow chart of material characterization process.

2.3. Decisive material parameters and clustering

In hygrothermal simulations some material parameters are more decisive than others and some are interrelated. Unfortunately, some decisive parameters may be difficult to determine, however, if the interrelated parameters are easier to estimate, it might be possible to estimate the decisive parameters through simple tests. Some materials have similar pore systems e.g. most historic building materials have open pore systems, which means that, density and open porosity are interrelated. Parameter studies, like the one described in this paper, are useful when determining which parameters are decisive, while determination of which parameters are interrelated can be done by making a statistical analysis on material parameters from materials where these are already known. The purpose of a statistical analysis is twofold:

- Determination of correlations between material parameters, in this way it will be possible to see which parameters can be estimated through other parameters that are easier to determine.
- Clustering of materials. Within groups of materials e.g. bricks there can be significant differences in hygrothermal properties. By defining decisive properties and analysing how materials differ, it is possible to cluster specific materials in groups and create generic material representing the cluster.

The work of Zhao et. al. [15] investigates different clustering techniques, and methods for deriving a generic material from a cluster. They emphasize that it is important to have found correlations between parameters first, otherwise some parameters will have too big an influence on the clustering. Generic materials can be used to overcome the problem of incomplete material data. Zhao et. al. [16] have also developed a concept for the inclusion of input uncertainties and a stochastic material database for probabilistic simulation rather than deterministic. Including the probability distributions of material properties, gives better estimations of the realism in achieved hygrothermal simulation results.

3. Method

3.1. Case study

For investigation of the importance in variation of various material parameters, a case study is used. The case study is a wall consisting of merely of brick and mortar. The wall is 1½ brick thick (348mm) and is internally rendered with 12-15mm of the same lime mortar used in the joints. The bricks used are new yellow softmolded bricks from Helligsø Teglværk, and the mortar for joints and rendering is a 7.7% lime adjusted wet mortar with grain size 0-4mm (air lime) which was produced to resemble characteristic mortar from year ~1900 in Denmark. The wall is built in a container wall with several other test walls, located in Kgs. Lyngby, Denmark, and the external side of the wall faces the actual climate, towards southwest. The interior conditions are set to be constant at 20°C and 60 % relative humidity, however natural fluctuations occur, e.g. no cooling system during warm periods. Temperature and relative humidity sensors are located in the wall at three locations, as seen in Figure 2. The sensors used are HYT-221 sensors, logging data every 10 minutes. Furthermore, temperature and relative humidity sensors are located on both external and internal side of the wall, for monitoring of boundary conditions.

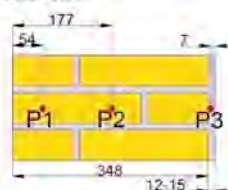


Figure 2: Cross section of wall, and indication of sensor locations. Exterior climate is on the left

3.2. Hygrothermal simulation

As 1D simulations are presented, the mortar joints are not included in the models. The model consists of 348mm brick, and 15mm mortar on the internal side. Material parameters for simulations are based on [17]. Local climate measurements from DTU weather station were implemented in the model. Climate data for one year, 2016, has been used and recycled for a 2nd year of simulation. Results from the 2nd year will be presented in this paper. Initial conditions for temperature and relative humidity in the construction were set as the measured values in 3 points, for each 1/3 of the construction thickness. The simulations are performed in the hygrothermal simulation software Delphin [18], and will constitute the base for the investigation of the significance of the various material parameters. Therefore

the base model must first be validated with measured data. Hereafter a variety of simulations can be made with variations in material parameters, in order to establish the effect on the obtained simulation results.

3.3. Variation of material parameters

To investigate the importance of the various basic material parameters, simulations with $\pm 10\%$ values were made for the following brick parameters; density, open porosity, thermal conductivity, water uptake coefficient and water vapour diffusion resistance factor. The alterations in some of the constant parameters effect some material functions in Delphin (e.g. A_w scales the liquid water conductivity). The implemented values, are shown in Table 2. Although some of the parameters are interrelated, e.g. thermal conductivity increasing with an increased density and decreased open porosity, the parameters are varied one by one.

For investigation of the correlation between parameters, additional simulations were made with actual material parameters provided by the Delphin database, on 2 different types of brick, with a large difference in density, see Table 2.

Table 2: Material parameter variations, and materials for simulation of correlation investigation.

	Original	-10%	+10%	High density Brick Bernhard	Low density Brick Schlagmann	Unit
Density, ρ	1713	1542	1884	2060	1396	kg/m ³
Open porosity, $\theta_{p,w}$	0.38	0.34	0.41	0.25	0.47	m ³ /m ³
Thermal conductivity, λ	0.52	0.47	0.57	1	0.27	W/mK
Water uptake coefficient, A_w	0.2	0.18	0.22	0.10	0.44	kg/m ² s
Water vapour diffusion resistance factor, μ	25	22.5	27.5	19	14	-

4. Results

4.1. Practical measurements, simulations and validation of model

Various simulations were run to establish a model validated through measurements. The combination of uncertainties in measurement and simulation, as well as unknown factors makes it difficult to achieve a simulation model 100% in accordance with measurements, especially for point P2; however a model considered validated continuous use in this work was obtained. With this validated model, the further simulations with material parameter variations become were performed.

4.2. Variation in material properties

Results from the simulations with varying material parameters, yield various results. Variations in density and open porosity alone show no effect to the results. In P1 and P2, variations in A_w and μ have an effect on relative humidity – especially in the fall season. A decreased A_w or an increased μ leads to increased relative humidity, and vice versa. A_w shows the largest impact on results. Thermal conductivity has a slight impact on temperature and relative humidity results in both P2 and P3; as the thermal conductivity is increased, the temperature decreases and the relative humidity subsequently increases – this effect is seen all year for P3.

Figure 3 and Figure 4 depict simulation results with the different brick types, Brick Bernhard and Brick Schlagmann from the entire 2nd year of simulation in the 3 measuring points, described in section 3.3.

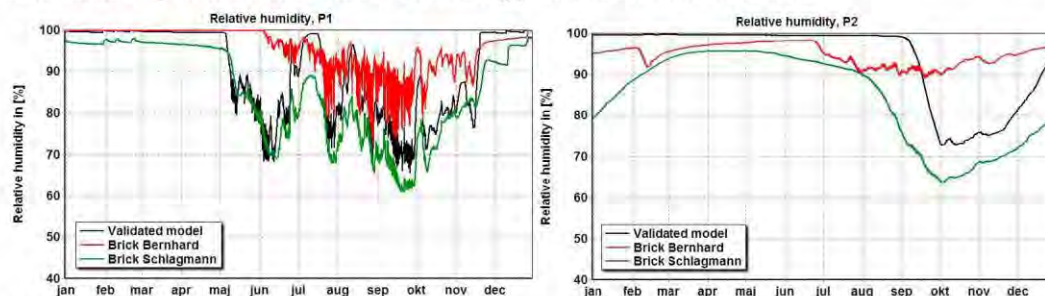


Figure 3: Relative humidity in P1 (left) and P2 (right) with different brick types.

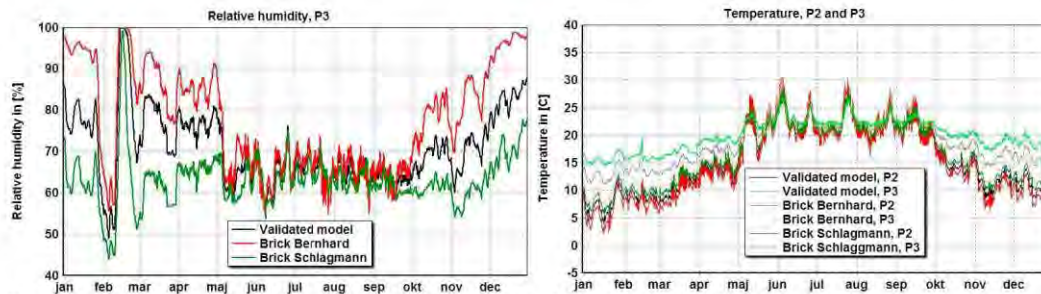


Figure 4: Relative humidity in P3 (left), and temperature in P2 and P3 (right) with different brick types.

5. Analysis/discussion

The validation of the simulation model does not reach a perfect fit; the simulations are performed in 1D without consideration to mortar joints, long wave emission has been omitted due to inexistent data, and exchange coefficients have been estimated. However, the validated model gives sufficient correlation in order to investigate the variations in material parameters.

Results from the various numerical simulations revealed the importance of certain material characteristics in hygrothermal conditions of a construction, while other parameters did not influence the simulation results. Table 3 gives an overview of the observed results and effects.

Table 3: Effects of variations in material parameters on the hygrothermal state of the construction.

Parameter	Significant effect	Effect
Density, ρ	-	
Open porosity, θ_{por}	-	
Thermal conductivity, λ	T (P3), RH (P2+P3)	Increased $\lambda \rightarrow$ decreased T and increased RH
Water uptake coefficient, A_w	RH (P1+P2)	Decreased $A_w \rightarrow$ increased RH in colder periods
Water vapour diffusion resistance factor, μ	RH (P1+P2)	Increased $\mu \rightarrow$ increased RH in colder periods

The simulations indicated that the water uptake coefficient (liquid transport) yields the largest impact on the relative humidity in both the external and middle part of the wall. The seasonal dependency can be explained partly by rain events not succeeded by fast drying from the solar radiation during summer. The influence of μ is partly explained by the reduced drying potential due to the increased diffusion resistance. The results are in consistency with findings in [1], with the exception of μ 's influence which was not found in their analysis.

The studied case is a brick wall with a given orientation and boundary conditions. Especially orientation of the wall, which in this case is the “worst case”, i.e. South-West orientation with heavy load of driving rain, may be a determining factor for the current conclusions. Another series of simulations with a less exposed orientation may result in a different conclusion.

The material parameter variation study was performed relatively simplistic, i.e. studying a single parameter at a time and the correlation of parameter variation was not included. In reality, many of the parameters correlate: e.g. thermal conductivity will normally decrease for decreasing density, which again decreases for increasing porosity. So the observed negligible effect of density and porosity within the $\pm 10\%$ variation on the temperature and moisture conditions in the studied construction must be linked to the observed significant effects of λ , μ and A_w , as these are functions of density and/or porosity. For this reason, further simulations were performed with 2 different types of brick. The results showed that the denser type of brick, Brick Bernhard, yielded results of higher relative humidity. The water uptake coefficient is lower in this brick type, underlining the effect demonstrated by the previous simulations. The lower relative humidity in Brick Schlagmann, can partly be explained by the increased temperatures. In Figure 4 it is apparent, that the material characteristics are dominantly influential in colder periods.

The simulations with Bernhard and Schlagmann bricks illustrate how different the outcome of hygrothermal simulations can be, depending on which brick was chosen for the simulation. Therefore the planner should not just choose any brick, but a correct brick type. A study of 23 specific bricks by Zhao et. al. [15] resulted in four different clusters; New bricks, Historical bricks of clay and loam, Historical bricks of clay, loam and sand and Bricks for external facades (high density and low moisture storage and transport capacity).

Therefore, information already available, e.g. construction period, or information on either density or transport capacity estimated by simple tests, e.g. Karsten tube, could be sufficient for determination of the correct cluster for better estimation of the hygrothermal performance.

6. Conclusion

For variations of $\pm 10\%$, the density and open porosity yielded no change in results for temperature and relative humidity. Water uptake coefficient, water vapour diffusion resistance factor and thermal conductivity all yielded results indicating seasonal impact on the effect of the various parameters. The water uptake coefficient turned out to be the most influential factor on relative humidity, of the parameters investigated. The seasonal variations indicate the material parameters dependency on external factors and conditions. If the water uptake coefficient can be estimated, or even just categorized, by use of Karsten tube, it may valuable information in regards to characterization of historic materials and hygrothermal simulations with clustered materials.

7. Acknowledgements

The presented work is a part of RIBuild project that has received funding from the European Union's Horizon 2020 research and innovation programme under grant agreement No 637268.

8. References

- [1] P. Kloda, Computational investigation of moisture problems related to internal insulation, DTU, 2017.
- [2] J. Zhao, R. Plagge, A. Nicolai, J. Grunewald, Stochastic study of hygrothermal performance of a wall assembly — The influence of material properties and boundary coefficients, HVAC R Res. 17 (2011).
- [3] A.H. Holm, H.M. Künzle, The influence of Measurement Uncertainties on the Calculated Hygrothermal Performance, in: *Insul. Mater. Test. Appl.* 4th Vol. Astm Spec. Tech. Publ. (2002)
- [4] EN 772-13 Methods of test for masonry units – Part 13: Determination of net and gross dry density of masonry units (except for natural stone), (2002).
- [5] DS/EN 1936:2002 Natural stone test method - Determination of real density and apparent density, and of total and open porosity, (2002).
- [6] Methods of test for masonry units - Part 3: Determination of net volume and percentage of voids of clay masonry units by hydrostatic weighing, (1998).
- [7] DS/EN 12664, Thermal performance of building materials and products - Determination of thermal resistance by means of guarded hot plate and heat flow meter methods, (2001).
- [8] ISO 15148 Hygrothermal performance of building materials and products - Determination of water absorption coefficient by partial immersion, (2002).
- [9] R. Plagge, G. Scheffler, J. Grunewald, Automatic Measurement of Water Uptake Coefficient of Building Materials, *Bauphysik*. 27 (2005).
- [10] R. Hendrickx, Using the Karsten tube to estimate water transport parameters of porous building materials, *Mater. Struct.* (2012)
- [11] EN/ISO 12572, Hygrothermal performance of building materials and products - Determination of water vapour transmission properties, (2001).
- [12] N.H. Bertelsen, Beskrivelse af udstyr til måling af fugttransport, DTU (1982).
- [13] H. Hens, Building Physics – Heat, Air and Moisture. Fundamentals and Engineering Methods with Examples and Exercises, Ernst & Sohn, A Wiley Company, 2007.
- [14] G.A. Scheffler, Validation of hygrothermal material modelling under consideration of the hysteresis of moisture storage, Dresden University of Technology, 2008.
- [15] J. Zhao, R. Plagge, N.M. Ramos, M.L. Simoes, J. Grunewald, Application of clustering technique for definition of generic objects in a material database, *J. Build. Phys.* 39 (2015).
- [16] J. Zhao, R. Plagge, N.M.M. Ramos, M.L. Simões, J. Grunewald, Concept for development of stochastic databases for building performance simulation - A material database pilot project, *Build. Environ.* 84 (2015)
- [17] H. Sandholdt, D. Dysted, Experimental and theoretical investigation of Interior insulations of solid brick walls with foam concrete and other silicate based materials (2015).
- [18] A. Nicolai, J. Grunewald, Delphin 5 User Manual and Program Reference, Program. (2006).

Appendix E

Paper V

Moisture transport properties of brick – comparison of exposed, impregnated and rendered brick

International RILEM Conference on Materials, Systems and Structures in Civil Engineering
Conference segment on Moisture in Materials and Structures
22-24 August 2016, Technical University of Denmark, Lyngby, Denmark

MOISTURE TRANSPORT PROPERTIES OF BRICK – COMPARISON OF EXPOSED, IMPREGNATED AND RENDERED BRICK

Tessa Kvist Hansen ⁽¹⁾, Søren Peter Bjarlov ⁽¹⁾, Ruut Peuhkuri ⁽²⁾

(1) Technical University of Denmark, Lyngby, Denmark

(2) Danish Building Research Institute, Copenhagen, Denmark

Abstract

In regards to internal insulation of preservation worthy brick façades, external moisture sources, such as wind-driven rain exposure, inevitably has an impact on moisture conditions within the masonry construction. Surface treatments, such as hydrophobation or render, may remedy the impacts of external moisture. In the present paper the surface absorption of liquid water on masonry façades of untreated, hydrophobated and rendered brick, are determined experimentally and compared. The experimental work focuses on methods that can be applied on-site, Karsten tube measurements. These measurements are supplemented with results from laboratory measurements of water absorption coefficient by partial immersion. Based on obtained measurement results, simulations are made with external liquid water loads for determination of moisture conditions within the masonry of different surface treatments. Experimental results showed a very clear reduction of the liquid water uptake for hydrophobated cases. However, hygrothermal simulations demonstrated clear differences in the effect of the surface treatments on the moisture content of brick depending on the brick type.

1. Introduction

Several studies have shown that external moisture sources, such as wind-driven rain (WDR), penetrate – especially thinner - masonry constructions. This inevitably influences the hygrothermal conditions of an internally insulated masonry building, which can essentially lead to health problems of inhabitants or general building degeneration. A single-leaf, untreated brick wall with high WDR loads was simulated and elevated relative humidities on internal walls were found, both with and without insulation [1]. Determination of WDR loads

International RILEM Conference on Materials, Systems and Structures in Civil Engineering
 Conference segment on Moisture in Materials and Structures
 22-24 August 2016, Technical University of Denmark, Lyngby, Denmark

and hygrothermal impact on solid brick walls has been conducted by hygrothermal simulations. The study showed, that WDR had a distinct impact on the relative humidity on the interior wall surfaces – especially during winter and summer [2]. Another study has also demonstrated the impact of WDR on the relative humidity in a masonry construction – in this case an embedded wooden beam. The study displayed critically high humidity conditions in beam ends, in cases with high rain intensity – based on hygrothermal simulations [3]. A significant impact of the magnitude of WDR loads on moisture conditions in the beam ends, has also been proven by 2D and 3D simulations [4]. The water uptake through the external surface must therefore be seen as a vital parameter for water penetration through the masonry.

The water absorption can be obstructed/limited by various means; render, paint, hydrophobisation, or water repelling surface treatment. Künzl [5] recommends a water repelling surface treatment before implementation of internal insulation, as the drying capacity and thermal resistance in the masonry is reduced by the hygrothermal changes following internal insulation, which can cause not only undesirable moisture conditions on the internal wall, but also frost damage to the façade. The impact of a hydrophobisation treatment on internally insulated walls has been documented by simulations, e.g. in [6]. The study included several cases with both capillary active and inactive insulation solutions on a 1-brick thick wall. Results showed significantly improved hygrothermal conditions in the masonry and humidity at the interface between insulation and original wall, in cases with external hydrophobisation treatment – also illustrating the impact of WDR [6].

In this present study, laboratory experiments were carried out in order to determine to which extent some guards of weather protection can limit the water absorption compared to untreated brick. The studied surface treatments were rendered and hydrophobisation. The water uptake was studied by means of Karsten tube and partial immersion methods. The results were supplemented by hygrothermal simulations for long term exposure and for the effect of different brick types beside the studied surface treatments. Water absorption through joints and mortar was not studied, even though it is acknowledged that penetration through these parts of masonry may be significant.

2. Materials and Methods

2.1 Materials

For laboratory experiments, three types of samples were used: 5 test specimens were rendered, 5 specimens were hydrophobized and the surfaces of 5 specimens were left untreated; these were used as reference specimens. A list of the components used for the test specimens are given in Table 1.

Table 1. The components used for test samples.

Brick	Yellow soft-molded brick from Helligsø Teglværk in Sydthy
Render	Standard 7.7% lime adjusted wet mortar, grain size 0–4mm (air lime)
Hydrophobisation	Funcosil FC from Remmers

The bricks were stored at a stationary indoor climate corresponding to the test conditions specified in prEN ISO 15148:2002 [7], until reaching a constant mass, i.e. the mass is not changing more than 0.1 % in 24 hours. Hereafter, 5 specimens were surface treated with air

International RILEM Conference on Materials, Systems and Structures in Civil Engineering
 Conference segment on Moisture in Materials and Structures
 22-24 August 2016, Technical University of Denmark, Lyngby, Denmark

lime render (approximately 1 cm thick) and 5 specimens with Funcosil hydrophobation (approximately 0.36 l/m²) respectively. Before laboratory experiments were carried out, the specimens should obtain constant conditions again, and it was ensured that the lime render was completely carbonated. The rendered specimens were placed in a climate chamber with a CO₂-supply in order to accelerate the carbonization process. The carbonation process was monitored by phenolphthalein on extra specimens. The hydrophobated specimens were tested 6 weeks after Funcosil application, according to manufacturer's recommendations.

2.2 Methods

The Karsten tube method is a non-destructive measuring method that can be implemented on in situ bricks. Mainly, Karsten tube measurements are performed for comparison purposes. Calculation methods developed by Roel Hendrickx [8] adds the option for conversion to sorptivity. Karsten tube experiments were carried out vertically on all specimens, and calculations performed according to the method described by Roel Hendrickx [8]. The specimens were subjected to demineralized water in the 4 ml tubes fixed to the center of the surface vertically. The water uptake was noted at 5 minute intervals for 30 minutes. The diameter of the contact area was registered individually, as variations occur due to the fixation. The diameter of the wetted area was measured at termination of each experiment, as the wet area became visible when removing tube and fixation. The calculations provided and described in [8] yield the value for sorptivity by the following calculations:

$$x(t) = R_{wet}(t) - \frac{D_e}{2} \quad (1)$$

$x(t)$: penetration of wet front at time t [mm]

R_{wet} : radius of effective contact area [mm]

D_e : diameter of wet area [mm]

$$V_{wet}(t) = \frac{2}{3} \cdot \pi \cdot (x(t)^3 + R_e \cdot x(t)) + \pi \cdot R_e^2 \cdot x(t) \quad (2)$$

$V_{wet}(t)$: wet volume at time t [mm³]

$$\theta_{cap}(t) = \frac{V_{abs}(t)}{V_{wet}(t)} \quad (3)$$

$\theta_{cap}(t)$: capillary saturated volume moisture content at time t [mm³/mm³]

$V_{abs}(t)$: absorbed volume at time t [ml].

$$V_{abs} = \pi \cdot R_e^2 \cdot S \cdot \sqrt{t} + \frac{\pi \cdot R_e \cdot \gamma \cdot S^2}{\theta_{cap}} \cdot t \quad (4)$$

S : sorptivity [cm/ $\sqrt{\text{min}}$]

γ : empirical factor of 0.75

The sorptivity is obtained by solving for S in Eq. 4, and finding the average of all times. Multiplying with $\frac{10}{\sqrt{60}}$ yields the common unit of sorptivity, S ; [$\frac{\text{kg}}{\text{m}^2 \cdot \sqrt{\text{s}}}$]. As previously implied, the wetted diameter could only be measured by the end of the experiment, hence no average value for the time can be found, however θ_{cap} should be a constant material parameter, why the value at termination, 30 minutes, is assumed and calculated.

International RILEM Conference on Materials, Systems and Structures in Civil Engineering
 Conference segment on Moisture in Materials and Structures
 22-24 August 2016, Technical University of Denmark, Lyngby, Denmark

After Karsten tube measurements, the specimens were dried until constant mass again was assumed. Epoxy was applied as a water and vapour tight sealant to the 4 sides of each stone, leaving the end surfaces blank, for water absorption by partial immersion.

For determination of short-term water absorption coefficient, the method described in prEN ISO 15148:2002 [7] was implemented. It was ensured that the test specimens were free of irregularities on the absorption surface, and had a water contact area larger than 50cm², as prescribed in the standard. Again, the specimens were conditioned until each mass was stabilized within 0.1 % of the mass within 24 hours.

The experiment was carried out as described here; each specimen was weighed with a scale of ± 0.1 % accuracy, and the initial mass registered as m_i . A water tank, capable of maintaining a constant water level, was filled with water, and specimens were placed in the tank, on point supporters. The water level was kept at 5 ± 2 mm above the base of the test specimen. A timer (accurate to 1 second) was started, as the specimens were immersed in water. 5 minutes after immersion, for each specimen, they were removed from the water, the surface blotted dry, the weight registered, m_{smin} , and the specimen put back in the tank. This procedure was repeated at time steps of 20 minutes, 1 hour, 2 hours, 4 hours, 8 hours, 9 hours and a last weighing 24 hours after initial immersion. The mass difference between each weighing relative to initial mass per area, Δm_t , is plotted against the square root of time. The curvature indicates the calculation method for obtaining the water absorption coefficient, A_w .

In cases where the graph results in a suddenly occurring straight, horizontal line, indicating liquid water at the specimen surface, the water absorption coefficient is calculated by the following method;

A linear trend line is placed through the initial results for Δm_t , until the slope's sudden decline. The value of Δm_t cuts the y-axis, is denoted $\Delta m'_0$.

$$A_w = \frac{\Delta m'_{tf} - \Delta m'_0}{\sqrt{t_f}} \quad (5)$$

t_f : duration of experiment [s]

$\Delta m'_{tf}$: value of Δm_t at time t_f [kg/m²]

In cases where the plot yields a curve, the calculations are made according to eq. 6;

$$A_{w,24} = \frac{\Delta m_{24}}{\sqrt{86400}} \quad (6)$$

$A_{w,24}$: water absorption coefficient related to 24 hours [kg/m²s^{1/2}]

Δm_{24} : mass gain per face area after 24 hours [kg/m²].

2.3 Simulations

The effect of surface treatment was also studied with hygrothermal dynamic simulations. One-dimensional models in calculation tool Delphin [11] were constructed and simulations were performed on various brick types with hydrophobisation, render and no surface treatment. The brick types investigated numerically were Brick Joens and Brick Bernhard, and Brick Schlagmann from the Delphin material database, as well as the yellow brick used in

experiments. The material parameters of yellow brick were partly based on Delphin database Historical Brick (cluster 4) and partly on experimental values obtained by Sandholdt et al. (2015) [9]. The simulations were performed on bricks of 228mm thickness, corresponding to a 1-brick thick external wall, typical in e.g. parapets or gables in historic Danish buildings. The render was a lime plaster (historical) with 1cm thickness. Material properties of the investigated brick types and the lime render are summarized in Table 2. In an attempt to simulate a hydrophobated surface treatment, the exterior 5mm of the brick was given a water uptake coefficient reduced by factor 15 – the factorial difference found between reference specimens and specimens with hydrophobisation treatment in Karsten tube experiments (see Results section).

Table 2. Material parameters for materials in Delphin simulations.

Material	Density [kg/m ³]	Thermal conductivity [W/mK]	Vapour diffusion resistance factor [-]	Open porosity [m ² /m ²]	Water uptake coefficient [kg/m ² s ^{1/2}]
Brick Joens	1790	0.87	14	0.36	0.23
Brick Bernhard	2060	1.00	19	0.25	0.10
Brick Schlagmann	1395	0.27	14	0.47	0.44
Yellow Brick	1713	0.52	12	0.33	0.31
Lime plaster	1800	0.82	12	0.30	0.13

The exterior climate for the simulations was constructed from a Danish reference year. It should be noted, that the rain has 6 hour intervals between values. The orientation of the external side was set to South West, which is most exposed to wind-driven rain in Denmark [10]. In addition to 6 hour summarized water loads, and South West orientation, the rain exposure coefficient was set to 1, so in periods the bricks were subjected to large rain loads. "Interior" conditions were set constant to 20°C and 50 % relative humidity. The simulations were run for two years, and the latter is displayed in the results. The simulation outputs for the present focus will be the relative humidity in 4 points through the brick – as seen in Figure 1, as well as the liquid moisture content in the entire brick.

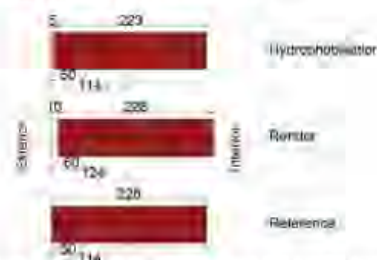


Figure 1. Output locations for Delphin simulations are marked by green lines. Output locations are, exterior, 5 cm from brick exterior, mid-brick and interior side.

International RILEM Conference on Materials, Systems and Structures in Civil Engineering
 Conference segment on Moisture in Materials and Structures
 22-24 August 2016, Technical University of Denmark, Lyngby, Denmark

The simulations were made for the purpose of surface treatment comparison, and for investigation of the influence of brick type.

3. Results

3.1 Laboratory

The Karsten tube measurements yielded results for sorptivity, as shown in Table 3. Specimens with a rendered surface absorbed nearly 25 times more water in 30 minutes, than the reference specimen. Specimens with hydrophobisation barely absorbed any water. The average calculated sorptivities and standard deviations are found in Table 3. It is clear, that the rendered surface exhibits a very high sorptivity, and surface with hydrophobisation a very low sorptivity relative to reference specimens. The results show that both hydrophobisation and render impacts the sorptivity of the brick surface.

Table 3. Average sorptivity and standard deviation for the 3 surface types obtained by Roel Hendrickx' method after Karsten tube experiment and partial immersion experiment

$\frac{kg}{m^2\sqrt{s}}$	Karsten tube		Partial immersion	
	$S_{average}$	$S_{standard\ deviation}$	$A_{w,average}$	$A_{w,standard\ deviation}$
Reference	0.129	0.070	0.16	0.04
Hydrophobisation	0.009	0.004	0.0004	0.0001
Render	2.229	0.368	0.30	0.03

The obtained results from partial immersion experiment are also displayed in Table 4. For reference and rendered specimens, the curvature, as seen in Figure 2, yielded the implementation of the calculation method described in eq. 5, whereas the hydrophobated specimens displayed a curve, and eq. 6 was used in this case. It is seen, that results differ from Karsten tube, particularly in hydrophobated and rendered specimens, but the same tendency is apparent; that the rendered surface absorbs the largest amount of water, whereas the hydrophobisation again exhibits a largely water repelling behavior. The difference between water absorption coefficient in reference and rendered specimens is less pronounced in the partial immersion experiment. It should be noted, that all reference and rendered specimens displayed water on the top surface, within 1 hour of immersion.

3.1 Simulations

Simulation results of the average water content in the various brick types, with the various surface treatments, are depicted in Figure 3. Figure 4 represent the relative humidity at the output location 5 cm from the exterior side of the brick. Simulation results clearly indicate differences in regards to surface treatment and brick type.

International RILEM Conference on Materials, Systems and Structures in Civil Engineering
 Conference segment on Moisture in Materials and Structures
 22-24 August 2016, Technical University of Denmark, Lyngby, Denmark

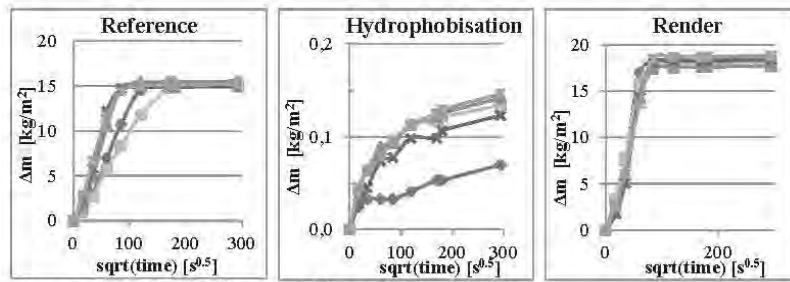


Figure 2. Plots of results from partial immersion experiments.

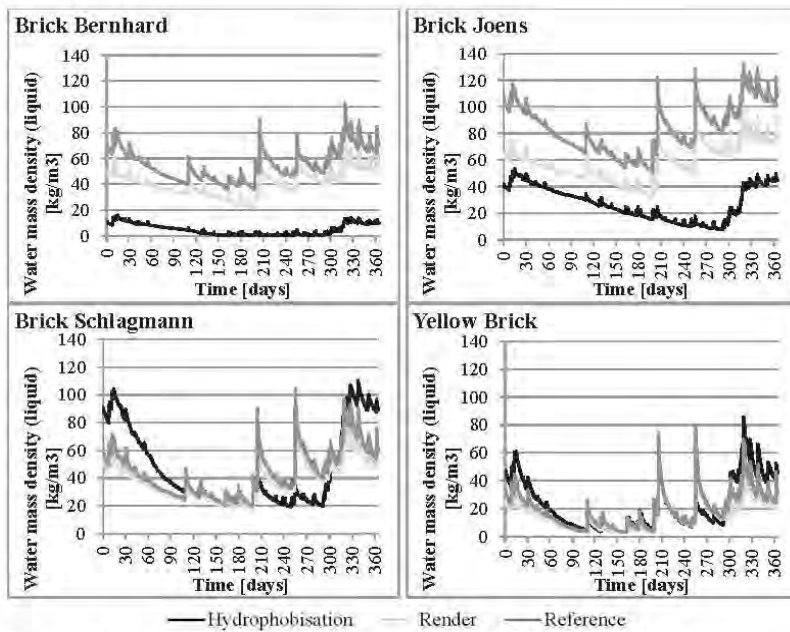


Figure 3. Average moisture content for the 2nd year of simulation and 3 surface types.

International RILEM Conference on Materials, Systems and Structures in Civil Engineering
 Conference segment on Moisture in Materials and Structures
 22-24 August 2016, Technical University of Denmark, Lyngby, Denmark

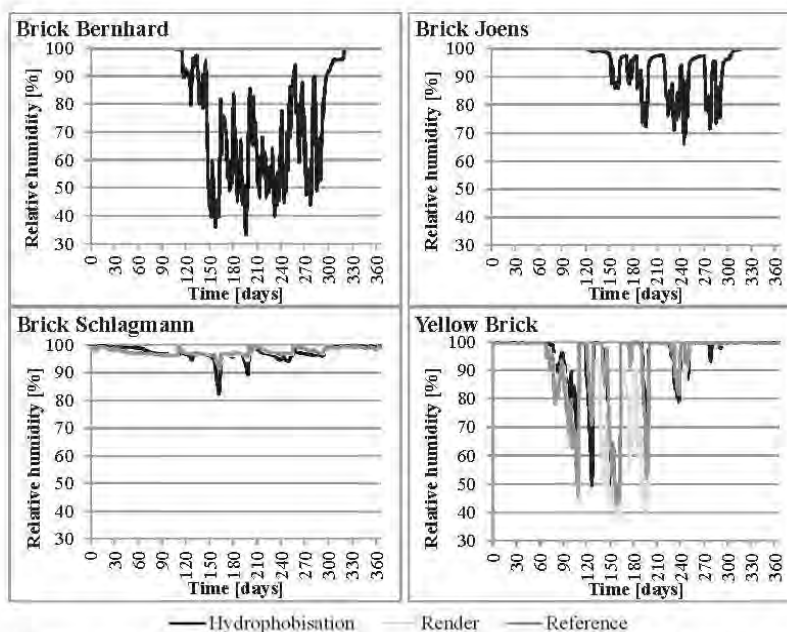


Figure 4. Relative humidity 5 cm from the brick surface for the 2nd year of simulation and the 3 surface types.

4. Discussion

The Karsten tube measurements show distinct variation in the absorption in regards to the type of surface. The surface with hydrophobisation treatment hardly absorbed any water – and on average 30 times less than the reference brick. The rendered surface absorbed nearly 25 times the amount of water compared to the reference brick. It was not investigated how the liquid distributed within the render and brick, however in one case a wet spot was observed on the bottom of the brick. The variation in results of the rendered specimens also indicates the unevenness of the surface treatment. The “film” of lime that appears on lime render surfaces, may be able to repel water better in reality with a lesser amount of water load, e.g. rain. The render surface is also assumed to be denser in reality and when executed by a professional, leaving it more weather proof. It should be noted, that the Karsten tube experiments were carried out vertically despite the bricks in real facades would require horizontal Karsten tube measurements. For comparison purposes, this did not cause concern for the results.

The partial immersion experiment showed same tendencies as the Karsten tube experiments for water uptake. Specimens with hydrophobisation treatment absorbed up to 124 times less

International RILEM Conference on Materials, Systems and Structures in Civil Engineering
Conference segment on Moisture in Materials and Structures
22-24 August 2016, Technical University of Denmark, Lyngby, Denmark

water in 24 hours relative to reference specimens. The rendered specimens absorbed a little more than reference specimens, but they also had a larger volume capable of retaining the liquid. The initial water absorption was highest in the rendered specimens. The rendered specimens also exhibited the largest amounts of water on the top surface of the specimen.

The fact that the rendered surface has the highest absorption found in both laboratory experiments seems rather curious. As mentioned, this can partly be due to inhomogeneity appearing as a result of non-professional execution. The extreme results obtained by Karsten tube can partly be explained by the poor adhesion of the tube to the rough surface, as some water may have escaped under the fixation. However, the fact that the absorption in the rendered surface is higher does not necessarily indicate further or faster penetration into the brick. It is possible, that the liquid distributes in render, and which possibly has better drying potential than the brick.

The differences observed between Karsten tube and partial immersion experiments, are assumed obtained partly due to the duration of time. The Karsten tube measurements were performed for only 30 minutes, whereas the partial immersion experiment lasts 24 hours. The initial water uptake in the partial immersion was faster than the Karsten tube.

Simulation results indicated that surface treatments such as either hydrophobisation or render could reduce the liquid moisture content in brick types such as Brick Bernhard or Brick Joens – hydrophobisation had the largest effect of the two treatments. The surface treatments however, seemed to have little to none effect in Brick Schlagmann and Yellow Brick. In the latter, hardly any effect of the surface treatment was observed. In Brick Schlagmann, the hydrophobisation displayed a negative effect in colder periods, but positive in summer.

The calculated relative humidity 5cm from the external brick side was for all brick types and surface treatments found to be very high in winter conditions. As mentioned, the simulations were made as a kind of “worst case” in regards to rain loads, and in winter periods there is only little drying potential. The hydrophobisation treatment again expressed positive impact in the brick types Brick Bernhard and Brick Joens during summer – most prominent in Brick Bernhard. 5 cm from the exterior in Brick Schlagmann no significant effect of the surface treatment was apparent. Within 5cm of the Yellow Brick, the brick seemed to be able to dry out during summer, regardless of the surface treatment.

5. Summary and conclusions

Karsten tube measurements and partial immersion experiment clearly showed the effect of a hydrophobisation surface treatment. Hardly any water was absorbed by specimens with hydrophobisation treatment. The rendered surface absorbed a large amount of water in Karsten tube experiment, but this is assumed to be partly caused by poor execution of rendering, poor adhesion of the tube, and the porosity of the lime render. The tendency of a high initial absorption in rendered specimens was also seen in the partial immersion experiment.

Simulation results made it very clear that the type of brick is a very important parameter when it comes to the effect of surface treatments. However, surfaces with both hydrophobisation and render did express a lower moisture content in Brick Bernhard and Brick Joens. For the

International RILEM Conference on Materials, Systems and Structures in Civil Engineering
 Conference segment on Moisture in Materials and Structures
 22-24 August 2016, Technical University of Denmark, Lyngby, Denmark

remaining brick types, the moisture content was generally lower than Brick Bernhard and Brick Joens, wherefore the effect is less significant. In both Brick Schlagmann and the Yellow Brick, the specimens with hydrophobisation treatment expressed higher moisture contents in colder periods – yet very little in the Yellow Brick. The conditions within 5 cm inside the brick indicated the effect of hydrophobisation during summer, in cases of Brick Bernhard and Brick Joens, however none effect of surface treatment was clear in Brick Schlagmann or Yellow Brick.

Future research should be done in the field of surface treatments of brick, as it potentially is essential to protect the façade from the climate when installing internal insulation. Research should focus on not only various treatments, but also how the treatments differ in effectiveness on different types of masonry. Surface treatments of mortar in joints should also be researched, as water penetration also occurs through joints. The effect of cracks and micro-cracks on surface treatments is also a highly relevant research area.

6. Acknowledgements

The presented work is a part of RIBuild project that has received funding from the European Union's Horizon 2020 research and innovation programme under grant agreement No 637268.

References

- [1] Vereecken, E., Roels, S., Capillary active interior insulation: do the advantages really offset potential disadvantages?, *Mater. Struct.* 48 (2015) 3009–3021
- [2] Abuku, M., Janssen, H., Roels, S., Impact of wind-driven rain on historic brick wall buildings in a moderately cold and humid climate: Numerical analyses of mould growth risk, indoor climate and energy consumption, 41 (2009) 101–110.
- [3] Morelli, M., Svendsen, S., Investigation of interior post-insulated masonry walls with wooden beam ends, *J. Build. Phys.* 36 (2012) 265–293
- [4] Morelli, M., Nielsen, T.R., Scheffler, G.A., Svendsen, S., Internal Insulation of Masonry Walls with Wooden Floor Beams in Northern Humid Climate, *Therm. Perform. Exter. Envel. Whole Build. XI Int. Conf.* (2010)
- [5] Künzle, H.M., Effect of interior and exterior insulation on the hygrothermal behaviour of exposed walls, *Mater. Struct.* 31 (1996) 99–103
- [6] Finken, G.R., Bjarlov, S.P., Peuhkuri, R.H., Effect of façade impregnation on feasibility of capillary active thermal internal insulation for a historic dormitory – A hygrothermal simulation study, *Constr. Build. Mater.* 113 (2016) 202–214
- [7] ISO 15148 Hygrothermal performance of building materials and products – Determination of water absorption coefficient by partial immersion, (2002)
- [8] Hendrickx, R., Using the Karsten tube to estimate water transport parameters of porous building materials, *Mater. Struct.* (2012) 1–12
- [9] Sandholdt, H., Dysted, D., Experimental and theoretical investigation of Interior insulations of solid brick walls with foam concrete and other silicate based materials, Master Thesis, 2015
- [10] Finken, G.R., Internal thermal insulation with hydrophilic materials, Master Thesis, 2014
- [11] Nicolai, A., Grünwald, J., Delphin 5, Version 5.8.3 User Manual and Program Ref. bauklimatik-dresden.de/downloads/documentation/Delphin_5_reference_manual_en.pdf

Appendix F

Paper VI

Correlation between certain material parameters in bricks

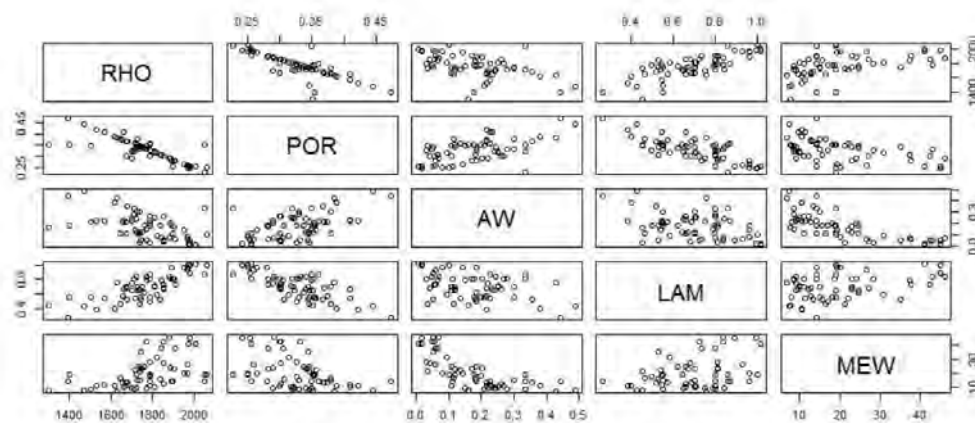
DTU

Correlation between certain material parameters in bricks

Introduction to applied statistics and R for PhD students
02935

Tessa Kvist Hansen

3/17/2017



Summary

Material parameters are vital in regards to hygrothermal simulations of buildings and building components. Hygrothermal simulations are also implemented for renovation purposes and in cases where material parameters are unknown. The density of brick can be determined in situ, why this can be assumed a known variable, and the estimation of other variables in regards to density is investigated. Applied statistics have been used in this project, in order to gain information on possible correlations between 5 different material parameters. A PCA analysis has indicated strong positive correlation between density and thermal conductivity, and a strong negative correlation between density and open porosity. Furthermore, a strong negative correlation between water uptake coefficient and water vapour diffusion resistance was found. Simple linear regression was applied for investigation of linear correlation between density and the other 4 parameters. Acceptable models were found for both open porosity and thermal conductivity in regards to the density, and reasonable estimations and predictions can be made. For water uptake coefficient and water vapour diffusion resistance factor the regression models cannot be accepted, and the same is true for the log transformed models, although an improvement could be seen.

Table of Contents

1	Introduction	2
2	Description of data	2
3	Statistical analyses, results and discussion	4
4	Conclusion.....	8
5	Appendices	10
5.1	R-script: Summary of data.....	10
5.2	R-script: PCA analysis.....	11
5.3	R-script: Simple linear regression	12

1 Introduction

Hygrothermal simulation tools are important for design and analysis of risks etc. in connection with e.g. interior insulation of historic buildings. Material parameters are essential for hygrothermal simulations, and some have proven to have a larger influence on results than others. It is not feasible in regards to time and economy, to send several samples to laboratory for a complete determination of all material parameters. In historic buildings there is even a large variation in e.g. bricks within the same square meter of wall. Some material parameters can be estimated by means of in situ tests. Some material parameters have a clear correlation to each other. It is sought to investigate the correlation of certain material parameters. As the density is the easiest parameter to estimate in situ and non-destructive, it is sought to estimate correlations between density and the other parameters. Material data is available on 63 types of brick, and there are five variables; density, open porosity, thermal conductivity, water uptake coefficient and water vapour diffusion resistance factor.

By means of PCA (principal component analysis) and simple regression, it is expected to shed light on the possible correlations.

2 Description of data

The data used in this project consists of 5 material parameters of 63 different types of brick. The data has been provided by the Delphin material database. Delphin is a hygrothermal simulation program, with a large material database of common building materials. All bricks from the database are included in this data, with the exception of perforated bricks, bricks with perlite content, and lime/sandstone bricks. The five material parameters given for each brick, is density (RHO), open porosity (POR), water uptake coefficient (AW), thermal conductivity (LAM) and water vapour diffusion resistance factor (MEW). A summary of the data can be found in Table 1.

Table 1: summary table of data

	Density, ρ [kg/m ³]	Open porosity [m ³ /m ³]	Water uptake coefficient [kg/m ² s ^{-1/2}]	Thermal conductivity, λ [W/mK]	Water vapour diffusion resistance factor, μ [-]
Denomination	RHO	POR	AW	LAM	MEW
Min.	1300	0.227	0.006	0.266	6.84
1 st quantile	1700	0.295	0.088	0.551	11.00
Median	1773	0.330	0.177	0.700	17.05
Mean	1769	0.327	0.178	0.704	20.21
3 rd quantile	1868	0.354	0.243	0.810	24.52
Max.	2060	0.474	0.489	1.012	46.21
Std. dev	159.69	0.051	0.113	0.173	11.52

The histograms of each parameter are shown in Figure 1. The histograms yield symmetry for parameters RHO, POR and LAM, and indicate a normal distribution. An asymmetry is however found in AW and MEW, which may lead to the use of log in the simple regression models. The histogram for AW seems right-skewed, as there is a natural limit to porosity (an open porosity of 1 corresponds to 100% of the material being air). The histogram of MEW however, looks bimodal, as it has two peaks.

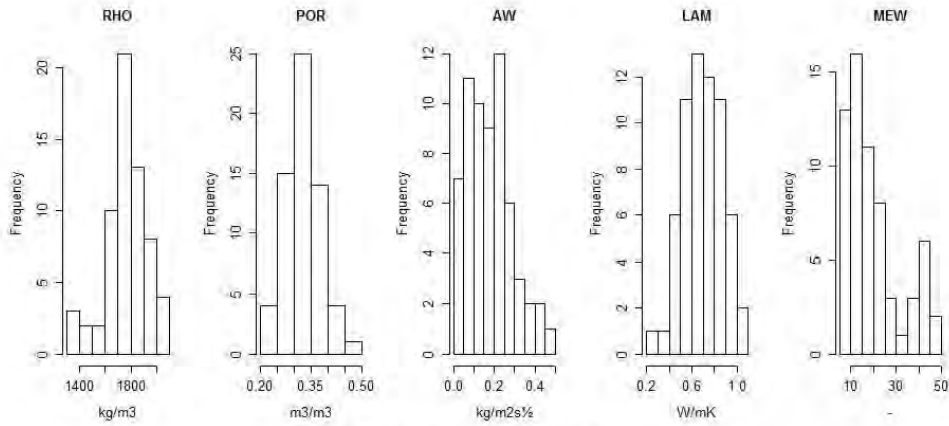


Figure 1: Histograms for all material parameters.

As the histograms, QQ plots can be used to check for normal distribution. As seen in Figure 2, most linearity is found in the parameters POR and LAM, while AW and MEW appear to be tailed, indicating more extreme values than expected for normal distribution.

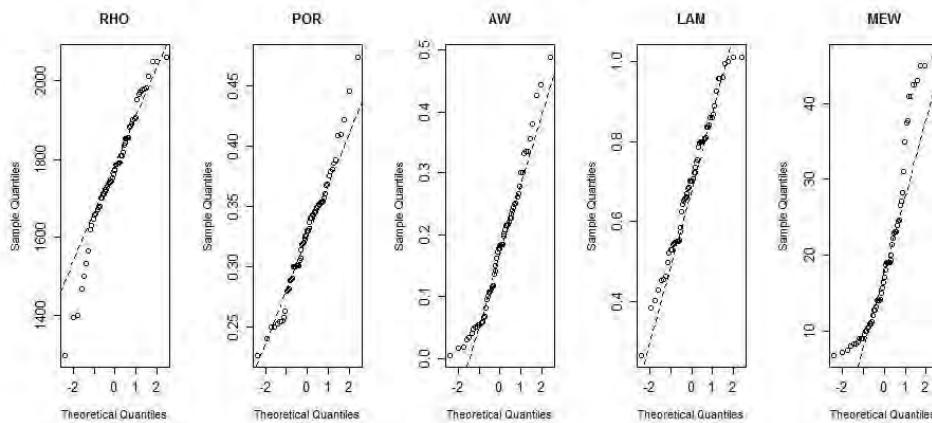


Figure 2: QQ Norm plots for all parameters

Plotting of the entire dataset can give an indication of any correlations. Figure 3 shows a clear indication of linear correlation between RHO and POR, RHO and LAM, POR and AW, and POR and LAM.

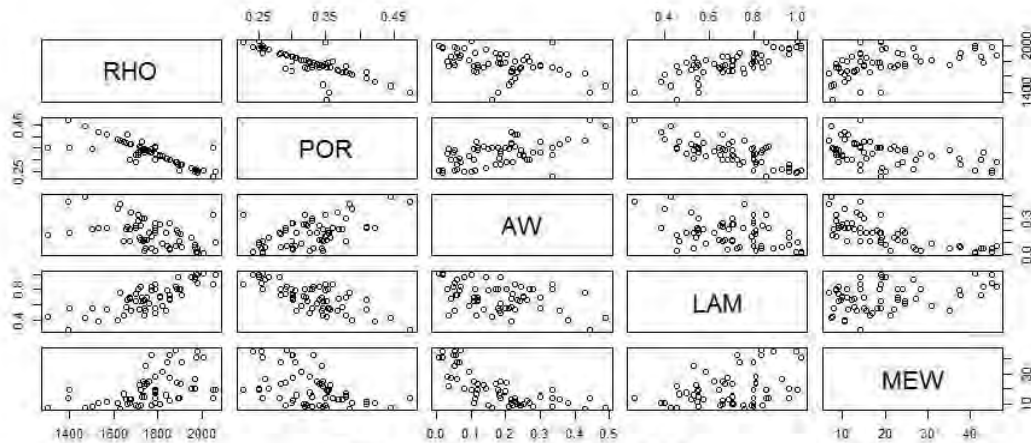


Figure 3: all variables plotted against each other.

As the only parameter that may be known/can be easily found, is RHO, the correlations between RHO and the other 4 parameters are in focus. Scatterplots of all the parameters vs. RHO have been made, and are seen in Figure 4. The figure clearly represents a sort of linearity between RHO and POR, and RHO and LAM. A linear correlation between RHO and AW, and RHO and MEW is not pronounced in the scatterplots.

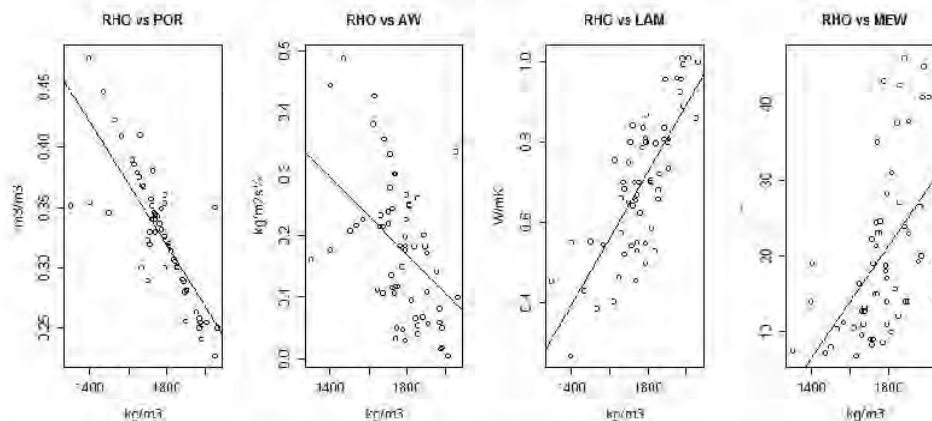


Figure 4: Scatterplots, relationship between 2 variables.

3 Statistical analyses, results and discussion

Initially a PCA, principal component analysis, is performed on the data. PCA is implemented in order to gain knowledge on the correlations between the various parameters and visualize clear patterns between the variables. PCA uses a transformation of the observations/bricks into variables called principal components.

This PCA was performed on standardized data. Standardization is implemented by scaling all the parameters. A plot of scores and loadings may be seen in Figure 5. A strong positive correlation is seen between RHO and LAM, and a strong negative correlation between RHO and POR. These results are not entirely

surprising, as the open porosity indicates the amount of pores, air, in a material. Hence the density was expected to decrease with an increased porosity. The same can be explained for the thermal conductivity; there is a higher heat transport through material than through air. Thus the more air/pores a material contains, the less heat will travel through and the thermal conductivity will be decrease. Also, a strong negative correlation is seen between AW and MEW. Both AW and MEW deal with moisture transport. The property of AW manages liquid water transport, whereas MEW describes the resistance to vapour transport. As MEW is a resistance, it makes sense for them to have a negative correlation. Also, as the angle between RHO and AW and MEW respectively, are in the vicinity of 90°, it can be said that there is little correlation between RHO and these two parameters.

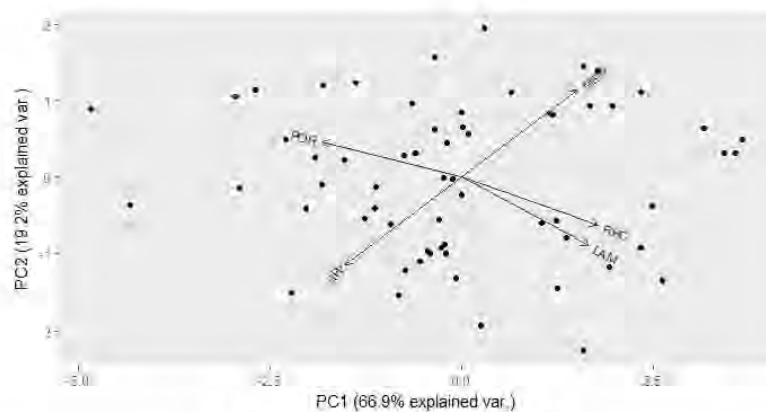


Figure 5: PCA biplot of scores and loadings.

In order to gather information on the correlations between RHO and the other material parameters, simple linear regression has been implemented. The histograms, QQ-plots and PCA have already revealed that MEW and AW may need transformation, but POR and LAM have already shown linear correlation.

The simple regression is firstly performed on the correlation between RHO and POR. RHO is the response variable, and the other material parameters are explanatory. The process will be described in the following. The correlations between RHO and the other parameters will have followed the same procedure in R, and results will be summarized in the end of this section.

The initial regression of RHO vs. POR can be seen in Figure 6. The coefficients for the regression line can be found in R, and yields the following linear function: $POR = 0.7778 - 0.00025 \cdot RHO$. The functions yield a p-value of $3.359e-15$ and R^2 value of 0.6411. R^2 is a measure that describes the degree of fit, and an R^2 value of 1 gives a perfect fit. An R^2 of 0.64 indicates a 64% variation in the response. The p-value states that the effect of RHO on POR is statistically significant in the 95% confidence interval, as it is below 5%, and the R^2 value indicates an acceptable fit, however the figure reveals some large discrepancies in some of the observations/bricks. By omitting these potential outliers, it may be possible to achieve a better fit and optimize the model.

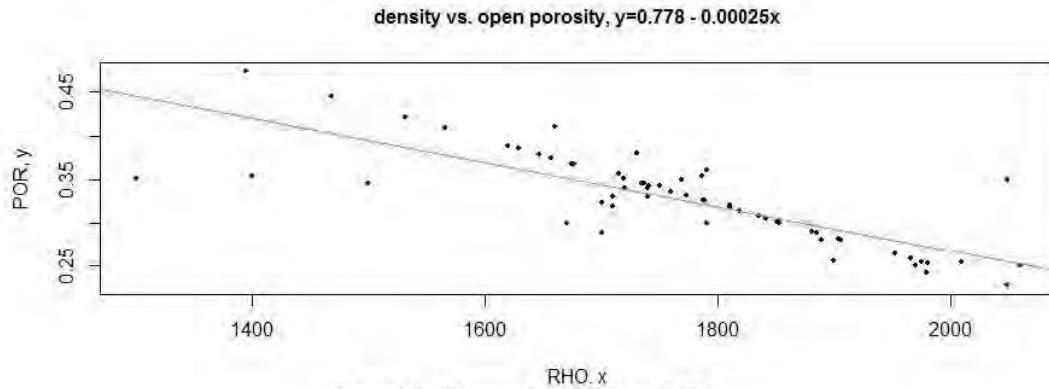


Figure 6: Initial regression for RHO vs. POR

The potential outliers can be identified via the residuals. The residual plots can be seen in Figure 7. The Residuals vs. Fitted plot shows a scattered tendency, indicating model adequacy, and the variance is more or less constant. In both the Residuals vs. Fitted, Normal Q-Q and Cook's distance charts, it is seen that observations/bricks no. 1, 3 and 62 are outliers. The outliers, in this case, consist of two low density bricks, with an average open porosity, and one high density brick with an average porosity.

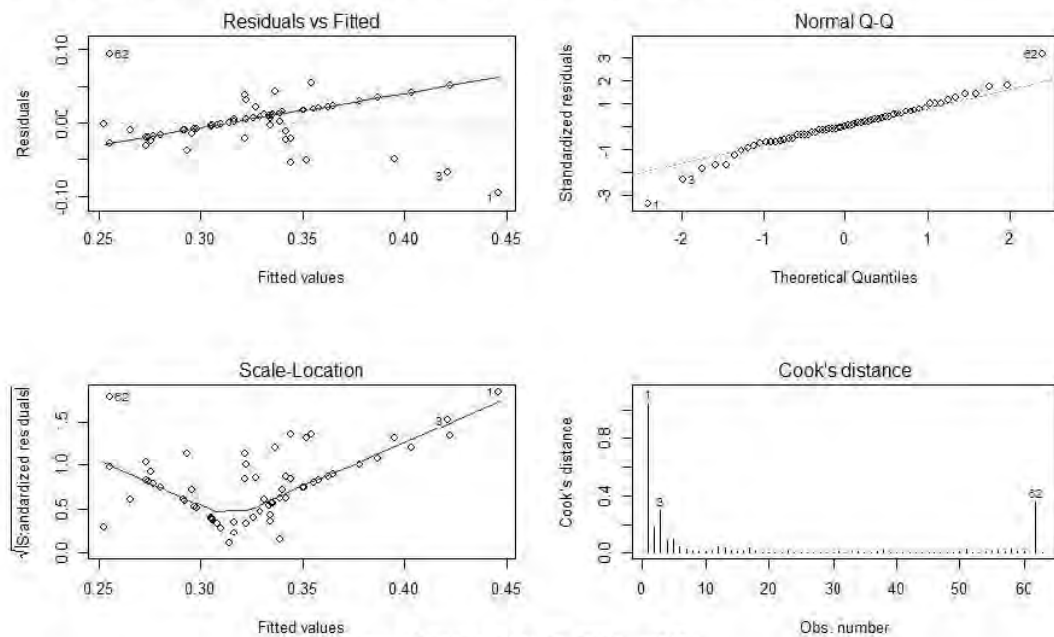


Figure 7: Residual plots for RHO vs. POR.

The regression is repeated with omission of observations/bricks 1, 3 and 62 for a better fit. The fitted model gives a p-value of less than $2.2e-16$, and R^2 value of 0.8308 – therefore a better fit is achieved. The new coefficients yield that: $POR = 0.9293 - 0.00034 \cdot RHO$; thus the estimated open porosity decreases with 0.00034 per kg/m^3 density increase. The new regression is shown in Figure 8 (blue line), and it is very apparent that a better fit is accomplished.

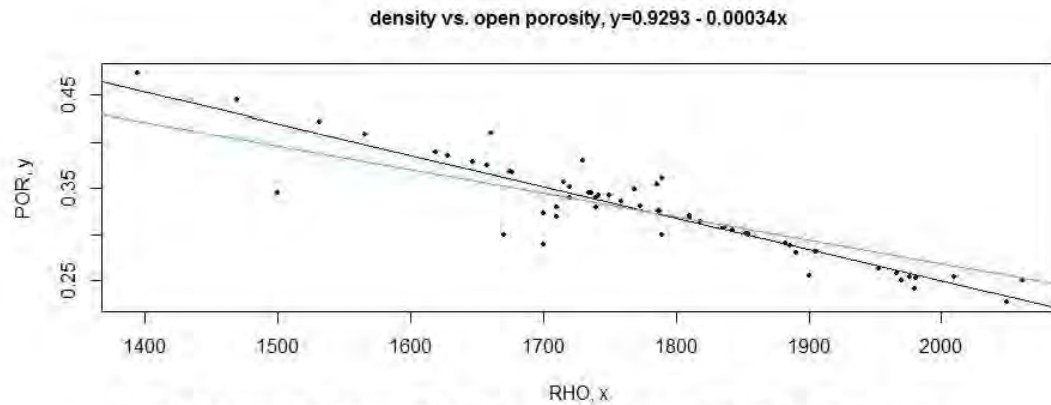


Figure 8: Fitted model and regressions for RHO vs. POR. Original model: green, fitted model: blue.

In Figure 9 the confidence and prediction intervals are depicted in red and orange respectively. Both should lie symmetrically around the regression line; however this was not possible to plot. R can also predict the open porosity for a given density. As an example of a density of 1780kg/m^3 , the open porosity is estimated to be 0.32 in the 95% confidence interval of 0.28 - 0.37.

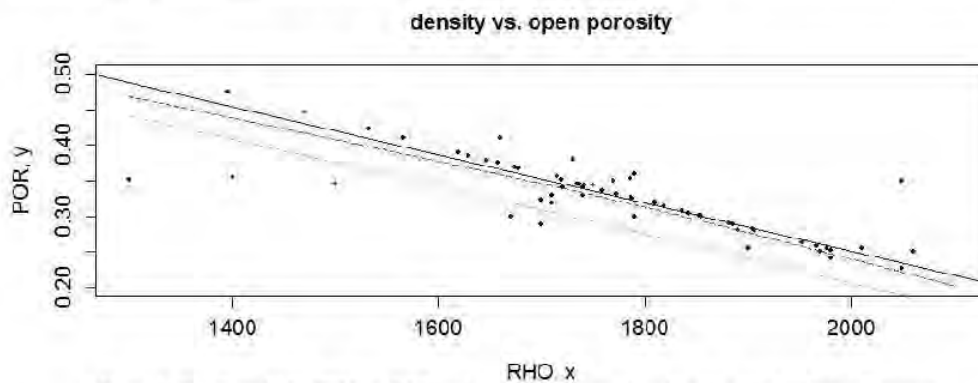


Figure 9: Fitted model for RHO vs. POR, and confidence interval: red, and prediction interval: orange.

The same procedure is performed on all the variables, and the outcomes can be seen in Table 2. It is seen in the table, that for all four parameters a better fit is achieved by omitting outliers. The best fit is found for RHO vs. POR, and the fitted model for RHO vs. LAM is also acceptable. The simple linear regressions for RHO vs. AW and RHO vs. MEW however, are not.

Table 2: Simple linear regression performed on RHO vs. the other material parameters.

RHO vs.	1 st model		Omitted observations /bricks	Fitted model			Example: prediction if RHO is 1780kg/m^3		
	R^2	p-value		R^2	p-value	function	fit	lower	upper
POR	0.64	$3.36\text{e-}15$	1, 3, 62	0.83	$<2.2\text{e-}16$	$y=0.93 - 0.00034x$	0.33	0.28	0.37
AW	0.19	$3.08\text{e-}4$	1, 61, 62	0.39	$1.07\text{e-}7$	$y=1.04 - 0.00049x$	0.17	-0.01	0.35
LAM	0.60	$1.08\text{e-}13$	1, 3	0.61	$1.01\text{e-}13$	$y=-0.97 + 0.00094x$	0.71	0.49	0.93
MEW	0.26	$1.82\text{e-}5$	3, 59, 62	0.29	$7.36\text{e-}6$	$y=-52.68 + 0.04108x$	20.44	1.09	39.80

An example of prediction of parameters is carried out for each parameter, assuming a RHO of 1780kg/m^3 is known. The results are given in Table 2, and the 95% confidence limits are found (upper and lower). It is clear that the intervals for AW and MEW are very large, again expressing the non-fit of these models.

As seen in the table, and previously in histograms and QQ-plots, a sort of transformation is needed for parameters AW and MEW , as they are not normally distributed; a nonconstant variance (trumpet) is also seen in the Residuals vs. Fitted plots in Figure 10 and yield very low R^2 values. Hence the fitted linear regression model is not accepted for these two parameters. A log transformation is implemented. The implemented log transformations give better residual vs. fitted plots, especially for AW , as seen in Figure 11.

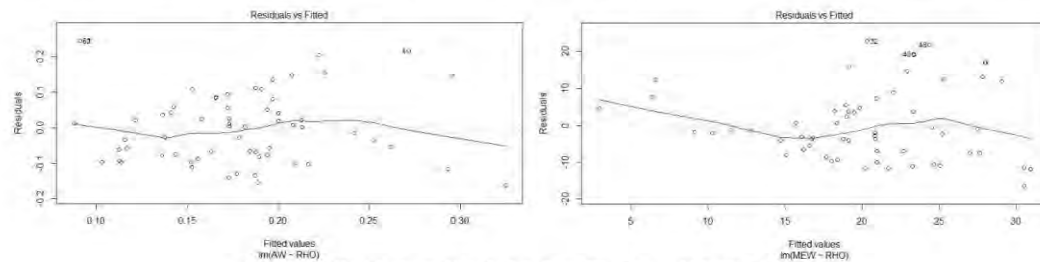


Figure 10: Residuals vs. Fitted plots for AW (left) and MEW (right).

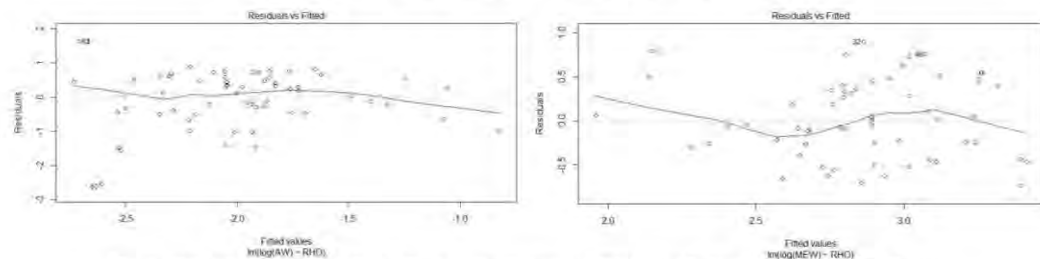


Figure 11: Residuals vs. Fitted plots for log transformed AW (left) and log transformed MEW (right).

The results from the log transformed and log transformed fitted models can be seen in Table 3. From the R^2 values, it is seen that better fits have been obtained, although they are still rather low. It is also seen in the table, that the interval for the example of expected estimated values of AW and MEW are very large. Thus the log transformations do not yield acceptable models for correlation between RHO and AW , and MEW respectively.

Table 3: Simple linear regression performed on RHO vs log transformed AW and MEW .

RHO vs.	1 st model, log transformed		Omitted observations /bricks	Fitted model, log transformed		Example: prediction if RHO is 1780kg/m^3			
	R^2	p-value		R^2	p-value	function	fit	lower	upper
AW	0.21	$1.51\text{e-}4$	1, 60, 62	0.26	$3.66\text{e-}5$	$\log(y)=2.93-0.0027x$	-2.00	-3.38	-0.62
						$y=\exp(2.93-0.0027x)$	0.14	0.03	0.54
MEW	0.31	$2.17\text{e-}6$	2, 3, 62	0.40	$4.81\text{e-}8$	$\log(y)=-1.54+0.0025x$	2.87	1.99	3.75
						$y=\exp(-1.54+0.0025x)$	17.64	7.32	42.52

4 Conclusion

The PCA analysis indicated strong correlations between RHO and POR , and RHO and LAM . These correlations were demonstrated with simple linear regression. By omitting outliers, reasonable models were

found for the correlations; $POR=0.93-0.00034 \cdot RHO$ and $LAM=-0.97+0.00094 \cdot RHO$. Linear regression was not found to be acceptable for parameters AW and MEW. Log transformed regression models of these parameters improved the fit, but still not categorized as reasonable or acceptable. AW and MEW also shown to be non-normally distributed in early presentation of the data (histograms and QQ-plots). Figure 3 did show possible linear correlation between POR and AW (POR and LAM), so it could be an option to fit this model, and find AW indirectly, however more uncertainties would apply. The outlying observations for the models were repeats in many cases; e.g. observation/brick no. 62 proved to be an outlier in all models, except RHO vs. LAM. Out of the 6 models (RHO vs. POR, RHO vs. AW, RHO vs. LAM, RHO vs. MEW, RHO vs. logAW, and RHO vs. logMEW), observations/bricks no. 1 and 3 were also represented 4 times each.

5 Appendices

The appendices will consist of three R-scripts. One for basic description of the data, one for PCA analysis and one for linear regression.

5.1 R-script: Summary of data

```
## Basic beginning

head(matp)
summary(matp)
par(mfrow=c(1,1))
attach(matp)
plot(matp[,1:5])

#histograms
par(mfrow=c(1,5))
hist(matp$RHO, main="RHO", xlab="kg/m3", cex.axis=1.2, cex.lab=1.2)
hist(matp$POR, main="POR", xlab="m3/m3", cex.axis=1.2, cex.lab=1.2)
hist(matp$AW, main="AW", xlab="kg/m2s1/2", cex.axis=1.2, cex.lab=1.2)
hist(matp$LAM, main="LAM", xlab="W/mK", cex.axis=1.2, cex.lab=1.2)
hist(matp$MEW, main="MEW", xlab="-", cex.axis=1.2, cex.lab=1.2)

#scatterplots
par(mfrow=c(1,5))
plot(matp$RHO, main="RHO", xlab="brick", ylab="kg/m3", cex.axis=1.2,
cex.lab=1.2)
plot(matp$POR, main="POR", xlab="brick", ylab="m3/m3", cex.axis=1.2,
cex.lab=1.2)
plot(matp$AW, main="AW", xlab="brick", ylab="kg/m2s1/2", cex.axis=1.2,
cex.lab=1.2)
plot(matp$LAM, main="LAM", xlab="brick", ylab="W/mK", cex.axis=1.2,
cex.lab=1.2)
plot(matp$MEW, main="MEW", xlab="brick", ylab="-", cex.axis=1.2,
cex.lab=1.2)

#scatterplots vs RHO, rho is x-axis
par(mfrow=c(1,4))
plot(matp$POR~matp$RHO, main="RHO vs POR", xlab="kg/m3", ylab="m3/m3",
cex.axis=1.2, cex.lab=1.2)
abline(lm(matp$POR ~ matp$RHO))
plot(matp$AW~matp$RHO, main="RHO vs AW", xlab="kg/m3", ylab="kg/m2s1/2",
cex.axis=1.2, cex.lab=1.2)
abline(lm(matp$AW ~ matp$RHO))
plot(matp$LAM~matp$RHO, main="RHO vs LAM", xlab="kg/m3", ylab="W/mK",
cex.axis=1.2, cex.lab=1.2)
abline(lm(matp$LAM ~ matp$RHO))
plot(matp$MEW~matp$RHO, main="RHO vs MEW", xlab="kg/m3", ylab="-",
cex.axis=1.2, cex.lab=1.2)
abline(lm(matp$MEW ~ matp$RHO))

#QQ Plots, observed quantiles plotted against theoretical quantiles,
#should give straight line
#normal data: POR, LAM. Light tails: RHO, AW and MEW.
```



```

par(mfrow=c(1,5))
qqnorm(matp$RHO, main="RHO", cex.axis=1.2)
qqline(matp$RHO, lty=2)
qqnorm(matp$POR, main="POR", cex.axis=1.2)
qqline(matp$POR, lty=2)
qqnorm(matp$AW, main="AW", cex.axis=1.2)
qqline(matp$AW, lty=2)
qqnorm(matp$LAM, main="LAM", cex.axis=1.2)
qqline(matp$LAM, lty=2)
qqnorm(matp$MEW, main="MEW", cex.axis=1.2)
qqline(matp$MEW, lty=2)

```

5.2 R-script: PCA analysis

```

###PCA - Principal component analysis

library(ChemometricsWithR)
# Basic PCA on correlations (WITH Standardization)
#ALLE parametre
par(mfrow=c(1,2))
matp_PC <- PCA(scale(matp[, 1:5]))
scores(matp_PC)
scoreplot(matp_PC, main="scores")
loadingplot(matp_PC, show.names = TRUE)

#with standardization - SCALE, all the parameters look to be equally
important.
par(mfrow=c(1,1))
biplot(matp_PC)

## A nicer biplot for PCA by prcomp or princomp:
matp_pca <- prcomp(matp,
                    center = TRUE,
                    scale. = TRUE)
library(devtools)
#install_github("ggbiplot", "vqv")
library(ggbiplot)
g <- ggbiplot(matp_pca, obs.scale = 1, var.scale = 1, ellipse = TRUE,
labels.size = 5)
g <- g + scale_color_discrete(name = '')
g <- g + theme(legend.direction = 'horizontal',
               legend.position = 'top')
print(g)

# Diagnostics using chemometrics package library(ChemometricsWithR)
# Basic PCA on correlations (WITH Standardization)
par(mfrow=c(1, 1))
matp_PC <- PCA(scale(matp[, 1:5]))
scores(matp_PC)
plot(scores(matp_PC)[, 1], scores(matp_PC)[, 2], scores(matp_PC)[, 3],
scores(matp_PC)[, 4], scores(matp_PC)[, 5])
var(scores(matp_PC)[, 1])

```

```

var(scores(matp.PC)[, 2])
var(scores(matp.PC)[, 3])
var(scores(matp.PC)[, 4])
var(scores(matp.PC)[, 5])
matp.PC$var
scoreplot(matp.PC, main = "Scores")
plot(matp.PC$var, cex=2, main="Scree type plot: variances")
lines(matp.PC$var)

#Diagnostics using chemometrics package library(chemometrics)
matp.PCA=princomp(matp[,1:5], cor = TRUE)
# The score distances res$SDist express the leverage values
# The orthogonal distances express the residuals
## Plots vs object number :
res=pcaDiagplot(matp[,1:5], matp.PCA, a=2)
## Plot of the two against each other:
plot(res$SDist, res$ODist, type="n")
text(res$SDist, res$ODist, labels=row.names(matp))
## Explained variance for each variable
pcaVarexpl(matp[,1:5], a=2)

```

5.3 R-script: Simple linear regression

```

### Simple linear regression.

attach(matp)
#####
#RHO vs. POR
RHOFOR<-data.frame(RHO,POR); RHOFOR
summary(RHOFOR)
par(mfrow=c(1,1))
plot(RHO,POR, pch=16, cex=.5)
abline(lm(POR~RHO))
ls()

reg1<-lm(POR~RHO)
coefficients(reg1) #POR=0.7778-0.00025*RHO=0.7778-0.00025*RHO
## Coefficients give us the slope and intercept (B0 and B1) fitted
regression line: y=0.778 - 0.00025x, = the estimated slope shows that the
estimated open porosity decreases by 0.00025 pr kg/m3 increase in density

par(mfrow=c(1,1))
plot(RHO,POR)
abline(reg1)
plot(RHO,POR,pch=16, cex=.5, cex.main=1, cex.axis=1, cex.lab=1,
      ylab= "POR, y", xlab= "RHO, x", main="density vs. open porosity,
y=0.778 - 0.00025x")
abline(reg1, col="green") ### this line is wrong
lines(lowess(matp$RHO,matp$POR), lty=2, col=3)
summary(reg1)
##P-value:3.4e-15 << 5% : The effect of RHO on POR is statistically
significant under the model

```

```
##R^2 = 0.641, R=0.8006

##Generic functions
par(mfrow=c(2,2))
print(reg1)
anova(reg1)
drop1(reg1)
drop1(reg1, test="F")
AIC(reg1) ##-256,1
coef(reg1)
confint(reg1, level=0.95) ## 95/5% is also default
par(mfrow=c(2,2))
plot(reg1)
predict(reg1)
residuals(reg1) ## residuals vs. fitted, randomly scattered: accept
plot(reg1)
plot(reg1, which=1:4)
names(reg1)
str(reg1)
vcov(reg1) ## Cooks distance highest in observations 1, 62, 3
str(reg1)

par(mfrow=c(1,1))

##Try to fit the model

rhopor<-data.frame(RHO,POR)
rhopor

## Omitting obs 1, 3 and 62 (the 3 largest cook dist and residual dist.)
reg1Min1362<-(lm(POR ~ RHO, data=rhopor[-c(1,3,62),]))
summary(reg1Min1362)
coefficients(reg1Min1362)
confint
par(mfrow=c(1,1))
plot(POR~RHO,data=matp[-c(1,3,62),],pch=16, cex=.5, cex.main=1,
      cex.axis=1, cex.lab=1,
      ylab= "POR, y", xlab= "RHO, x", main="density vs. open porosity,
      y=0.9293 - 0.00034x")

abline(reg1Min1362, col="blue") ### this line is wrong
abline(reg1, col="green")

## Confidence and prediction intervals
newx1<-seq(1300,2100)
newx1
newdatax1=data.frame(RHO=newx1)

predCI<-predict(reg1Min1362,newdata=newdatax1, interval="confidence",
level=0.95, type="response")
predCI
predPI<-predict(reg1Min1362,newdata=newdatax1,interval="prediction",
level=0.95, type="response")
```

```

predPI

plot(RHO,POR,xlim=c(0,2100),ylim=c(0.2,1), pch=16, cex=0.5,
     ylab="POR, y", xlab="RHO, x", main="density vs. open porosity",
     cex.axis=1.2,
     cex.lab=1.2, cex.main=1.2)
abline(reg1Min1362, col="blue") #
lines(newx1,predCI[,2],col="red", lty=2)
lines(newx1,predPI[,2],col="orange", lty=2)

### Predict POR when RHO is 1780
predPIx1780<-
predict(reg1Min1362,newdata=data.frame(RHO=1780),interval="prediction",
       level=0.95, type="response");predPIx1780

## the 95% prediction limits for the new y is: 0.28-0.37, fit is 0.32

#####
#RHO vs. AW
RHOAW<-data.frame(RHO,AW); RHOAW
summary(RHOAW)
par(mfrow=c(1,1))
plot(RHO,AW, pch=16, cex=.5)
abline(lm(AW~RHO))
ls()

reg2<-lm(AW~RHO)
coefficients(reg2) #AW=0.7309 - 0.00031*RHO
## Coefficients give us the slope and intercept (B0 and B1) fitted
regression line: y=0.7309 - 0.00031x, = the estimated slope shows that
the estimated water uptake coefficient decreases by 0.00031 perkg/m3
increase in density

par(mfrow=c(1,1))
plot(RHO,AW)
abline(reg2)
plot(RHO,AW,pch=16, cex=.5, cex.main=1, cex.axis=1, cex.lab=1,
     ylab= "AW, y", xlab= "RHO, x", main="density vs. water uptake
coefficient, y=0.778 - 0.00025x")
abline(reg2, col="green") ### this line is wrong
lines(lowess(matp$RHO,matp$AW), lty=2, col=3)

summary(reg2)
##P-value:3.08e-4 << 5% : The effect of RHO on AW is statistically
significant under the model
##R^2 = 0.1936

##Generic functions
par(mfrow=c(2,2))
print(reg2)
anova(reg2)
drop1(reg2)
drop1(reg2, test="F")

```

```

AIC(reg2) ##-104
coef(reg2)
confint(reg2, level=0.95) ## 95/5% is also default
par(mfrow=c(2,2))
plot(reg2)
predict(reg2)
residuals(reg2) ## residuals vs. fitted, trumpet.. noaccept
plot(reg2)
plot(reg2, which=1:4)
names(reg2)
str(reg2)
vcov(reg2) ## Cooks distance highest in observations 1, 61, 62
str(reg2)

par(mfrow=c(1,1))

##Try to fit the model

rhoaw<-data.frame(RHO,AW)
rhoaw

## Omitting obs 1, 3 and 62 (the 3 largest cook dist and residual dist.)
reg2Min16162<-(lm(AW ~ RHO, data=rhoaw[-c(1,61,62),]))
summary(reg2Min16162)
coefficients(reg2Min16162)
plot(reg2Min16162, which=1:4)
confint
par(mfrow=c(1,1))
plot(AW~RHO,data=matp[-c(1,61,62),],pch=16, cex=.5, cex.main=1,
     cex.axis=1, cex.lab=1,
     ylab="AW, y", xlab="RHO, x", main="density vs. water uptake
     coefficient, y=1.03939 - 0.0004899x")

abline(reg2Min16162, col="blue") ### this line is wrong
abline(reg2, col="green")

## Confidence and prediction intervals
newx2<-seq(1300,2100)
newx2
newdatax2=data.frame(RHO=newx2)

predCI<-predict(reg2Min16162,newdata=newdatax2, interval="confidence",
level=0.95, type="response")
predCI
predPI<-predict(reg2Min16162,newdata=newdatax2,interval="prediction",
level=0.95, type="response")
predPI

plot(RHO,AW,xlim=c(0,2100),ylim=c(0.2,1), pch=16, cex=0.5,
     ylab="AW, y", xlab="RHO, x", main="density vs. water uptake
     coefficient", cex.axis=1.2,
     cex.lab=1.2, cex.main=1.2)
abline(reg2Min16162, col="blue") #

```



```

lines(newx2,predCI[,2],col="red", lty=2)
lines(newx2,predPI[,2],col="orange", lty=2)

plot(RHO,AW,xlim=c(1300,2100),ylim=c(0.2,1), pch=16, cex=0.5,
      ylab="AW, y", xlab="RHO, x", main="density vs. water uptake
coefficient", cex.axis=1.2,
      cex.lab=1.2, cex.main=1.2)
abline(reg2Min16162, col="blue") #
lines(newx2,predCI[,2],col="red", lty=2)
lines(newx2,predPI[,2],col="orange", lty=2)

### Predict AW when RHO is 1780
predPIx1780<-
predict(reg2Min16162,newdata=data.frame(RHO=1780),interval="prediction",
        level=0.95, type="response");predPIx1780

## the 95% prediction limits for the new y is: -0.011-0.35, fit is 0.17

#####
#RHO vs. LAM
RHOLAM<-data.frame(RHO,LAM); RHOLAM
summary(RHOLAM)
par(mfrow=c(1,1))
plot(RHO,LAM, pch=16, cex=.5)
abline(lm(LAM~RHO))
ls()

reg3<-lm(LAM~RHO)
coefficients(reg3) #LAM=-0.7799 + 0.0008386*RHO
## Coefficients give us the slope and intercept (B0 and B1) fitted
regression line: y=-0.7799 + 0.00084x, = the estimated slope shows that
the estimated thermal conductivity increases by 0.00084 per kg/m3
increase in density

par(mfrow=c(1,1))
plot(RHO,LAM)
abline(reg3)
plot(RHO,LAM,pch=16, cex=.5, cex.main=1, cex.axis=1, cex.lab=1,
      ylab="LAM, y", xlab="RHO, x", main="density vs. thermal
conductivity, y=-0.7799 + 0.00084x")
abline(reg3, col="green") ###
lines(lowess(matp$RHO,matp$LAM), lty=2, col=3)

summary(reg3)
##P-value:1.75e-13 << 5% : The effect of RHO on LAM is statistically
significant under the model
##R^2 = 0.5984

##Generic functions
par(mfrow=c(2,2))
print(reg3)
anova(reg3)
drop1(reg3)

```

```

drop1(reg3, test="F")
AIC(reg3) ##-94.66
coef(reg3)
confint(reg3, level=0.95) ## 95/5% is also default
par(mfrow=c(2,2))
plot(reg3)
predict(reg3)
residuals(reg3) ## residuals vs. fitted, trumpet.. accept
plot(reg3)
plot(reg3, which=1:4)
names(reg3)
str(reg3)
vcov(reg3) ## Cooks distance highest in observations 1, 2, 3
str(reg3)

par(mfrow=c(1,1))

##Try to fit the model

rholam<-data.frame(RHO,LAM)
rholam

## Omitting obs 1 and 3 (the 2 largest cook dist and residual dist.)
reg3Min13<-(lm(LAM ~ RHO, data=rholam[-c(1,3),]))
summary(reg3Min13)
coefficients(reg3Min13)
confint
par(mfrow=c(1,1))
plot(LAM~RHO,data=matp[-c(1,3),],pch=16, cex=.5, cex.main=1, cex.axis=1,
cex.lab=1,
ylab="AW, y", xlab="RHO, x", main="density vs. thermal
conductivity, y=-0.97 + 0.000944x")

abline(reg3Min13, col="blue")
abline(reg3, col="green")

## Confidence and prediction intervals
newx3<-seq(1300,2100)
newx3
newdatax3=data.frame(RHO=newx3)

predCI<-predict(reg3Min13,newdata=newdatax3, interval="confidence",
level=0.95, type="response")
predCI
predPI<-predict(reg3Min13,newdata=newdatax3,interval="prediction",
level=0.95, type="response")
predPI

plot(RHO,LAM,xlim=c(0,2100),ylim=c(-1,1), pch=16, cex=0.5,
ylab="LAM, y", xlab="RHO, x", main="density vs. thermal
conductivity", cex.axis=1.2,
cex.lab=1.2, cex.main=1.2)
abline(reg3Min13, col="blue") #

```

```

lines(newx3,predCI[,2],col="red", lty=2)
lines(newx3,predPI[,2],col="orange", lty=2)
plot(RHO,LAM,xlim=c(1300,2100),ylim=c(0.2,1), pch=16, cex=0.5,
      ylab="LAM, y", xlab="RHO, x", main="density vs. thermal
conductivity", cex.axis=1.2,
      cex.lab=1.2, cex.main=1.2)
abline(reg3Min13, col="blue") #
lines(newx3,predCI[,2],col="red", lty=2)
lines(newx3,predPI[,2],col="orange", lty=2)

### Predict POR when RHO is 1780
predPIx1780<-
predict(reg3Min13,newdata=data.frame(RHO=1780),interval="prediction",
        level=0.95, type="response");predPIx1780

## the 95% prediction limits for the new y is: 0.49-0.93, fit is 0.707

#####
#RHO vs. MEW
RHO_MEW<-data.frame(RHO,MEW); RHO_MEW
summary(RHO_MEW)
par(mfrow=c(1,1))
plot(RHO,MEW, pch=16, cex=.5)
abline(lm(MEW~RHO))
ls()

reg4<-lm(MEW~RHO)
coefficients(reg4) #LAM=-45.09 + 0.036907*RHO
## Coefficients give us the slope and intercept (B0 and B1) fitted
regression line: y=-45.09 + 0.036907x, = the estimated slope shows that
the estimated mew increases by 0.036907 per kg/m3 increase in density

par(mfrow=c(1,1))
plot(RHO,MEW)
abline(reg4)
plot(RHO,MEW,pch=16, cex=.5, cex.main=1, cex.axis=1, cex.lab=1,
      ylab= "MEW, y", xlab= "RHO, x", main="density vs. water vapour
diffusion resistance factor, y=-45.09 + 0.036907x")
abline(reg4, col="green") ###
lines(lowess(matp$RHO,matp$MEW), lty=2, col=3)

summary(reg4)
##P-value:1.82e-5 << 5% : The effect of RHO on MEW is statistically
significant under the model
##R^2 = 0.2681

##Generic functions
par(mfrow=c(2,2))
print(reg4)
anova(reg4)
drop1(reg4)
drop1(reg4, test="F")
AIC(reg4) ##-94.66

```

```

coef(reg4)
confint(reg4, level=0.95) ## 95/5% is also default
par(mfrow=c(2,2))
plot(reg4)
predict(reg4)
residuals(reg4) ## residuals vs. fitted, trumpet... accept
plot(reg4)
plot(reg4, which=1:4)
names(reg4)
str(reg4)
vcov(reg4) ## Cooks distance highest in observations 1, 61, 62
str(reg4)

par(mfrow=c(1,1))

##Try to fit the model

rhomew<-data.frame(RHO,MEW)
rhomew

## Omitting obs 3, 59 and 62 (the 3 largest cook dist and residual dist.)
reg4Min35962<-lm(MEW ~ RHO, data=rhomew[-c(3,59,62),])
summary(reg4Min35962)
coefficients(reg4Min35962)
confint
par(mfrow=c(1,1))
plot(MEW~RHO,data=matp[-c(3,59,62),],pch=16, cex=.5, cex.main=1,
cex.axis=1, cex.lab=1,
      ylab= "MEW, y", xlab= "RHO, x", main="density vs. water vapour
diffusion resistance factor,  $y=-0.97 + 0.000944x$ ")
abline(reg4Min35962, col="blue") ### this line is wrong
abline(reg4, col="green")

## Confidence and prediction intervals
newx4<-seq(1300,2100)
newx4
newdatax4=data.frame(RHO=newx4)

predCI<-predict(reg4Min35962,newdata=newdatax4, interval="confidence",
level=0.95, type="response")
predCI
predPI<-predict(reg4Min35962,newdata=newdatax4,interval="prediction",
level=0.95, type="response")
predPI

plot(RHO,MEW,xlim=c(0,2100),ylim=c(0,50), pch=16, cex=0.5,
      ylab="MEW, y", xlab="RHO, x", main="density vs. water vapour
diffusion resistance factor", cex.axis=1.2,
      cex.lab=1.2, cex.main=1.2)
abline(reg4Min35962, col="blue") #
lines(newx4,predCI[,2],col="red", lty=2)
lines(newx4,predPI[,2],col="orange", lty=2)
plot(RHO,MEW,xlim=c(1300,2100),ylim=c(0,50), pch=16, cex=0.5,

```

```

      ylab="LAM, y", xlab="RHO, x", main="density vs. thermal
conductivity", cex.axis=1.2,
      cex.lab=1.2, cex.main=1.2)
abline(reg4Min35962, col="blue") #
lines(newx4,predCI[,2],col="red", lty=2)
lines(newx4,predPI[,2],col="orange", lty=2)

### Predict POR when RHO is 1780
predPIx1780<-
predict(reg4Min35962,newdata=data.frame(RHO=1780),interval="prediction",
      level=0.95, type="response");predPIx1780

## the 95% prediction limits for the new y is: 1.08-39.79, fit is 20.44

#####
#Log transformations of AW and MEW

##AW
reglogaw<-lm(log(AW)~RHO,data=matp)
par(mfrow=c(1,1))
plot(log(AW)~RHO,data=matp)
abline(reglogaw)
coefficients(reglogaw)
par(mfrow=c(2,2))
plot(reglogaw, 1:4)
##largest cook's distances: 1, 60, 62
summary(reglogaw)

rhologaw<-data.frame(RHO=log(AW))
rhologaw

## Omitting obs 1, 60 and 62 (the 3 largest cook dist and residual dist.)
reg5<-(lm(log(AW) ~ RHO, data=matp[-c(1,60,62),]))
summary(reg5)
coefficients(reg5)
plot(reg5, which=1:4)
confint
par(mfrow=c(1,1))
plot(log(AW)~RHO,data=matp[-c(1,60,62),],pch=16, cex=.5, cex.main=1,
cex.axis=1, cex.lab=1,
      ylab= "log(AW), y", xlab= "RHO, x", main="density vs. log water
uptake coefficient, y=2.9222 - 0.002766x")

abline(reglogaw, col="red")
abline(reg5, col="orange")

## Confidence and prediction intervals
newx5<-seq(1300,2100)
newx5
newdatax5=data.frame(RHO=newx5)

predCI<-predict(reg5,newdata=newdatax5, interval="confidence",
level=0.95, type="response")

```



```

predCI
predPI<-predict(reg5,newdata=newdatax5,interval="prediction", level=0.95,
type="response")
predPI

plot(RHO,log(AW),xlim=c(0,2100),ylim=c(-6,0), pch=16, cex=0.5,
      ylab="log(AW), y", xlab="RHO, x", main="density vs. log water uptake
coefficient", cex.axis=1.2,
      cex.lab=1.2, cex.main=1.2)
abline(reg5, col="blue") #
lines(newx5,predCI[,2],col="red", lty=2)
lines(newx5,predPI[,2],col="orange", lty=2)

plot(RHO,log(AW),xlim=c(1300,2100),ylim=c(-6,0), pch=16, cex=0.5,
      ylab="log(AW), y", xlab="RHO, x", main="density vs. log water uptake
coefficient", cex.axis=1.2,
      cex.lab=1.2, cex.main=1.2)
abline(reg5, col="blue") #
lines(newx5,predCI[,2],col="red", lty=2)
lines(newx5,predPI[,2],col="orange", lty=2)

### Predict AW when RHO is 1780
predPIx1780<-
predict(reg5,newdata=data.frame(RHO=1780),interval="prediction",
        level=0.95, type="response");predPIx1780

## the 95% prediction limits for the new y is: -0.011-0.35, fit is 0.17

#####

#MEW
reglogmew<-lm(log(MEW)~RHO,data=matp)
par(mfrow=c(1,1))
plot(log(MEW)~RHO,data=matp)
abline(reglogmew)
coefficients(reglogmew)
par(mfrow=c(2,2))
plot(reglogmew, 1:4)
##largest cook's distances: 2, 3, 62
summary(reglogmew)

rhologmew<-data.frame(RHO,log(MEW))
rhologmew

## Omitting obs 2, 3 and 62 (the 3 largest cook dist and residual dist.)
reg6<-(lm(log(MEW) ~ RHO, data=matp[-c(2,3,62),]))
summary(reg6)
coefficients(reg6)
plot(reg6, which=1:4)
confint
par(mfrow=c(1,1))
plot(log(MEW)~RHO,data=matp[-c(2,3,62),],pch=16, cex=.5, cex.main=1,
cex.axis=1, cex.lab=1,

```

```

      ylab= "log(AW), y", xlab= "RHO, x", main="density vs. log water
uptake coefficient,  $y=-1.5429 + 0.0024787x$ ")

abline(reglogmew, col="red")
abline(reg6, col="orange")

## Confidence and prediction intervals
newx6<-seq(1300,2100)
newx6
newdatax6=data.frame(RHO=newx6)

predCI<-predict(reg6,newdata=newdatax6, interval="confidence",
level=0.95, type="response")
predCI
predPI<-predict(reg6,newdata=newdatax6,interval="prediction", level=0.95,
type="response")
predPI

plot(RHO,log(MEW),xlim=c(0,2100),ylim=c(0,5), pch=16, cex=0.5,
      ylab="log(MEW), y", xlab="RHO, x", main="density vs. log water
vapour diffusion resistance factor", cex.axis=1.2,
      cex.lab=1.2, cex.main=1.2)
abline(reg6, col="blue") #
lines(newx6,predCI[,2],col="red", lty=2)
lines(newx6,predPI[,2],col="orange", lty=2)

plot(RHO,log(MEW),xlim=c(1300,2100),ylim=c(1,4), pch=16, cex=0.5,
      ylab="log(MEW), y", xlab="RHO, x", main="density vs. log water
vapour diffusion resistance", cex.axis=1.2,
      cex.lab=1.2, cex.main=1.2)
abline(reg6, col="blue") #
lines(newx6,predCI[,2],col="red", lty=2)
lines(newx6,predPI[,2],col="orange", lty=2)

### Predict MEW when RHO is 1780
predPIx1780<-
predict(reg6,newdata=data.frame(RHO=1780),interval="prediction",
        level=0.95, type="response");predPIx1780

## the 95% prediction limits for the new y is: 1.99-3.75, fit is 2.87

```

Internal insulation is a method for reduction of heat loss in historic buildings with preservation worthy façades. The application of internal insulation to solid masonry makes the existing wall colder and damper. Thus, the threat of moisture accumulation and moisture associated risks is increased. Dynamic simulations are useful for the prediction of hygrothermal performance, but the quality of the results is highly dependent on the input. This thesis investigates vital input parameters and their influence on the hygrothermal performance of internally insulated solid historic masonry.

DTU Civil Engineering
Technical University of Denmark

Brovej, Bygning 118
2800 Kongens Lyngby
Tel. 45 25 17 00

www.byg.dtu.dk

ISBN 9788778774965
ISSN 1601-2917